Factors Affecting the Reactivity of Granular Iron in contact with Chlorinated Solvents

Rubina Firdous

M.Sc., Department of Geology, University of Karachi

Submitted to the Department of Geology
and the Faculty of the Graduate School of the University of Kansas
in partial fulfillment of the requirements for the Degree of
Doctor of Philosophy

September 2013

Advisory Committee:

_____
Dr. J. F. Devlin, Chair

_____
Dr. Craig P. Marshall, Committee Member

_____
Dr. Jennifer Roberts, Committee Member

_____
Dr. George Tsoflias, Committee Member

_____
Dr. Daniel Hirmas, Committee Member

_____
Dr. Andrea Brookfield, Committee Member

Date Defended 09/06/2013

The Dissertation Committee for Rubina Firdous certifies that this is the approved version of the Following dissertation:

Factors Affecting the Reactivity of Granular Iron in contact with Chlorinated Solvents

Advisory Committee:

_____

Dr. J. F. Devlin, Chair

Date Approved 11/15/2013

Abstract

This study investigates, at various scales, the factors that affect the reactivity of granular iron (GI) toward chlorinated solvents and link these scale-specific processes with each other. The Kinetic Iron Model (KIM), provides a separate estimate for both the sorption and reaction processes of contaminant degradation, was used to determine the macro-scale kinetic and sorption parameters in all column experiments associated with this work. The intermediate scale corresponding to pore spaces was investigated by image analysis technique. This technique was used to examine the effects of diluting iron with sand on the availability of reactive iron surface. Two morphological parameters were measured in sections: i) grain perimeter, which reflects surface in contact with solution, and ii) total grain area in section. Morphological analysis showed grain areas exposed in section were highest for 100% iron packings and decreased with increasing sand content. However, the estimated iron grain perimeter length for 85% iron-by weight mixture was found to be the similar to that of 100% iron by weight. This study supported the use of 15% sand (by weight) in iron-sand mixture for the optimum performance of a permeable reactive barrier (PRB). Another pore scale issue examined was the effect of GI packing in column experiments. Among the tested packing variations- vertical packing with long axes preferentially along the flow showed higher reaction rates (2-4 times) compared to packings with long axes preferentially perpendicular to flow (horizontal packing) or randomly arranged (regular packing). The pore-scale differences in grain surface availability to solution through image analysis showed that grain surface availability partially accounted for reactivity differences between columns of different packings. It was suggested that micro-scale changes to the iron surfaces accounted for the remaining differences in reactivity. In order to examine the micro-scale changes that occur on the iron surface due to corrosion and to link these changes with macro-scale KIM parameters, long term column experiments were performed under

dynamic flow conditions. Micro-scale grain characteristics were made by recovering single grains from sampling port along the length of columns, and examining them through time using Raman spectroscopy and scanning electron microscopy (SEM)/Energy dispersive spectroscopy (EDS). Trichloroethylene (TCE) reduction kinetics showed considerable changes in both TCE sorption and reaction with time. Similarly, spectroscopic studies also indicated profound changes to the iron grain surfaces. It was found that over time, with exposure to TCE and water, iron tended to loose small number of sorption sites associated with highest reactivities (k) whereas large number of less reactive sorption sites increased in number. Raman spectra collected along the column showed the loss of hematite, and transition of intermediate phases to magnetite. Weakening of Raman signals for surface carbon correspond to declining k values and the non-reactive sorption parameter, suggesting that surface carbon serves as non-reactive sorption sites as well as a reactive one. Further the role of carbon present in GI during reductive dechlorination was assessed by comparing 2 iron types of GI in column experiments: Connelly Iron (GI)(~3% C) and Electrolytic Iron (EI) (≤ 0.01% C). Kinetic data suggested a shift in rate constant (k) and sorption parameters for both iron types with time. This work demonstrated the implication of carbon during the retardation (R_{app}) of TCE i.e high R_{app} for GI and low for EI.

Acknowledgments

Above all I would like to pay my warmest thanks to my advisor and mentor, Dr. John Frederick Devlin, for his excellent guidance and support throughout my PhD studies. It was his dedication, encouragement and trust that helped me out in a timely completion of this thesis. His passion to make his students thorough professionals is remarkable. Alongside supervising our research and studies, Dr. Devlin provided me and all of my other colleagues every possible opportunity to interact and collaborate with other scholars, workers and professionals, as available in the field of our studies. This generous and broad minded approach certainly played pivotal role in grooming our skills as competent Geoscientists. It was not only that his office was always a welcome place for me to discuss and sort out any kind of research issues but much more than the superb academic support, that I received from him, the personal cooperation, compassionate understanding and accommodating gestures during the initial days when I and my family came to USA for the first time – particularly with reference to the hardships of raising a young daughter – shall remain to be a memory to cherish in days to come.

I also want to express my deep gratitude to my PhD committee members, Dr. Craig P. Marshall, Dr. Jennifer Roberts, Dr. George Tsoflias, Dr. Daniel Hirmas, and Dr. Andrea Brookfield for their guidance and comments on the dissertation. I am especially thankful to Dr. Marshall for allowing me to use his laboratory, the training on Raman Instrument that he provided to me and for the expert advices on Raman Analysis during frequent discussions. I truly appreciate Dr. Bei Huang, then PhD candidate, who helped me during experimental work and data analysis. I would also like to thanks Dr. Luis Gonzalez for providing GTA support to continue my research, uninterruptedly. I shall be very unjustified on my part if I forget to appreciate the useful tips and buck up remarks that I received all the time from my colleagues

Dr. Peter Schillig, Ian Bowen, Natalie Burris, Kevin Walter, Angela Eichler and Brian Gibson. Furthermore, I would like to acknowledge the help from Mr. Wayne C. Dickerson who provided equipment support / guidance in preparing sections for morphological studies and Mr. Ian J. Rowell for the troubleshooting the computer related issues.

This acknowledgement will remain incomplete without mentioning the Institute of International Education (IIE) and the bureau of education and cultural affairs, United States Department of State for selecting me for the prestigious "Fulbright Science and Technology Award 2008 - 2011" in recognition of my capabilities and interest in the field of my choice. Similarly, without the indulgence of the staff at the United States Education Foundation in Pakistan (USEFP) all the necessary documentation for the visa processing and travel arrangements could not be possible.

In the end I would like to say thank you to my mother, my husband and my daughter for their support, understanding and encouragement throughout my studies. Specially, I shall remain extremely grateful to my husband for accompanying me in the United States, far away from his career service in Pakistan, for looking after his family while I was concentrating on my work. Without their cooperation it could not be possible for me to successfully complete the degree program, at all.

Table of Contents

List of Figures

List of Tables

1. Introduction

The goal of this thesis is to investigate, at various scales, the factors that affect reactivity of granular iron toward chlorinated solvents and to gain insight into how the scale-specific processes relate to each other. The Kinetic Iron Model (KIM) (Devlin, 2009) was used to determine the macro-scale kinetic and sorption parameters in column experiments. Spectroscopic and scanning techniques were used to investigate micro-scale characteristics on the iron grains as a function of age. A novel column design was adopted with which it was possible to obtain data sets from both the micro and macro scales. Between the column scale (macro) and the sub grain scale (micro) is an intermediate scale corresponding to pore spaces. Image analysis techniques were used to explore factors that might be of importance at that intermediate scale. Finally, different iron types with known compositional differences that would influence micro-scale processes were examined at the column scale to observe factors that directly connect the micro and macro scales.

1.1. Chlorinated Solvents

Chlorinated solvents are common groundwater contaminants found at hazardous waste sites and many industrial properties. Their widespread and extensive use, indiscriminate disposal history, leaks and spills have caused an important threat to groundwater resources (Gavaskar, 1998) and posed serious health affects to human population (WHO, 2003). Chlorinated compounds and some of the intermediate breakdown products that form in the subsurface tend to be highly toxic or carcinogenic at low concentrations (parts per billion) and have been designated as priority pollutants by the United States Environmental Protection Agency (EPA). For

example, the maximum contaminant level (MCL) standards of trichloroethene (TCE) for drinking water has been set to 5µg/l with a maximum contaminant level goal (MCLG) of 0 µg/l (Jia and Chu, 2009).

Many chlorinated solvents have densities greater than water and belong to a class of pollutant know as dense non-aqueous phase liquids (DNAPLs). When they are spilled, they move downward, below the water table, under the influence of gravity until they encounter a low permeability zone or aquitard. Their physio-chemical properties allow them to partition into several phases including the aqueous phase, or so-called "dissolved phase", they may volatilize into soil gas, the so-called "vapor phase", they may become sorbed to subsurface geological material, the "sorbed phase" or remain in an undissolved liquid phase known as a "residual phase". Due to their low solubilities, a contaminant source zone containing chlorinated solvents in an aquifer can persist from years to several decades. Relatively small amounts of these compounds can result in large scale groundwater contamination. Due to their low solubilities, tendencies to sink and resistance to degradation in many aquifers, these compounds pose a serious challenge to both detection in the subsurface and subsequent remediation (Brusseau *et al.*, 1999).

1.2. Permeable Reactive Barriers

Early methods of remediating contaminated groundwater focused on pumping, followed by above-ground treatment, a practice commonly called "pump-and-treat" (Kim *et al.*, 2010). Because of the nature and behavior of DNAPLs in the subsurface, coupled with the heterogeneity and complexity of groundwater systems, this treatment proved to be lengthy, expensive and ineffective at most of the hazardous sites (NAS, 1994; Mackay and Cherry, 1989). The inefficiency of pump-and-treat systems led to the development of alternate technologies. In

particular, *in-situ* methods for groundwater remediation were favored because they promised to be effective and relatively inexpensive over the long term.

The selection of a remediation technology depends on site specific conditions, long-term performance, and cost effectiveness. Permeable reactive barriers (PRBs) have been put forward as potential alternatives to pump-and-treat. A PRB treatment system consists of a reactive porous medium, placed *in situ* in the path of contaminated groundwater that flows under a natural hydraulic gradient. The reactive material sorbs or degrades contaminants thus immobilizing or converting them into potentially non-toxic compounds, respectively (Liang *et al.*, 2000). PRBs require low operating and maintenance costs and are highly effective for wide range of chlorinated solvents (Gillham and O'Hannesin, 1994; Phillips *et al.*, 2000) as well as inorganic contaminants (Blowes *et al.*, 2000).

1.3. Zero valent iron

Zero-valent iron (Fe^0), or its commercial equivalent, granular iron (GI) is the leading reactive material used in a PRB because it is capable of chemically reducing a wide variety of groundwater contaminants (Burris *et al.*, 1995; Gillham and O'Hannesin, 1994; Matheson and Tratnyek, 1994). GI consists of granular or platy grains of a light steel or cast iron (Burris *et al.*, 1998) mixed in a rotary kiln at several hundred degrees Fahrenheit. The kiln atmosphere, cooling time, and milling procedure leads to different surface morphologies and chemical compositions (Landis, 2001) which lead to slight variations in the commercially available GI brands. For example Connelly® Iron, exhibits platy texture (Bi *et al.*, 2009) and is covered with layers of several types of iron oxide (Odziemkowski *et al.*, 1998). Other zero valent metals like Cu^0, Al^0, galvanized Zn^0 (Gavaskar, 1998) have been investigated for their potential to reduce chlorinated compounds but, except for applications involving a small number of specific contaminants

resistant to degradation by iron, they have been found to offer no significant advantages over GI (Roh *et al.*, 2000b). Bimetallic Fe-Pd media have also been investigated for its dechlorination efficiency and found to enhance reaction rates by factor of 10 or more (Gui and Gillham, 2002; Wan *et al.*, 1999) because of the catalytic effect of Pd (Gavaskar, 1998). However, their use in PRB is limited mainly because of high cost compared to the GI. Similar studies have demonstrated advantages in other bimetallic systems, most notably Fe-Ni (Gunawardana and Swedlund, 2011; Kim and Carraway, 2003; Nyer and Vance, 2001). GI based PRBs have received much attention as a passive and cost-effective remediation technique for contaminated groundwater. However, its cost effectiveness is directly linked to its long-term performance in removing contaminants from groundwater. The main issues that might decrease the efficiency of a GI in PRB are 1) loss of reactivity (Gotpagar *et al.*, 1997) and 2) reduction in permeability through clogging (Mackenzie *et al.*, 1999; Roh *et al.*, 2000). Researchers have paid much attention to the passivation of the iron surface due to corrosion and precipitation (Mackenzie *et al.*, 1999; Ritter *et al.*, 2002) and have identified it as the major factor contributing to declining PRB performance (Devlin and Allin, 2005; Henderson and Demond, 2007; Vikesland *et al.*, 2003). Macro-scale factors, including solution composition, iron type, and available surface area are also know to affect reactivity (Bi *et al.*, 2009; Devlin and Allin, 2005; Su and Puls, 1999).

1.4. Reaction mechanism, corrosion and oxide formation

The carbon atoms in chlorinated solvents, such as TCE, are in an oxidized state because of the presence of chlorine, and undergo a reduction when the molecules come into contact with GI. Omitting the mechanistic details, which are still not fully understood, the solvent reduction is accompanied by iron oxidation, and by the disassociation of water (Gillham and O'Hannesin, 1994). Several mechanisms have been suggested for contaminant degradation in Fe^0-H_2O system which include direct electron transfer or catalyzed hydrogenolysis by H_2 (Matheson and

Tratnyek, 1994), β-elimination (Roberts *et al.*, 1996) or by catalytic hydrogenation (Farrell *et al.*, 2000). Studies have shown a combination of both hydrogenolysis and β-elimination (TCE → chloroacetylene → acetylene) pathways occur at the same time during the reduction of TCE (Roberts *et al.*, 1996b). In any of these cases, the GI core is believed to be the ultimate source of electrons in the reduction process (equation 1.1),

$$Fe^0 \rightarrow Fe^{2+} + 2e^- \qquad 1.1$$

This half reaction is coupled with the reduction of chlorinated compounds

$$RCL + 2e^- + H^+ = RH + Cl^- \qquad 1.2$$

Other important electron acceptors present in the system are H_2O and O_2, which undergo the following reductions (Johnson *et al.*, 1996),

$$\frac{1}{2} O_2 + H_2O + 2e^- \rightarrow 2OH^- \qquad 1.3$$

$$2H_2O + 2e^- \rightarrow H_{2(g)} + 2OH^- \qquad 1.4$$

Combining half reactions 1.1 and 1.4

$$Fe^0 + 2H_2O = Fe^{2+} + H_{2(g)} + 2OH^- \qquad 1.5$$

Several of the above reactions produce OH^- which increase the solution pH (Henderson and Demond, 2007; Matheson and Tratnyek, 1994)(equation 1.5). The corrosion and the increased pH lead to the precipitation of ferrous hydroxide ($Fe(OH)_2$) due to availability of iron ions in solution (Matheson and Tratnyek, 1994) (equation 1.6).

$$Fe^0 + 2H_2O = Fe(OH)_2 + 2H^+ + 2e^-$$

The overall reaction can thus be written,

$$Fe^0 + RCL + 2H_2O = Fe(OH)_2 + RH + H^+ + Cl^- \qquad 1.7$$

$Fe(OH)_2$ is thermodynamically unstable in the presence of Fe^0 and is further converted to magnetite (Fe_3O_4) (Odziemkowski *et al.*, 1998; Pourbaix, 1973; Reardon, 1995) which occurs as the dominant corrosion product on the iron surface under anaerobic conditions (equation 1.8).

$$3Fe(OH)_2 \rightarrow Fe_3O_4 + H_2 + 2H_2O \qquad 1.8$$

Magnetite (Fe_3O_4) acts as a conductor, which permits the exchange of electrons between Fe^0 and an oxidant (Schultze, 1978) through a process referred to as electron tunneling (Stimming and Schultze, 1979). Hematite (Fe_2O_3) can also be present as an outer oxide layer on GI. It may be removed by an auto-reduction reaction when in contact with solution and Fe^0 (Odziemkowski *et al.*, 1998), but can also build up on the GI surface if the flux of oxidant to the surface is sufficiently high. Hematite has been described as a semi-conductor (Schultze, 1978), or insulator (Cohen, 1978). Nevertheless, relative to magnetite or Fe^0, it will inhibit electron transfer (Ritter *et al.*, 2002).

Depending on the type of contaminants and ambient groundwater chemistry different corrosion products can form on the iron surface. Over time, mixed valent iron oxyhydroxides (Fe^{2+} and Fe^{3+}), also known as green rusts, form on the iron surface. These later act as intermediates in the formation of magnetite (Sumoondur *et al.*, 2008). Formation of goethite (α-FeOOH), lepidocrocite (γ- FeOOH) and magnetite (Fe_3O_4) have all been reported on Master builders GI contacting an anaerobic solution for 72 hours (Allin, 2000). Likewise, Ritter *et al* (2000) identified maghemite, which precipitated during nitrate reduction on Connelly Iron. Besides oxides, carbonates such as aragonite($CaCO_3$), calcite ($CaCO_3$), siderite ($FeCO_3$) and carbonate green rust have been identified on Peerless GI from Y-12 PRB, installed to treat U and NO_3 in high carbonate and calcium rich groundwater (Phillips *et al.*, 2003).

1.5. Surface characterization

Researchers have used various methods to identify and characterize the GI surface (Farrell *et al.*, 2001; Odziemkowski *et al.*, 1998; Phillips *et al.*, 2000). Among them are spectroscopy, diffractometry, thermal analysis and microscopy. Spectroscopic methods are widely used because they are non-invasive and provide useful information about any oxide phases on the iron surface. This is important because, with the exception of some platinum group elements, zero-valent metals – including iron – are not thermodynamically stable under normal environmental conditions on the Earth's surface, and tend to become covered with thin films of oxides (Chawla and Gupta, 1993) when exposed to the atmosphere, or dissolved oxygen.

Raman Spectroscopy has been used to investigate corrosion products on GI surfaces (Thibeau *et al.*, 1978) and gained importance in the characterization of near-surface Fe phases and carbonaceous materials because the method is sensitive to these phases, i.e., they are strong Raman scatterers. Raman techniques are widely accepted as they are nondestructive, require little or no sample preparation, and provide chemical and structural information at the micrometer scale (Marshall and Marshall, 2011). In addition, spectra of water-metal interfaces can be obtained *in-situ* (Devine, 1991). In prior work reported concerning GI, Raman spectra of dry Connelly iron showed the presence of magnetite (Fe_3O_4), maghemite (α-Fe_3O_4) and hematite (Fe_2O_3)(Odziemkowski *et al.*, 1998; Ritter *et al.*, 2002) whereas magnetite, maghemite and wustite were observed on the pristine Peerless iron surface (Satapanajaru *et al.*, 2003).

Scanning electron microscopy (SEM) and energy dispersive X-ray spectroscopy (EDS) have also been used to evaluate the morphology and elemental composition of the solid phases formed on the GI surface due to corrosion and precipitation (Lee and Wilkin, 2010; Min *et al.*, 2008; Min *et al.*, 2009). For example, micrographs of iron grains collected from Elizabeth city

PRB showed the presence of needle like crystals on the iron surface with an elemental composition close to that of the iron-carbonate phase, chukanovite (Lee and Wilkin, 2010).

Raman and SEM/EDS mapping techniques are available and have been applied to the study of graphite surfaces (Costa *et al.*, 2008; Dresselhaus *et al.*, 2010) They offer the possibility of establishing the special distributions of various phases – including oxides and carbonaceous phases – on a surface, and to highlight changes in those distributions over time. This methods has yet to be applied to the examination of GI surfaces.

As alluded to above, the GI grain surface has been demonstrated to be composed of variety of mineral phases, and elemental impurities with which contaminants might interact. Sorption and chemical reduction of many chlorinated solvents is believed to be fast at surface sites not covered with oxides, or only thinly covered (Huang, 2011). Additionally, the presence of impurities, such as carbon, further increases the complexity of the iron surface as they have been associated with non-reactive sites (Burris *et al*., 1998). Notably and paradoxically, carbon has also been shown to serve as a reactive site (Oh *et. al*., 2002).

In addition, the surface is morphologically complex, with pits, edges, and corners that may serve as sorption or reaction sites for contaminants. Changes in the nature and composition of oxide phases developed during the manufacturing process commonly exhibit stress points in oxide coating (Chawla and Gupta, 1993). These can lead to fractures and crevices within the oxide layers (Gotpagar *et al.*, 1999), which in turn serve as high energy points for corrosion when immersed in solution (Roh *et al.*, 2000).

1.6. Reactive and Non-Reactive Sites

Despite the known heterogeneous nature of granular iron surfaces, most studies treat them as being homogenous, and all sorption sites are assumed reactive. In light of the preceding

discussion, this view is oversimplified. Some of the various sites mentioned have the potential for chemical reactions with contaminants over relevant time frames (reactive sites) while others may not (non-reactive sites) (Burris *et. al*., 1998). Distinguishing between them is important since the non-reactive sites represent temporary storage of contaminants, not permanent removal.

Attempts have been made to quantify the proportions of "reactive" and "non-reactive" sites (Burris *et. al*., 1998). A conceptual model put forward by Huang (2011) divided the iron surface into 4 types of sites; (1) non-reactive and non-sorptive; (2) non-reactive sorption; (3) slow reactive sorption and (4) fast reactive sorption. The occurrence of these sites is presumed dependent, in part, on the thickness of the oxide layers. The terminology of "reactive sites" and "non-reactive sites" was adopted for this work where "reactive sites" refers to locations on GI where a chemical reaction can take place in a time frame relevant to the period of observation (the column pore volume exchange time was about 0.5 to 1 hour in the experiments conducted here). Non-reactive sites are capable of sorption but do not support chemical reactions over the relevant time period. Both reactive and non-reactive sites can decrease contaminant mass in solution, but complete and permanent removal only occurs at reactive sites (Bi *et al.*, 2010).

1.7. Iron-Sand Mixtures

Mass transfer limitations to sorption of TCE on GI have been shown to be practically insignificant in 100% iron media due to the close proximity of grains (Bi *et al.*, 2009). However, diluting GI with sand – generating media <100% iron – is a common field practice adopted to prevent clogging and reduce cost (O'Hannesin and Gillham, 1998; Yabusaki *et al.*, 2001a). A variety of iron-sand mixture ratios have been examined, - ranging from 10% iron to as high as 100% iron by weight (Bi *et al.*, 2009; Miyajima and Noubactep, 2013; Sivavec *et al.*, 2002). Various mixing ratios resulted in different reaction rates not necessarily proportional to the

fraction of iron in the medium (Bi *et al.*, 2009), the reasons for these differences have not been fully elucidated. Further work in this area could be of practical importance for PRB design.

1.8. Grain Geometry

The effect of grain shape on the reactivity of commercially available GI has received little attention. This seems like an oversight since studies conducted on other granular media have shown grain shape to be a factor of hydrologic importance, and by extension (more efficient contact between the solution and the GI surface leads to faster corrosion) of chemical importance (Dullien, 1991). Commercially available GI, for example the Connelly product, is platy in texture and therefore may pack in different orientations relative to the flow direction. Wu *et. al*., (2005) reported the differences of 10% in model-fitted parameters for identically prepared columns, and these variations attributed to differences due to grain packing. However, despite these differences, the effect of grain packing on reactivity has never been experimentally established.

1.9. TCE Dechlorination Reaction Kinetics involving GI

Knowledge of reaction rates of chlorinated solvents is essential for PRB design. A kinetic model should ideally account for all the chemical processes that affect dechlorination rates. In the past, reductive dechlorination by GI has been modeled by pseudo-first order kinetics (Devlin, 2009; Johnson *et al.*, 1996).

$$\frac{dC}{dt} = -k_{obs}C \qquad 1.9$$

Where C is the aqueous concentration of chlorinated solvents (M/L^3); k_{obs} is the observed first order rate constant (T^{-1}); and t is time (T). This simple approach fits any particular experimental data reasonably well with an empirically fitted value of k_{obs} (Bi *et al.*, 2009; Johnson *et al.*, 1996). However, this model does not represent the reaction processes realistically, as reaction rates depend on both the amount of iron and the aqueous concentration of the reactant (Johnson *et al.*, 1996). This is immediately apparent by virtue of the fact that k_{obs} is experiment specific and not a true constant. To partially address this deficiency, researchers have incorporated the iron surface area into the rate equation as shown in the following equation,

$$\frac{dC}{dt} = -k_{SA}\rho_a C \qquad 1.2.0$$

where k_{SA} is surface area normalized reaction rate constant ($L^3T^{-1}M^{-2}$), ρ_a is the surface concentration of Fe^0 (m^2L^{-1}). Eq 1.2.0 represents an improvement in the representation of TCE dechlorination on GI, but it does not account for self-competition for the surface by the reacting organic. Since in reality the surface is finite, the kinetics of reaction can be better represented by the Langmuir-Hinshelwood (L-H) rate equation (Lee and Batchelor, 2002).

$$\frac{dC}{dt} = \frac{kC_{max}Fe/V}{1/J+C}C \qquad 1.2.1$$

where k (min^{-1}) is the first order rate constant for the surface reaction, C_{max} is a parameter representing sorption capacity ($\mu molg^{-1}$), J is the sorption affinity to reactive sites on the surface (μM^{-1}), Fe/V is the iron mass to column pore water volume ratio ($g\ L^{-1}$) and C is the aqueous concentration of TCE (μM). The basic assumptions in this model are that target compounds sorb to a finite number of reactive site on the iron surface; reductive dechlorination occurs at these sites by first order reaction; absorption of chlorinated compounds and desorption of daughter products are both very fast compared to the chemical reaction that produces the

daughter; and sorption can be described by the Langmuir isotherm (Arnold and Roberts, 2000; Burris *et al.*, 1995; Devlin and Allin, 2005). The model accounts for sorption and electron transfer, which are fundamentally different processes, but two of the associated parameters are lumped in the kC_{max} term in the L-H rate equation making it impossible to uniquely identify their individual values and characterize the two processes separately.

$$\frac{dC}{dt} = \frac{kC_{max}Fe/V}{1/J + \frac{C_{max\,R}\,Fe/V}{1 + J_R C_o} + C_o} C_o = k_{app} C_o \qquad 1.2.2$$

To overcome this limitation, Devlin (2009) introduced Kinetic Iron Model (KIM), which is a generalized form of the L-H model, and can be used to obtain unique estimates of the surface-reaction rate constant (k), sorption capacity of reactive sites (C_{max}) and the sorption affinity of reactive sites (J), in some cases. The parameters are typically estimated with a non-linear optimization algorithm (Devlin, 1994). However, preliminary estimations can sometimes be obtained using a linearization approximation (Devlin, 2009; Marietta and Devlin, 2005). As part of this work, these procedures were coded together in the Visual Basic environment, within Excel, to streamline the analysis.

1.10. Hypothesis and Objectives of this Dissertation

The overall objective of this study is to establish cross-scale links between iron grain surface chemistry and macroscopic kinetic measurements. The specific tasks are geared at testing the following hypotheses: (1) a reported enhancement in reactivity associated with the addition of 15% sand to GI is due to increased GI surface area exposure at the pore scale; (2) Grain packing affects the GI surface area available to solution at the pore scale and therefore it also affects macro-scale reactivity: (3) the primary locations associated TCE reactions and sorption on GI are associated with micro-scale occurrences of carbon in the oxide layer or on the

metal surface, (4) the micro-scale surface carbon sites change in number and type as GI weathers with a corresponding effect on macro-scale kinetics.

1.11. Organization and Scope of this Dissertation

This document is organized into chapters based on the objectives listed above. Chapter 2 addresses mixing non-reactive media (sand) with GI in varying ratios, and compares trends in the pore-scale morphological parameters with those in the kinetic estimates. The effect of grain packing on the kinetics of TCE dechlorination is investigated in Chapter 3. Column experiments with different grain orientation were performed to evaluate the variability in the reactivity due to different packing practices, supported by pore scale investigations to observe the difference in morphological parameters among packings. In all experiments, comparisons of observations at the various scales were made with macro (column)-scale tests. In these experiments, the KIM parameters were identified using a VBA Excel Program presented in Chapter 4. This program code is embedded with two optimization algorithms, one transport code and two solution methods for the KIM. In Chapter 5, a comparison is made between iron types (Connelly iron with 3% carbon by weight, and an electrolytic iron, 99.99% pure by weight) The goal was to investigate the variability in sorption and reaction parameters connected to iron types with (relatively) high and low carbon contents. A comparison of the results of macro-scale column tests involving iron samples of differing ages and associated changes in micro-scale grain surface characteristics is reported in chapter 6. Column experiments were performed in a custom design column to recover grains for Raman spectroscopy and SEM/EDS analyses. The mapping tools available on the SEM instruments were used to document the changes in surface phases over time. The thesis concludes with a summary of the overall findings of the work.

References

Adamson, A.W., Gast, A.P., 1997. Physical chemistry of surfaces. Wiley New York.

Allin, K., 2000. Effect of water Geochemistry on the reactivity of granular iron., Earth Sciences. Waterloo, Ontario.

Arnold, W.A., Ball, W.P., Roberts, A.L., 1999. Polychlorinated ethane reaction with zero-valent zinc: pathways and rate control. Journal of Contaminant Hydrology, v. 40, no. 2, 183-200.

Arnold, W.A., Roberts, A.L., 2000. Inter- and Intraspecies Competitive Effects in Reactions of Chlorinated Ethylenes with Zero-Valent Iron in Column Reactors. Environmental Engineering Science, v. 17, no. 5, 291-302.

Bartzas, G., Komnitsas, K., 2010. Solid phase studies and geochemical modelling of low-cost permeable reactive barriers. Journal of Hazardous Materials, v. 183, no. 1–3, 301-308.

Bi, E., Devlin, J.F., Huang, B., 2009. Effects of Mixing Granular Iron with Sand on the Kinetics of Trichloroethylene Reduction. Ground Water Monitoring and Remediation, v. 29, no. 2, 56-62.

Bi, E., Devlin, J.F., Huang, B., Firdous, R., 2010. Transport and Kinetic Studies To Characterize Reactive and Nonreactive Sites on Granular Iron. Environmental Science and Technology, v. 44, no. 14, 5564-5569.

Blowes, D.W., Ptacek, C.J., Benner, S.G., McRae, C.W.T., Bennett, T.A., Puls, R.W., 2000. Treatment of inorganic contaminants using permeable reactive barriers. Journal of Contaminant Hydrology, v. 45, no. 1–2, 123-137.

Brusseau, M.L., Gierke, J.S., Sabatini, D.A., 1999. Field Demonstrations of Innovative Subsurface Remediation and Characterization Technologies: Introduction, Innovative Subsurface Remediation. American Chemical Society, pp. 2-5.

Burris, D., Allen-King, R., Manoranjan, V., Campbell, T., Loraine, G., Deng, B., 1998. Chlorinated Ethene Reduction by Cast Iron: Sorption and Mass Transfer. Journal of Environmental Engineering, v. 124, no. 10, 1012-1019.

Burris, D.R., Campbell, T.J., Manoranjan, V.S., 1995. Sorption of Trichloroethylene and Tetrachloroethylene in a Batch Reactive Metallic Iron-Water System. Environmental Science and Technology, v. 29, no. 11, 2850-2855.

Chawla, S.L.G., R. K., 1993. Materials selection for Corrosion Control. ASM International, Materials Park, OH, 7 pp.

Cohen, M., 1978. The passivity and breakdown of passivity on iron. The Electrochemical Society, Pennington, NJ., 521-545 pp.

Costa, S., Borowiak-Palen, E., Kruszynska, M., Bachmatiuk, A., Kalenczuk, R., 2008. Characterization of carbon nanotubes by Raman spectroscopy. Mater Sci Poland, v. 26, no. 2, 433-441.

Devine, T.M., 1991. Use of Surface-Enhanced Raman Spectroscopy in Studies of Electrode-Electrolyte Interfaces, In: Ferreira, M.S., Melendres, C. (Eds.), Electrochemical and Optical Techniques for the Study and Monitoring of Metallic Corrosion. Springer Netherlands, pp. 389-437.

Devlin, J.F., 1994. A Simple and Powerful Method of Parameter Estimation Using Simplex Optimization. Ground Water, v. 32, no. 2, 323-327.

Devlin, J.F., 2009. Development and Assessment of a Rate Equation for Chemical Transformations in Reactive Porous Media. Environmental Science & Technology, v. 43, no. 11, 4113-4118.

Devlin, J.F., Allin, K.O., 2005. Major Anion Effects on the Kinetics and Reactivity of Granular Iron in Glass-Encased Magnet Batch Reactor Experiments. Environmental Science & Technology, v. 39, no. 6, 7p.

Dresselhaus, M., Jorio, A., Saito, R., 2010. Characterizing graphene, graphite, and carbon nanotubes by Raman spectroscopy. Annu. Rev. Condens. Matter Phys., v. 1, no. 1, 89-108.

Dullien, F.A., 1991. Fluid transport and pore structure. Academic Press, San Diego, CA.

Farrell, J., Melitas, N., Kason, M., Li, T., 2000. Electrochemical and Column Investigation of Iron-Mediated Reductive Dechlorination of Trichloroethylene and Perchloroethylene. Environmental Science and Technology, v. 34, no. 12, 2549-2556.

Farrell, J., Wang, J., O'Day, P., Conklin, M., 2001. Electrochemical and spectroscopic study of arsenate removal from water using zero-valent iron media. Environ Sci Technol, v. 35, no. 10, 2026-2032.

Gavaskar, A.R., 1998. Permeable barriers for groundwater remediation : design, construction, and monitoring. Battelle Press, Columbus.

Gillham, R.W., O'Hannesin, S.F., 1994. Enhanced Degradation of Halogenated Aliphatics by Zero-Valent Iron. Ground Water, v. 32, no. 6, 958-967.

Gotpagar, J., Grulke, E., Tsang, T., Bhattacharyya, D., 1997. Reductive dehalogenation of trichloroethylene using zero-valent iron. Environmental Progress, v. 16, no. 2, 137-143.

Gotpagar, J., Lyuksyutov, S., Cohn, R., Grulke, E., Bhattacharyya, D., 1999. Reductive Dehalogenation of Trichloroethylene with Zero-Valent Iron: Surface Profiling Microscopy and Rate Enhancement Studies. Langmuir, v. 15, no. 24, 8412-8420.

Gui, L., Gillham, R.W., 2002. Evaluating the performance of palladium-plated granular iron for reductive dechlorination of TCE. IAHS PUBLICATION, 403-408.

Gunawardana, B., Swedlund, P., 2011. Review Papers: Degradation of Chlorinated Phenols by Zero Valent Iron and Bimetals of Iron: A Review. Environmental Engineering Research (EER), v. 16, no. 4, 187-203.

Henderson, A.D., Demond, A.H., 2007. Long-term performance of zero-valent iron permeable reactive barriers: A critical review. Environmental Engineering Science, v. 24, no. 4, 401-423.

Higgins, M.R., Olson, T.M., 2009. Life-Cycle Case Study Comparison of Permeable Reactive Barrier versus Pump-and-Treat Remediation. Environmental Science and Technology, v. 43, no. 24, 9432-9438.

Huang, B., 2011. Separating the Kinetic and Sorption Parameters of Mixed Chlorinated Solvents in Contact with Granular Iron, Geology. University of Kansas, Lawrence, p. 163.

Jia, J., Chu, W., 2009. The photodegradation of trichloroethylene with or without the NAPL by UV irradiation in surfactant solutions. Journal of Hazardous Materials, v. 161, no. 1, 196-201.

Johnson, T.L., Scherer, M.M., Tratnyek, P.G., 1996. Kinetics of Halogenated Organic Compound Degradation by Iron Metal. Environmental Science and Technology, v. 30, no. 8, 2634-2640.

Kim, Y.H., Carraway, E.R., 2003. Reductive dechlorination of TCE by zero valent bimetals. Environmental Technology, v. 24, no. 1, 69-75.

Landis, R.L., Gillham, R. W., Reardon, E. J., Fagan, R., Focht, R. M., Vogan, J.L., 2001. An examination of zero-valent iron sources used in permeable reactive barriers., 3rd International Containment Technology Conference. Florida State University, Tallahassee, Orlando, FL, p. 5.

Lee, J.-Y., Lee, K.-J., Youm, S., Lee, M.-R., Kamala-Kannan, S., Oh, B.-T., 2010. Stability of Multi-Permeable Reactive Barriers for Long Term Removal of Mixed Contaminants. Bulletin of Environment Contamination and Toxicology, v. 84, no. 2, 250-254.

Lee, T.R., Wilkin, R.T., 2010. Iron hydroxy carbonate formation in zerovalent iron permeable reactive barriers: Characterization and evaluation of phase stability. Journal of Contaminant Hydrology, v. 116, no. 1–4, 47-57.

Lee, W., Batchelor, B., 2002. Abiotic reductive dechlorination of chlorinated ethylenes by iron-bearing soil minerals. 1. Pyrite and magnetite. Environmental Science & Technology, v. 36, no. 23, 5147-5154.

Liang, L., Korte, N., Gu, B., Puls, R., Reeter, C., 2000. Geochemical and microbial reactions affecting the long-term performance of in situ 'iron barriers'. Advances in Environmental Research, v. 4, no. 4, 273-286.

Mackay, D.M., Cherry, J.A., 1989. Groundwater contamination: pump-and-treat remediation. Environmental Science & Technology, v. 23, no. 6, 630-636.

Mackenzie, P.D., Horney, D.P., Sivavec, T.M., 1999. Mineral precipitation and porosity losses in granular iron columns. Journal of Hazardous Materials, v. 68, no. 1–2, 1-17.

Marietta, M.L., Devlin, J.F., 2005. In Bringing Groundwater Quality Research to the Watershed Scale 4th International Groundwater Quality Conference. IAHS, Waterloo, Canada, pp. 376-382.

Marshall, C.P., Marshall, A.O., 2011. Hematite and carbonaceous materials in geological samples: A cautionary tale. Spectrochimica Acta, Part ASpectrochimica Acta Part A: Molecular and Biomolecular Spectroscopy, v. 80, no. 1, 133-137.

Matheson, L.J., Tratnyek, P.G., 1994. Reductive Dehalogenation of Chlorinated Methanes by Iron Metal. Environmental Science and Technology, v. 28, no. 12, 2045-2053.

Miyajima, K., Noubactep, C., 2013. Impact of Fe0 amendment on methylene blue discoloration by sand columns. Chemical Engineering Journal, v. 217, no. 0, 310-319.

NAS.,1994. Alternatives for ground water cleanup. N. A. o. Sciences. Washington, DC., National Academy Press: Washington, DC.

Nyer, E.K., Vance, D.B., 2001. Nano-Scale Iron for Dehalogenation. Ground Water Monitoring & Remediation, v. 21, no. 2, 41-46.

O'Hannesin, S.F., Gillham, R.W., 1998. Long-Term Performance of an In Situ "Iron Wall" for Remediation of VOCs. Ground Water, v. 36, no. 1, 164-170.

Odziemkowski, M.S., Schuhmacher, T.T., Gillham, R.W., Reardon, E.J., 1998. Mechanism of oxide film formation on iron in simulating groundwater solutions: Raman spectroscopic studies. Corrosion Science, v. 40, no. 2–3, 371-389.

Phillips, D.H., Gu, B., Watson, D.B., Roh, Y., 2003. Impact of sample preparation on mineralogical analysis of zero-valent iron reactive barrier materials. J Environ Qual, v. 32, no. 4, 1299-1305.

Phillips, D.H., Gu, B., Watson, D.B., Roh, Y., Liang, L., Lee, S.Y., 2000. Performance Evaluation of a Zerovalent Iron Reactive Barrier: Mineralogical Characteristics. Environmental Science and Technology, v. 34, no. 19, 4169-4176.

Phillips, D.H., Nooten, T.V., Bastiaens, L., Russell, M.I., Dickson, K., Plant, S., Ahad, J.M.E., Newton, T., Elliot, T., Kalin, R.M., 2010. Ten Year Performance Evaluation of a Field-Scale Zero-Valent Iron Permeable Reactive Barrier Installed to Remediate Trichloroethene Contaminated Groundwater. Environmental Science and Technology, v. 44, no. 10, 3861-3869.

Pourbaix, M., 1973. Lectures on Electrochemical Corrosion. Plenum, New York, 202 pp.

Reardon, E.J., 1995. Anaerobic Corrosion of Granular Iron: Measurement and Interpretation of Hydrogen Evolution Rates. Environmental Science and Technology, v. 29, no. 12, 2936-2945.

Roberts, A.L., Totten, L.A., Arnold, W.A., Burris, D.R., Campbell, T.J., 1996. Reductive Elimination of Chlorinated Ethylenes by Zero-Valent Metals. Environmental Science and Technology, v. 30, no. 8, 2654-2659.

Roh, Y., Lee, S.Y., Elless, M.P., 2000. Characterization of corrosion products in the permeable reactive barriers. Environmental Geology, v. 40, no. 1-2, 184-194.

Satapanajaru, T., Shea, P.J., Comfort, S.D., Roh, Y., 2003. Green rust and iron oxide formation influences metolachlor dechlorination during zerovalent iron treatment. Environ Sci Technol, v. 37, no. 22, 5219-5227.

Schultze, J., 1978. Electron transfer reactions on passive films. J. W. Schultze, Free Univ. of Berlin, W. Germany, Passivity of Metals, Frankenthal and Kruger(eds.), 82-101.

Sivavec, T., Krug, T., Berry-Spark, K., Focht, R., 2002. Performance Monitoring of a Permeable Reactive Barrier at the Somersworth, New Hampshire Landfill Superfund Site, Chlorinated Solvent and DNAPL Remediation. American Chemical Society, pp. 259-277.

Stimming, U., Schultze, J.W., 1979. A semiconductor model of the passive layer on iron electrodes and its application to electrochemical reactions. Electrochimica Acta, v. 24, no. 8, 859-869.

Su, C.M., Puls, R.W., 1999. Kinetics of trichloroethene reduction by zerovalent iron and tin: Pretreatment effect, apparent activation energy, and intermediate products. Environmental Science and Technology, v. 33, no. 1, 163-168.

Sumoondur, A., Shaw, S., Ahmed, I., Benning, L., 2008. Green rust as a precursor for magnetite: an in situ synchrotron based study. Mineralogical Magazine, v. 72, no. 1, 201-204.

Thibeau, R.J., Brown, C.W., Heidersbach, R.H., 1978. Raman Spectra of Possible Corrosion Products of Iron. Applied Spectroscopy, v. 32, no. 6, 532-535.

Vikesland, P.J., Klausen, J., Zimmermann, H., Roberts, A.L., Ball, W.P., 2003. Longevity of granular iron in groundwater treatment processes: changes in solute transport properties over time. J Contam Hydrol, v. 64, no. 1-2, 3-33.

Wan, C., Chen, Y.H., Wei, R., 1999. Dechlorination of chloromethanes on iron and palladium-iron bimetallic surface in aqueous systems. Environmental Toxicology and Chemistry, v. 18, no. 6, 1091-1096.

WHO, 2003. Trichloroethene in drinking-water. Background document for preparation of WHO Guidelines for drinking-water quality. Geneva, World Health Organization (WHO/SDE/WSH/03.04/22)

Yabusaki, S., Cantrell, K., Sass, B., Steefel, C., 2001. Multicomponent Reactive Transport in an In Situ Zero-Valent Iron Cell. Environmental Science and Technology, v. 35, no. 7, 1493-1503.

2. Visualizations and Optimization of Iron-Sand Mixtures for Permeable Reactive Barriers.

2.1. Abstract

Diluting granular iron with sand is a common practice performed to minimize clogging and to reduce the cost of permeable reactive barrier (PRB) installations. A variety of mixture ratios have been tested, ranging from 16% iron to 100% iron by weight. However, a determination of the iron:sand ratio to achieve optimal performance from granular iron PRBs (GIPRB) has received little attention. This study used a pore-scale image analysis technique to examine the effects of mixing sand with iron on the availability of reactive iron surface. Four mixing ratios (100%, 85%, 75% and 50% iron by weight) were compared on the basis of two morphological parameters measured in section: 1) grain perimeter available to solution, which reflects surface in contact with solution, and 2) total grain area in section, which is most closely related to the total amount of iron present. Grain areas exposed in section were highest for 100% iron packings and decreased with increasing sand content, as expected. Counter-intuitively, the estimated iron grain perimeter lengths in sections of the 85% iron-by weight mixtures were found to be similar as of 100%, and followed by 75%, and 50% iron mixtures. This analysis supports an earlier hypothesis that the addition of sand to iron opens up the packing structure, exposing more grain surface. The full benefit of the associated enhancement in reactivity appears to be realized in the 85% iron mixtures, and declines in more dilute iron mixtures due to overall lower iron surface area and the onset of mass transport controlled reaction rates.

2.2. Introduction

Granular iron permeable reactive barriers (GIPRB) have emerged as an effective groundwater remediation technology (Agrawal and Tratnyek, 1995; Matheson and Tratnyek, 1994; O'Hannesin and Gillham, 1998; Puls *et al.*, 1999). The use of iron as a reactive media in

PRBs is most common due to its ability to remediate wide variety of groundwater contaminants (Baciocchi *et al.*, 2003; Farrell *et al.*, 2000; Higgins and Olson, 2009; Phillips *et al.*, 2010). The success of a PRB depends on its long term ability to remove groundwater contaminants while maintaining permeability within the barrier. While reactivity losses are expected to be the main limits on PRB lifetimes (Henderson and Demond, 2007), the potential for clogging has received much attention (Btatkeu K *et al.*, 2013; Gu *et al.*, 1999; Liang *et al.*, 2000). Indeed, clogging has been documented in field studies (Korte *et al.*, 1997) and can cause the development of preferential flow paths and, in some cases, promote complete bypassing of the barrier (Benner *et al.*, 1999; Moraci and Calabrò, 2010).

Out of concern for the effects of clogging, and in order to reduce the cost of the barrier backfill (Bi *et al.*, 2009), the idea of diluting granular iron with sand (O'Hannesin and Gillham, 1998; Yabusaki *et al.*, 2001) and other non-reactive materials (Moraci and Calabrò, 2010) was conceived and put into practice. It was hoped that non-reactive granular material would maintain permeability in the barrier; prolonging the time that water could access the iron surface and be subject to treatment. To evaluate the performance of iron-sand backfill mixtures researchers have examined various iron:sand ratios in benchtop experiments (Bi *et al.*, 2009; Wu *et al.*, 2005). A variety of mixture ratios have been tested, ranging from as low as 10% iron to as high as 100% iron by weight (Miyajima and Noubactep, 2013; Sivavec *et al.*, 2002). However, an iron content of 50% by weight has received the most attention (RTDF, 2001). A recent study reported the iron:sand ratio of 30 to 50% by volume was the most efficient mixture based on methylene blue disappearances in columns of 0% through 100% iron, with 10% increments of sand by volume. However, the removal rates varied considerably over the tested range with the highest tested removal coming from the 0% column. Thus, the conclusion must be considered provisional. The earliest work on iron-sand mixtures showed that a linear relationship exists

between the iron surface area (or mass) and apparent reactivity (expressed as the pseudo first order rate constant, or rate) (Agrawal and Tratnyek, 1995; Gillham and O'Hannesin, 1994). However, a more detailed study indicated that 100% iron backfill and 85% iron 15% sand backfill (% by weight) exhibited nearly identical reactivities (Bi *et al.*, 2009). Bi *et al*. (2009) also noted that iron grains used in their experiments were platy and prone to packing in a fashion that could restrict full access of the solution to the iron surface. Therefore, the loss of total iron surface in going from 100% iron backfill to 85% backfill was hypothesized to be offset by an increase in iron surface available to solution due to the separation of platy grains by sand.

The objective of this work was to test the explanation given by Bi *et al*. (2009) by examining iron and sand mixtures at the pore scale. This was achieved through direct observations of serially sectioned media, and subjecting the sections to image analyses to obtain computer aided visualizations, and quantifications of the pore geometries in the different iron-sand mixtures.

2.3. Materials and Methods

All chemicals were used as received. Connelly Iron was provided by GMP Inc. Iron grains were hand sieved and grain sizes ranging from 0.71 to 2.0 mm were used. Fine silica sand was received from Quikrete Company was mixed with iron to get different iron: sand ratios for image analysis.

Table 2.1: Summary of the image characteristics of iron-sand mix packings

Packing type	Slice thickness (mm)	No. of slices	Original image size (pixel x pixel)	Image size for analysis (pixel x pixel)	Image size for analysis (mm x mm)
100:0*	0.05	25	615 x 382	510 x 368	20.99 x 15.14
85:15*	-	1	616 x 434	510 x 368	20.99 x 15.14
75:25*	-	1	626 x 442	510 x 368	20.99 x 15.14
50:50*	-	1	619 x 473	510 x 368	20.99 x 15.14

**mass iron:mass sand*

2.3.1. Sample preparation for pore scale investigations/Digital Image Processing

Pore scale investigations were carried out by preparing the desired iron:sand mixtures in plastic vials of diameter 2.9 cm, which closely matched the cross-sectional dimensions of the columns used by Bi *et al*. (2009). Vials were flooded and subsequently cemented with epoxy (EPO-TEK 301). Vertical cross-sections of the cemented material were cut from the solid

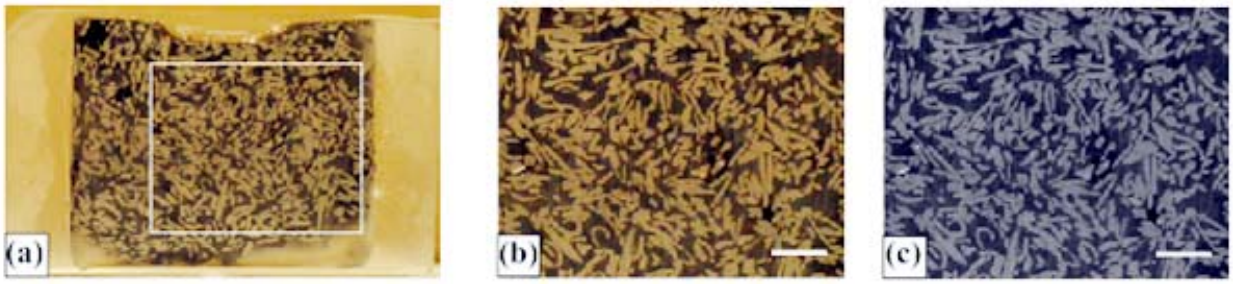

Figure 2.1: Pre-processing of raw data for image analysis (a) Original image of rectangle block on glass slide, (b) cropped image, (c) 8-bit grey scale image . The scale bars are 3 mm in length.

cylinders and mounted on glass slides. Altogether, 25 serial sections of 100% iron, and single sections for each of 85%, 75% and 50 % iron were prepared by grinding the surfaces in 50 μm steps using Hillquist Thin Sectioner. In 25 serial sections completed with the 100% iron-packed medium, the variability between morphological estimates, perimeter and area, was found not to exceed 10%, justifying further analysis on the basis of single sections. At each step the surface was photographed using a Olympus Stylus-5010 digital camera. All images were saved at 600

dpi, however analysis of dpi versus morphological parameters showed minimum of 300 dpi can be used effectively for the optimal result (appendix E). All original images were of 710 x 604 pixels size in 24 bit (Figure 2.1a), and were cropped to extract a common-sized region of interest (ROI) for image analysis (Figure 2.1b). Final images were stored as 8-bit grey level images (Figure 2.1c) (Table 2.1). The image analysis was based on methods given by Rasband (2007), using image analysis software NIH Image J (Rasband, 2007).

The following steps were taken to quantify pore geometry in Image J: 1) 8-bit grey level images were converted to binary representations of solid iron grains (white) and spaces between iron grains, containing sand (black) and pore space; ii) binary images were stacked together and 3D reconstructions made to render the total volume and porosity (Figure 2.2); iii) perimeters, area and grain counts were estimated for each prepared section using the "Analyze particles" function in Image J (Figure 2.3)(Table 2.2).

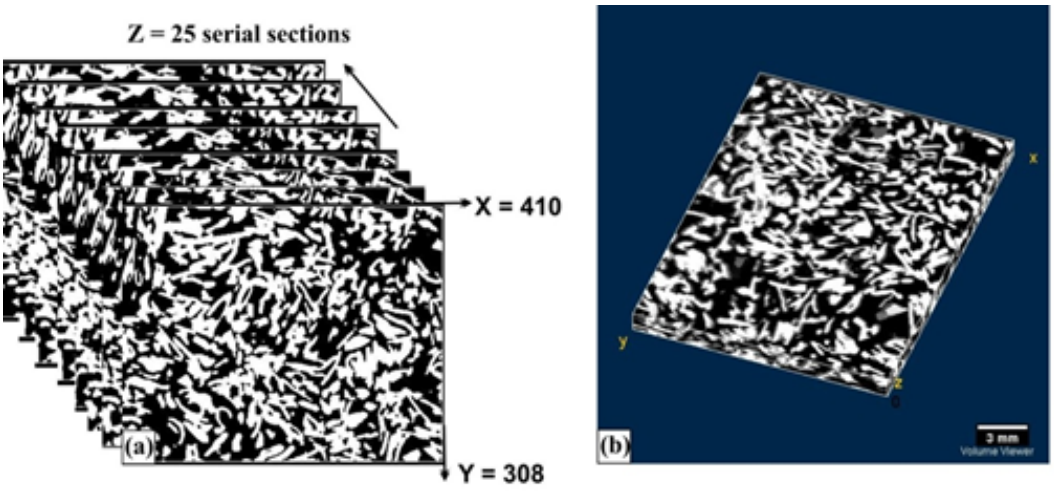

Figure 2.2: Post processing of the data using Image J freeware (a) serial binary images , (b) 3-D reconstruction for pore scale analysis. X and Y are pixel size.

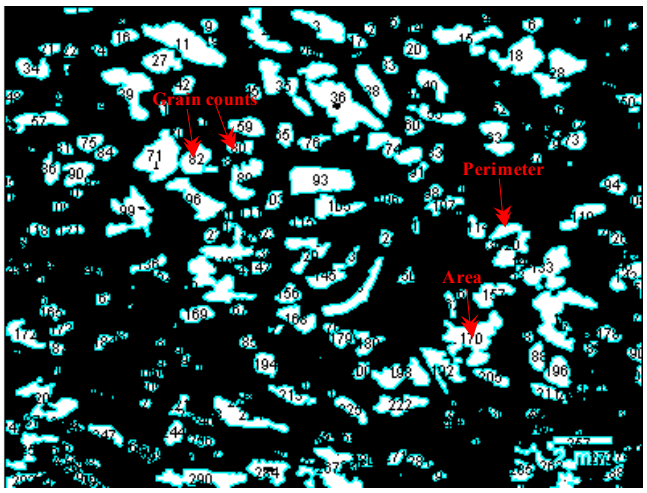

Figure 2.3: 75:25 Iron:sand mixture showing the grain boundaries in green as perimeter and white as grain area. Sand grains and pore spaces are shown by black pixels.

Table 2.2: Summary of pore analysis for iron:sand mixtures

Iron: Sand	Total perimeter (mm)	Total Area (mm2)	Iron area %
100:00	1050.03	172.25	54
85:15	1010.17	130.16	40.7
75:25	576.05	66.00	21
50:50	504.79	54.80	18

2.4. Results and Discussion

2.4.1. Image Analysis of Pore-Scale Changes Due to mixing

The structure of the porous medium and shape of the grains are known to affect flow and transformation rates of dissolved substances (Loraine, 2001). Other, related, factors with similar influence include porosity and permeability of the porous medium (Nield, 1992; Phillips, 1991; Zhao *et al.*, 2008). Therefore, the pore morphologies of porous media consisting of 100% iron, and mixtures of iron and sand, are relevant to PRB backfill material characterization. The image analysis technique used in this work clearly showed differences in grain packings between the different media investigated (Figure 2.4). As mentioned in the Introduction, the iron grains used in this study were platy and tended to pack with a high proportion of pores likely to restrict water

flow (Figure 2.4a). In 25 serial sections completed with the 100% iron-packed medium, the variability between morphological estimates, perimeter and area, was found not to exceed 10%, justifying further analysis on the basis of single sections. In contrast, a visual inspection of the spatial distributions of the iron grains showed large variations in packings where sand was present (Figure 2.4). As expected, the presence of sand in the medium opened pore spaces between closely packed iron grains (Figures 2.4b, c & d).

As mentioned previously, Bi *et al*. (2009) found that 85% iron (by weight) reacted with trichloroethene (TCE) with about the same initial reaction rate (k_{obs} * C_o) as 100% iron despite the lower iron content. Two important morphological parameters were considered to explain this finding: *solution accessible grain perimeter*, hereafter referred to as the 'perimeter', which is defined as the cumulative lengths of the outside boundaries of the grains, and the grain *area visible in section*, hereafter referred to as the 'area', which is defined as the cumulative 2-dimensional spaces bounded by the perimeters (Figure 2.3).

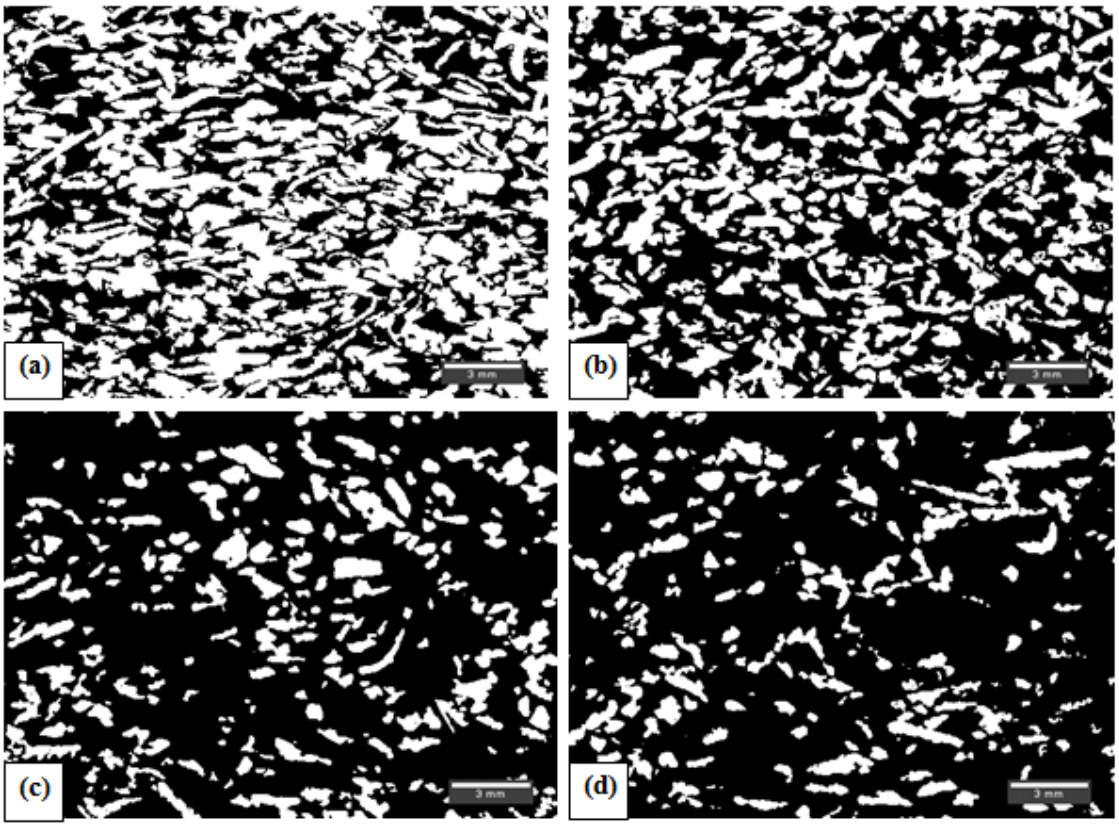

Figure 2.4: Binary images of iron-sand mix (showing iron grains in white) (a) 100% iron by weight (b) 85% iron (c) 75% iron and (d) 50% iron.

Estimated perimeters serve as a metric for the amount of iron surface accessible by solution, and areas serve as a metric for the total iron mass present. The image analysis showed that the perimeter of a mixture of 85% iron by weight is very close to a 100% iron medium despite the fact that the trend in areas was exactly the reverse (Figure 2.5a) (Table 2.2). This supports the hypothesis that portions of the iron surface is partially unavailable to the solution in the case of the 100% iron medium, presumably due to the close proximity of iron grains to one another.

Table 2.3: Summary of KIM parameters analyzed on different iron to sand ratios.

	Iron %	Porosity	Fe/V (gL^{-1})	k (min^{-1})	C_{max} ($\mu molg^{-1}$)	J (μM^{-1})
80 g iron	100%	0.55	4577	0.030	0.0210	0.0327
68 g iron : 12 g sand	85%	0.46	4416	0.011	0.0731	0.0279
60 g iron : 20 g sand	75%	0.49	3548	0.178	0.0048	0.0062
40 g iron : 40 g sand	50%	0.47	2223	0.032	0.0166	0.0098

The addition of 15% sand noticeably maintained the estimated perimeter by opening the pore spaces and exposing more of the iron surface to solution. Therefore, these results support the hypothesis proposed by Bi *et al*. (2009), that the lower iron mass in the 85% column was offset by the higher available iron surface.

To test the hypothesis further, the Kinetic Iron Model (KIM) (Devlin, 2009), eq 2.1, was utilized to estimate the maximum sorption capacity of the granular iron, C_{max}.

$$\left(\frac{dC}{dt}\right)_o = \frac{kC_{max}\frac{Fe}{V}}{\frac{1}{J} + \frac{C_{max}\frac{Fe}{V}}{1+JC} + C_o} C_o \qquad 2.1$$

where k is first order rate constant (min^{-1}), C_{max} represents maximum sorption capacity ($\mu molg^{-1}$), and J is sorption affinity to reactive sites (μM^{-1}) and Fe/V is the iron mass to water volume ratio (g/L). If solution accessible surface was truly limiting in selected iron-sand packed columns, then sorption capacity would be expected to be less in those cases than in the 85% iron columns. At the same time, the reactivity of the surface, indicated by k, and the affinity of the surface for TCE, indicated by J, would not be expected to change as a function of the amount of available surface. As predicted, both C_{max} and the perimeter estimates corresponded well, showing their highest values for 85% iron packed columns (Figure 2.5a). Furthermore, on the basis of the error estimates, the C_{max} for 85% iron was found to be significantly greater than other values while C_{max} estimates for the 100% and 50% packings were found not to be significantly different from each other. These data provide independent and corroborating evidence for the hypothesis of Bi *et al*. (2009) to explain the similar reactivities of 100% and 85% iron packed columns (Appendix A).

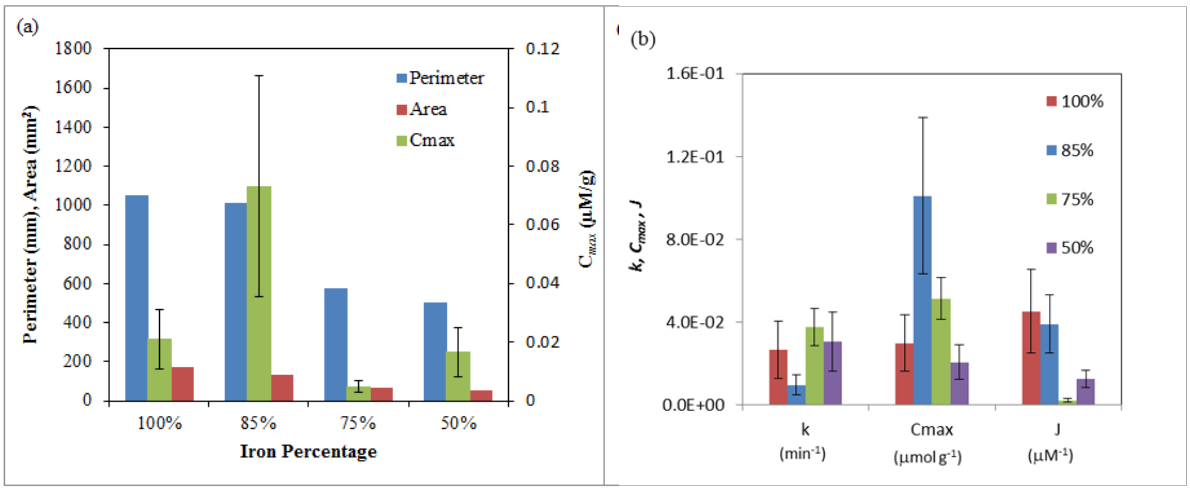

Figure 2.5: Comparison of morphological data through image analysis and KIM parameters in column experiment. a) *k*, C_{max}, and *J* estimated from each of the sand-iron packed columns. b) Comparison of perimeter, area, and C_{max} of 100:0, 85:15, 75:25 and 50:50 iron –sand mix packings. Error bars represent ± one standard deviation, σ. The σ for *k*, C_{max}, *J* were estimated from a Monte Carlo analysis of the rate vs. C_o data and eq. 2.1.

2.5. Conclusions and Implications

The analysis of iron and sand mixtures at the pore scale and by chemical kinetics analysis supports the hypothesis suggested by Bi *et al*. (2009) that the optimum reactivity of an iron PRB can be achieved by mixing the iron with about 15% sand by weight. Barriers constructed without sand will achieve grain packings that limit solution availability to the iron surface, particularly when the iron grains are platy in texture. The addition of more than 15% sand by weight may reduce the cost of a barrier, but it is also expected to reduce the reactive surface area of the iron, making the barrier less reactive. Moreover, as grains are separated by greater and greater distances, the kinetics of contaminant removal are likely to become increasingly mass transfer controlled.

References

Agrawal, A., Tratnyek, P.G., 1995. Reduction of Nitro Aromatic Compounds by Zero-Valent Iron Metal. Environmental Science & Technology, v. 30, no. 1, 153-160.

Baciocchi, R., Boni, M.R., D'Aprile, L., 2003. Characterization and Performance of Granular Iron as Reactive Media for TCE degradation by Permeable Reactive Barriers. Water, Air, and Soil Pollution, v. 149, no. 1, 211-226.

Benner, S.G., Blowes, D.W., Gould, W.D., Herbert, R.B., Ptacek, C.J., 1999. Geochemistry of a Permeable Reactive Barrier for Metals and Acid Mine Drainage. Environmental Science & Technology, v. 33, no. 16, 2793-2799.

Bi, E., Devlin, J.F., Huang, B., 2009. Effects of Mixing Granular Iron with Sand on the Kinetics of Trichloroethylene Reduction. Ground Water Monitoring and Remediation, v. 29, no. 2, 56-62.

Btatkeu K, B.D., Miyajima, K., Noubactep, C., Caré, S., 2013. Testing the suitability of metallic iron for environmental remediation: Discoloration of methylene blue in column studies. Chemical Engineering Journal, v. 215–216, no. 0, 959-968.

Devlin, J.F., 2009. Development and Assessment of a Rate Equation for Chemical Transformations in Reactive Porous Media. Environmental Science and Technology, v. 43, no. 11, 4113-4118.

Farrell, J., Melitas, N., Kason, M., Li, T., 2000. Electrochemical and Column Investigation of Iron-Mediated Reductive Dechlorination of Trichloroethylene and Perchloroethylene. Environmental Science and Technology, v. 34, no. 12, 2549-2556.

Gillham, R.W., O'Hannesin, S.F., 1994. Enhanced Degradation of Halogenated Aliphatics by Zero-Valent Iron. Ground Water, v. 32, no. 6, 958-967.

Gu, B., Phelps, T.J., Liang, L., Dickey, M.J., Roh, Y., Kinsall, B.L., Palumbo, A.V., Jacobs, G.K., 1999. Biogeochemical Dynamics in Zero-Valent Iron Columns: Implications for Permeable Reactive Barriers. Environmental Science & Technology, v. 33, no. 13, 2170-2177.

Henderson, A.D., Demond, A.H., 2007. Long-term performance of zero-valent iron permeable reactive barriers: A critical review. Environmental Engineering Science, v. 24, no. 4, 401-423.

Higgins, M.R., Olson, T.M., 2009. Life-Cycle Case Study Comparison of Permeable Reactive Barrier versus Pump-and-Treat Remediation. Environmental Science & Technology, v. 43, no. 24, 9432-9438.

Korte, N.E., West, O.R., Liang, L.Y., Pelfrey, M.J., Houk, T.C., 1997. A field-scale test facility for permeable reactive barriers at the portsmouth gaseous diffusion plant. Federal Facilities Environmental Journal, v. 8, no. 3, 105-114.

Liang, L., Korte, N., Gu, B., Puls, R., Reeter, C., 2000. Geochemical and microbial reactions affecting the long-term performance of in situ 'iron barriers'. Advances in Environmental Research, v. 4, no. 4, 273-286.

Loraine, G.A., 2001. Effects of alcohols, anionic and nonionic surfactants on the reduction of PCE and TCE by zero-valent iron. Water Res, v. 35, no. 6, 1453-1460.

Matheson, L.J., Tratnyek, P.G., 1994. Reductive Dehalogenation of Chlorinated Methanes by Iron Metal. Environmental Science & Technology, v. 28, no. 12, 2045-2053.

Miyajima, K., Noubactep, C., 2013. Impact of Fe0 amendment on methylene blue discoloration by sand columns. Chemical Engineering Journal, v. 217, no. 0, 310-319.

Moraci, N., Calabrò, P.S., 2010. Heavy metals removal and hydraulic performance in zero-valent iron/pumice permeable reactive barriers. Journal of Environmental Management, v. 91, no. 11, 2336-2341.

Nield, D.A., Bejan, A. , 1992. Convection in porous media. Springer-Verlag, New York.

O'Hannesin, S.F., Gillham, R.W., 1998. Long-Term Performance of an In Situ "Iron Wall" for Remediation of VOCs. Ground Water, v. 36, no. 1, 164-170.

Phillips, D.H., Nooten, T.V., Bastiaens, L., Russell, M.I., Dickson, K., Plant, S., Ahad, J.M.E., Newton, T., Elliot, T., Kalin, R.M., 2010. Ten Year Performance Evaluation of a Field-Scale Zero-Valent Iron Permeable Reactive Barrier Installed to Remediate Trichloroethene Contaminated Groundwater. Environmental Science & Technology, v. 44, no. 10, 3861-3869.

Phillips, O.M., 1991. Flow and reactions in permeable rocks. Cambridge University Press, Cambridge.

Puls, R.W., Blowes, D.W., Gillham, R.W., 1999. Long-term performance monitoring for a permeable reactive barrier at the U.S. Coast Guard Support Center, Elizabeth City, North Carolina. Journal of Hazardous Materials, v. 68, no. 1–2, 109-124.

Rasband, W., 2007. ImageJ: National Institute of Health, 1.46b ed, Bethesda, MD, USA, p. http://rsb.info.nih.gov/ij/index.html.

RTDF, 2001. Permeable reactive barrier installation profiles. Remediation Technologies Development Forum.

Sivavec, T., Krug, T., Berry-Spark, K., Focht, R., 2002. Performance Monitoring of a Permeable Reactive Barrier at the Somersworth, New Hampshire Landfill Superfund Site, Chlorinated Solvent and DNAPL Remediation. American Chemical Society, pp. 259-277.

Wu, Y., Slater, L.D., Korte, N., 2005. Effect of Precipitation on Low Frequency Electrical Properties of Zerovalent Iron Columns. Environmental Science and Technology, v. 39, no. 23, 9197-9204.

Yabusaki, S., Cantrell, K., Sass, B., Steefel, C., 2001. Multicomponent Reactive Transport in an In Situ Zero-Valent Iron Cell. Environmental Science & Technology, v. 35, no. 7, 1493-1503.

Zhao, C., Hobbs, B., Ord, A., Hornby, P., Peng, S., 2008. Effect of Reactive Surface Areas Associated with Different Particle Shapes on Chemical-Dissolution Front Instability in Fluid-Saturated Porous Rocks. Transport in Porous Media, v. 73, no. 1, 75-94.

3. The Effect of Grain Packing on Reductive Dechlorination Rates of TCE in Granular Iron Columns

3.1. Abstract

Commercial granular iron (GI) is light steel that is widely used in Permeable Reactive Barriers (PRBs). Investigations into the reactivity of GI have focused mainly on its chemical nature and little direct work has been done to account for the effects of grain shape and packing on the reactivity of a PRB. Both of these factors are expected to influence available grain surface area, which is known to correlate to reactivity. Commercial granular iron grains are platy and therefore pack in preferential orientations. Three packing variations were investigated using Connelly Iron and trichloroethylene (TCE). The experimental data showed reaction rates 2-4 times higher when grains were packed with long axes preferentially parallel to flow (VP) compared to packings with long axes preferentially perpendicular to flow (HP) or randomly arranged (RP). The possibility that packing-related pore-scale differences in grain surface availability to solution was assessed by conducting an image analysis of the pore structure of sectioned columns. The analyses showed that grain surface availability partially accounted for reactivity differences between columns of different packings. It is hypothesized that smaller scale features on the grain surfaces account for the remaining differences.

3.2. Introduction

Granular iron (GI) is the most common reactive material used in Permeable Reactive Barriers (PRB) (Baciocchi *et al.*, 2003; Farrell *et al.*, 2000; Higgins and Olson, 2009; Phillips *et al.*, 2010). The chemical behavior of GI, which is commercially available as an oxide covered light steel, has been intensively investigated in laboratory tests that regularly substitute pure iron, i.e., zero valent iron (ZVI), for the commercial products for the sake of simplifying the experimental interpretations. Since the morphology of ZVI is not necessarily the same as that of

the product that is used in field PRBs, there is the possibility that factors related to reactivity differences between laboratory and field studies have been overlooked. The objective of this work was to address this need, specifically by comparing the effects of grain packing, differentiated on the basis of differing grain orientations, on the reactivity of commercial GI towards TCE in column experiments. The context for this investigation is given below.

Reactive media like GI are selected for their propensity to degrade, sorb, or otherwise attenuate groundwater pollutants including chlorinated solvents (Liang, 1997; Mackenzie *et al.*, 1999), trace elements like arsenic (Wilkin *et al.*, 2009), selenium (Sasaki *et al.*, 2008), radionuclides such as uranium (Gu *et al.*, 2002; Simon *et al.*, 2003) and a variety of other substances like nitrates (Lee *et al.*, 2010; Robertson *et al.*, 2008), acid mine drainage (AMD) (Bartzas and Komnitsas, 2010) and even landfill leachate (Lee *et al.*, 2010). Macro-scale factors, including solution composition, iron type, and total available surface area (Su and Puls, 1999) are known to affect GI reactivity (Devlin and Allin, 2005; VanStone *et al.*, 2004), which is defined here as a property directly related to the rate of a specified reactant transformation in the presence of the GI surface. Relative reactivity of an iron sample can thus be compared in series of experiments involving the same reactant.

It is noted that the GI surface consists of a variety of mineral phases (Burris *et al.*, 1998), as well as physical features such as edges and corners, that may serve as sorption or reaction sites for groundwater contaminants. The number and availability of these sites is expected to have a direct effect on GI reactivity. However, it is also noted that transformation rates may be affected by the delivery rates of dissolved substances to the GI surface. The formation of precipitates within the GI porous medium, related to corrosion (Mackenzie *et al.*, 1999; Odziemkowski *et al.*, 1998; Ritter *et al.*, 2002), can diminish the permeability of packed GI (Mackenzie *et al.*, 1999; Roh *et al.*, 2000) hence decreasing contaminant flux through the GI medium and, consequently,

also the apparent reactivity (Puls *et al.*, 1999). These concepts are well established in the literature and continue to receive attention.

Another factor affecting PRB performance that has received attention is the grain surface area (Gotpagar *et al.*, 1997; Johnson *et al.*, 1996; Sivavec and Horney, 1995). Linear relationships between iron surface area (or mass) and reactivity (expressed as the pseudo first order rate constant, or rate) have been noted by different investigators (Agrawal and Tratnyek, 1996; Gillham and O'Hannesin, 1994). This linearity has been rationalized in several models of the reaction kinetics (Arnold and Roberts, 2000; Devlin, 2009; Johnson *et al.*, 1996; Wüst *et al.*, 1999). Reactive transport models that account for these effects have also been developed (Huang, 2011; Jeen *et al.*, 2007; Mayer *et al.*, 2001). With the introduction of nano-scale iron, several related studies have dealt with the issue of grain size, hence surface area density (g-Fe/L-solution), effects on reactivity (Gillham, 2003; Wang and Zhang, 1997).

A relevant factor that has received virtually no attention in the literature is the effect of GI grain packing on reactivity. Commercially available GI, for example the Connelly product, is platy in texture and therefore may pack in different orientations relative to the flow direction. The shape of granular material and its arrangement (Dullien, 1991), is known to affect flow and transformation rates of dissolved substances (Willingham *et al.*, 2008), as well as porosity and permeability of the porous medium (Nield, 1992; Phillips, 1991; Zhao *et al.*, 2008). The structure of granular media may also affect transport (Coelho *et al.*, 1997; Friedman and Robinson, 2002; Sperry and Peirce, 1995; Wyllie and Gregory, 1955; Yang and Xiaofeng, 2007). For example, work done on the micro-structure of undisturbed till showed a directional property of hydraulic conductivity (Nyborg, 1989); the parameter was smaller in the direction normal to the long axis of grains as compared to the direction parallel to the grain axes. The effective

diffusion coefficient also depends on the shape and tortuosity of the pore framework, which is in turn largely dependent on the shape of the granular media (Friedman and Robinson, 2002). Furthermore, grain packing is known to affect physical properties such as porosity and bulk density (Lebron and Robinson, 2003).

Despite efforts to achieve homogenous packing, column experiments performed with the same iron type have sometimes given notably different results (Ritter *et al.*, 2002). Differences of 10% have been reported in model-fitted parameters for duplicate columns , and the variations hypothesized to be due to differences in grain packing (Wu *et al.*, 2005). Differences in corrosion rates between 4 iron types have similarly been attributed to the combined effects of iron surface composition and geometric factors such as packing and shape of the grains (Jin suk *et al.*, 2009). To validate these speculations, it remains to be shown experimentally that packing does influence apparent reaction rates in GI media.

3.3. Materials and Methods

3.3.1. Materials

All chemicals were used as received. Trichloroethylene (TCE, 99%) was obtained from Acros Organics and methanol (HPLC grade) from Fisher Scientific. Connelly Iron was provided by GMP Inc. Iron grains were hand sieved and grain sizes ranging from 0.71 to 2.0 mm were used in the experiments. Stock solutions for analytical calibration were prepared in methanol and stored refrigerated at about 4 ^{o}C for not more than a month.

Table 3.1: Characterization of packed columns

Packing type	mass iron (g)	column internal diameter (cm)	column packed length (cm)	Pore Volume Vp (ml)	Porosity	Fe/V* (g L^{-1})
VP-1	80	1.59	16.60	18.56	0.56	4310
VP-2	80	1.59	15.70	15.95	0.51	5010
HP-1	80	1.59	15.70	17.99	0.57	4444
HP-2	80	1.59	15.70	17.75	0.57	4489
RP-1	80	1.59	16.75	19.42	0.58	4119
RP-2 (ref)	80	1.59	15.80	17.50	0.55	4571

**Fe/V refers to the mass of GI divided by the volume of solution in a saturated packed medium.*

3.3.2. Column Packings

All experiments were conducted with 1.59 cm diameter by 40 cm long pyrex glass columns. Vertical packing (VP) – grains preferentially aligned with the flow direction – was achieved by pouring small quantities of GI, 10-12 g at a time, into a column standing vertically on the bench-top. The column was then gently shaken by hand until the grains became aligned with the long axis of the column (Figure 3.1a). Great care was taken to disturb the surface coatings of the grains as little as possible during this procedure. The packing continued until the column was filled with 80 g of GI. Horizontal packing (HP) – with preferential grain alignment perpendicular to flow – was achieved by pouring 8-10 grains at a time into a vertically oriented glass column (Figure 3.1b). No shaking or tapping was necessary for the grains to acquire a strong horizontal grain alignment.

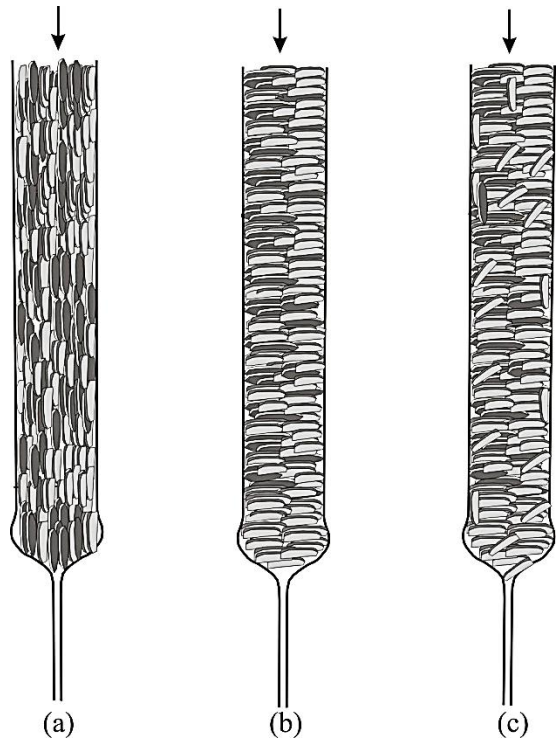

Figure 3.1: Schematic diagram showing different grain orientation in columns (a) Vertical Packing (b) Horizontal Packing and (c) Random Packing. Arrows indicate the flow direction in columns.

Random packing (RP) was achieved by adding 10-12 g at a time to a vertically oriented column with gentle tapping on the column glass to randomly redistribute the grains (Figure 3.1c) (Robinson and Friedman, 2001).

3.3.3. Methods

Each column was packed with 80 g Connelly GI (Table 3.1) and fitted with machined Plexiglass® end plugs. The weight of the columns and length of the packed material were measured for later porosity determinations. Prior to flooding, all packed columns were flushed with CO_2 gas for 20 minutes. The columns were then saturated with 8 mM electrolyte solution (1.124 g/L $NaClO_4$), which had been presparged with N_2 for 20 min to remove dissolved oxygen (DO). DO levels were measured in the sparged electrolyte solution with a Chemetrics kit and found to contain less than 0.5 mg/L $O_{2(aq)}$. Column flooding was undertaken with a flow rate (Q)

of 1 ml/min from air-tight PTFE (polytetrafluoroethylene) bags for at least for 8 hours before introducing TCE, to permit the iron surface to approach an equilibrium with the solution. $NaClO_4$ was used as a background electrolyte due to its low reactivity on the granular iron surface (Devlin and Allin, 2005; Moore *et al.*, 2003). After flooding, the columns were reweighed and the difference used to determine porosity (n).

After pretreatment, the solutions in the PTFE bags were spiked with the TCE stock solution and used as influent reservoirs for the column experiments. The solutions were pumped through the column using a peristaltic pump with Viton tubing in the pump heads. TCE concentrations were not noticeably different before and after the pump head in prior testing of the system (Huang, 2011).

The influent solutions were adjusted to pH 10 with the drop-wise addition of NaOH solution, prior to de-aeration by nitrogen sparging (minimum 20 minutes). The choice of pH 10 was made for consistency with prior work and to represent conditions within the center of a PRB (Devlin and Allin, 2005; Gavaskar, 1998; Yabusaki *et al.*, 2001).

Column experiments were conducted with a flow rate of 1 ml/min. TCE was introduced to the column at a selected influent concentration (C_o) until a steady state TCE effluent concentration was achieved. The column was then flushed with pre-sparged $NaClO_4$ for at least 12 hours to remove any TCE or chlorinated transformation products present from the earlier experiment. The C_o in the reservoir bag was subsequently adjusted upward and another test conducted. This was repeated for six different C_o values per experimental suite. Altogether, 5 different experimental suites were performed: 2 with vertically oriented grains; 2 with horizontally oriented grains; 1 with randomly orientation of the grains.

Effluent samples were collected in 2 ml vials at predetermined times. The collected samples were placed in a centrifuge for 5 minutes at 10,000 RPM to drive any solids to the

bottom of the vials. Samples were analyzed immediately after completing an experiment using an Agilent 1100 series High Performance Liquid Chromatography (HPLC) with autosampler and diode array detector (Marietta and Devlin, 2005). Two sets of standards covering the range of the initial concentrations (25 μM to 500 μM) were analyzed with the samples for calibration purposes. The calibration standards were used to determine accuracy and precision (*54*) which was generally within 2 – 10%. The detection limit of the method was found to be 0.5 μM.

A chloride tracer test was performed on both VP and HP to assess the possibility of physical non-equilibrium (PNE) transport dominating the apparent reaction rates. Evidence for PNE was sought in the form of noticeable tailing in the breakthrough curves. Chloride was analyzed using HACH Chloride Test Kit model 8-P Cat. No. 1440-01. Samples were collected in 2 ml vials, which were diluted with deionized (DI) water to make up the 6 ml sample volume necessary for the analysis. Once the breakthrough curves reached a plateau, the columns were flushed with DI water to remove the chloride tracer. Chloride concentrations were analyzed over the range of 60 mg/L to 300mg/L.

3.3.4. Determination of reaction kinetics and retardation factors

Effluent concentrations were plotted as breakthrough curves, which were fitted using BEARPE, a solution to the advection-dispersion equation with sorption and reaction (eq 3.1) coded with a non-linear optimizer (Bear, 1979; Devlin, 1994). The curves were fitted on velocity, v (cm/min), dispersivity, α (cm), pseudo first order rate constant, k_{app} (min^{-1}), and, when v was known in advance, retardation factor R_{app} (Appendix B).

$$C(x,t) = \frac{C_0}{2}\left\{\exp\left[\frac{vx}{2D}\left(1-\sqrt{1+\frac{4k_{app}D}{v^2}}\right)\right] erfc\left[\frac{R_{app}x - vt\sqrt{1+\frac{4k_{app}D}{v^2}}}{2\sqrt{DR_{app}t}}\right]\right\} \qquad 3.1$$

where C_o is the influent TCE concentration (μM), D is dispersion coefficient (m^2s^{-1}:, $D=\alpha v+D^*$), α is dispersivity (m), v is water velocity ($m\ s^{-1}$) and D^* is effective diffusion coefficient ($m^2\ s^{-1}$) that was assumed negligible in these experiments compared to αv, x is column length (cm).

3.3.5. Kinetic Modeling

The removal of TCE from groundwater in iron-based PRBs is the combined result of sorption and chemical reduction on the iron surface (Devlin *et al.*, 1998). The Kinetic Iron Model (KIM) (eq 3.2) (Devlin, 2009), which is capable of separating both the sorption and reaction processes, was used in this work to document possible changes in these parameters in connection with varying grain orientation. Changes in surface availability would be expected to affect the capacity term, C_{max}, to a greater degree than the other terms.

$$\frac{dC}{dt} = \frac{kC_{maxR}Fe/V}{1/J + \frac{C_{max\,R}\,Fe/V}{1+J_R C_o} + C_o} C_o = k_{app}C_o \qquad 3.2$$

where k (min^{-1}) is the first order rate constant for the surface reaction, C_{maxR} is the maximum sorption capacity to reactive sites ($\mu molg^{-1}$), J_R is the sorption affinity to reactive sites on the surface (μM^{-1}), Fe/V is the iron mass to column pore water volume ratio ($g\ L^{-1}$) and C_o is the aqueous influent concentration of TCE (μM).

3.4. Results and Discussion

3.4.1. Effect of grain packing variation on non-reactive sorption

The iron grain surface can be conceptualized as consisting of reactive and non-reactive

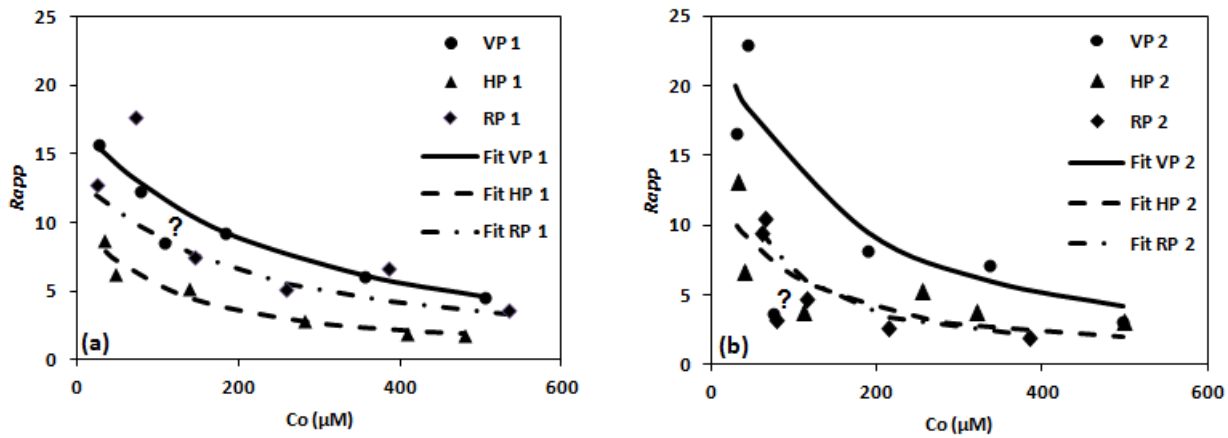

Figure 3.2: Relationship between retardation factor and injected TCE concentration for all packing columns (a) the solid curve fit the data for the VP-1, dash line for HP-1, and dash dotted line for RP-1(b) the solid curve fit the data for the VP-2, dash line for HP-2, and dash dotted line for RP-2. Data points labeled "?" were not used in model fits.

sites (Bi *et al.*, 2010; Burris *et al.*, 1995). Over a sufficiently large range of C_o, there is non-linear sorption to both types of sites (Bi *et al.*, 2010). The non-reactive sorption can be analyzed using the transient portion of the breakthrough curve (Bi *et al.*, 2010). Using eq 3.1, the k_{app} and R_{app} were fitted from the breakthrough curves (Appendix B). The maximum sorption capacity C_{maxN} (µmolg^{-1}) and sorption affinity, J_N (µM^{-1}), to non-reactive sites in the iron columns were then fitted with eq 3.3 (Bi *et al.*, 2010) (Figure 3.2) (Table 3.2).

$$R_{app} = 1 + \frac{Fe}{V} K_{dFe} \qquad 3.3$$

where,

$$K_{dFe} = \frac{J_N C_{maxN}}{(1+J_N C_o)^2} \qquad 3.4$$

The lower the K_{dFe} value, the lower the retardation factor (R_{app}), and the faster the reacting solute migrates through the material. For non-sorbing species, K_{dFe} will be zero and R_{app} will be equal

to 1, corresponding to a solute that migrates at the average linear speed of the water. Generally, R_{app} was found to decrease with increasing influent concentration, as previously reported (Bi *et al.*, 2010). This behavior was observed consistently in all experiments, but was particularly noticeable for $C_o > 100$ μM (Figure 3.2).

Sorption was most pronounced at lower influent concentrations (<100 μM) in all experiments. However, the two VP replicate columns showed higher retardation values at all injected TCE concentrations compared to the HP and RP experiments (Figure 3.2). Note that this result is inconsistent with PNE retarded transport, which would be expected to be most pronounced in the horizontally packed columns where the nature of the grain packing would make PNE transport most likely (due to the higher number of pores cut off from the main direction of flow). In the present work, the mass of Fe was kept constant (80 g for all columns), so any change in the availability of sorption sites, as suggested by the higher sorption in the VP experiments, appears to have been associated with the grain packing and orientation rather than the amount of iron present. Apparently, the vertical orientation of grains fostered increased availability of the surface for sorption compared to the other packing arrangements.

The *Fe/V* term (eq 3.2, 3.3) is sometimes reported as surface area and sometimes as mass. However, the overall solid surface area of packed GI increases over time due to oxide production as the iron corrodes (Allin, 2000), producing surfaces that are not necessarily as reactive as the original surfaces. This, and a reported linear relationship between initial surface areas and iron mass (Gillham and O'Hannesin, 1994), justifies the use of *Fe/V* expressed in terms of iron mass, which changes very little over an experimental suite. The mass of solid iron in a column is greatly in excess of what can be removed during an experiment, based on typical corrosion rates (0.1- 0.7 mmol Kg^{-1} day^{-1}) and iron leaching rates (max 6 mg L^{-1} in effluent) (Gillham and

O'Hannesin, 1994; Reardon, 1995). The changing surface area (reactive and non-reactive) is primarily taken into account in the C_{max} parameters, which is intuitively reasonable since the surface area and C_{max} terms are both related to sorption capacity.

Table 3.2: Summary of fitted kinetic and sorption parameters for reactive and nonreactive sites on GI packed in three different (predominant) orientations.

Packing	C_{maxN} (μMg^{-1})	J_N (μM^{-1})	k (min^{-1})	C_{maxR} (μMg^{-1})	J_R (μM^{-1})
VP-1	1.70	0.0026	0.0097	0.32	0.065
VP-2	1.34	0.0034	0.010	0.11	0.099
HP-1	0.47	0.0044	0.010	0.06	0.07
HP-2	0.54	0.0048	0.008	0.06	0.16
RP-1	1.20	0.0024	0.010	0.085	0.055

The calculated C_{maxN} followed the trend VP>RP>HP for all columns (Table 3.2). This order was similar to that of the R_{app} estimates, for which VP>RP ≥ HP (Figures 3.2 a and b). In contrast, there was no clear trend in the J_N parameter estimates if an uncertainty of ± 0.001 μM^{-1} was applied, based on the differences between replicates. A t-test was performed to compare the means of the estimated parameters from the various tests (Appendix C). It was found there was only a 9% chance that the means of C_{maxN} were identical between the HP and RP *vs*. VP packings, compared to a 57% chance the means of J_N were identical. The absence of systematic variations in J_N indicates the affinity of the iron for TCE was independent of grain packing, which was as expected.

3.4.2. Effect of grain packing variation on reactive sorption

The kinetics of transformation, and equilibrium reactive sorption on the iron surface was investigated using the TCE concentrations in the steady state portion ($dC_{effluent}/dt = 0$) of the effluent breakthrough curves and equation 3.2 (Bi *et al.*, 2010). Using a 2-step linearization approximation (Marietta and Devlin, 2005), preliminary estimates of C_{maxR}, J_R, and k were

calculated for all experiments. These were then used as initial guesses for nonlinear regression in the KIM (Devlin, 2009), from which the best fit parameters were estimated (Table 3.2). The values of C_{maxR} for the HP and RP were in the range previously reported (Bi *et al.*, 2010) and repeatedly less than those obtained from the VP experiments. Again, t-tests were performed to compare the means of the three packing type tests. They indicated only about a 16% chance that the means were the same for the C_{maxR} parameter, a 78% chance they were the same for the J_R parameter, and a 92% chance the means were the same for the k parameter. This result indicates that the higher reaction rates in the VP columns were mainly attributable to a greater number of available reactive sites rather than higher sorption affinity (through J) or inherent chemical reactivity (through k).

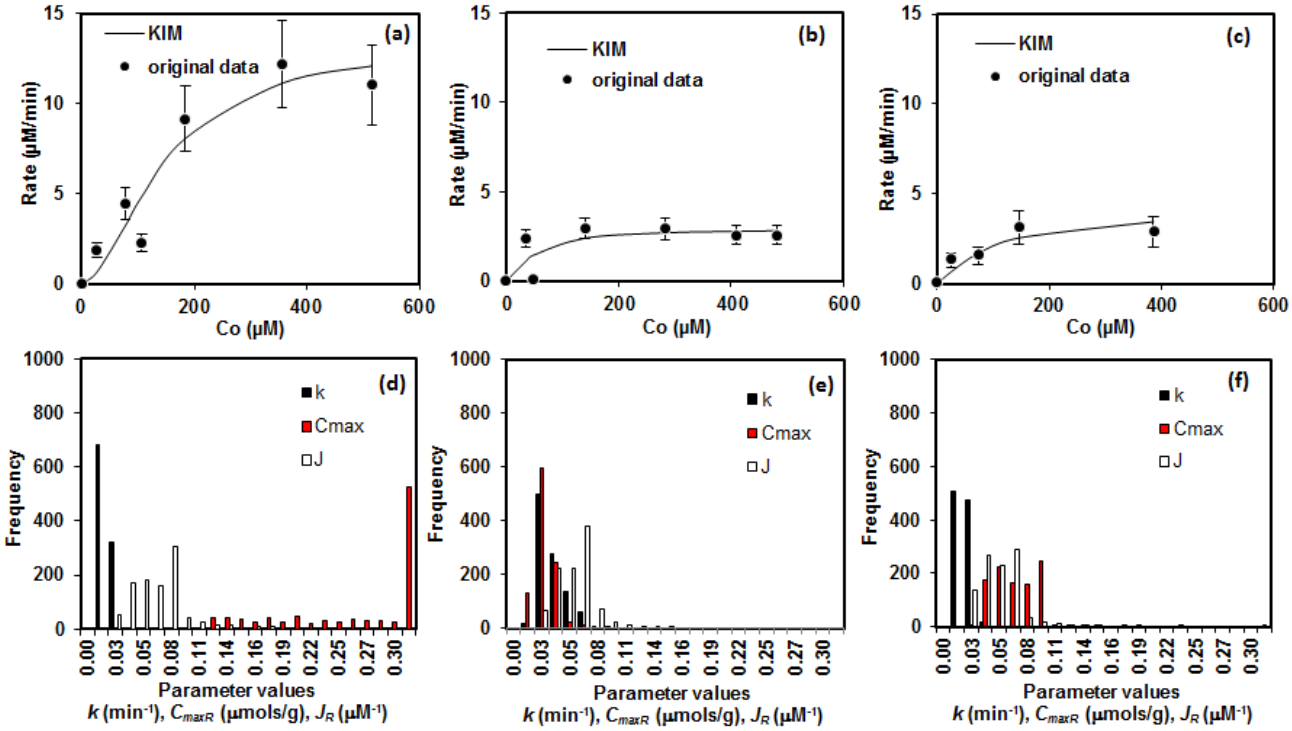

Figure 3.3: Relationship between TCE concentration and reduction rates using KIM (eq 3.2) (a) for VP (b) for HP (c) for RP (d) distribution of parameters estimates using Monte Carlo analysis for VP (e) for HP and (f) for RP. Note that the best fit parameters represent a single realization and

may not correspond to the parameter values with the highest frequencies determined in the Monte Carlo analysis.

The estimates of J_R were found to be consistently higher than those of J_N, suggesting slightly greater affinity of TCE for the reactive sites compared to non-reactive sites in these experiments.

A further check on the possibility that the C_{max} terms were significantly different between the VP experiments and the other tests was undertaken by performing a Monte Carlo analyses on the data sets assuming 20% error on each column rate point (Figures 3.3 a, b, and c) to generate distributions of fitted C_{maxR}, k, and J_R parameters (Figures 3.3 d, e, and f). The Monte Carlo exercise was based on 1000 realizations. The distributions tended to be slightly asymmetrical in all cases and for all packings. Nevertheless, there were differences in the results from the variously packed columns: all three parameters exhibited relatively narrow distributions in HP and RP experiments, while in both VP tests, the C_{maxR} parameter exhibited a very wide distribution indicating high uncertainties on the best fit values (Figure 3.3d). The wide distribution in C_{maxR} makes the parameter difficult to define with precision, but nonetheless points to likelihood that its value tends to be greater on average in the VP tests than in the HP and RP tests, as concluded previously.

The possibility that the differences in the C_{max} terms were influenced by PNE rather than sorption was examined with chloride tracer tests. It was reasoned that stream lines perpendicular to the average flow direction would be more common in the HP columns than in the VP columns and that these would create conditions favorable for PNE in the HP columns. This would occur because in HP columns some streamlines would exhibit much higher water speeds than others. Where PNE is important, solute breakthrough curves would be expected to show significant tailing due to the slow release of solute from the restricted pores. These

occurrences would affect tracer breakthrough curves in VP columns, where PNE is expected to be minimal, differently from HP columns, where PNE is more likely to occur. However, experimentally, both types of column packings produced nearly identical breakthrough curves (Appendix D). This result suggests that PNE in the HP columns was not a major factor in the transport behavior in these columns. Therefore, the C_{max} terms must primarily reflect differences in sorption rather than biases introduced by PNE.

The important result of this work is that it demonstrates that grain packing and orientation in the GI porous medium affects observable transformation rates of TCE. The initial reaction rates ($dC/dt= k_{obs}C_o$) in HP and RP tests were found to be very similar, and agreed with previously reported experiments (Bi *et al.*, 2010). However, the reaction rates in duplicate VP experiments were 2-4 times higher than those from the other packings, apparently due to an increased availability of reactive sorption sites.

3.4.3. Pore-Scale Visualization Experiments

The possibility that the reactivity differences could be rationalized on the basis of solution accessible surface areas in the differently packed columns was evaluated using NIH Image J software (Rasband, 2007). The VP and HP pore networks were found to be quite distinct from one another (Figures 3.4a and b). The vertical packing resulted in a more open structure with more apparent solution available grain surface than the horizontal packing. This observation is supported by an examination of skeletonized images, which facilitate visualization of the interconnectedness of the pore networks by digitally removing the grains from the images and displaying connected pores throats with lines (Figures 3.4c & d) (Baldissera *et al.*, 2011); the denser network is seen to correspond to the VP case (Figure 3.4c). Further support comes from consideration of porosity differences between the columns, which were found to be higher on

average in the VP cases. A t-test of the means of the measured porosities from the VP and HP columns indicated only a 19% chance they were identical. The grain perimeters were on average greater in the VP columns, but not greatly so. It was calculated that the average perimeters for the VP and HP columns had a ~33% chance of being identical (Appendix E). Nevertheless, the spatial distribution of grains and a more evenly distributed pore network in the VP columns allowed better grain to solution contact in those cases. The grain areas were expected to be higher in the more densely packed medium (HP) while lower areas (fewer grains per image) were expected for the less densely packed medium (VP), as estimated by image analysis. Further t-tests provided support that this expectation was realized; the grain areas showed only 15% chance they were identical (Appendix E).

An increased availability of iron for corrosion in the VP columns is likely to be responsible for some of the increased reactivity that was observed (factor of 2 to 4). This raises the possibility that the different packings led to different rates of oxide formation, due to an increase in grain-solution contact. This could have fostered increases in reactive surface area (at least initially) at a scale too small to assess by the image analysis. This idea is supported by reported increases in BET surface area of 300% for 8 mM $NaClO_4^-$contacted granular iron (Master Builder's iron) in batch tests (Allin, 2000). However, in order for the hypothesis to be plausible, the oxides formed would have had to include a high proportion of reactive phases, i.e., oxides of mixed valency in iron, or carbon sorption sites capable of participating in electron transfer to TCE – both possibilities that are supported by previous work (Odziemkowski *et al.*, 1998; Oh *et al.*, 2002; Ritter *et al.*, 2002). Microscopic analysis of the iron surface is required to address these possibilities for the current experimental conditions.

3.5. Implications for granular iron reactive barriers

This work helps to account for variability in the sorption and kinetic behavior of GI in column experiments. On the basis of this work, attention should be paid to grain packing in treatability tests in order to reduce variability between individual column tests, between laboratory and field tests, and improve confidence in PRB design calculations. The HP and RP packings were found to lead to quite similar GI reactivities (through the *k* term). This is a favorable outcome for lab testing repeatability since these packings require little effort to achieve. However, HP and RP packings may not be very representative of packings in PRBs where horizontally oriented grains are aligned parallel to flow. The VP columns, in which grains

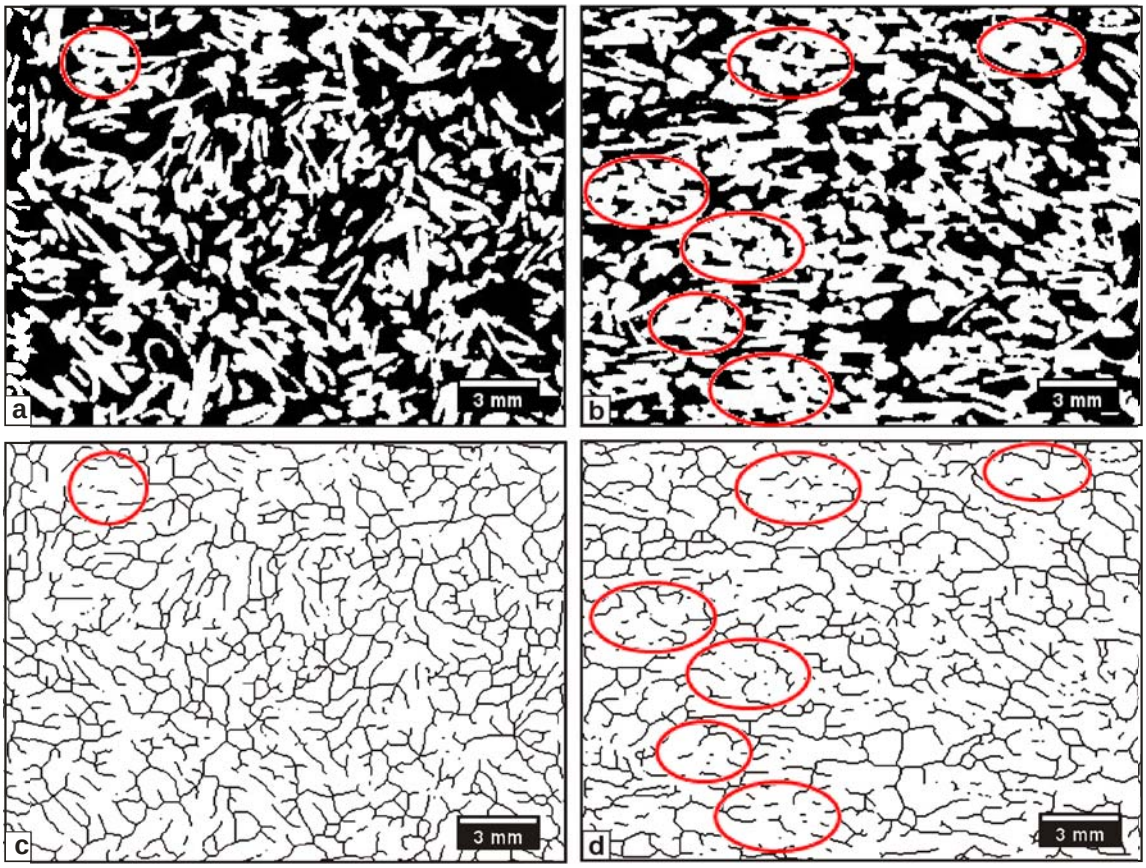

Figure 3.4: Threshold images (a) VP-1and (b) HP-1, skeletonize images (c) VP-1 and (d) HP-1 showing pore network. Red circles indicate selected areas of dense packing and reduced grain surface-solution contact.

were oriented parallel to flow, were found to be more reactive (based on reaction rates, *dC/dt*) than the HP and RP cases. Therefore, existing field installation practices for 100% iron PRBs may be inadvertently packing the iron to great advantage, though some additional optimization might be possible.

It is assumed that mass transfer does not initially limit reaction rates in the 100% iron media due to close proximity of grains in the columns (Bi *et al.*, 2009). However, if lower reactivity in the HP and RP columns occurs due to a decrease in the available iron surface, or immobile zones in the columns, (as shown to exist in the morphological study) this could create mass transfer limitations in a 100% HP or RP GI medium. This possibility was not discernible in the chloride tracer tests performed here, but remains a possibility for other iron media nonetheless. As suggested by others (Bi *et al.*, 2009) the addition of sand, or another inert granular material, could improve the solution-GI contact and increase transformation rates, at least in the short term, by physically separating the grains.

References

Agrawal, A., Tratnyek, P.G., 1996. Reduction of nitro aromatic compounds by zero-valent iron metal. Environmental Science and Technology, v. 30, no. 1, 153-160.

Allin, K.O., 2000. Effect of water geochemistry on the reactivity of granular iron. University of Waterloo, Waterloo, Ont.

Arnold, W.A., Roberts, A.L., 2000. Inter- and Intraspecies Competitive Effects in Reactions of Chlorinated Ethylenes with Zero-Valent Iron in Column Reactors. Environmental Engineering Science, v. 17, no. 5, 291-302.

Baciocchi, R., Boni, M.R., D'Aprile, L., 2003. Characterization and Performance of Granular Iron as Reactive Media for TCE degradation by Permeable Reactive Barriers. Water, Air, and Soil Pollution, v. 149, no. 1, 211-226.

Baldissera, M.R., Rios, P.R., Hein, L.R.O., Sandim, H.R.Z., 2011. Three-dimensional characterization of pores in Ti-6Al-4V alloy. Materials Research, v. 14, 102-106.

Bartzas, G., Komnitsas, K., 2010. Solid phase studies and geochemical modelling of low-cost permeable reactive barriers. Journal of Hazardous Materials, v. 183, no. 1–3, 301-308.

Bear, J., 1979. Hydraulics of Groundwater. McGraw- Hill International Book Co, New York.

Bi, E., Devlin, J.F., Huang, B., 2009. Effects of Mixing Granular Iron with Sand on the Kinetics of Trichloroethylene Reduction. Ground Water Monitoring and Remediation, v. 29, no. 2, 56-62.

Bi, E., Devlin, J.F., Huang, B., Firdous, R., 2010. Transport and Kinetic Studies To Characterize Reactive and Nonreactive Sites on Granular Iron. Environmental Science and Technology, v. 44, no. 14, 5564-5569.

Burris, D., Allen-King, R., Manoranjan, V., Campbell, T., Loraine, G., Deng, B., 1998. Chlorinated Ethene Reduction by Cast Iron: Sorption and Mass Transfer. Journal of Environmental Engineering, v. 124, no. 10, 1012-1019.

Burris, D.R., Campbell, T.J., Manoranjan, V.S., 1995. Sorption of Trichloroethylene and Tetrachloroethylene in a Batch Reactive Metallic Iron-Water System. Environmental Science and Technology, v. 29, no. 11, 2850-2855.

Coelho, D., Thovert, J.F., Adler, P.M., 1997. Geometrical and transport properties of random packings of spheres and aspherical particles. Physical Review E, v. 55, no. 2, 1959-1978.

Devlin, J.F., 1994. A Simple and Powerful Method of Parameter Estimation Using Simplex Optimization. Ground Water, v. 32, no. 2, 323-327.

Devlin, J.F., 2009. Development and Assessment of a Rate Equation for Chemical Transformations in Reactive Porous Media. Environmental Science & Technology, v. 43, no. 11, 4113-4118.

Devlin, J.F., Allin, K.O., 2005. Major Anion Effects on the Kinetics and Reactivity of Granular Iron in Glass-Encased Magnet Batch Reactor Experiments. Environmental Science & Technology, v. 39, no. 6, 7p.

Devlin, J.F., Klausen, J., Schwarzenbach, R.P., 1998. Kinetics of Nitroaromatic Reduction on Granular Iron in Recirculating Batch Experiments. Environmental Science and Technology, v. 32, no. 13, 1941-1947.

Dullien, F.A., 1991. Fluid transport and pore structure. Academic Press, San Diego, CA.

Farrell, J., Melitas, N., Kason, M., Li, T., 2000. Electrochemical and Column Investigation of Iron-Mediated Reductive Dechlorination of Trichloroethylene and Perchloroethylene. Environmental Science and Technology, v. 34, no. 12, 2549-2556.

Friedman, S.P., Robinson, D.A., 2002. Particle shape characterization using angle of repose measurements for predicting the effective permittivity and electrical conductivity of saturated granular media. Water Resour. Res., v. 38, no. 11, 1236.
Gavaskar, A.R., 1998. Permeable barriers for groundwater remediation : design, construction, and monitoring. Battelle Press, Columbus.
Gillham, R.W., 2003. Discussion of Papers/Discussion of Nano-Scale Iron for Dehalogenation. Ground Water Monitoring and Remediation, v. 23, no. 1, 6-8.
Gillham, R.W., O'Hannesin, S.F., 1994. Enhanced Degradation of Halogenated Aliphatics by Zero-Valent Iron. Ground Water, v. 32, no. 6, 958-967.
Gotpagar, J., Grulke, E., Tsang, T., Bhattacharyya, D., 1997. Reductive dehalogenation of trichloroethylene using zero-valent iron. Environmental Progress, v. 16, no. 2, 137-143.
Gu, B., Watson, D.B., Wu, L., Phillips, D.H., White, D.C., Zhou, J., 2002. Microbiological characteristics in a zero-valent iron reactive barrier. Environ Monit Assess, v. 77, no. 3, 293-309.
Higgins, M.R., Olson, T.M., 2009. Life-Cycle Case Study Comparison of Permeable Reactive Barrier versus Pump-and-Treat Remediation. Environmental Science and Technology, v. 43, no. 24, 9432-9438.
Huang, B., 2011. Separating the Kinetic and Sorption Parameters of Mixed Chlorinated Solvents in Contact with Granular Iron, Geology. University of Kansas, Lawrence, p. 163.
Jeen, S.W., Mayer, K.U., Gillham, R.W., Blowes, D.W., 2007. Reactive transport modeling of trichloroethene treatment with declining reactivity of iron. Environmental Science and Technology, v. 41, no. 4, 1432-1438.
Jin suk, O., Jeen, S.-W., Gillham, R.W., Gui, L., 2009. Effects of initial iron corrosion rate on long-term performance of iron permeable reactive barriers: Column experiments and numerical simulation. Journal of Contaminant Hydrology, v. 103, no. 3–4, 145-156.
Johnson, T.L., Scherer, M.M., Tratnyek, P.G., 1996. Kinetics of Halogenated Organic Compound Degradation by Iron Metal. Environmental Science and Technology, v. 30, no. 8, 2634-2640.
Lebron, I., Robinson, D.A., 2003. Particle Size Segregation during Hand Packing of Coarse Granular Materials and Impacts on Local Pore-Scale Structure. Vadose Zone Journal, v. 2, no. 3, 330-337.
Lee, J.-Y., Lee, K.-J., Youm, S., Lee, M.-R., Kamala-Kannan, S., Oh, B.-T., 2010. Stability of Multi-Permeable Reactive Barriers for Long Term Removal of Mixed Contaminants. Bulletin of Environment Contamination and Toxicology, v. 84, no. 2, 250-254.
Liang, L.Y., N. Korte, JD, Goodlaxson, J, Clausen al. , 1997. Byproduct formation during the reduction of TCE by zero-valence iron and palladized iron. Ground Water Monitoring and Remediation, v. 17, no. 1, 122-127.
Mackenzie, P.D., Horney, D.P., Sivavec, T.M., 1999. Mineral precipitation and porosity losses in granular iron columns. Journal of Hazardous Materials, v. 68, no. 1–2, 1-17.
Marietta, M.L., Devlin, J.F., 2005. In Bringing Groundwater Quality Research to the Watershed Scale 4th International Groundwater Quality Conference. IAHS, Waterloo, Canada, pp. 376-382.
Mayer, K.U., Blowes, D.W., Frind, E.O., 2001. Reactive transport modeling of an in situ reactive barrier for the treatment of hexavalent chromium and trichloroethylene in groundwater. Water Resour. Res., v. 37, no. 12, 3091-3103.

Moore, A.M., De Leon, C.H., Young, T.M., 2003. Rate and Extent of Aqueous Perchlorate Removal by Iron Surfaces. Environmental Science and Technology, v. 37, no. 14, 3189-3198.

Nield, D.A., Bejan, A. , 1992. Convection in porous media. Springer-Verlag, New York.

Nyborg, M.R., 1989. A Model for the Relationship between the Hydraulic Conductivity and Primary Sedimentary Structures of Till. Nordic Hydrology, v. 20, 137-152.

Odziemkowski, M.S., Schuhmacher, T.T., Gillham, R.W., Reardon, E.J., 1998. Mechanism of oxide film formation on iron in simulating groundwater solutions: Raman spectroscopic studies. Corrosion Science, v. 40, no. 2–3, 371-389.

Oh, S.-Y., Cha, D.K., Chiu, P.C., 2002. Graphite-Mediated Reduction of 2,4-Dinitrotoluene with Elemental Iron. Environmental Science & Technology, v. 36, no. 10, 2178-2184.

Phillips, D.H., Nooten, T.V., Bastiaens, L., Russell, M.I., Dickson, K., Plant, S., Ahad, J.M.E., Newton, T., Elliot, T., Kalin, R.M., 2010. Ten Year Performance Evaluation of a Field-Scale Zero-Valent Iron Permeable Reactive Barrier Installed to Remediate Trichloroethene Contaminated Groundwater. Environmental Science and Technology, v. 44, no. 10, 3861-3869.

Phillips, O.M., 1991. Flow and reactions in permeable rocks. Cambridge University Press, Cambridge.

Puls, R.W., Blowes, D.W., Gillham, R.W., 1999. Long-term performance monitoring for a permeable reactive barrier at the U.S. Coast Guard Support Center, Elizabeth City, North Carolina. Journal of Hazardous Materials, v. 68, no. 1-2, 109-124.

Rasband, W., 2007. ImageJ: National Institute of Health, 1.46b ed, Bethesda, MD, USA, p. http://rsb.info.nih.gov/ij/index.html.

Reardon, E.J., 1995. Anaerobic Corrosion of Granular Iron: Measurement and Interpretation of Hydrogen Evolution Rates. Environmental Science and Technology, v. 29, no. 12, 2936-2945.

Ritter, K., Odziemkowski, M.S., Gillham, R.W., 2002. An in situ study of the role of surface films on granular iron in the permeable iron wall technology. Journal of Contaminant Hydrology, v. 55, no. 1-2, 87-111.

Robertson, W.D., Vogan, J.L., Lombardo, P.S., 2008. Nitrate Removal Rates in a 15-Year-Old Permeable Reactive Barrier Treating Septic System Nitrate. Ground Water Monitoring and Remediation, v. 28, no. 3, 65-72.

Robinson, D.A., Friedman, S.P., 2001. Effect of particle size distribution on the effective dielectric permittivity of saturated granular media. Water Resour. Res., v. 37, no. 1, 33-40.

Roh, Y., Lee, S.Y., Elless, M.P., Cho, K.S., 2000. Electro-enhanced remediation of radionuclide-contaminated groundwater using zero-valent iron. Journal of Environmental Science and Health Part a-Toxic/Hazardous Substances & Environmental Engineering, v. 35, no. 7, 1043-1059.

Sasaki, K., Blowes, D.W., Ptacek, C.J., Gould, W.D., 2008. Immobilization of Se(VI) in mine drainage by permeable reactive barriers: column performance. Applied Geochemistry, v. 23, no. 5, 1012-1022.

Simon, F.-G., Segebade, C., Hedrich, M., 2003. Behaviour of uranium in iron-bearing permeable reactive barriers: investigation with 237U as a radioindicator. Science of the Total Environment, v. 307, no. 1–3, 231-238.

Sivavec, T.M., Horney, D.P., 1995. Reductive Dechlorination of Chlorinated Ethenes by Iron Metal. Abstracts of Papers of the American Chemical Society, v. 209, 128-ENVR.

Sperry, J.M., Peirce, J.J., 1995. A Model for Estimating the Hydraulic Conductivity of Granular Material Based on Grain Shape, Grain Size, and Porosity. Ground Water, v. 33, no. 6, 892-898.

Su, C.M., Puls, R.W., 1999. Kinetics of trichloroethene reduction by zerovalent iron and tin: Pretreatment effect, apparent activation energy, and intermediate products. Environmental Science and Technology, v. 33, no. 1, 163-168.

VanStone, N.A., Focht, R.M., Mabury, S.A., Lollar, B.S., 2004. Effect of Iron Type on Kinetics and Carbon Isotopic Enrichment of Chlorinated Ethylenes During Abiotic Reduction on Fe(0). Ground Water, v. 42, no. 2, 268-276.

Wang, C.-B., Zhang, W.-x., 1997. Synthesizing Nanoscale Iron Particles for Rapid and Complete Dechlorination of TCE and PCBs. Environmental Science and Technology, v. 31, no. 7, 2154-2156.

Wilkin, R.T., Acree, S.D., Ross, R.R., Beak, D.G., Lee, T.R., 2009. Performance of a zerovalent iron reactive barrier for the treatment of arsenic in groundwater: Part 1. Hydrogeochemical studies. Journal of Contaminant Hydrology, v. 106, no. 1–2, 1-14.

Willingham, T.W., Werth, C.J., Valocchi, A.J., 2008. Evaluation of the Effects of Porous Media Structure on Mixing-Controlled Reactions Using Pore-Scale Modeling and Micromodel Experiments. Environmental Science and Technology, v. 42, no. 9, 3185-3193.

Wu, Y., Slater, L.D., Korte, N., 2005. Effect of Precipitation on Low Frequency Electrical Properties of Zerovalent Iron Columns. Environmental Science and Technology, v. 39, no. 23, 9197-9204.

Wüst, W.F., Köber, R., Schlicker, O., Dahmke, A., 1999. Combined Zero- and First-Order Kinetic Model of the Degradation of TCE and cis-DCE with Commercial Iron. Environmental Science and Technology, v. 33, no. 23, 4304-4309.

Wyllie, M.R.J., Gregory, A.R., 1955. Fluid Flow through Unconsolidated Porous Aggregates. Industrial and Engineering Chemistry, v. 47, no. 7, 1379-1388.

Yabusaki, S., Cantrell, K., Sass, B., Steefel, C., 2001. Multicomponent Reactive Transport in an In Situ Zero-Valent Iron Cell. Environmental Science and Technology, v. 35, no. 7, 1493-1503.

Yang, Z., Xiaofeng, P., 2007. Micro-CT scanning analysis for inner structure of porous media. Heat Transfer—Asian Research, v. 36, no. 4, 208-214.

Zhao, C., Hobbs, B., Ord, A., Hornby, P., Peng, S., 2008. Effect of Reactive Surface Areas Associated with Different Particle Shapes on Chemical-Dissolution Front Instability in Fluid-Saturated Porous Rocks. Transport in Porous Media, v. 73, no. 1, 75-94.

4. BEARKIMPE: A VBA Excel Program for Characterizing Granular Iron in Treatability Studies

4.1. Abstract

The selection of a suitable kinetic model to investigate the reaction rate of a contaminant with Granular Iron (GI) can be essential to optimize the Permeable Reactive Barrier (PBR) performance in term of its reactivity. The newly developed Kinetic Iron Model (KIM) uniquely determines: rate constant (k) and sorption parameters (C_{max} & J) which was not possible with earlier models. The code presented in this work was written in a Visual Basic Application (VBA) for Microsoft Excel is adopted from BEARPE and KIMPE codes written in FORTRAN. The program is organized in several user interface screens (UserForms) that guide the user step by step through the analyses. BEARKIMPE uses non-linear optimization algorithm based on simplex optimization to calculate transport and chemical kinetic parameters.

4.2. Introduction

The disappearance rates of groundwater contaminants in the presence of zero-valent iron (Fe^0) are important to understand for the purposes of groundwater remediation (Bi *et al.*, 2010; Gillham and O'Hannesin, 1994; Puls *et al.*, 1999), -in particular where Permeable Reactive Barrier (PRB) designs are concerned. Over the last two decades this technology has proven to be effective for removing various pollutants, most notably trichloroethene (TCE) from groundwater (Agrawal and Tratnyek, 1996; O'Hannesin and Gillham, 1998; Puls *et al.*, 1999). The choice of an appropriate kinetic model to investigate the reaction rate of a contaminant with GI can be essential to optimize the barrier performance in term of its reactivity (Henderson and Demond, 2007; Roh *et al.*, 2000a, b)

Much of the existing literature on GI kinetics suggest that reactions with organic groundwater pollutants is first order (Gillham and O'Hannesin, 1994; Johnson *et al.*, 1996), or

second order if the iron is (more correctly) treated as a reactant (Devlin *et al.*, 1998; Johnson *et al.*, 1996). Recent studies have shown that the reaction processes between GI and contaminants depend on both electron transfer (k) and sorption that occurs to the surface of iron (Arnold and Roberts, 2000; Bi *et al.*, 2010; Devlin, 2009). For example, the Langmuir-Hinshelwood model (L-H) accounts for surface saturation and reactivity and have employed sorption capacity of solid surface (C_{max}), sorption affinity (J) and rate constant (k) (Arnold and Roberts, 2000). Unfortunately, the rate constant (k) and maximum sorption capacity (C_{max}) only occur as a product kC_{max} in the model equation, making it impossible to estimate the individual values uniquely (Arnold and Roberts, 2000; Bi *et al.*, 2010; Gillham and O'Hannesin, 1994).

The newly developed Kinetic Iron Model (KIM) is a more general version of the L-H model and is capable of separating these processes and uniquely determine: rate constant (k) and sorption parameters (C_{max} & J) (Devlin, 2009). In order to make these estimations, a suite of column tests, performed with various influent concentrations of the contaminant of interest – TCE is used here as an example – are conducted. Details on the methodology of column experiment can be found elsewhere, together with an assessment of the approach compared to other methods (Bi *et al.*, 2010). Upon completion of each test, the column effluent samples are analyzed for TCE and breakthrough curves (BTCs) are generated. The BTCs are then fitted with a solution of the advection-dispersion equation (with reaction and sorption terms) to obtain an estimate of the pseudo-first order rate constant, k_{app}. These values were then used in a 2 step linearization approximation of the L-H and KIM equations to obtain preliminary estimates of k, C_{max} and J parameters (Marietta and Devlin, 2005) followed by non-linear optimization to improve on the preliminary estimates (Figure 4.1). Each of the steps has until now been facilitated with command line driven codes prepared in FORTRAN, which required considerable

file management in the Windows environment, and manipulations including imports to spreadsheets or plotting software.

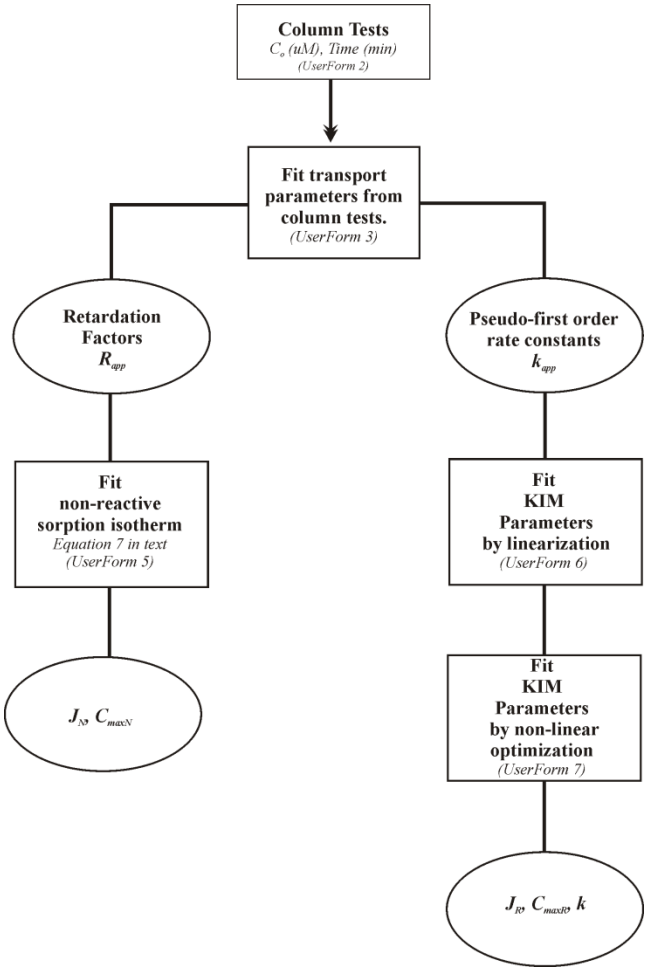

Figure 4.1: Flow chart illustrating the data analysis steps to assess reactions with GI.

The FORTRAN codes included BEARPE, to fit the advection-dispersion equation, KIM2PE, to perform L-H and KIM linearizations, and KIMPE, to perform the non-linear optimizations. The procedure involving these codes was satisfactory for single-pass analyses of the data, but was found to be inefficient if multiple passes were required. Multiple passes were frequently desirable to correct irregularities in fitted lines in one or more steps. To improve the

ease of movement through the process, and reduce file manipulations at the operating system level, the codes were adapted to VBA within the Excel environment.

The purpose of the present work was to convert the BEARPE, KIM2PE, and KIMPE simplex optimization codes into a visual basic procedure in the Excel environment, and to adapt the codes to interact seamlessly. BEARKIMPE, name of a new code, uses graphical user interface and straightforward Userforms for its functions. The program is also customized to make graphic representation of observed and calculated data, which was not possible in the earlier work (Appendix F).

4.3. Breakthrough curves analysis and kinetics analysis

BEARKIMPE calculates transport and chemical kinetic parameters for the column tests by fitting the experimental data with eqs 4.1 and 4.2, by minimizing the residual sum of square (RSS) objective function (eq 4.3).

$$C(x,t) = \frac{C_o}{2}\left\{\exp\left[\frac{vx}{2D}\left(1-\sqrt{1+\frac{4k_{app}D}{v^2}}\right)\right] erfc\left[\frac{R_{app}x - vt\sqrt{1+\frac{\sqrt{4k_{app}D}}{v^2}}}{2\sqrt{DR_{app}t}}\right]\right\} \tag{4.1}$$

$$\frac{dC}{dt} = k_{app}C_o = \frac{kC_{max}Fe/V}{1/J + \frac{C_{max\,R}\,Fe/V}{1+J_R C_o} + C_o}C_o \tag{4.2}$$

$$RSS = \sum_{i=1}^{n}[y_i - f(x_i)]^2 \tag{4.3}$$

Where y_i is the ith observed concentration and $f(x_i)$ is the calculated concentration from a solution to advection-dispersion Equation (eq 4.1) (Bear, 1979) or the KIM (eq 4.2). Where C_o is the influent TCE concentration (μM), D is dispersion coefficient (m^2s^{-1}), $D=\alpha v+D^*$, α is dispersivity (m), v is water velocity ($m\ s^{-1}$) and D^* is effective diffusion coefficient ($m^2\ s^{-1}$) that was assumed negligible in these experiments compared to αv, x is column length (cm), dC/dt is the observed rate and $f(x_i)$ is the calculated rate, k_{app} is the apparent or observed pseudo-first order rate constant (min^{-1}), k is the first order rate constant for the surface reaction (min^{-1}), C_{maxR} is the maximum sorption capacity ($\mu molg^{-1}$), J_R is the sorption affinity to reactive sites on the surface (μM^{-1}), Fe/V is the iron mass to column pore water volume ratio ($g\ L^{-1}$) and C_o is the aqueous influent concentration of TCE (μM).

The non-linear optimization algorithm is based on simplex optimization (Devlin, 1994; Jurs, 1984). Briefly, a simplex or geometrical shape is created in space with N+1(where N is the total number of parameters to be estimated) vertices on a response surface, which consists of the RSS for all possible sets of parameter values. Initial guesses of parameters serve as the vertices of the initial simplex. Upon initialization, the simplex moves by stretching, contracting and flipping on the response surface. The response surface is searched until convergence is achieved at the lowest RSS location, which corresponds to the optimal parameter estimates.

4.4. Setup for optimizer

The BEARKIMPE code is written in VBA and requires Microsoft Excel version of 2007 or later. Installation is performed by simply saving the "BEARKIMPE" Excel file to hard disk. This program contains macros, therefore security settings within Excel should be adjusted accordingly (with macros enabled). The only input file required by the program is a spreadsheet

listing the effluent TCE concentrations and their corresponding times for each of the tests (varying C_o) in a suite. A sample input file is provided with the program file.

Upon initializing the BEARKIMPE program the "*Welcome to BEARKIMPE*" UserForm will appear on screen and prompt the user to select either "Import external data" or "Cancel" command button as seen in Figure 4.2.

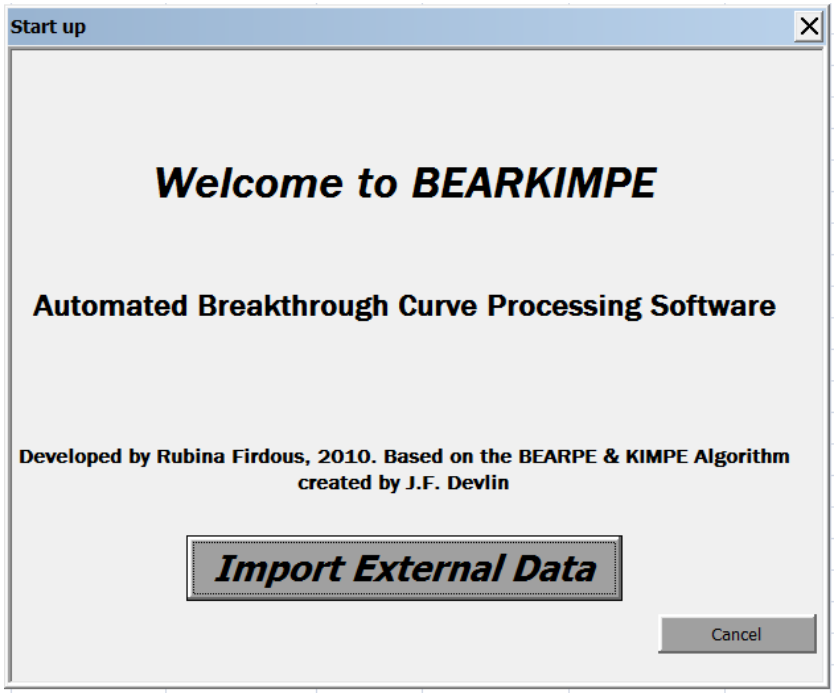

Figure 4.2: Screen capture of UserForm 1 "*We1come to BEARKIMPE*" screen.

Selecting "Cancel" button disables the code and the spreadsheet can subsequently only be used for simple excel work. Clicking "Import External Data" allows the user to select the target input file from a file directory. Once the user selects the input file, a message box appears requesting verification that correct file was selected. Selecting "No" in the message box returns the user to the file directory to reselect the input file. Choosing "Yes" causes the VBA code to continue executing. The data are imported and stored in a spreadsheet named "BearPE2".

Upon successfully importing the data, UserForm 2 appears (Figure 4.3). The code associated with this form creates up to 6 spreadsheets for column test data from a suite with editable C_o values to be filled in for purpose of naming worksheets. The input data from the BearPe sheet are parsed by test (i.e., C_o) and copied to the new spreadsheets. Graphical representations of BTCs for the observed data are also created during this step.

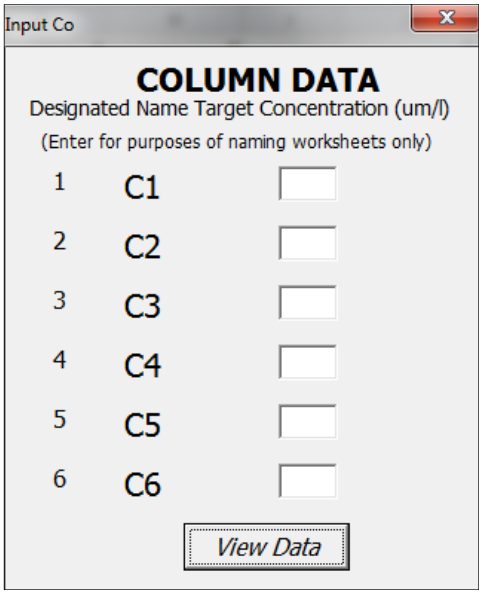

Figure 4.3: Screen capture of UserForm 2 "Input Co" showing designated names and target concentrations. By default target concentrations are suggested for the naming of 6 new spreadsheets added to the workbook when "View Data" command button is selected

4.5. Fitting the Observed data with the Simplex Optimizer

With the individual tests spreadsheets created, UserForm 3, "BEARPE First Approximation Screen" (Figure 4.4), appears. This form prompts for input from the user on which to base the fitting of eq 4.1 to the column BTC data for each test. This form leads to first approximations of the eq. 4.1 parameters, which can be evaluated by the user and improved further along in the process.

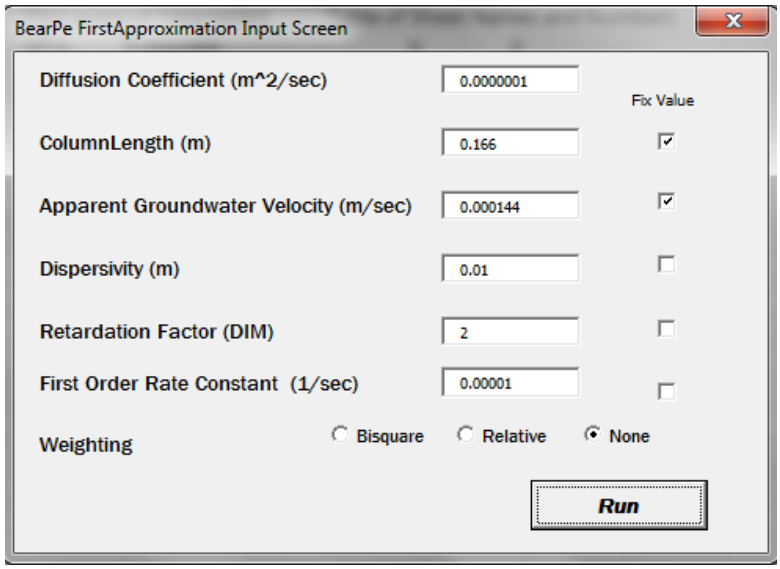

Figure 4.4: Screen capture of First approximation input screen. By default column length and velocity are fixed.

Any of the parameters can be held constant in the optimization process by simply clicking the "Fix" check box on the parameter line. Column velocity and column length are expected to be fixed in the experimental design, therefore both are fixed by default in this UserForm 3 (Figure 4.4). Column experiments are generally conducted at flow rates that swamp diffusion. For this reason there is no option to optimize on the diffusion coefficient.

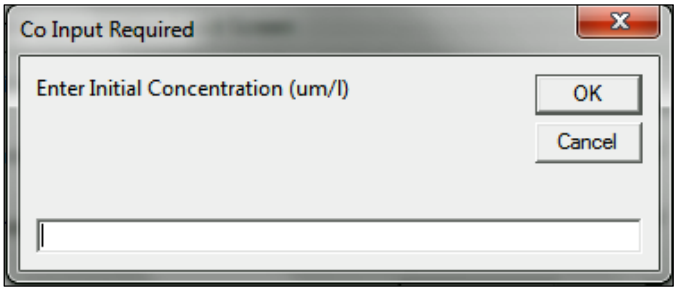

Figure 4.5: Screen capture of message box for Initial Concentration Co Input.

The user can choose between 3 weighting options: "Relative", Bisquare", and "None". By default "None" is selected which simply fits the effluent column data weighting each point equally, as indicated in eq 4.3. "Relative" weighting modifies eq 4.3 by weighting the residual sums by the magnitude of the concentration, C_i (eq 4.4).

$$RSS_{Relative} = \sum_{i=1}^{n} \left[\frac{[y_i - f(x_i)]}{C_i} \right]^2 \tag{4.4}$$

The effect of this change is that each point is given relatively equal weighting in the optimization process. In practice, the fitting procedure de-emphasizes the highest concentration points compared to the "None" option.

The third weighting option is called "Bisquare" weighting, and this has the effect of de-emphasizing points that depart from the fitted line, i.e., potential outliers – the greater the disagreement, the less the weighting in the final fit. The RSS function in this case is modified as follows (Robinson, 1985):

$$Wt_i = \left[1 - \left[\frac{n[y_i - f(x_i)]}{6(RSS)} \right]^2 \right]^2 for \left[\frac{n[y_i - f(x_i)]}{6(RSS)} \right] \leq 1, otherwise\ Wt_i = 0 \tag{4.5}$$

$$RSS_{Bisquare} = \sum_{i=1}^{n} Wt_i [y_i - f(x_i)]^2 \tag{4.6}$$

Upon selecting the "Run" command, the initial guesses entered into the form are applied to all BTCs. As each BTC is considered, the user is prompted for the experimental C_o (as opposed to the approximate value used to name the sheet (Figure 4.5). Once the experimental C_o is entered and the "Ok" command button selected, the simplex optimizer runs and the transport/reaction parameters estimated (Figure 4.6).The procedure moves sequentially through the spreadsheets until all the BTCs are fitted with the simplex optimizer.

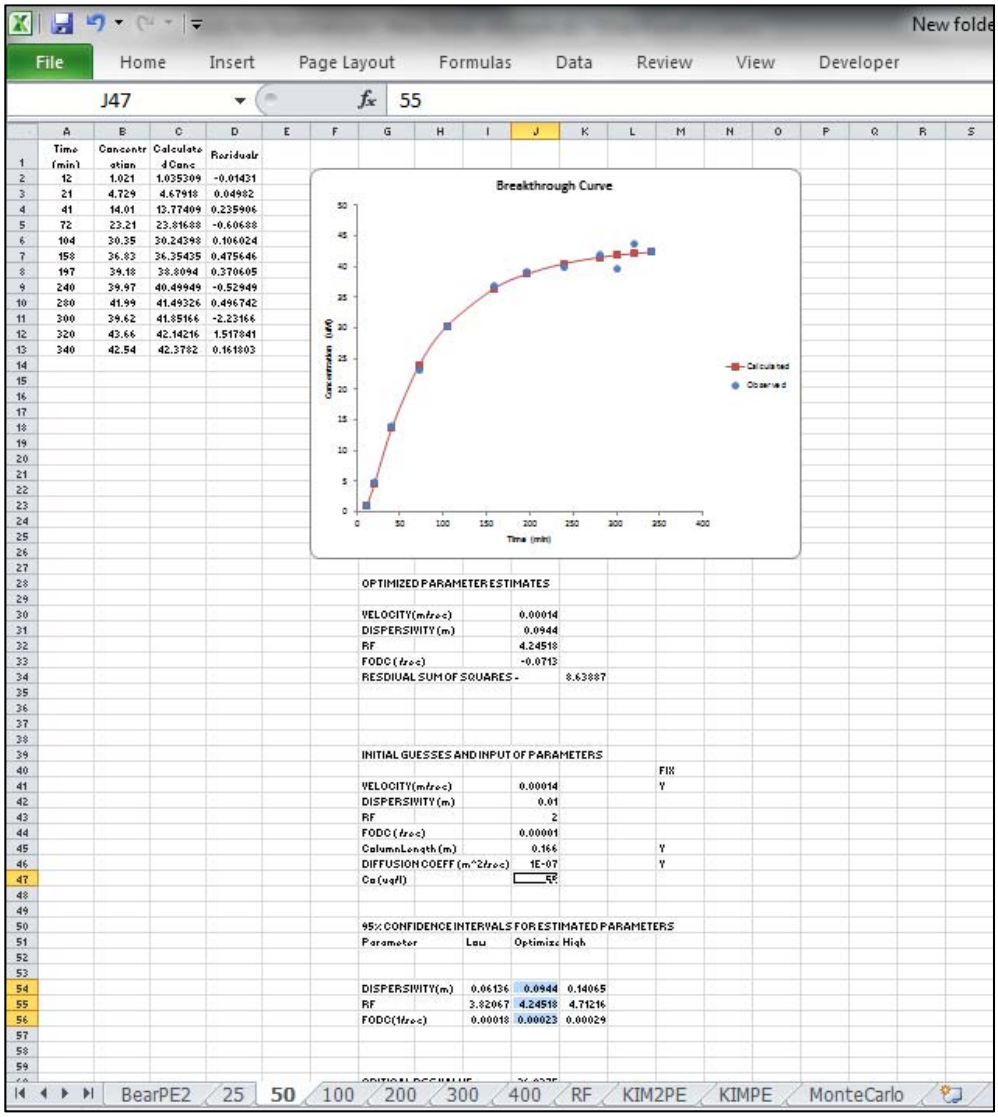

Figure 4.6: Output of BEARPE approximation UserForm 3 showing optimized transport parameters and RSS values.

Usually, the calculated BTC displays a good match with the observed one, but sometimes the initial guesses are poor and the optimizer converges on a local RSS minimum on the response surface, rather than the global minimum that is sought. In this case manual adjustment of parameter estimates is needed, and is done from UserForm 4 (Figure 4.7). The UserForm

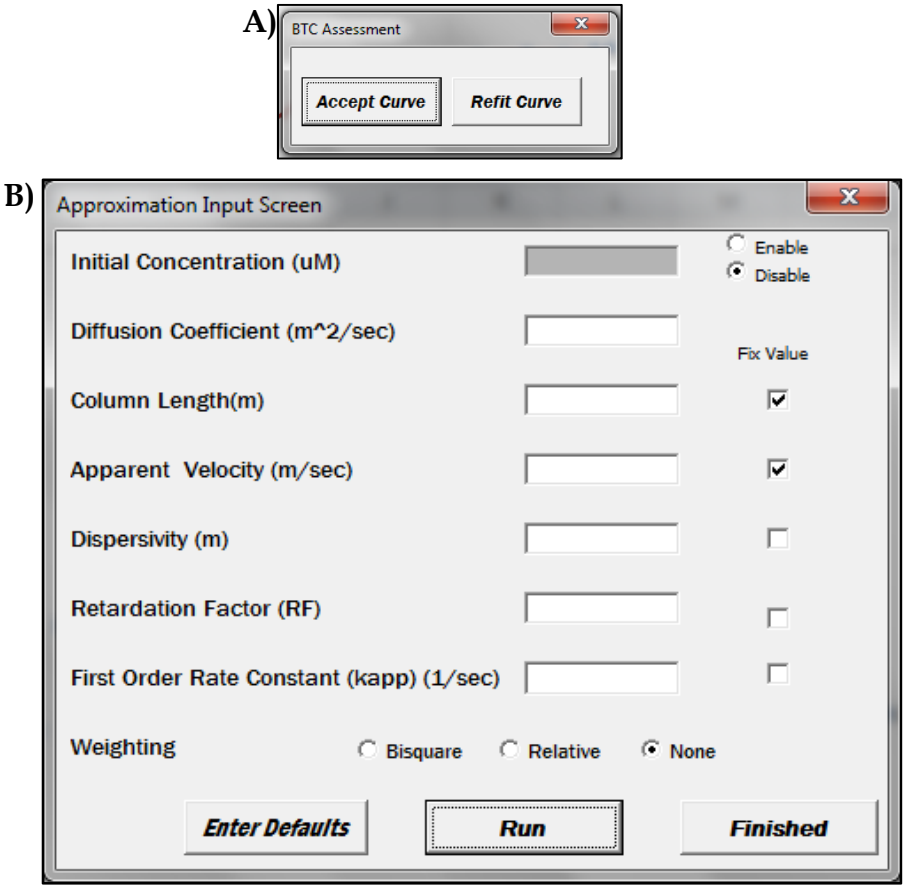

Figure 4.7: Screen Capture of (A) Message for BTC assessment and (B) UserForm 4 for second optimization

,"BTC Assessment" allow user to refit or accept the breakthrough curve. If "refit curve" is selected the UserForm 4 "Approximation Input Screen", utilizes the same simplex optimization code called from UserForm 3 will appear on screen. This form allows the user to re-enter the initial parameter guesses and rerun the optimization routine. The initial parameters can be called by "Enter Defaults" command button or by manual input. In addition, it has an entry option for the "Initial Concentration (μmL^{-1})" which can be either "enabled" or "disabled" by checking an option button. This allows users to revise the experimental C_o (Figure 4.7B). Once the curve fitted, the UserForm 4 appears on screen for next C_o and procedure moves sequentially through the spreadsheets until all the BTCs are refitted with the simplex optimizer. User can skip these

steps if first approximation (UserForm 3) fits data well by selecting "accept curve" command button (Figure 4.7A).

4.6. Collecting the data for analyzing retardation and non-reactive sorption

Non-reactive sorption is analyzed using the transient portion of the breakthrough curve. The apparent rate constant (k_{app}) and retardation factor (R_{app}) are fitted from BTC using eq 4.1. Non-reactive sorption is further characterized by examining the dependency of R_{app} on C_o, assuming a Langmuir isotherm describes the sorption.

$$R_{app} = 1 + \frac{Fe}{V}\frac{J_N C_{maxN}}{(1 + J_N C_o)^2} \tag{4.7}$$

Where C_{maxN} is maximum sorption capacity (μMg^{-1}) and J_N is sorption affinity, (μML^{-1}), to non-reactive site (Bi *et al.*, 2010).

The value of the parameter *Fe/V*, the iron mass to column pore water volume ratio (g L^{-1}), is required for calculating both non-reactive (eq 4.7) and reactive sorption (eq 4.2). UserForm 5 is designed to prompt for *Fe/V* and then read the fitted R_{app} and k_{app} estimates from the various C_o spreadsheets and incorporate them into a new sheet called "RF". Also on the same sheet, a button "*non-reactive sorption*" is displayed and linked to the Solver option in Excel. Solver is another nonlinear optimizer that minimizes the RSS objective function by fitting C_{maxN} and J_N.

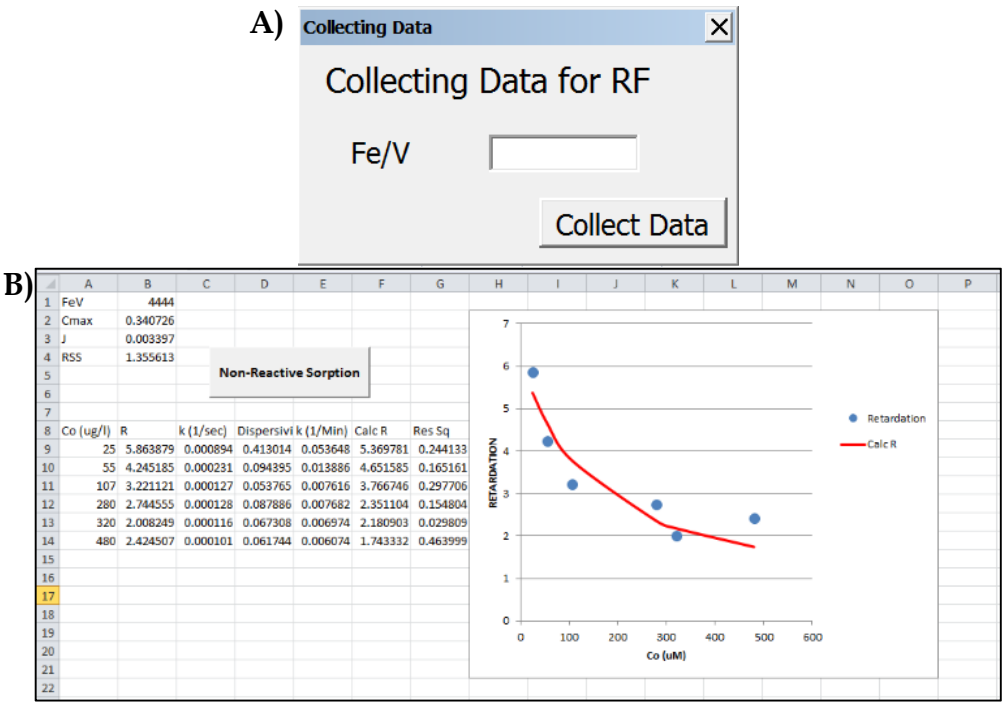

Figure 4.8: Screen captures of A) UserForm 5 and B) output file for non-reactive sorption.

4.7. Running 2 Step linearization for kinetic and sorption parameters

Once the non-reactive sorption calculations are complete, the program proceeds to UserForm 6, coded with a 2-step linearization approximation (Marietta and Devlin, 2005) (Figure 4.9). This method provides the preliminary estimate of the reactive sorption parameters (C_{maxR}, J_R), and rate surface constant (k). These estimates are then used as initial guesses for nonlinear regression in the KIM. In the first step, the L-H model is used to obtain estimates of the parameter J, and the parameter product kC_{max} (Marietta and Devlin, 2005). Briefly, the observed dataset from all BTCs is placed into the matrix form, from which the parameter estimates of $1/J$ and kC_{max} is calculated (Devlin and Allin, 2005). In the second step, the estimated J parameter from L-H model is used in a linearized form of the KIM (eq 4.5) to obtain the best fit estimates of k and C_{maxR} (Marietta and Devlin, 2005). In equation 4.5, each row represents the linearized form of eq 4.2 for each C_o experiment.

$$\begin{bmatrix} \left(\frac{C_o+\frac{1}{J_R}}{\frac{Fe}{V}}\right)_1 & \left(\frac{1}{k_{app}}\right)_1 \\ \left(\frac{C_o+\frac{1}{J_R}}{\frac{Fe}{V}}\right)_2 & \left(\frac{1}{k_{app}}\right)_2 \\ \dots & \dots \\ \left(\frac{C_o+\frac{1}{J_R}}{\frac{Fe}{V}}\right)_n & \left(\frac{1}{k_{app}}\right)_n \end{bmatrix} \begin{bmatrix} 1/C_{maxR} \\ k \end{bmatrix} = \begin{bmatrix} \left(\frac{1}{1+J_R C_o}\right)_1 \\ \left(\frac{1}{1+J_R C_o}\right)_2 \\ \dots \\ \left(\frac{1}{1+J_R C_o}\right)_n \end{bmatrix} \tag{4.8}$$

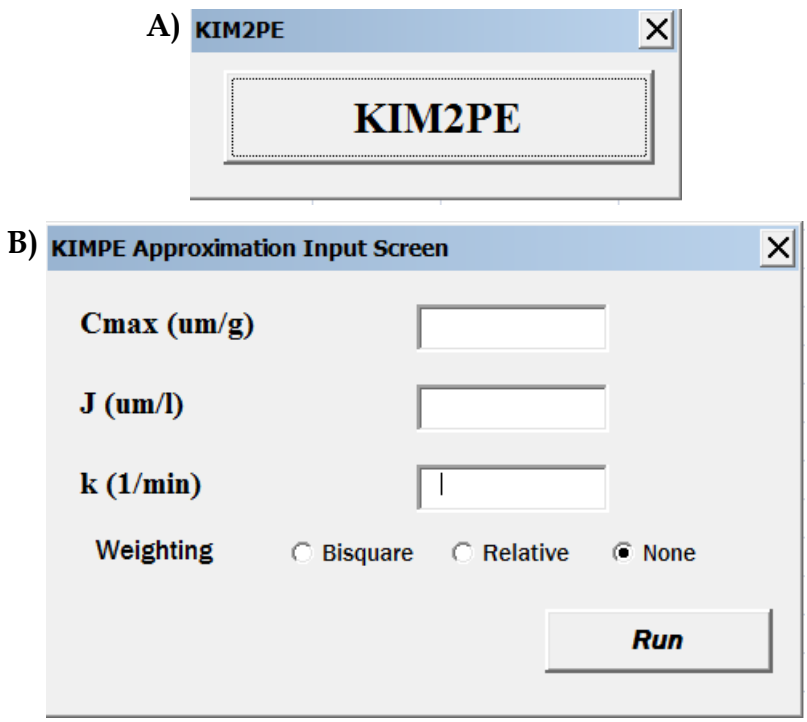

Figure 4.9: Screen captures of (A) UserForm 6, KIM2PE and (B) UserForm 7, KIMPE Approximation Input for KIM parameters.

Once these estimated parameters values are calculated, they serve as initial guesses for the "KIMPE Optimization Input screen", UserForm 7. Selecting "Run" command button will initiate the optimizer and run until convergence is successfully met.

4.8. Data for the Monte Carlo analysis

To quantify the uncertainty attached to the fitted C_{maxR}, k, and J_R estimates, a Monte Carlo analysis can be performed to generate probability distributions of each parameter. The Monte Carlo procedure was described by Devlin (2009), and was not duplicated here.

4.9. Summary and conclusion

The KIM was used in this study to obtain unique estimates of reaction and sorption parameters for the organic reactions with granular iron, which was not possible with earlier kinetic models. The procedure was initially developed using codes developed in FORTRAN, which was time intensive. This prompted the development of a user friendly program executable in a commonly available spreadsheet environment. The BEARKIMPE spreadsheet contains code written in Visual Basic for Excel, adapted from the FORTRAN programs BearPE2 and KIMPE. It requires only a single input file to perform a complete analysis of a suite of column tests to determine reactive and non-reactive sorption parameters and a first-order rate constant for the surface reaction. The program is structured in several user interface screens (UserForms) that guide the user step by step through the analyses. BTCs are fitted with simplex optimizer on transport parameters. BEAKIMPE also utilizes "Solver", which is also a nonlinear optimizer that minimizes the RSS objective function, is operated to optimize non-reactive sorption and retardation. Further, the program is coded with a 2 step linearization method that gives approximate estimates of k, C_{max} and J. Once these estimated parameters are processed with a nonlinear optimizer to improve them, they are saved in a new file suitable for export to a separate spreadsheet capable of running Monte Carlo analyses to quantify parameter uncertainty. On completion, user can save the project file on a system for documentation purposes.

References

Agrawal, A., Tratnyek, P.G., 1996. Reduction of nitro aromatic compounds by zero-valent iron metal. Environmental Science and Technology, v. 30, no. 1, 153-160.

Arnold, W.A., Roberts, A.L., 2000. Inter- and Intraspecies Competitive Effects in Reactions of Chlorinated Ethylenes with Zero-Valent Iron in Column Reactors. Environmental Engineering Science, v. 17, no. 5, 291-302.

Bear, J., 1979. Hydraulics of Groundwater. McGraw- Hill International Book Co, New York.

Bi, E., Devlin, J.F., Huang, B., Firdous, R., 2010. Transport and Kinetic Studies To Characterize Reactive and Nonreactive Sites on Granular Iron. Environmental Science and Technology, v. 44, no. 14, 5564-5569.

Devlin, J.F., 1994. A Simple and Powerful Method of Parameter Estimation Using Simplex Optimization. Ground Water, v. 32, no. 2, 323-327.

Devlin, J.F., 2009. Development and Assessment of a Rate Equation for Chemical Transformations in Reactive Porous Media. Environmental Science and Technology, v. 43, no. 11, 4113-4118.

Devlin, J.F., Allin, K.O., 2005. Major Anion Effects on the Kinetics and Reactivity of Granular Iron in Glass-Encased Magnet Batch Reactor Experiments. Environmental Science and Technology, v. 39, no. 6, 1868-1874.

Devlin, J.F., Klausen, J., Schwarzenbach, R.P., 1998. Kinetics of Nitroaromatic Reduction on Granular Iron in Recirculating Batch Experiments. Environmental Science and Technology, v. 32, no. 13, 1941-1947.

Gillham, R.W., O'Hannesin, S.F., 1994. Enhanced Degradation of Halogenated Aliphatics by Zero-Valent Iron. Ground Water, v. 32, no. 6, 958-967.

Henderson, A.D., Demond, A.H., 2007. Long-term performance of zero-valent iron permeable reactive barriers: A critical review. Environmental Engineering Science, v. 24, no. 4, 401-423.

Johnson, T.L., Scherer, M.M., Tratnyek, P.G., 1996. Kinetics of Halogenated Organic Compound Degradation by Iron Metal. Environmental Science and Technology, v. 30, no. 8, 2634-2640.

Jurs, P.C., 1984. Computer software application in chemistry. John Wiley and Sons, Toronto, 125-140 pp.

Marietta, M.L., Devlin, J.F., 2005. In Bringing Groundwater Quality Research to the Watershed Scale 4th International Groundwater Quality Conference. IAHS, Waterloo, Canada, pp. 376-382.

O'Hannesin, S.F., Gillham, R.W., 1998. Long-Term Performance of an In Situ “Iron Wall” for Remediation of VOCs. Ground Water, v. 36, no. 1, 164-170.

Puls, R.W., Blowes, D.W., Gillham, R.W., 1999. Long-term performance monitoring for a permeable reactive barrier at the U.S. Coast Guard Support Center, Elizabeth City, North Carolina. Journal of Hazardous Materials, v. 68, no. 1-2, 109-124.

Robinson, J.A., 1985. Determining microbial kinetic parameters using nonlinear regression analysis. In: Advances in Microbial Ecology. K.C. Marshal, ed. Plenum Press, New York, 61-114pp.

Roh, Y., Lee, S.Y., Elless, M.P., Cho, K.S., 2000a. Electro-enhanced remediation of radionuclide-contaminated groundwater using zero-valent iron. Journal of Environmental Science and Health Part a-Toxic/Hazardous Substances & Environmental Engineering, v. 35, no. 7, 1043-1059.

Roh, Y., Lee, S.Y., Elless, M.P., Cho, K.S., 2000b. Electro-enhanced remediation of radionuclide-contaminated groundwater using zero-valent iron (vol A35, pg 1043, 2000). Journal of Environmental Science and Health Part a-Toxic/Hazardous Substances & Environmental Engineering, v. 35, no. 10, 1995-+.

5. Accessing the importance of carbon in the granular iron during the reductive dechlorination process.

5.1. Abstract

Granular iron (GI) is commonly used reactive material in the permeable reactive barriers (PRBs) to treat wide variety of groundwater contaminants. Commercially available GI which replaced electrolytic iron has been investigated in laboratory. A notable difference between commercial GI and EI is presence of carbon and other impurities on the surface. Column experiments were conducted to compare 2 types of GI, Connelly and Electrolytic Iron (EI), to document the effects on sorption and kinetic parameters as iron aged in TCE solution. It was observed that retardation factor (R_{app}) for GI followed non-linear relation and dropped significantly as iron age in TCE solution. Whereas R_{app} values for EI were substantially lower than GI and varied minimally through the injected TCE concentrations and with aging. Kinetic data suggested a shift in rate constant (k) and sorption parameters for both iron types. This work demonstrates the implication of carbon during the retardation of TCE i.e high R_{app} for GI (~3% carbon) and low for EI (≤ 0.01%). Furthermore, hydrocarbon tests performed on GI suggested the background carbon as a possible source of hydrocarbon formation in Fe/H_2O system.

5.2. Introduction

Commercially available Granular iron (GI) is the leading reactive material used in the permeable reactive barriers (PRBs) (Farrell *et al.*, 2000; Gillham *et al.*, 2010; Higgins and Olson, 2009) and able to treat wide variety of groundwater contaminants (Blowes *et al.*, 2000; Mackenzie *et al.*, 1999; O'Hannesin and Gillham, 1998; Sasaki *et al.*, 2008). Differences in the manufacturing processes of GI lead to differences in grain morphology as well as chemical and physical properties of iron surface. The chemical nature of GI from various manufacturers has

been intensively investigated in laboratory tests (Burris *et al.*, 1998; Su and Puls, 1999; VanStone *et al.*, 2004), which have sometimes - substituted electrolytic iron (EI) for commercial GI, for the purposes of limiting the investigation to a relatively simple metallic surface, which is inferred to provide the active sites where reactions take place (Baciocchi *et al.*, 2003). A notable difference between commercial GI and EI is presence of carbon and other impurities on the surface. The importance of this difference was first raised by Burris *et al.* (1998) who examined cast iron as a surrogate for GI. They found that carbon was important to the sorption of hydrophobic chemicals to the iron surface at sites where no reductions took place – so-called non-reactive sites. Later studies have attempted to quantify the sorption to sites where reductions could take place (Bi *et al.*, 2010; Deng *et al.*, 2003; Dries *et al.*, 2005), but these did not localize the sorption to sites of a particular composition or type (Deng *et al.*, 2003).

It is well established that the condition of the GI surface has a significant effect on reaction rates (Dries *et al.*, 2005; Phillips *et al.*, 2010). The presence of a variety of oxides (Burris *et al.*, 1998) as well as physical features, like edges and corners (Stumm, 1992), offer many possibilities for sorption or reaction sites. Despite detailed investigations of the surface phases present on GI, the roles of these various surface phases and features in aqueous solute reductions remains uncertain. A possible site for reaction on the GI surface is carbon originating from the steel or during the manufacturing process (Oh *et al.*, 2002). Carbon is also known for its strong propensity to act as a sorbent of hydrophobic substances (Cornelissen *et al.*, 2005). For example, activated carbon is used for the removal of organic and inorganic contaminants from water (Oliveira *et al.*, 2002). Commercially available GI, used in PRBs, is typically a cast iron or light steel that contains 2.85 – 3.23% by weight carbon (Appendix G). The carbon on cast iron comes, at least in part, from decomposition of carbide/cementite ($Fe_3C = 3Fe + C$) which

promotes graphitization (Chawla and Gupta, 1993). Different morphologies of graphite for example flaky or nodular and rounded, have been described and may depend on kiln temperature and rate of cooling (Chawla and Gupta, 1993).

Early investigations identified the role of surface carbon as a non-reactive sorption site (Burris *et al.*, 1998). Later work suggested that carbon can also serve as a reactive sorption site for contaminants (Oh *et al.*, 2002). In another study, granular activated carbon was mixed with nano-scale zero-valent iron and assessed as a conductor for the shuttling of electrons to improve the reactivity of corroded iron (Tang *et al.*, 2011).

Efforts to examine the role of carbon have been complicated by the formation of hydrocarbons in metallic iron/water system (Fe/H_2O) - both in the presence and absence of chlorinated solvents (Burris *et al.*, 1997; Deng *et al.*, 1997; Hardy and Gillham, 1996) . Primary reductive pathways for chlorinated ethylenes is believed to be through β –elimination and or hydrogenolysis which could lead to the formation of C_2 hydrocarbons (acetylene, ethane, and ethane) (Arnold *et al.*, 1999; Roberts *et al.*, 1996). Aqueous CO_2 and chloroethylene have also been shown as possible source for C1 –C5 hydrocarbon (Hardy and Gillham, 1996; Yabusaki *et al.*, 2001).

The objective of this work was to evaluate the importance of surface carbon on the reactivity of GI towards trichloroethylene (TCE). Two iron types were compared in column tests to make this assessment: Connelly Iron GI, a commercial brand with ~3% carbon by weight, and Sigma Aldrich EI which is 99.99% Fe. Quantification of reactive sorption was accomplished using the kinetic iron model (KIM) (Devlin, 2009; Bi *et al.,* 2010) and the effects of surface carbon evaluated by contrasting TCE reduction kinetics in the presence of the two iron types.

5.3. *Materials and Methods*

5.3.1. Materials

All chemicals were used as received. Connelly® Iron was provided by GMP Inc. The iron grains were platy in appearance and hand sieved to isolate sizes ranging from 0.71 to 2.0 mm in diameter. Electrolytic iron (EI) (>99.99%), was purchased from Sigma Aldrich, was granular in appearance with grain diameters between 0.42 and 2.0 mm. Trichloroethylene (TCE, 99%) was obtained from Acros Organics, methanol, pentane (HPLC grade) from Fisher Scientific, and CO_2, O_2, He gases (99+%) were purchased from Air gas, Topeka.

$NaClO_4$ feed solution (8 mM) was prepared with deionized water (Barnstead International Nano Pure Infinity Ultra-pure Water System Series 896). $NaClO_4$ was selected as the background electrolyte because is known to be minimally active on the granular iron surface (Devlin and Allin, 2005; Huang, 2011; Moore *et al.*, 2003). The solution was adjusted to pH 10 with the drop wise addition of either 1.1 mM perchloric acid or 0.35 mM sodium hydroxide solution. The choice of pH 10 was made for consistency with prior work and to represent conditions within the center of a PRB (Devlin and Allin, 2005; Gavaskar, 1998). The $NaClO_4$ electrolyte solution was pre-sparged with ultra-high purity nitrogen gas (Air gas, Topeka) for 20 minutes to remove dissolve oxygen before introducing it to a granular iron column. Chemetrics dissolved oxygen (DO) kit (K-7512 and K-7501) was used to confirm that DO levels in the influent was less than 0.5 mg/L.

Stock solutions of TCE were prepared in methanol at concentrations of 5 mM and 100 mM for the purpose of analytical calibration and spike source for feed reservoir, respectively. Stock solutions were stored refrigerated at about 4° C for times not exceeding one month. PTFE (polytetrafluoroethylene) bags obtained from American Durafilm® served as source reservoirs for all column experiments. They were outfitted with stainless steel fittings for the purpose of

connecting Peak® tubing to or from a peristaltic pump with Viton® tubing (Cole Parmer) in the pump head. Columns were each custom-made in 3 parts: a glass cylindrical tube, 1.59 cm in diameter and 25 cm long, a funnel shaped glass effluent port fitted at the outlet end of the column with a fritted-glass connection, and a machined Plexiglas® end plug at the inlet end of the column.

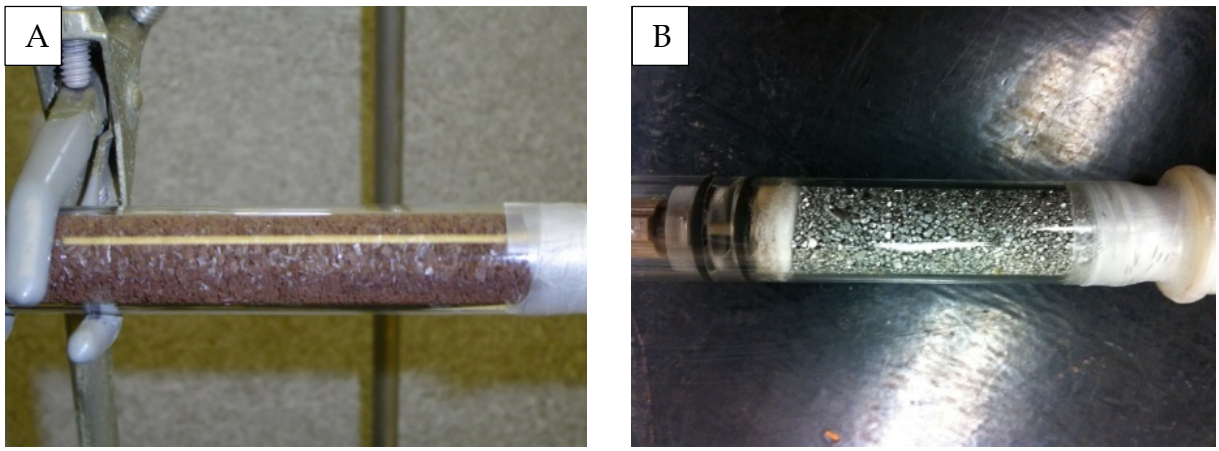

Figure 5.1: Glass columns packed with 80 g of (A) Connelly Iron (GI) and (B) Electrolytic Iron (EI).

5.3.2. Methods

Glass columns were packed with 80 g of either Connelly granular Iron (GI) or electrolytic iron from Sigma Aldrich (EI) (Figure 5.1;Table 5.1). The length of the packed material and weight of the columns prior to and after saturation were noted for the calculation of porosity. Columns were then flushed with the CO_2 gas for 20 minutes to replace the atmosphere inside the column and facilitate saturation. Next, the columns were flooded with the deoxygenated, pH 10, 8 mM $NaClO_4$ solution (1.124 g/L). The influent was pumped at a flow rate (Q) of 1 ml/min for at least 8 hours before introducing TCE, to permit the iron surface to approach an equilibrium with the electrolyte solution.

Table 5.1: Parameters of packed columns

Iron type	mass iron (g)	column internal diameter (cm)	column packed length (cm)	Pore Volume VP (ml)	Porosity	Fe/V ($g\ L^{-1}$)
GI	80	1.59	16.60	18.56	0.56	4310
EI	80	1.59	9.80	5.67	0.29	14159

Following pretreatment, the $NaClO_4$ solutions in the PTFE bags were spiked with TCE stock solution, and were then used as the influent reservoirs for the column experiments.

Figure 5.2: Experimental setup for GI column experiment showing PTFE bag, peristaltic pump and column.

The TCE in the reservoir was sequentially spiked to predetermined concentrations (C_o) that were maintained at each step until steady state TCE effluent concentrations were achieved. At the end of each experimental step, the columns were flushed with deoxygenated $NaClO_4$ for at least 12 hours to remove any TCE or chlorinated by products present from the earlier experiment. The C_o in the reservoir bag was then adjusted upward and the next test conducted. This was repeated

for six different C_o values per experimental suite. Altogether, four experimental suites were completed, two with each iron type (GI and EI).

Effluent samples were collected in 2 ml glass vials at predetermined times. The collected samples were centrifuged using an IEC Micromax centrifuge (model OM 3590) for 5 minutes at 10,000 RPM to drive any suspended particles to the bottom of the vials. Samples were then immediately analyzed using an Agilent 1100 series High Performance Liquid Chromatography (HPLC) with autosampler and diode array detector (Marietta and Devlin, 2005). Two sets of standards covering the range of the initial concentrations (25 μM to 500 μM) were analyzed with the samples for calibration purposes. The calibration standards were used to determine accuracy and precision which was generally within 2 – 10% (Devlin, 1996).

Hydrocarbons from inorganic sources were determined in the headspace of control Fe^0/H_2O batch test vials. Control bottles (40 ml glass vials), containing no iron, were calibrated with known amounts of pentane (5μM, 10 μM, 20 μM, 50 μM, 100 μM). In the active vials, approximately 50 g GI was saturated with DI water, leaving a small headspace, and stored for 24 hours. Vials were sealed with crimped, Teflon-lined septum caps. Samples were manually injected into an Agilent 6890 series gas chromatograph (GC) equipped with fused silica capillary column and a flame ionization detector (FID). Helium was used as the carrier gas with a flow rate of 2ml/min. The oven was maintained at 50ºC for 1 min and then ramped to 170 ºC for 4 min. The column pressure was maintained at 14.88 psi. TCE (50 μM) as used as an internal standard in all cases.

5.3.3. SEM Analysis

GI and EI grains were recovered from columns inside a glove box under an ultrapure nitrogen atmosphere. Iron grains were rinsed with methanol, dried and stored in nitrogen filled glass vials for transport to the SEM laboratory. SEM/EDS analyses were also performed on the

untreated iron grains to permit an assessment of the changes on the iron surface as the iron aged in the TCE solution. Grains were carefully mounted on the specimen holder. SEM images were collected on Carl Zeiss Leo 1550 Field Emission Scanning Electron Microscope using an in-lens detector operated at 10 kV. EDS (energy dispersive X-ray spectroscopy). Analysis was performed on selected sites of the grains using a Si (Li) detector with the Genesis software package (EDAX, U.S.).

5.3.4. Determination of reaction kinetics and retardation factors

Effluent concentrations were plotted as breakthrough curves, which were fitted using a solution to the advection-dispersion equation with sorption and reaction (eq 5.1), using a non-linear optimizer (Bear, 1979; Devlin, 1994) coded in visual basic, in the Excel® spreadsheet environment, as BEARKIMPE-2 (Firdous and Devlin, 2013). The curves were fitted on velocity, v (cm/min), dispersivity, α (cm), pseudo-first order rate constant, k_{app} (min^{-1}), and, when v was known in advance, retardation factor R_{app} .

$$C(x,t) = \frac{C_0}{2}\left\{\exp\left[\frac{vx}{2D}\left(1-\sqrt{1+\frac{4k_{app}D}{v^2}}\right)\right] erfc\left[\frac{R_{app}x - vt\sqrt{1+\frac{4k_{app}D}{v^2}}}{2\sqrt{DR_{app}t}}\right]\right\} \qquad 5.1$$

where C_o is the influent TCE concentration (μM), D is dispersion coefficient (m^{2}s^{-1}), $D=\alpha v+D^*$, α is dispersivity (m), v is water velocity (m s^{-1}) and D^* is effective diffusion coefficient (m^2 s^{-1}) (assumed negligible in these experiments compared to αv), x is column length (cm).

5.3.5. Modeling kinetics

The KIM (eq 5.2) (Devlin, 2009), was used in this work to determine possible changes in sorption and reaction parameters for reactive sites, on both the GI and EI.

$$\frac{dC}{dt} = \frac{kC_{max}Fe/V}{1/J + \frac{C_{max\,R}\,Fe/V}{1 + J_R C_o} + C_o} C_o = k_{app} C_o \qquad 5.2$$

where k (min^{-1}) is the first order rate constant for the surface reaction, C_{maxR} is the maximum sorption capacity ($\mu molg^{-1}$), J_R is the sorption affinity to reactive sites on the surface (μM^{-1}), Fe/V is the iron mass to column pore water volume ratio (g L^{-1}) and C_o is the aqueous influent concentration of TCE (µM).

The maximum sorption capacity C_{maxN} ($\mu molg^{-1}$) and sorption affinity J_N (μM^{-1}) to non-reactive sites in the iron columns were fitted with eq 5.3 (Figure 5.3, 5.4)(Table 5.2). Both equations 5.2 and 5.3 were included in the BEARKIMPE Excel program for fitting.

$$\mathrm{R_{app}} = 1 + \frac{Fe}{V}\,\frac{J_N C_{maxN}}{(1+J_N C_o)^2} \qquad 5.3$$

5.4. *Results and Discussion*

5.4.1. Role of carbon in non-reactive sorption

Non-reactive sorption was analyzed using the transient portion of the breakthrough curves (BTC) (Bi *et al.*, 2010). In all experiments, the BTCs for GI exhibited delayed arrivals of TCE at the column outlets, relative to the time predicted for a conservative solute, establishing retarded transport (Figure 5.3).

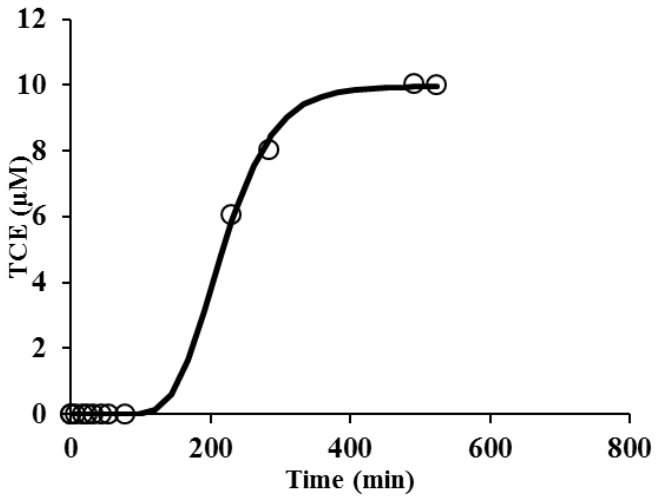

Figure 5.3: Breakthrough curve from Connelly Iron (GI-1) column for Co = 25 µM, fitted with eq 5.2. Symbols represent data points and the line represents the best fit. The column was aged 2 days at the time of the experiment. Fitted parameter values are given in Tables 5.1 and 5.2, respectively.

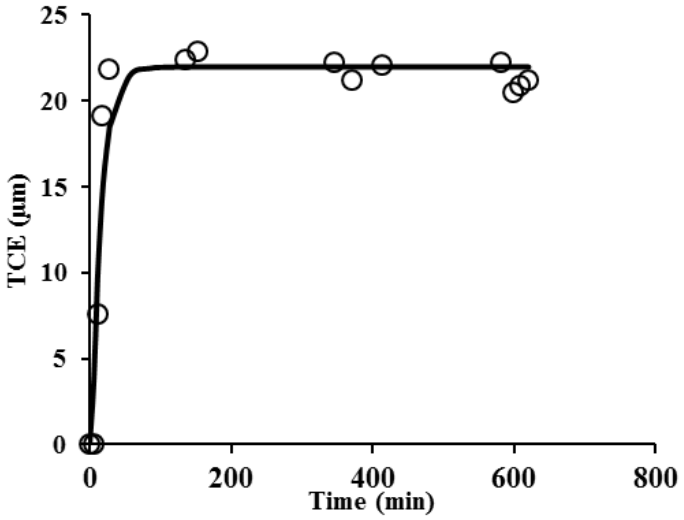

Figure 5.4: Breakthrough curve from the Electrolytic Iron (EI) column for C_o = 25 µM, fitted with eq 5.2. Symbols represent data points and the line represents the best fit. The column was aged 2 days at time of experiment. Fitted Parameter values are given in Tables 5.1 and 5.2, respectively.

However, the EI column exhibited comparatively little retardation (Figure 5.4, Table 5.3). The difference in behaviors between the EI and GI BTCs can be explained by the comparative

absence of a surface phase on EI associated with non-reactive adsorption of TCE. It was hypothesized that carbon was the dominant sorbing phase in this case.

Table 5.2: Comparison of best fit C_{maxN} and J_N using eq. 5.3 and C_{maxR} J_R and k using eq 5.2 in columns packed with GI and EI.

Packing (time since saturation)	C_{maxN} (μMg^{-1})	J_N (μM^{-1})	k (min^{-1})	C_{maxR} (μMg^{-1})	J_R (μM^{-1})
EI (0-10 days)	0.372	0.00026	0.05	0.024	0.00095
EI (0-90 days)	0.25	0.00045	0.0023	0.082	0.052
GI (0-10 days)	1.4	0.0025	0.045	0.022	0.016
GI (0-90 days)	1.01	0.003	0.009	0.149	0.027

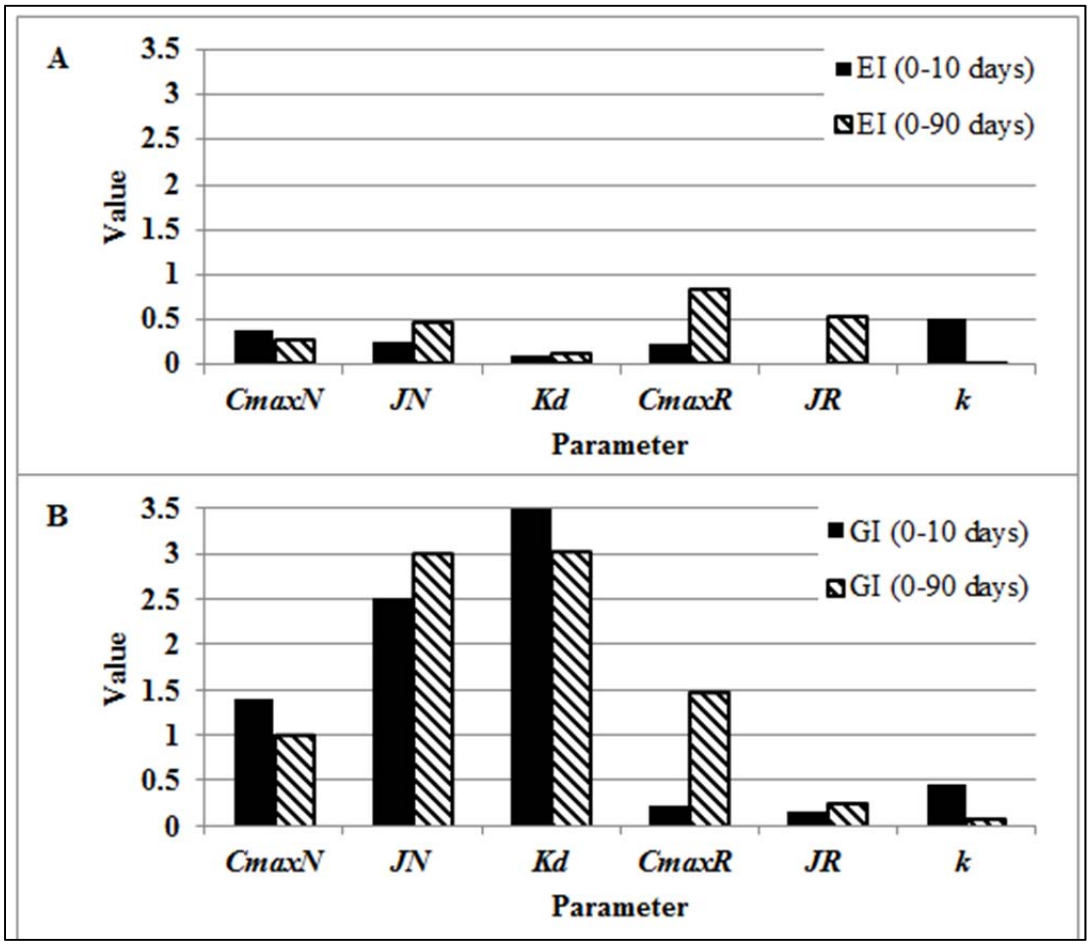

Figure 5.5: Comparison of 0-10 days and 0-90 days sorption and kinetic parameters for (A) EI and (B) GI. Note: Parameter estimates are multiplied to show on graph. J_N x 10^3 μM^{-1}, C_{maxR} x 10 μMg^{-1}, J_R x 10 μM^{-1} and k x 10 min^{-1}.

Table 5.3: Comparison of the values of apparent first order rate constants (k_{app}) and retardation factors (R_{app}) using eq. 5.1 for Connelly Iron and Pure Iron columns.

Connelly Iron (GI-1)							
0-10 days				0-90 days			
k_{app}(s^{-1})	C_o	R_{app}	Calc. R_{app}	k_{app} (s^{-1})	C_o	R_{app}	Calc. R_{app}
8.68E-04	24.9	12.72	12.89768	4.42E-04	36.5	12	11.70477
3.57E-04	73.19	17.7	10.58749	5.00E-04	73.77	9.99	9.73674
2.15E-04	145.4	5.44	8.211794	2.39E-04	160.8	5.9	6.816906
5.27E-04	258.5	4.538	5.943354	2.66E-04	194.3	4.836	6.072745
1.24E-04	386.4	6.618	4.464012	2.00E-04	391	6	3.631451
4.12E-04	534.3	4.083	3.45288	1.89E-04	447.1	3.6	3.256924

Electrolytic Iron (EI)							
0-10 days				0-90 days			
k_{app} (s^{-1})	C_o	R_{app}	Calc. R_{app}	k_{app} (s^{-1})	C_o	R_{app}	Calc. R_{app}
1.67E-04	23.22	2.3	2.395534	7.88E-04	31.5	2.28	2.548703
8.61E-05	44.26	1.9	2.380034	1.60E-04	58.02	2.55	2.512889
1.12E-04	108.6	3.12	2.334204	1.52E-04	99.5	2.6	2.459313
2.13E-04	217.3	1	2.261803	1.17E-04	204.2	2.2	2.336092
8.26E-05	313.7	1.998	2.202413	1.30E-04	353	2.5	2.18615
1.51E-04	437.3	2.1	2.132208	1.71E-07	395	3.096	2.148386

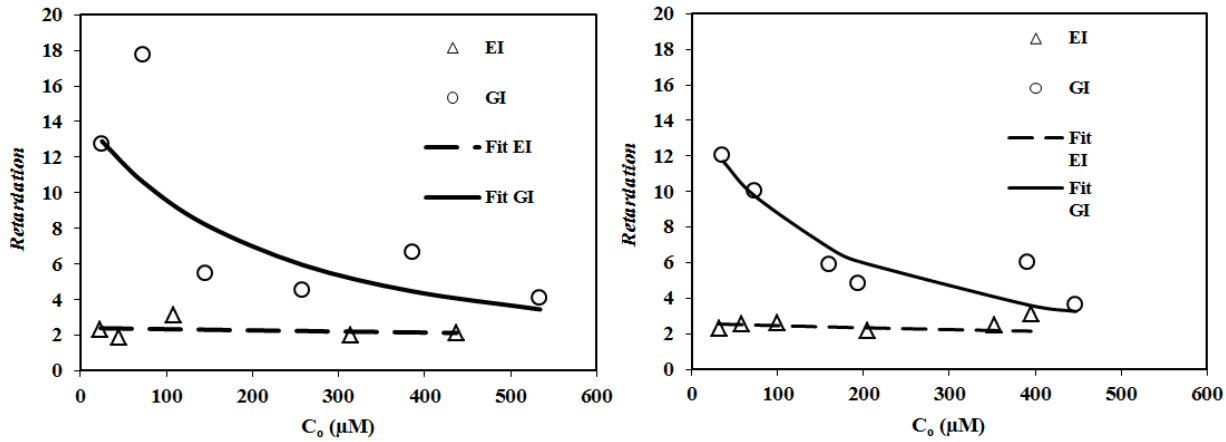

Figure 5.6: Relationship between retardation factor and injected TCE concentration for Connelly Iron (CI-1) and Pure iron (PI) (a) represents 0- 10 days: the solid curve fit the data for the CI-1, dash line for PI, circle markers were observed data for CI-1 and triangle markers were observed data for PI (b) represents 90 days: the solid curve fit the data for the CI-1, dash line for PI, circle markers were observed data for CI-1 and triangle markers were observed data for PI.

The retardation factors observed in the GI column were found to vary non-linearly with TCE concentrations (Figure 5.6). Retardation was particularly high when C_o was less than 100 μM and decreased with increasing concentrations. This result is consistent with the presence of a limited number of non-reactive sorption sites for TCE molecules, and saturation of these sites at the higher C_o values. This finding is also consistent with previously reported results (Bi *et al.*, 2010) (Figure 5.7).

The observed non-reactive sorption on the iron surface can be described by a Langmuir isotherm that requires 2 parameters to fully define: the maximum sorption capacity (C_{maxN}), and the sorption affinity (J_N). These parameters were investigated using eq 3 and R_{app} values from BTCs. C_{maxN} was observed to vary between 0.68 and 0.9 μmol $g^{-1}$with no systematic trend as the iron aged (Table 5.4). However, J_N continuously decreased in magnitude, with increasing GI age, ending up at a quarter of its initial value after about 300 days of GI in the column. Overall, a decrease in R_{app} was observed over the 9 month period of the GI-2 column (Figure 5.7), apparently due to mainly to the declining J_N parameter (Table 5.4).

Table 5.4: Comparison of C_{maxN} and J_N using eq. 5.3 for 3 suits of experiments on Connelly Iron (GI-2).

	Connelly Iron (GI-2)		
	0-10 days	**150-180 days**	**280-300 days**
C_{maxN} (μmolg^{-1})	0.68	0.58	0.90
J_N (μM^{-1})	0.0040	0.0021	0.0010

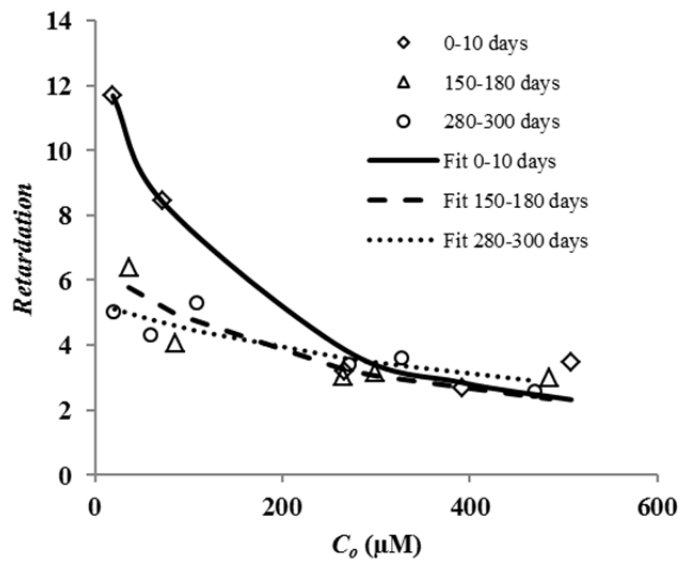

Figure 5.7: Effect of GI age on apparent retardation factors (R_{app}).

Estimations of C_{maxN} and J_N were also attempted for EI . In contrast to the findings for GI, R_{app} values for EI were comparatively low and showed no dependency on C_o (Figure 5.6;Table 5.3). This lack of dependency indicated that any sorption that was occurring could be described with a linear sorption isotherm ($C_{sorbed} = K_d C_{aqueous}$). A comparison of the associated partition coefficients, K_d, suggests that if any change to the sorption of TCE occurs as EI ages, it is to increase the affinity of the iron surface for TCE (Figure 5.5). However, this suggestion is weak and a more conservative conclusion is that there was no practical difference in the R_{apps} in young and aged EI columns.

The pronounced difference in affinities for TCE to the EI and GI surfaces is difficult to explain in terms of sorption to oxides or other minerals known to exist on the grain surfaces because i) these phases are expected to be common to both types of iron and ii) none of these inorganic phases are expected to participate strongly in hydrophobic sorption. A more likely explanation for the differences is the relatively strong presence of reduced carbon on the GI

compared to the EI surface, supported by the work of Burris *et al,* (1998) who identified graphite nodules embedded in cast iron grains and suggested these features to be nonreactive sorption sites. Unfortunately, that study was not able to provide insights into the nature of reactive sorption.

5.4.2. Assessment of reactive sorption in two iron types

Equilibrium reactive sorption and reaction rate of transformation of TCE was calculated using the steady state portion of the BTC and the method described by Bi *et al.* (2010) (Table 5.2). Monte Carlo analyses based on 1000 realizations were then performed, as described by Devlin (2009) to assess the uncertainty on these parameters.

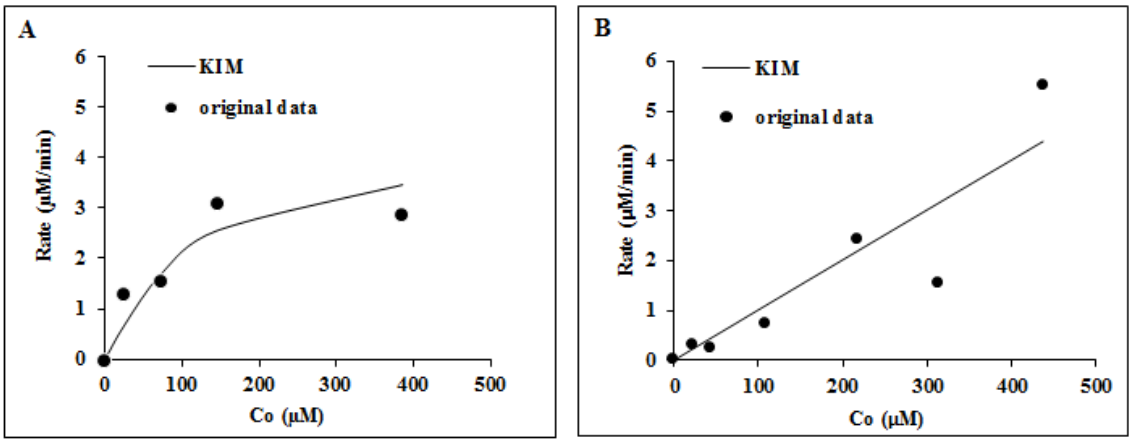

Figure 5.8: Relationship between TCE concentration and reduction rates for iron aged 0-7 days, using KIM (eq 2) (A) for Connelly Iron GI-1, (B) for Electrolytic Iron (EI). Solid circles represent observed rates and lines are fitted with KIM.

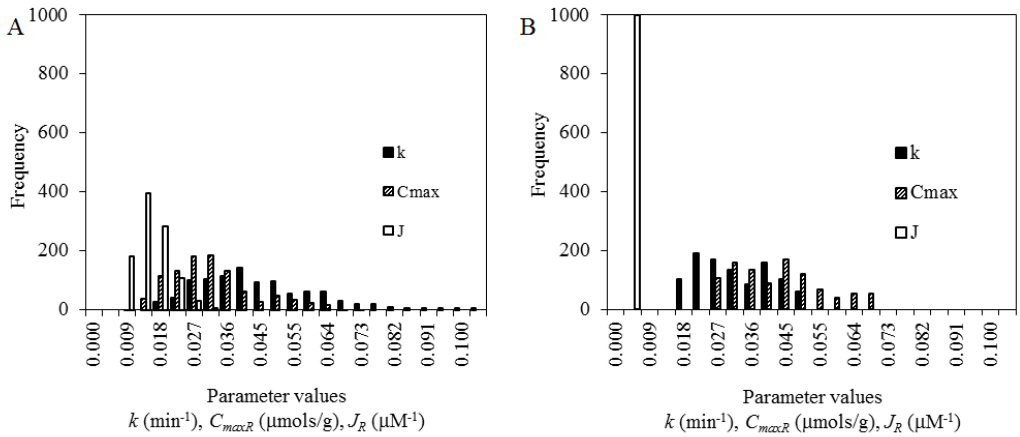

Figure 5.9: Distribution of parameters estimates using Monte Carlo analysis for 0-7 days aged (A) GI-1 and (B) EI.

The rate data exhibited moderate scatter, which is typical in the analysis of untreated commercial granular iron (Figure 5.8).This scatter is reflected in the ranges of possible parameter values revealed in the Monte Carlo analysis (Figure 5.9). In spite of the notable uncertainties a clear difference can be discerned between the commercial GI and the EI. Connelly iron is characterised by a considerably larger value of J_R than EI, consistent with expectations based on a carbon phase acting as the reactive sorption site.

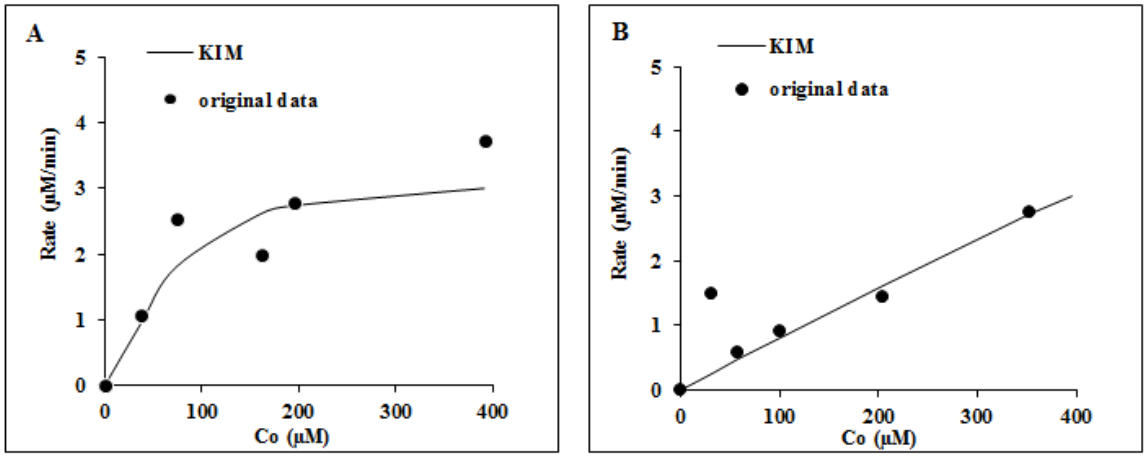

Figure 5.10: Relationship between TCE concentration and reduction rates using KIM (eq 2) (A) for Connelly Iron CI-1, (B) for Electrolytic Iron (EI) both aged 0-90 days. Solid circles represent observed rate for all injected C_o and solid lines are fitted with KIM.

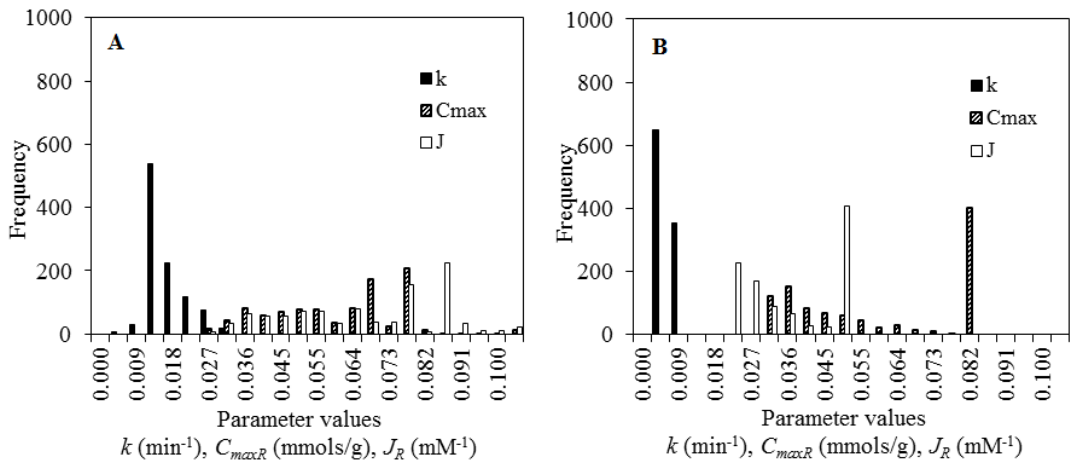

Figure 5.11: Distribution of parameters estimates using Monte Carlo analysis for 0-90 days aged (A) CI-1 and (B) EI.

The same analysis was repeated after the two columns were aged 3 months (90 days) (Figures 5.10 and 5.11). Both iron types were found to have altered parameter values after aging, though the EI product exhibited the more profound changes. Connelly iron was found to have lost inherent reactivity (declining k) and gained sorption capacity (increasing C_{maxR}), with a possible moderate increase in J_R. This result was also reported by Bi *et al.* (2010) and Huang (2011).

In contrast to the GI product, the EI exhibited more dramatic changes in inherent reactivity (k), which declined, and sorption affinity (J_R), increased, accompanied by a moderate increase in capacity (C_{maxR}). These changes, in particular that to the affinity parameter, suggest a fundamental change to the character of the reactive sorption sites on the EI.

A possible interpretation of the above trends in KIM parameters is that Connelly iron begins with carbon-dominated reactive sites, exhibiting relatively high sorption affinities to TCE, and EI begins with inorganic-dominated sites characterized by low sorption affinities. As the Connelly iron ages, the accumulation of oxides and alteration of surface carbon (Burris *et al.*,

1998; Lee and Wilkin, 2010; Mackenzie *et al.*, 1999) cause a loss of the most reactive sites. Now, reactivity is increasingly dominated by carbon-dominated sites with lower inherent reactivities but which are more plentiful, resulting in an increase in sorption capacity, and a minimal overall change to the iron reactivity.

The same reasoning applies to the declining k and increasing C_{maxR} parameters on EI – with a notable difference. The large increase in J_R indicates that the most active locations on the EI surface change in character from sites with low sorption affinities to sites with affinities similar to Connelly iron. This finding suggests that carbon-based sorption sites may develop on the aged EI product.

Several previous studies provide clues to the processes that might explain how surface carbon changes with time. Hardy and Gillham, (1996) reported the production of hydrocarbons (HC) in Fe^0/H2O systems. They tentatively ruled out graphitic carbon from the GI, and firmly ruled out background organics in their influent water as sources of the HC carbon, concluding that carbon dioxide reduction was the chief process generating the HCs. Deng et al, (1997) examined several different iron types and also detected HCs in the pore water. They found HC concentrations that increased nearly linearly with time. They further suggested background carbon in the form of a carbide phase on the GI was a possible source of HC production in Fe/H2O systems. These reports support the idea that surface carbon is a dynamic phase on GI, and that CO_2 can be a source of reduced carbon on EI (conversion to a sorbing phase remains an unconfirmed possibility), explaining the reactivity trends documented here.

5.4.3. Demonstration of carbon transformations in GI/H_2O systems

If the EI developed new carbon-based sorption sites over time, it should be possible to document an increase in surface carbon on the EI surface over time. An attempt to do this was made by examining fresh EI, before exposure to water, and 90 day old EI recovered from a column, using a scanning electron microscope (SEM) and electron dispersive x-rays (EDS) (Figure 5.12 A-D).

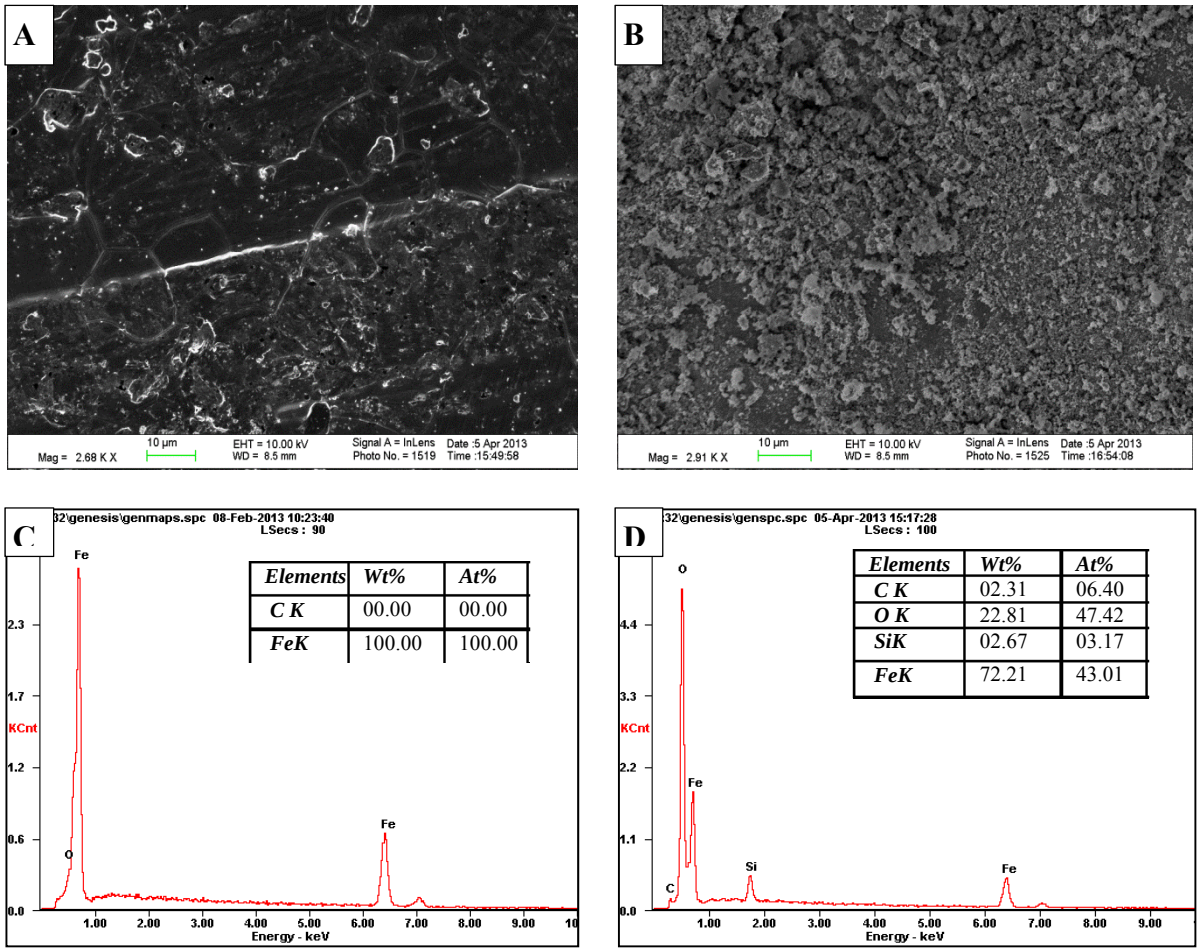

Figure 5.12: Scanning Electron Microscope images and EDX spectra of EI (A& C) Untreated (B&D) treated. EDS also shows elemental distribution in inset table.

The images clearly show the absence of detectable carbon on the fresh iron sample (Figure 5.12A,C) and the presence of surface carbon on the 90-day aged sample (Figure B,D). Further work is needed to establish unequivocally that the carbon occurrence is of a type conducive to sorption of TCE. Nevertheless, in principle it is possible to reduce carbon dioxide to graphite on the EI surface (Nagasawa *et al.*, 2013), so the carbon detected here is supportive of the carbon-based sorption interpretation described above.

It was postulated above that the Connelly iron surface transitioned from one dominated by a relatively low number of highly reactive sites to one characterized by a larger number of less reactive sites. In both cases the magnitude of the J_R parameter suggested the involvement of surface carbon in the sorption. This model suggests that the surface carbon may be subject to alterations as the GI ages – possibly related to burial under oxide minerals, or by direct transformations. Evidence for the latter was obtained in a headspace experiment in which GI produced 1.4 to 24 μM of C1-C4 hydrocarbons (HC) in deionized water – Fe^0 batch vials.

5.5. Conclusions

Retardation factors, R_{app}, for TCE in GI-packed columns vary non-linearly as a function of input TCE concentrations, rising to values approaching 15 for C_o < 100 to 200 μmol. In contrast, R_{app} values for TCE in EI-packed columns were independent of TCE concentrations, and tended to remain in the range 1 to 3.

Aging of the iron columns had no noticeable effect on the R_{app} values from the EI column, but were found to decline significantly with aging (particularly C_o < 200 μmol) in the GI column.

Overall reactivities for both young and aged iron samples of both GI and EI types changed little during these experiments, but the underlying reasons for the reactivity appeared to shift emphasis toward an increasing role for sorption. For example, the GI column showed an increase in available reactive sorption sites with time, shifting rate control from a small number of highly reactive sites to a larger number of less reactive sites. In the case of EI, the sorption affinity toward TCE appeared to increase as the solid aged.

This work suggests that carbon plays an important role in both reactive and non-reactive sorption. On Connelly iron, a replacement of highly reactive sites with more numerous sites of lower reactivity – all with sorption affinities in the range expected for surface carbon phases – occurred as the iron aged. On the electrolytic iron surface, a low initial sorption affinity grew with aging to one similar to that observed with the Connelly iron, suggesting a transition to reactive sites similar in character to those on the Connelly product. More precise descriptions of the character of the reactive sites may be possible with additional work aimed at examining the iron surfaces at the micro-scale.

References

Arnold, W.A., Ball, W.P., Roberts, A.L., 1999. Polychlorinated ethane reaction with zero-valent zinc: pathways and rate control. Journal of Contaminant Hydrology, v. 40, no. 2, 183-200.

Baciocchi, R., Boni, M.R., D'Aprile, L., 2003. Characterization and Performance of Granular Iron as Reactive Media for TCE degradation by Permeable Reactive Barriers. Water, Air, and Soil Pollution, v. 149, no. 1, 211-226.

Bear, J., 1979. Hydraulics of Groundwater. McGraw- Hill International Book Co, New York.

Bi, E., Devlin, J.F., Huang, B., Firdous, R., 2010. Transport and Kinetic Studies To Characterize Reactive and Nonreactive Sites on Granular Iron. Environmental Science and Technology, v. 44, no. 14, 5564-5569.

Blowes, D.W., Ptacek, C.J., Benner, S.G., McRae, C.W.T., Bennett, T.A., Puls, R.W., 2000. Treatment of inorganic contaminants using permeable reactive barriers. Journal of Contaminant Hydrology, v. 45, no. 1–2, 123-137.

Burris, D., Allen-King, R., Manoranjan, V., Campbell, T., Loraine, G., Deng, B., 1998. Chlorinated Ethene Reduction by Cast Iron: Sorption and Mass Transfer. Journal of Environmental Engineering, v. 124, no. 10, 1012-1019.

Burris, D.R., Wells, J.R., Campbell, T.J., Roberts, A.L., 1997. Trichloroethylene and tetrachloroethylene reduction in a metallic iron-water-vapor batch system. Environmental Toxicology and Chemistry, v. 16, no. 4, 0p.

Chawla, S.L., Gupta, R.K., 1993. Materials selection for Corrosion Control. ASM International, Materials Park, OH, 7 pp.

Cornelissen, G., Gustafsson, Ö., Bucheli, T.D., Jonker, M.T.O., Koelmans, A.A., van Noort, P.C.M., 2005. Extensive Sorption of Organic Compounds to Black Carbon, Coal, and Kerogen in Sediments and Soils: Mechanisms and Consequences for Distribution, Bioaccumulation, and Biodegradation. Environmental Science & Technology, v. 39, no. 18, 6881-6895.

Deng, B., Campbell, T.J., Burris, D.R., 1997. Hydrocarbon Formation in Metallic Iron/Water Systems. Environmental Science & Technology, v. 31, no. 4, 1185-1190.

Deng, B., Hu, S., Whitworth, T.M., Lee, R., 2003. Trichloroethylene Reduction on Zero Valent Iron: Probing Reactive versus Nonreactive Sites, Chlorinated Solvent and DNAPL Remediation. American Chemical Society, pp. 181-205.

Devlin, J.F., 1994. A Simple and Powerful Method of Parameter Estimation Using Simplex Optimization. Ground Water, v. 32, no. 2, 323-327.

Devlin, J.F., 1996. A Method to Assess Analytical Uncertainties Over Large Concentration Ranges With Reference to Volatile Organics in Water. Ground Water Monitoring and Remediation, v. 16, no. 3, 179-185.

Devlin, J.F., 2009. Development and Assessment of a Rate Equation for Chemical Transformations in Reactive Porous Media. Environmental Science & Technology, v. 43, no. 11, 4113-4118.

Devlin, J.F., Allin, K.O., 2005. Major Anion Effects on the Kinetics and Reactivity of Granular Iron in Glass-Encased Magnet Batch Reactor Experiments. Environmental Science & Technology, v. 39, no. 6, 7p.

Dries, J., Bastiaens, L., Springael, D., Agathos, S.N., Diels, L., 2005. Combined Removal of Chlorinated Ethenes and Heavy Metals by Zerovalent Iron in Batch and Continuous Flow Column Systems. Environmental Science and Technology, v. 39, no. 21, 8460-8465.

Farrell, J., Melitas, N., Kason, M., Li, T., 2000. Electrochemical and Column Investigation of Iron-Mediated Reductive Dechlorination of Trichloroethylene and Perchloroethylene. Environmental Science and Technology, v. 34, no. 12, 2549-2556.

Firdous, R., Devlin, J.F., BEARKIMPE-2: A VBA Excel program for Characterizing Granular Iron in Treatability Studies. Computers & Geosciences, http://dx.doi.org/10.1016/j.cageo.2013.10.005.

Gavaskar, A.R., 1998. Permeable barriers for groundwater remediation : design, construction, and monitoring. Battelle Press, Columbus.

Gillham, R.W., Vogan, J., Gui, L., Duchene, M., Son, J., 2010. Iron Barrier Walls for Chlorinated Solvent Remediation.In Situ Remediation of Chlorinated Solvent Plumes, In: Stroo, H.F., Ward, C.H. (Eds.). Springer New York, pp. 537-571.

Hardy, L.I., Gillham, R.W., 1996. Formation of Hydrocarbons from the Reduction of Aqueous CO2 by Zero-Valent Iron. Environmental Science & Technology, v. 30, no. 1, 57-65.

Higgins, M.R., Olson, T.M., 2009. Life-Cycle Case Study Comparison of Permeable Reactive Barrier versus Pump-and-Treat Remediation. Environmental Science and Technology, v. 43, no. 24, 9432-9438.

Huang, B., 2011. Separating the Kinetic and Sorption Parameters of Mixed Chlorinated Solvents in Contact with Granular Iron, Geology. University of Kansas, Lawrence, p. 163.

Lee, T.R., Wilkin, R.T., 2010. Iron hydroxy carbonate formation in zerovalent iron permeable reactive barriers: Characterization and evaluation of phase stability. Journal of Contaminant Hydrology, v. 116, no. 1–4, 47-57.

Mackenzie, P.D., Horney, D.P., Sivavec, T.M., 1999. Mineral precipitation and porosity losses in granular iron columns. Journal of Hazardous Materials, v. 68, no. 1–2, 1-17.

Marietta, M.L., Devlin, J.F., 2005. In Bringing Groundwater Quality Research to the Watershed Scale 4th International Groundwater Quality Conference. IAHS, Waterloo, Canada, pp. 376-382.

Moore, A.M., De Leon, C.H., Young, T.M., 2003. Rate and Extent of Aqueous Perchlorate Removal by Iron Surfaces. Environmental Science and Technology, v. 37, no. 14, 3189-3198.

Nagasawa, S., Kitagawa, H., Nakanishi, T., Tanabe, S., Hong, W., 2013. An approach toward automatic graphitization of CO2 samples for AMS 14C measurements. Nuclear Instruments and Methods in Physics Research Section B: Beam Interactions with Materials and Atoms, v. 294, no. 0, 266-269.

O'Hannesin, S.F., Gillham, R.W., 1998. Long-Term Performance of an In Situ “Iron Wall” for Remediation of VOCs. Ground Water, v. 36, no. 1, 164-170.

Oh, S.-Y., Cha, D.K., Chiu, P.C., 2002. Graphite-Mediated Reduction of 2,4-Dinitrotoluene with Elemental Iron. Environmental Science & Technology, v. 36, no. 10, 2178-2184.

Oliveira, L.C.A., Rios, R.V.R.A., Fabris, J.D., Garg, V., Sapag, K., Lago, R.M., 2002. Activated carbon/iron oxide magnetic composites for the adsorption of contaminants in water. Carbon, v. 40, no. 12, 2177-2183.

Phillips, D.H., Nooten, T.V., Bastiaens, L., Russell, M.I., Dickson, K., Plant, S., Ahad, J.M.E., Newton, T., Elliot, T., Kalin, R.M., 2010. Ten Year Performance Evaluation of a Field-Scale Zero-Valent Iron Permeable Reactive Barrier Installed to Remediate Trichloroethene Contaminated Groundwater. Environmental Science and Technology, v. 44, no. 10, 3861-3869.

Roberts, A.L., Totten, L.A., Arnold, W.A., Burris, D.R., Campbell, T.J., 1996. Reductive Elimination of Chlorinated Ethylenes by Zero-Valent Metals. Environmental Science and Technology, v. 30, no. 8, 2654-2659.

Sasaki, K., Blowes, D.W., Ptacek, C.J., Gould, W.D., 2008. Immobilization of Se(VI) in mine drainage by permeable reactive barriers: column performance. Applied Geochemistry, v. 23, no. 5, 1012-1022.

Stumm, W., 1992. Chemistry of the solid-water interface: Processes at the mineral-water and particle-water interface in natural systems. John Wiley & Son Inc.

Su, C.M., Puls, R.W., 1999. Kinetics of trichloroethene reduction by zerovalent iron and tin: Pretreatment effect, apparent activation energy, and intermediate products. Environmental Science and Technology, v. 33, no. 1, 163-168.

Tang, H., Zhu, D., Li, T., Kong, H., Chen, W., 2011. Reductive dechlorination of activated carbon-adsorbed trichloroethylene by zero-valent iron: carbon as electron shuttle. J Environ Qual, v. 40, no. 6, 1878-1885.

VanStone, N.A., Focht, R.M., Mabury, S.A., Lollar, B.S., 2004. Effect of Iron Type on Kinetics and Carbon Isotopic Enrichment of Chlorinated Ethylenes During Abiotic Reduction on Fe(0). Ground Water, v. 42, no. 2, 268-276.

Yabusaki, S., Cantrell, K., Sass, B., Steefel, C., 2001. Multicomponent Reactive Transport in an In Situ Zero-Valent Iron Cell. Environmental Science and Technology, v. 35, no. 7, 1493-1503.

6. Assessment of granular iron reactivity at micro and macro scales.

6.1. Abstract

Long term column experiments were carried out under dynamic flow conditions to link the micro-scale changes that occur on the iron surface due to corrosion, to macro-scale KIM parameters. Micro-scale grain characteristics were investigated by recovering single grains from sampling ports along the length of columns, and examining them through time using Raman spectroscopy and SEM/Energy dispersive spectroscopy (EDS). TCE reduction kinetics showed considerable changes in both TCE sorption and reactivity within the first 150 days. Likewise, the Raman spectra indicated that most profound changes to the grain surfaces also occurred within the first 150 days of experiment. The spectroscopic data showed two main types of changes: 1) rapid (within 15 days of exposure to solution) and column-wide partial degradation of the surface carbon signals, and 2) a more complete loss of the carbon signals associated with a reaction front, which had progressed about halfway along the columns (~10 cm) in 240 days. Associated with the carbon changes, Raman spectra collected along the column showed the loss of hematite, and the transition of intermediate phases to magnetite. Weakening of Raman signals for surface carbon, assumed to correspond to both physical and chemical losses of the graphitic carbon, corresponded to declining *k* values and the declines in the non-reactive sorption capacity, providing new evidence that surface carbon on granular iron is actively involved in non-reactive as well as reactive sorption.

6.2. Introduction

The use of granular iron permeable reactive barriers (GIPRBs) has gained much attention as an innovative and cost effective technology (Blowes *et al.*, 2000; Gillham and O'Hannesin, 1994; Gillham *et al.*, 2010; Gu *et al.*, 2002; Landis, 2001; Wilkin *et al.*, 2009) to treat wide variety of organic (Bi *et al.*, 2010; Burris *et al.*, 1997; Gillham and O'Hannesin, 1994; Liang, 1997) and inorganic groundwater contaminants (Blowes *et al.*, 2000; Lo *et al.*, 2007; Ritter *et al.*, 2003; Sasaki *et al.*, 2008; Wilkin *et al.*, 2009). Despite of its removal efficiencies, this technology suffers from issues such as loss of reactivity (Gotpagar *et al.*, 1997) and reduction in permeability with time (Liang *et al.*, 2000). Loss in reactivity due to corrosion and precipitation (Mackenzie *et al.*, 1999; Phillips *et al.*, 2000; Ritter *et al.*, 2002) have been identified as the major factor affecting the GIPRB longevity (Vikesland *et al.*, 2003). Although macro-scale factors, including solution composition, iron type, and available surface area are also known to affect reactivity (Bi *et al.*, 2009a; Devlin and Allin, 2005; Su and Puls, 1999).

Long term reactivity of the reactive media depends on the ability of the granular iron (GI) surface to transfer electrons for the reduction of chlorinated solvents (Farrell *et al.*, 2000). GI, such as the product sold by Connelly- GPM, Inc., consists of platy grains (Bi *et al.*, 2009b) of a light steel or cast iron (Burris *et al.*, 1998) where the iron core is covered with different oxides (Odziemkowski *et al.*, 1998). Reactivity is believed to be associated with both the metal cores of the grains and a thin oxide coating that covers most of the grains' surfaces (Huang, 2011), particularly the conductive oxides such as magnetite (Odziemkowski *et al.*, 1998). Graphite from the steel is another possible surface phase connected to reactivity (Oh *et al.*, 2002), although there is evidence that it is also connected to non-reactive sorption (Burris *et al.*, 1998).

Various methods have been employed to identify and characterize the GI surface (Farrell *et al.*, 2001; Odziemkowski *et al.*, 1998; Phillips *et al.*, 2000). Among them, spectroscopy and microscopic techniques have featured prominently because they can be non-invasive and are well suited to the detection and characterization of oxide phases on the iron surface. A notable example is the examination of dry Connelly iron by Raman spectroscopy, which showed the presence of 3 oxide layers coating a granular iron grain; magnetite (Fe_3O_4) dominating the inner layer, an increasing presence of maghemite (α-Fe_3O_4) in the middle layer and hematite (Fe_2O_3)occupying the outer layer (Odziemkowski *et al.*, 1998; Ritter *et al.*, 2002). The distinction between the layers is important because magnetite can act as a conductor (Schultze, 1978), while outermost hematite is usually considered a semi-conductor (Schultze, 1978), or insulator (Cohen, 1978), with significant implications for electron transfer from the metal core. The application of Raman spectroscopy first revealed an auto reduction reaction on iron that converted passivating oxides into phases that supported electron transfer (Odziemkowski and Gillham, 1997).

Depending on the type of contaminants, ambient groundwater chemistry, and experimental conditions, different corrosion products can form on the iron surface. Over time, the formation of mixed valent iron oxyhydroxides (Fe^{2+} and Fe^{3+}), including green rusts, goethite (α-FeOOH), lepidocrocite (γ- FeOOH) and magnetite (Fe_3O_4) has been reported to occur on GI (Allin, 2000; Min *et al.*, 2009; Roh *et al.*, 2000). Besides oxides, microscopic, X-ray diffraction and spectroscopic analyses have identified carbonates such as aragonite ($CaCO_3$), calcite ($CaCO_3$), siderite ($FeCO_3$) and carbonate green rust (Furukawa *et al.*, 2002; Phillips *et al.*, 2003; Phillips *et al.*, 2000; Roh *et al.*, 2000). Interestingly, the detailed spectroscopic work conducted on GI has remained focused on the examination of oxide phases to the virtual exclusion of everything

else. Notably ignored are the occurrences of carbon on the GI surface despite the fact that sp^2 carbonaceous material (CM) are strong Raman scatters, and therefore well suited to Raman spectroscopic analysis (Pimenta *et al.*, 2007).

Changes to the iron surface due to corrosion occur on the grain scale, but they clearly exert macro-scale effects on PRB performance in the form of reactivity and permeability changes. These changes are typically assessed in bench-scale studies that measure contaminant disappearance rates through kinetic modeling (Hansson *et al.*, 2008; Jeen *et al.*, 2007; Min *et al.*, 2009), sometimes coupled with solid phase investigations involving spectroscopic techniques (Hansson *et al.*, 2006). To evaluate PRB performance and longevity, efforts to reconcile the macro-scale parameters and pore scale processes were undertaken but with limited success (i.e., primarily qualitative analyses limited to oxide behaviors) due to inadequate kinetic models and instrument limitations. Development of the Kinetic Iron Model (KIM) (Devlin, 2009) and more powerful spectroscopic instruments has since raised the possibility of improved insights across the scales of investigation by re-examining the GI system with linked kinetic and Raman spectroscopic tools.

The objective of this work was to link the kinetic and sorption parameters of the KIM, determined at the bench scale, to specific surface phase changes using Raman spectroscopy and Scanning electron microscopy (SEM). This was accomplished using long-term (up to 8 months) column experiments to assess the macro-scale KIM parameters. Micro-scale grain characteristics were investigated by recovering single grains from various locations in the columns, and examining them through time

6.3. Materials and Methods

6.3.1. Materials

All chemicals were used as received. Trichloroethylene (TCE, CAS# 79-01-6, 99%) was purchased from Acros Organics and methanol (CAS# 67-56-1; HPLC grade) from Fisher Scientific. Connelly® Iron was provided by GMP Inc. Iron grains were hand sieved and grain sizes ranging from 0.71 to 2.0 mm were used in all experiments. N_2 and CO_2 gases (99+%) were purchased from Air gas, Topeka, Kansas.

8 mM $NaClO_4$ feed solution was prepared using deionized water (Barnstead International Nano Pure Infinity Ultra-pure Water System Series 896). The pH of solution was adjusted to 10 with the drop wise addition of either 1.1 mM perchloric acid or 0.35 mM sodium hydroxide solution to mimic the geochemical conditions inside a PRB (Bi *et al.*, 2009b; Bi *et al.*, 2010). The $NaClO_4$ solution was sparged with nitrogen gas for 20 minutes to remove dissolve oxygen.

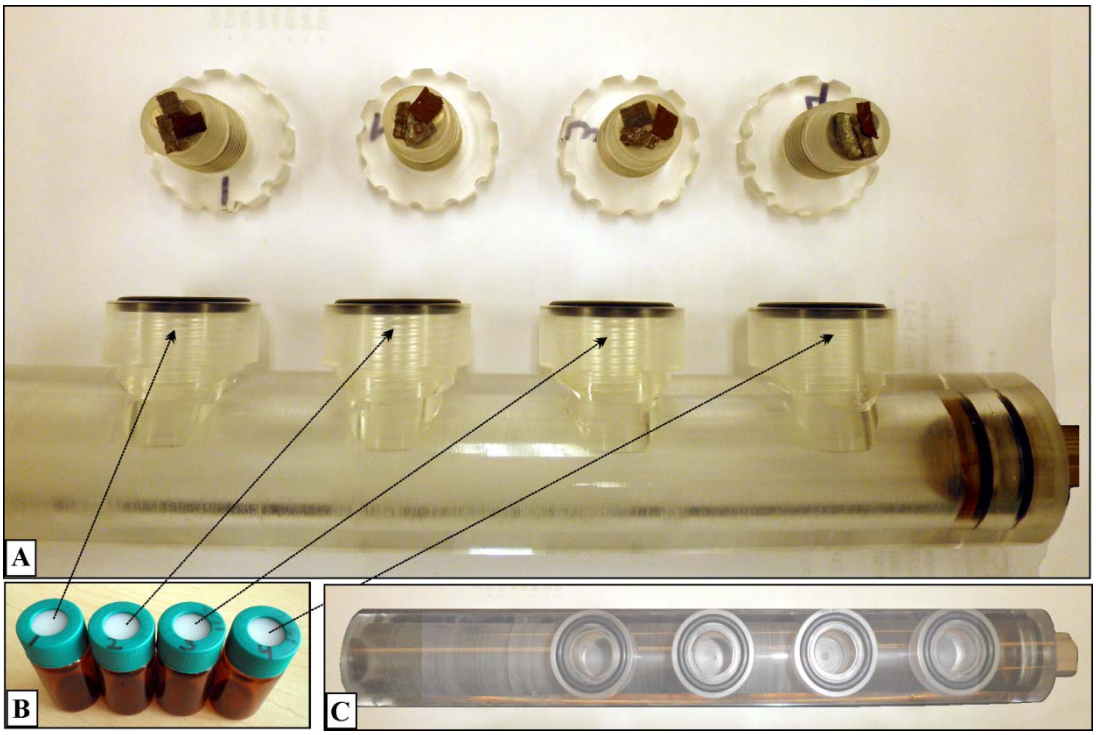

Figure 6.1: Column design for KIM analysis and Spectroscopic investigations (A) Side view showing 4 ports with lids designed to hold iron grains magnetically. Ports were fitted with O-rings to create a watertight seal, (B) Glass vials for transferring the grains to the Raman and SEM labs, and (C) Top view of the column.

Stock solutions of TCE were prepared in methanol at concentrations of 5 mM and 100 mM for the purposes of analytical calibration and to serve as a spike source for the feed reservoirs, respectively. Stock solutions were stored refrigerated at about 4° C for no more than a month. PTFE (polytetrafluoroethylene) bags were used as source reservoirs for column experiments. They were obtained assembled from American Durafilm®. Stainless steel fittings for the bags were obtained from Swagelock®.

Figure 6.2: Experimental setup of the column test showing plexiglas® column, peristaltic pump and Teflon bag used as reservoir for TCE solution.

The 25 cm long, 1.59 cm inside diameter, columns were custom manufactured from plexiglas® with 4 sampling ports 2 cm deep and 4 cm apart for holding iron grains that could be recovered repeatedly for time series analyses (Figure 6.1). Each column was fitted with machined Plexiglas® end plugs. Peak® tubing, obtained from Fisher Scientific was used to connect the columns with PTFE bags through a (Cole Parmer) peristaltic pump with a Viton® tubing in the pump head.

6.3.2. Methods

Columns were packed with 80 g of Connelly® Iron (CI) (Table 6.1). The length of the packed section of each column (~19 cm), and the weight of each column prior to and after saturation, were noted for porosity estimation purposes. Recoverable iron grains were placed in the column sampling ports. The sampling ports were constructed with slit openings inside the columns to permit the flow-through of pore water. This allowed the resampled grains to

equilibrate with location-specific pore water multiple times throughout the experiment. Accordingly, the grains were removed from the ports at selected times for examination by Raman spectroscopy and SEM/EDS analysis. Immediately following packing, and before flooding, the columns were flushed with the CO_2 gas for 20 minutes to replace atmospheric air trapped between the grains. The CO_2 flush was followed by water flooding with an 8 mM electrolyte solution (1.124 g/L $NaClO_4$), pH 10 that had been pre-sparged with N_2 gas for at least 20 min in order to remove the dissolved oxygen. The electrolyte solution was pumped into columns at a flow rate (Q) of 1 ml/min from the PTFE (polytetrafluoroethylene) reservoir bags for at least 8 hours before introducing TCE, to permit the iron surface to approach equilibrium with the solution. $NaClO_4$ was used as the background electrolyte due to its low reactivity on the granular iron surface (Devlin and Allin, 2005; Huang, 2011; Moore *et al.*, 2003) (Figure 6.2).

Table 6.1: Parameters of packed column

Iron type	Connelly Iron
mass iron (g)	80
column internal diameter (cm)	1.59
column packed length (cm)	19
Pore Volume PV (ml)	18
Porosity	0.48
Fe/V (= ρ_b/n) (g L^{-1})	4444

Following pretreatment, the solution in the PTFE reservoir source bag was spiked with TCE from the stock solution, using glass micro-liter syringes (Fisher Scientific). Column experiments were conducted with a flow rate of 1 ml/min, which could be reliably maintained with the peristaltic pump and generated water velocities within the columns that were comparable to groundwater velocities in highly permeable media (~ 2 m/day). Column experiments were performed at selected TCE concentrations (C_o), which were allowed to reach

steady state TCE effluent concentrations. At the end of each experiment, the columns were flushed with de-aerated $NaClO_4$ for at least 12 hours to remove any TCE or chlorinated by-products that might be held over from the prior experiment. The influent C_o was then adjusted upward and another test was conducted. This was repeated for six different C_o values per experimental suite. Altogether, three experimental suits were performed to assess the changes in TCE removal kinetics over a period of 8 months.

Effluent samples were collected in 2 ml glass vials, placed in an IEC Micromax centrifuge (model OM 3590) and spun for 5 minutes at 10,000 RPM to drive any suspended particles to the bottom of the vials. Samples were analyzed immediately after completing an experiment using an Agilent 1100 series High Performance Liquid Chromatography (HPLC) with autosampler and diode array detector (Marietta and Devlin, 2005). Two sets of standards covering the range of the initial concentrations (25 μM to 500 μM) were analyzed with the samples for calibration purposes. The calibration standards were used to determine accuracy and precision (Devlin, 1996) which was generally within 2 – 10%.

Figure 6.3: Setup for recovering iron grains from a column placed in a nitrogen filled glove bag. Grains were rinsed with methanol, $N_{2(g)}$ dried and placed in $N_{2(g)}$ filled glass vials all within the glove bag.

Micro-scale grain characteristics were investigated by recovering individual grains from the sampling ports along the column (Figure 6.1), and examining them with Raman spectroscopy and SEM/EDS. This process was repeated 3 times over 8 month period of the experiment. The grains were removed from the columns in an anaerobic glove bag under a nitrogen atmosphere. Grains were washed with methanol and allowed to dry under a nitrogen atmosphere for 10-15 minutes before being sealed under nitrogen in glass vials with Teflon® -lined lids, and then transported immediately to the appropriate spectroscopy lab (Figure 6.3). Raman analyses were completed with each sampling, SEM/EDS analyses were completed on the fresh grains and the grains at the end of the experiment.

6.3.3. Raman Spectroscopy

A Renishaw InVia Reflex Raman microprobe with a multi-wavelength facility operating at 514.5 nm, from a 50 mW Ar^+ laser (Spectra-Physics Stabilite 2017 laser) orientated normal to the sample, was used to record spectra from the granular iron samples. The collection optics were based on a Leica DMLM microscope. A refractive glass 50× objective lens was used to

focus the laser onto a 2 μm spot in order to collect the backscattered light. Two sets of spectral acquisition parameters were used, depending on the condition of the iron surface: (1) fresh iron surfaces could be effectively analyzed with 1 accumulation, 10 s acquisition, 1-5 mW laser power, and (2) corroded iron required 3-5 accumulations, 10 s acquisition, 1-5 mW laser power to produce acceptable spectra. The laser power impinging the oxides and carbonaceous material was kept between 1-5mW to minimize laser-induced heating of the samples (Marshall et al., 2010). A scan range of 100-1800 cm^{-1} was selected because it spans the finger print region of both the iron oxyhydroxides and sp^2 carbonaceous materials. The spectra were deconvoluted using Guassian/Lorentzian fit routine using GRAMS/32 Software. During these analyses, all the characteristics of Raman spectra, *i.e*. the band position, the band intensity, and crystallite size (L_a), were noted. Dry iron grains were removed from the sealed vials and placed, on glass slides under room air for the analyses. On average, 5-8 Raman spectra were obtained from each grain after each experiment.

6.3.4. SEM Analysis

Prior to a column experiment, SEM/EDS analyses were performed on the pristine iron grains to establish the background conditions of the surfaces. Grains were removed from the sealed vials, mounted on the specimen holders, and placed under vacuum for the analyses. SEM images were collected using a Carl Zeiss Leo 1550 Field Emission Scanning Electron Microscope using an inlens detector operated at 10 kV. EDS analyses on selected sites of the grains were collected using a Si (Li) detector with the Genesis software package (EDAX, U.S.).

6.3.5. Determination of reaction kinetics and retardation factors

Effluent concentrations of TCE were plotted as breakthrough curves (BTC), which were fitted using BEARKIMPE, an Excel VBA-coded solution to advection-dispersion equation with sorption and reaction (eq 6.1) and a simplex non-linear optimizer (Bear, 1979; Devlin, 1994).

The BTCs were fitted on velocity, v (ms^{-1}), dispersivity, α(cm), pseudo-first order rate constant, k_{app} (min^{-1}), and, when v was known in advance, retardation factor, R_{app} .

$$C(x,t) = \frac{C_0}{2}\left\{\exp\left[\frac{vx}{2D}\left(1-\sqrt{1+\frac{4k_{app}D}{v^2}}\right)\right] erfc\left[\frac{R_{app}x - vt\sqrt{1+\frac{4k_{app}D}{v^2}}}{2\sqrt{DR_{app}t}}\right]\right\} \quad 6.1$$

where C_o is the influent TCE concentration (μM), D is dispersion coefficient (m^2s^{-1}), $D=\alpha v+D^*$, and D^* is effective diffusion coefficient ($m^2\ s^{-1}$), , x is the length of the packed section of the column (cm).

The KIM (eq 6.2) (Devlin, 2009), was used in this work to determine possible changes in sorption and reaction parameters among two types of GI.

$$\frac{dC}{dt} = \frac{kC_{max}Fe/V}{1/J + \frac{C_{max\,R}\,Fe/V}{1+J_RC_o} + C_o}C_o = k_{app}C_o \quad 6.2$$

where k (min^{-1}) is the first order rate constant for the surface reaction, C_{maxR} is the maximum reactive-sorption capacity ($\mu molg^{-1}$), J_R is the reactive-sorption affinity (μM^{-1}), Fe/V is the iron mass to column pore water volume ratio, equivalent to the bulk dry density to porosity ratio (ρ_b/n) (Bi *et al.,* 2010) ($g\ L^{-1}$) and C_o is the aqueous influent concentration of TCE (μM).

The non-reactive maximum sorption capacity C_{maxN} ($\mu molg^{-1}$) and non-reactive-sorption affinity J_N (μM^{-1}) in the iron columns were fitted with eq 6.3.

$$R_{app} = 1 + \frac{Fe}{V}\frac{J_NC_{maxN}}{(1+J_NC_o)^2} \quad 6.3$$

where R_{app} = the apparent retardation factor (dimensionless), assuming a Langmuir type isotherm describes the sorption.

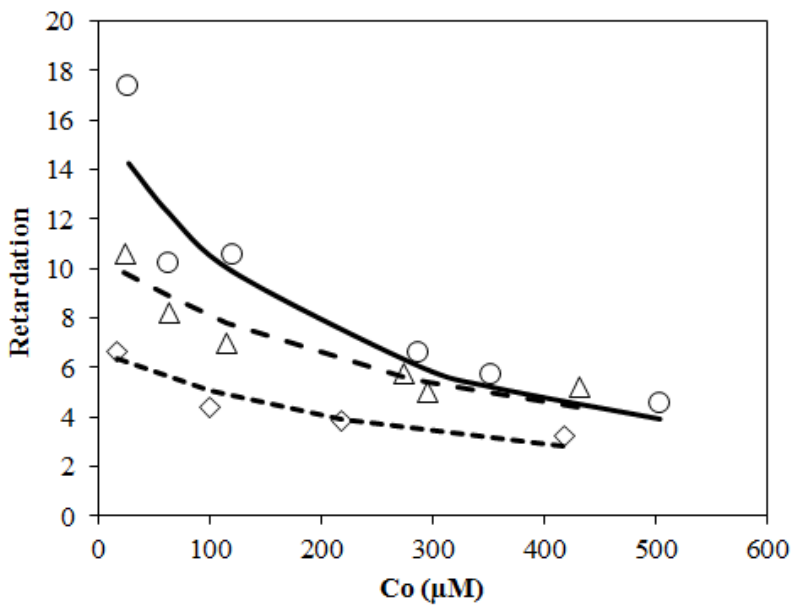

Figure 6.4: Relationship between retardation factors and injected TCE concentration. Symbols indicate measurement values and lines depict model fits. Circle symbols and solid line represents 0-15 days. Triangle symbols and long dashed line represents 140- 154 days. Diamond symbols and short dashed line represents 220 - 240 days.

6.4. Results and Discussion

6.4.1. Effect of aging on reactive and non-reactive sorption.

The removal of TCE from water in an iron-based PRB is the combined result of sorption and chemical reduction on the grain surfaces (Devlin *et al.*, 1998). Effluent BTCs led to best fit k_{app} and retardation factors R_{app} estimations that declined with increasing C_o and with increasing time (Table 6.2).

Table 6.2: Comparison of the values of apparent first order rate constants (k_{app}) and retardation factors (R_{app}) using eq. 6.1 for T_1, T_2 and T_3.

Time$_1$(0-15 days)			
k_{app}(s^{-1})	C_o (μM)	R_{app}	Calc. R_{app}
2.30E-03	27.1	17.41	15.46
8.60E-04	63.39	10.23	13.13
5.27E-04	120.7	10.57	10.44
2.72E-04	287.1	6.65	6.25
1.86E-04	353.4	5.77	5.33
2.02E-04	503.7	4.62	3.96
Time$_2$ (140-154 days)			
k_{app} (s^{-1})	C_o(μM)	R_{app}	Calc. R_{app}
3.75E-04	23.55	10.69	9.82
2.29E-04	63	8.26	8.86
4.20E-04	114.7	7.06	7.81
1.50E-04	274	5.80	5.63
5.56E-05	295.8	5.07	5.42
8.47E-05	431.5	5.24	4.37
Time$_3$ (220-240 days)			
k_{app}(s^{-1})	C_o(μM)	R_{app}	Calc. R_{app}
2.21E-04	16.3	6.69	4.78
1.88E-04	43.9	1.43	4.35
6.99E-05	99.56	4.45	3.68
2.19E-04	218	3.88	2.78
4.93E-05	263	0.80	2.56
9.05E-05	418.2	3.30	2.04

The trends observed in R_{app} were consistent with previous work (Bi *et al.*, 2010) which showed a non-linear relation over the range of input TCE concentrations (Figure 6.4). Retardation factors were highest when C_o was less than 100 μM and decreased with increasing concentrations (Figure 6.4). High retardation values at low C_o are thought to be due to an overabundance of available sorption sites for TCE molecules; sites that eventually became saturated at higher C_o values.

Table 6.3: Comparison of C_{maxN} and J_N using eq. 6.3 and C_{maxR} J_R and k using eq 6.2 in GI column.

Time (days)	Days	C_{maxN} (μMg^{-1})	J_N (μM^{-1})	k (min^{-1})	C_{maxR} (μMg^{-1})	J_R (μM^{-1})
T_1	0-15	1.58	0.0025	0.1223	0.0085	0.05
T_2	140-154	1.35	0.0015	0.016	0.037	0.057
T_3	220-240	0.70	0.0018	0.0028	0.23	0.075

The Langmuir parameters for non-reactive sites, C_{maxN} and J_N, both declined with increasing time. The C_{maxN} parameter steadily declined from 1.58 to 0.70 μmol g^{-1} over a period of 240 days (Table 6.3). The J_N parameter declined initially (between days 16 and 154) but then rebounded slightly between days 155 and 240, suggesting minimal changes in this parameter (Table 6.3). The decrease in the sorption capacity and affinity for non-reactive sites resulted in an overall decrease in R_{app} over the 240 days period of the experiment, and suggests the loss of non-reactive sorption sites, particularly at early time (Table 6.3) (Figure 6.4).

Within each data set, the KIM was fitted to data plotted as initial rate, $(dC/dt)_o$, *vs*. C_o to estimate the reaction and reactive-sorption parameters k, C_{maxR} and J_R (Figure 6.5) (Table 6.3). Monte Carlo analyses based on 1000 realizations of the rate data, assuming an effective error of about ±30%, were performed to assess the uncertainties on the KIM parameters (Figures 6.6, 6.7, 6.8). Estimated reaction rates were generally consistent with previous column experiments performed with Connelly Iron (Bi *et al.*, 2010), for similarly packed columns. In all experiments reaction rates declined over time, as expected. The largest decreases occurred during first 140 days of GI column (~ 4 to 2 μM/min) with little or no change in rate after 140 days despite the fact that similar effluent volumes were pumped through the column before and after 140 days.

However, a detailed examination of the reactive-sorption parameters suggested that steady changes did occur in the column over the duration of the experiment.

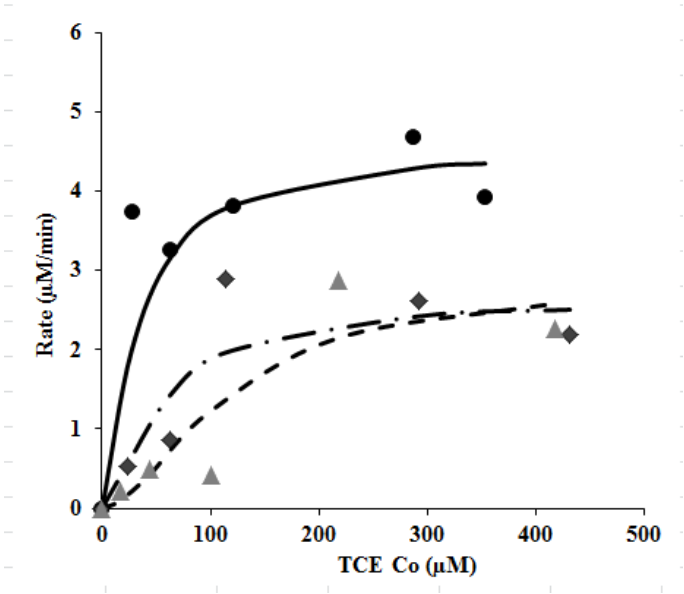

Figure 6.5: Relationship between TCE concentration and reduction rates using KIM (eq 2). Symbols indicate measurement values and lines depict model fits. Circle symbols and solid line represents 0-15 days. Diamond symbols and long dashed line represents 140- 154 days. Triangle symbols and short dashed line represents 220 - 240 days.

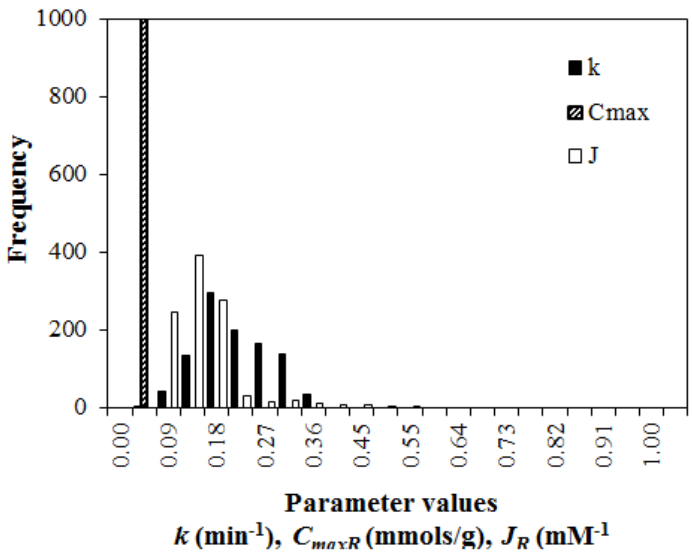

Figure 6.6: Distribution of parameters estimates using Monte Carlo analysis for 0-15 days aged GI column.

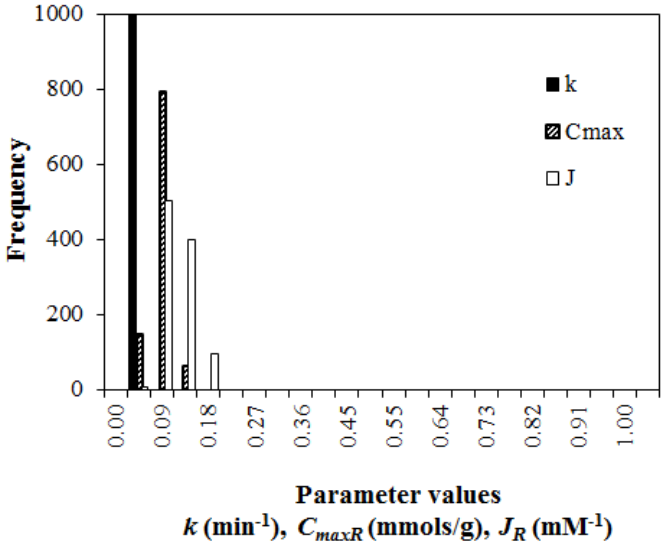

Figure 6.7: Distribution of parameters estimates using Monte Carlo analysis for 140-154 days aged GI column.

The comparison of histograms from the Monte Carlo analyses indicates that the early-time columns exhibited reaction kinetics dominated by highly reactive sites, characterized by high *k* and relatively small C_{maxR} (Figure 6.6). The decline in reaction rates from early time to

approximately day 140 is largely explainable by the decline in the parameter *k* over this period (Figure 6.7).

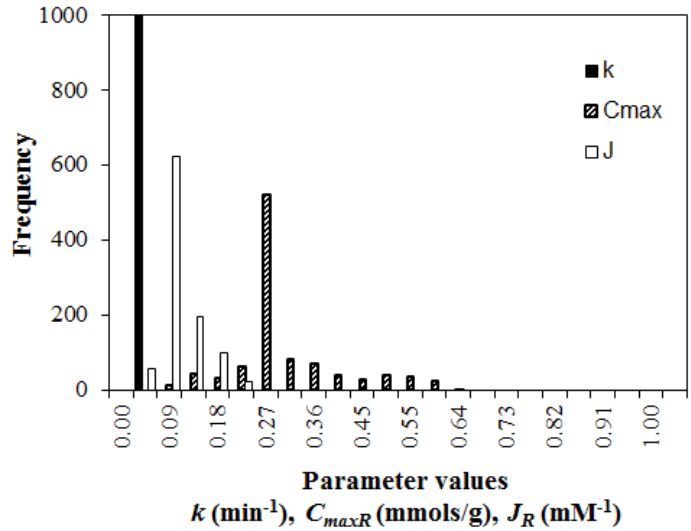

Figure 6.8: Distribution of parameters estimates using Monte Carlo analysis for 220-240 days aged GI column.

In contrast, the values of the reactive sorption capacity term, $C_{maxR,}$ were found to increase over the duration of the experiment (Figures 6.6- 6.8) (Table 6.3). In comparison to the other parameters, J_R was found to change relatively little with the aging of the grains. Taken together, these findings suggest that the reaction kinetics are initially dominated by a relatively small number of very reactive sites, but as the iron ages they become dominated by a larger number of less reactive sites. The similarity of J_R throughout the tests may indicate that both kinds of sites are associated with the same, or related, phases with similar sorption affinities for TCE.

6.4.2. Surface Analyses

6.4.2.1. Identification of surface phases on untreated GI

The iron oxide and hydroxide Raman bands in the collected spectra were assigned based on literature values (Dünnwald and Otto, 1989; Hanesch, 2009; Thibeau *et al.*, 1978). Three iron

oxide species were identified on untreated Connelly iron: αFe_2O_3 (Hematite), γFe_2O_3 (maghemite) and Fe_3O_4 (magnetite) (Figure 6.10A,B) (Hanesch, 2009; Ritter *et al.*, 2002) The presence of these oxide films on the iron surface is associated with the manufacturing process, which involves firing in a kiln at temperatures reaching ~ 700 to 1100 ^{o}C (Hardy and Gillham, 1996). Iron exposed to these temperatures, in the presence of oxygen and or with other oxidizing gases, promotes the formation of solid oxidation products (Chawla and Gupta, 1993). Accordingly, the first and second mineral layers formed on the iron surface in

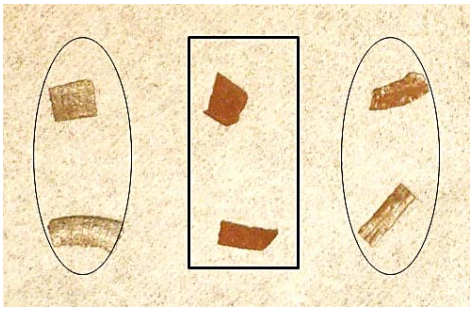

Figure 6.9: Connelly Iron showing platy grains with shiny side in oval and red side in rectangular shape.

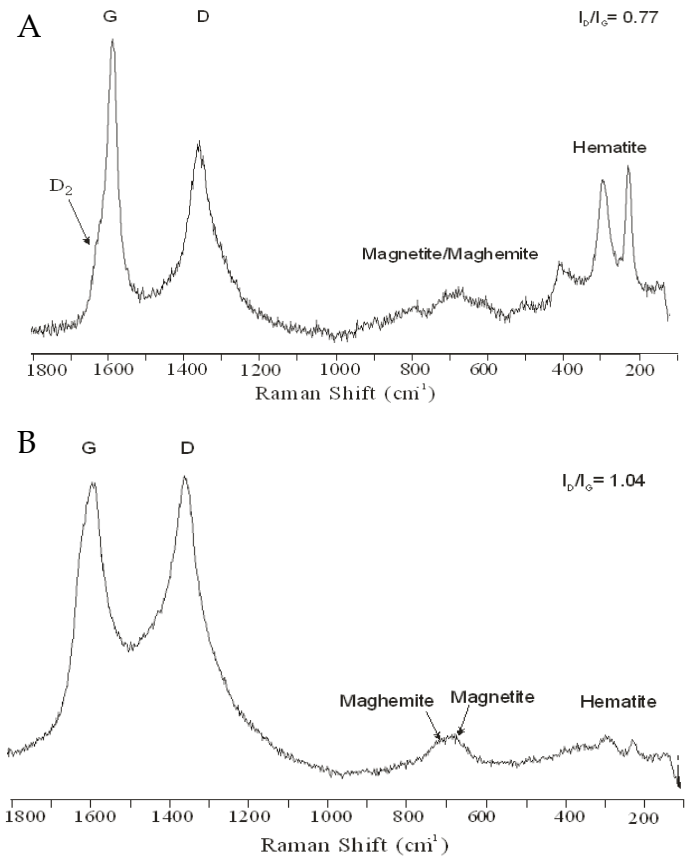

Figure 6.10: Raman spectra of untreated Connelly Iron collected on A) Red side and B) Shiny side.

the kiln are oxides that form strong chemical bonds (chemisorption) with metallic iron surface; any oxide beyond second layer is merely physical adsorbed (Uhlig, 1956). The total thickness of these oxides covering the commercial iron fillings was reported to be about to be 2.25µm (Sivavec and Horney, 1995).

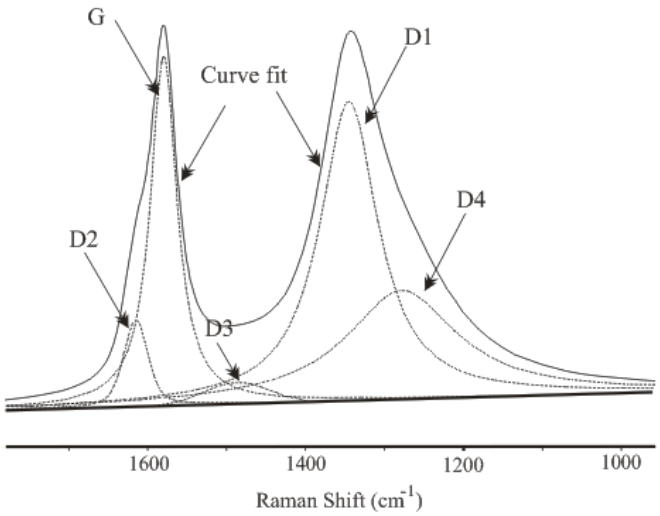

Figure 6.11: Example of decomposition of carbon first-order region of a Raman spectrum from the shiny side of Connelly Iron. Five bands can be resolved into Gaussian-Lorentzian bands, D2 (disorder sp^2 lattice), G (in plane C=C in an aromatic ring stretching vibrational mode with E_{2g2} symmetry), D3(amorphous carbon), D1(A_{1g} symmetry), and D4(sp^3 bonds or C-C and C=C stretching vibrations).

The Connelly iron used in these experiments exhibited a platy texture possessing two different faces. One side, often slightly convex, tended to be shiny while the other side, slightly concave, was dull red in color and well coated with oxides (Figure 6.9). Raman spectra collected on the red sides showed strong bands associated with hematite at 225 cm^{-1}, 291 cm^{-1} and 410 cm^{-1} (Figure 6.10A). These same bands were visible in much lower intensities in spectra collected from the shiny sides (Figure 6.10B). Maghemite and magnetite bands were observed at 720 cm^{-1} and 670 cm^{-1} respectively (Figure 6.10A, B). The Raman spectrum of carbonaceous material can be divided into first (800-1800cm^{-1}) and second-order (2200-3400cm^{-1}) region depending upon the crystallinity, the first-order spectral region contains most of the structural information of CM (Marshall and Marshall, 2011) and hence is used in this work. The first band referred to as D band is located at ~1350 cm^{-1} and is assigned to A_{1g} symmetry and second band located at 1582 cm^{-1}, is assigned to G band, an in-plane C=C in an aromatic ring stretching vibrational mode with E_2g_2 symmetry. The D band, only becomes active due to disorder in the

sp^2 carbon network (Ferrari and Robertson, 2000). Disorder in graphite may be induced by relative rotation of adjacent layers, by puckering sheets, or by disruption of the interlayer spacings (Rouzaud *et al.*, 1983). The ratio of the D and G band intensities (I_D/I_G) can be used as a metric for the degree of disorder in the CM; with increasing disorder the I_D/I_G is expected to increase compared to crystalline graphite (Ferrari and Robertson, 2000). By using band deconvolution, D and G bands can be separated and a more accurate measurement of I_D/I_G can be obtained, and subsequently used to provide a better quantitative estimate of the structural organization of sp^2 carbonaceous materials (Figure 6.11) (Marshall and Marshall, 2011).

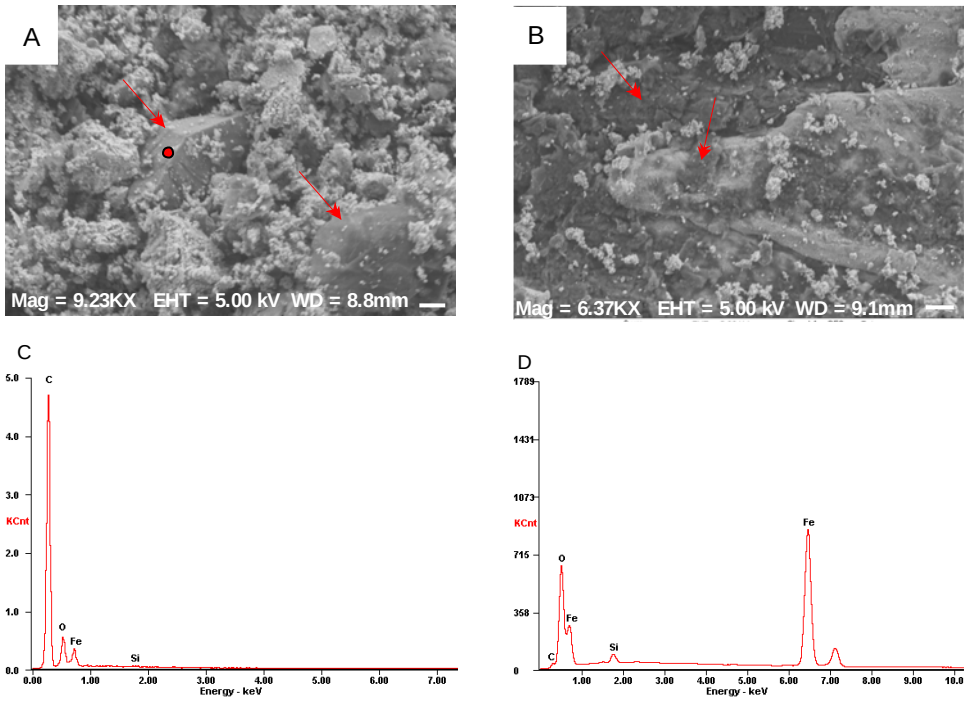

Figure 6.12: SEM micrographs of untreated GI showing A) spheroidal/nodular CM on red side marked with arrows and B) lamellar CM on shiny side (marked with arrows) of untreated iron surface. (C) representative EDS of the spheroidal CM (circle marked on A) and (D) oxide coating on iron surface.

On average, spectra collected on the red side of iron showed a narrow and more intense G band with a calculated I_D/I_G ratio of 0.82 ± 0.05, while shiny side showed a broader G band with I_D/I_G of 1.08 ± 0.17. The relative intensity of D to G also provides a good indicator for determining the

in-plane crystallite size (La) or the amount of disorder in the carbonaceous material(Tuinstra and Koenig, 1970). The formula $L_a = 44[I_D/I_G]^{-1}$ (nm) used in this work to determine the L_a was based on empirical expression derived by Knight and White (1989) and is only valid for 514.5 nm laser line. It was found that microcrytalline planer size ranges from 49 – 53nm for CM present on red while 32-44nm for the shiny side of grain. Comparison of the intensity of the D band, I_D/I_G ratio and L_a on both sides of the grain revealed the present of two different types of CM on Connelly Iron (Marshall *et al*., 2012).

SEM imaging of untreated iron samples showed clusters of oxides and dark patches on the iron surface (Figure 6.12A,B). The EDS analyses of these dark patches showed the presence of high levels of carbon, specifically 75.25% – 98.97% carbon, 7.96 – 1.03% O, and 16.34 – 0% Fe while the clusters of oxides were dominated by other elements, specifically, 72.85% Fe, 25.48% O, by weight and a small fraction of silica (1.67%). The distributions of the weight% of these elements did vary on iron surface, depending upon specific phase (Figure 6.12C, D). Nonetheless, the percentages given are reasonably good indicators of the typical cases.

Various forms of graphite have been reported to occur on cast/grey iron, such as spheroidal, lamellar, and nodular (Ritter *et al.*, 2002; Ritter *et al.*, 2003). Careful examination of micrographs collected in this work also showed differences in the CM forms, including more spheroidal/nodular varieties on the red sides of the grains, and flaky or lamellar varieties on the shiny sides (Figure 6.12A,B). The detailed effect of the graphite morphology and its effect on corrosion has not been tested in this study, however, based on the Raman analyses performed here, the spheroidal/nodular graphite may be more ordered form of CM, and therefore the variety that dominates TCE sorption, at least in the early times of the column experiments.

6.4.3. Phase distributions and transitions associated with aging of the iron surface.

Systematic investigations of the grain surfaces from all 4 column sampling ports provided comprehensive details concerning changes occurring to iron grains at the micro-scale. Hematite bands in the Raman spectra, which were present on untreated iron (Figures 6.10A), were removed from grains in all ports within 24 hours of column operation (Figure 6.13, 6.14), indicating that immersion in water was sufficient to drive a hematite transformation. The process of hematite removal is well discussed in literature (Odziemkowski and Gillham, 1997; Ritter *et al.*, 2002), and is thought to involve an autoreduction reaction ultimately producing magnetite.

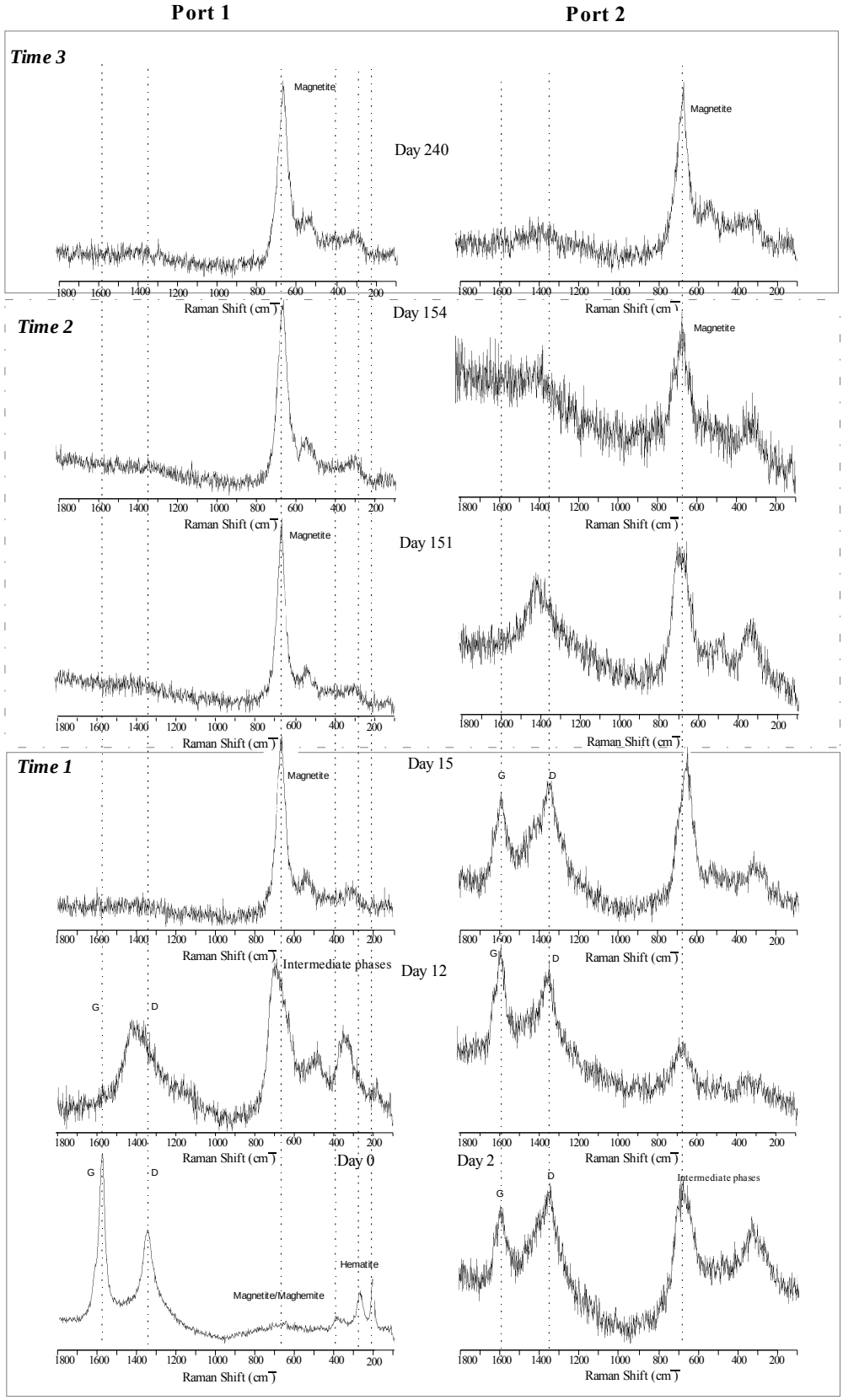

Figure 6.13: Raman spectra collected on red side from port 1 and 2 during T_1, T_2 and T_3.

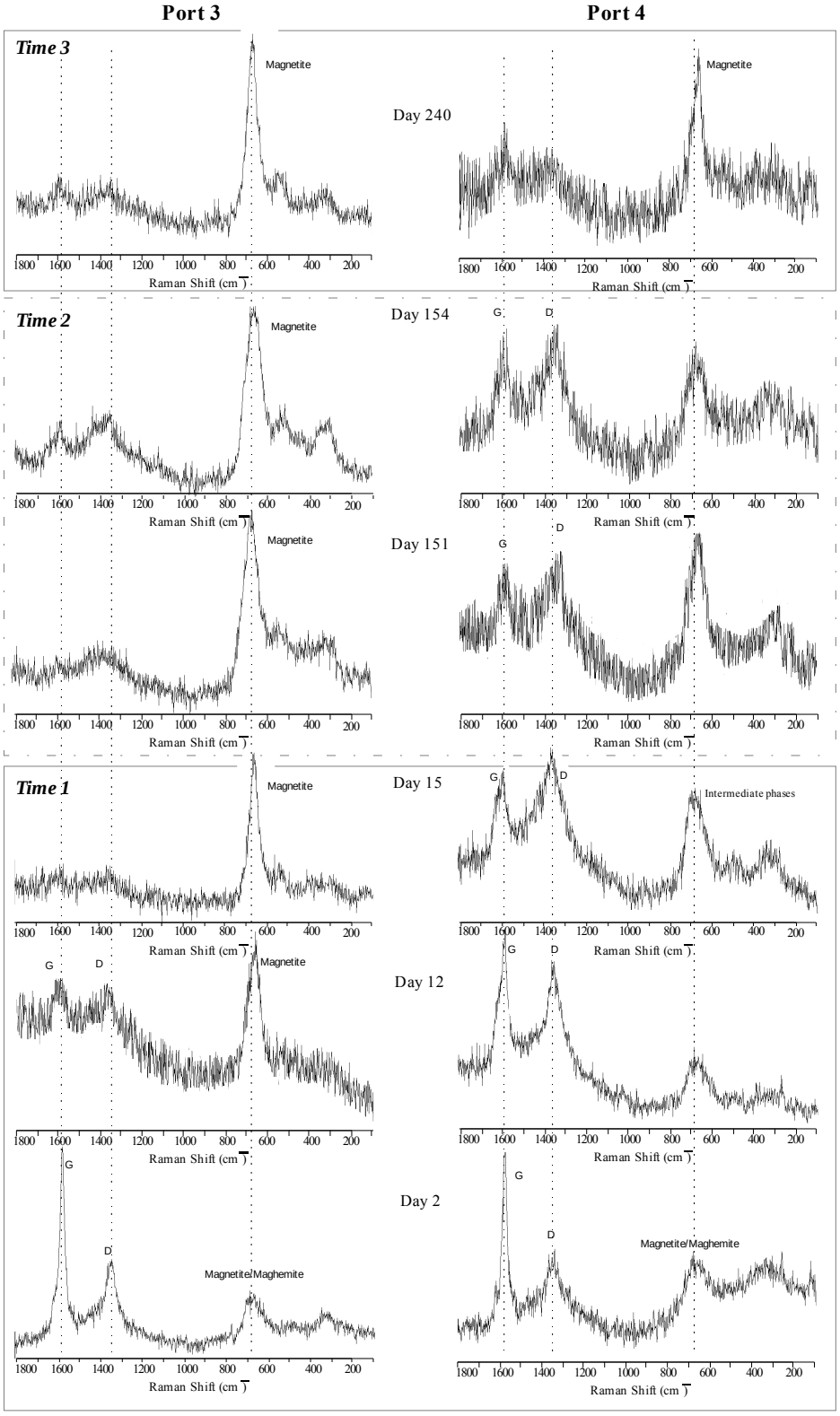

Figure 6.14: Raman spectra collected on red side from port 3 and 4 during T_1, T_2 and T_3.

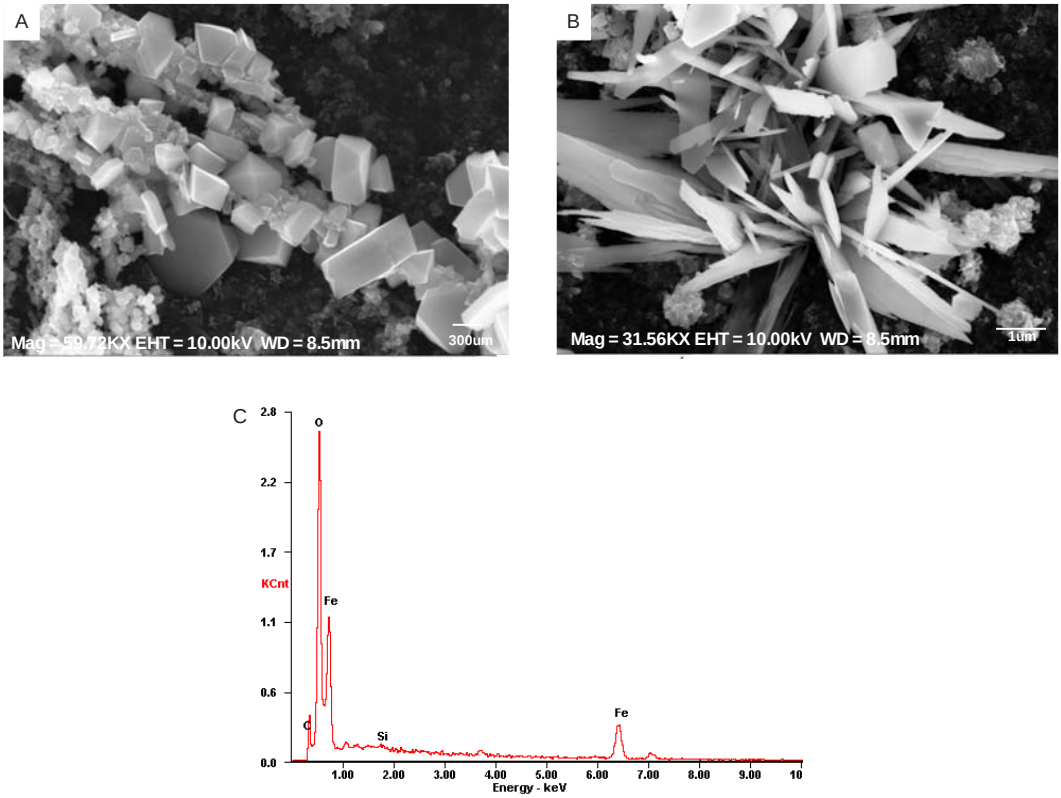

Figure 6.15: SEM images collected after T_3 showing (A) octahedral crystals tentativelyu identified as magnetite and (B) a lath-like or tabular mineral tentatively identified as lepidocrocite. Identificatoins were based on crystal habit and chemical composition as determined by EDS. (C) representative EDS analysis of (A).

The maghemite band occurring as a shoulder on the magnetite band, at 715 cm^{-1}, also disappeared soon after the grains were immersed in water.

The appearance of bands at 345 cm^{-1}, 510 cm^{-1} and 710 cm^{-1}, which are in the finger print region of iron oxides and (oxy)hydroxides, including the possible phases ferrihydrite (Hanesch, 2009), $Fe(OH)_3$ and/or amorphous FeOOH, goethite (α-FeOOH) and lepidocrocite (γ-FeOOH), green rust (de Faria *et al.*, 1997; Dünnwald and Otto, 1989; Roh *et al.*, 2000), appeared within 48 hours of column flooding. They were especially noticeable on the grain from port 1 which was closest to the inlet. These phases may have acted as intermediates in the formation of magnetite (Sumoondur *et al.*, 2008) and are therefore regarded here as intermediate phases. In

the presence of Fe^{2+}, lepidocrocite has been shown to transform gradually to crystals of magnetite (Eq. 6.4) (Tamaura *et al.*, 1983) (Figure 6.15A, B)

$$2FeOOH + Fe^{2+} \rightarrow Fe_3O_4 + 2H^+ \qquad \text{Eq. 6.4}$$

Goethite and magnetite bands close to 700cm^{-1} may overlap when both phases are present, but magnetite produces the stronger signal and therefore tends to dominates if both are present in quantity (Neff *et al.*, 2004). The shift from a broad band at 710 cm^{-1} to a sharp, narrow band at 670cm^{-1} is associated with the completion of a phase transition to magnetite (Dünnwald and Otto, 1989).

It was noted that the occurrence and predominance of the mineral phases or phase transitions varied with distance along the column. It is clearly evident from spectra collected from all 4 ports that a transformation front, evident at early time near influent end of the column, progressed at least halfway down the column after 240 days (ports 2, 3 and 4) (Figures 6.13 and 6.14). The greater progress of corrosion at port 1 at the end of the experiment was due its close proximity to inlet source and therefore a relatively high degree of exposure to TCE and traces of dissolve oxygen that may have been present in the influent. By comparison, the other ports would have been exposed to less of these solutes because they were reduced as they moved through the columns.

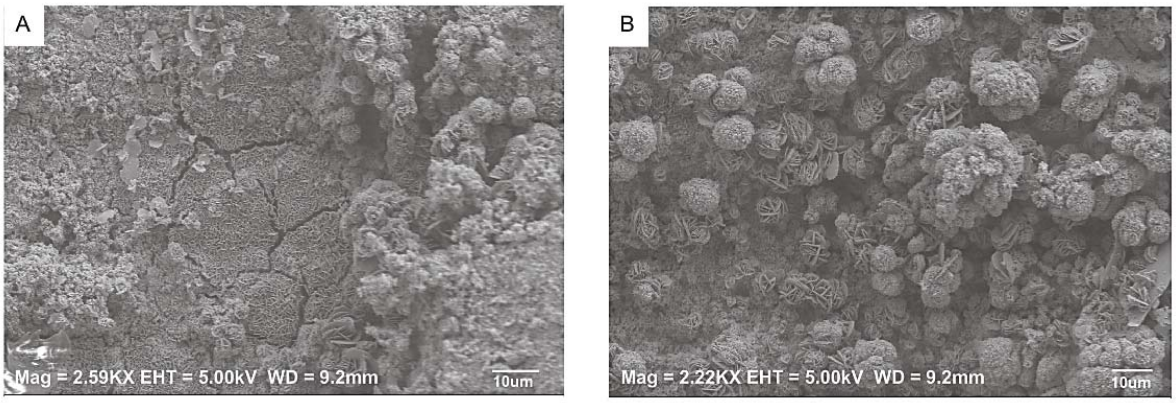

Figure 6.16: SEM micrographs of treated iron surface showing (A) Fe (oxy)hydroxides (B) goethite

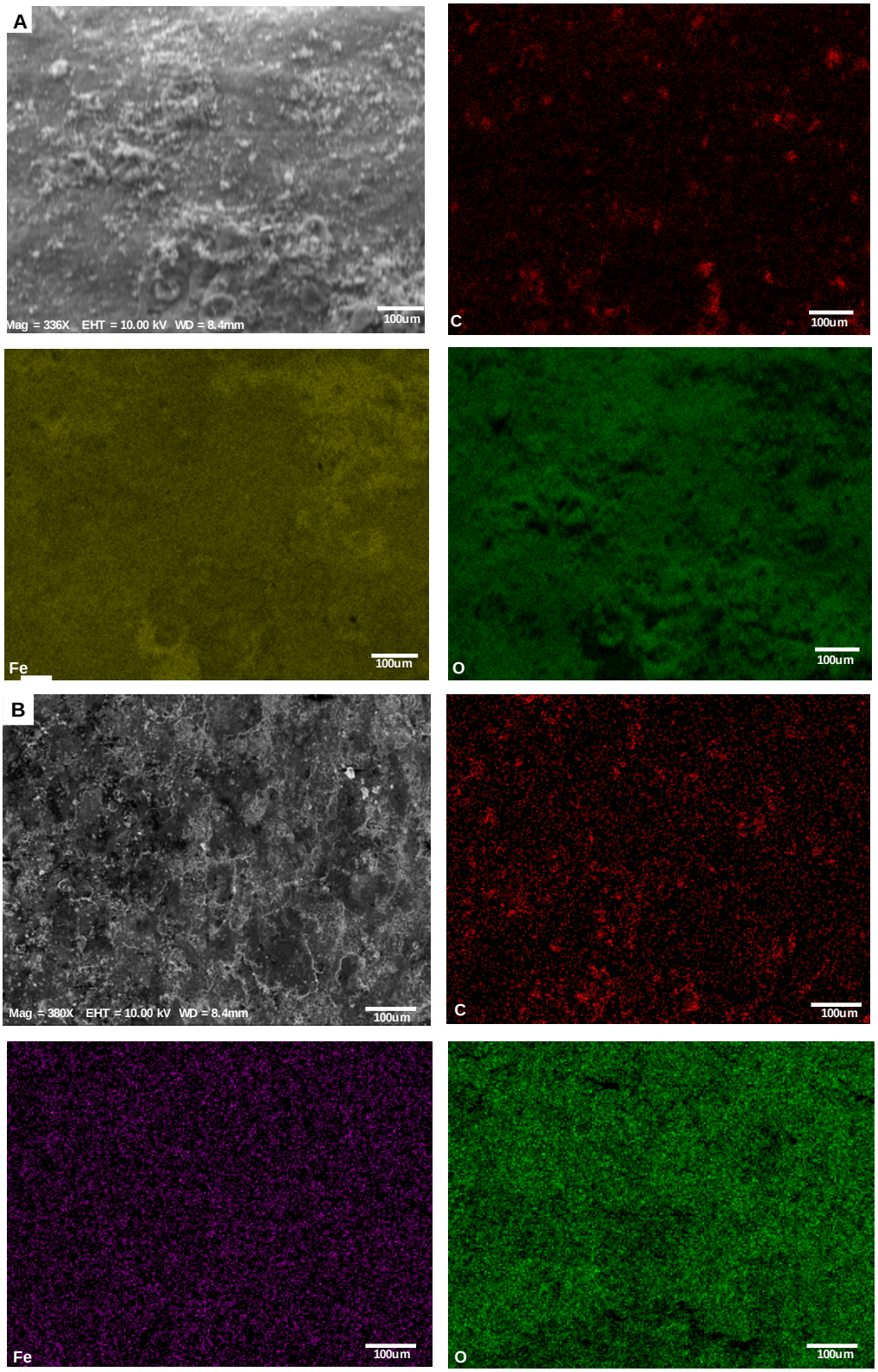

Figure 6.17: EDS maps for elemental distribution of C, Fe, and O on (A) untreated GI and (B) after 240 days of treatment.

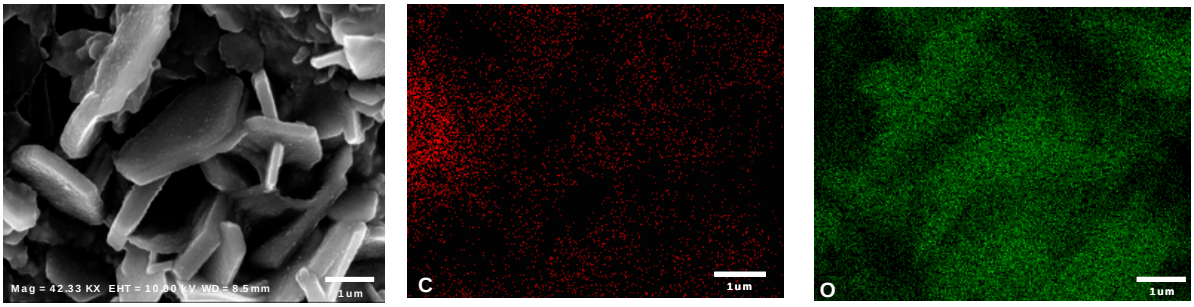

Figure 6.18: SEM micrograph of green rust and elemental distribution of C and O after 240 days of treatment. The presence of carbon in these micrographs suggests the presence of inorganic carbon on the aged grains.

As in the cases of the iron phases, surface carbon also underwent changes, as indicated by variations in the D and G Raman bands. High corrosion close to inlet resulted in disappearance of carbon bands from port 1 during the first 15 days of exposure to solution, whereas ports 2 and 3 only experienced a more gradual decrease in intensities over a 5 month period (Figures 6.13, 6.14). In keeping with this trend, the D and G bands weakened but never completely disappeared in spectra collected from ports 3 and 4 over the approximately 8 month time of the experiment (Figure 6.14).

SEM micrographs and EDS collected on the untreated iron surface and on the iron surface aged in the column for 240 days showed differences in carbon distribution. The untreated grains showed more intense and patchy distributions of carbon compared to the aged grains (Figure 6.17A, B). Much of the carbon distribution on EDS map after 240 days was found to be similar with respect to oxygen indicated a difference in the characteristics of surface carbon- from sp^2 CM to the form found in the corrosion product such as green rust (Min *et al.*, 2009) (Figure 6.18).

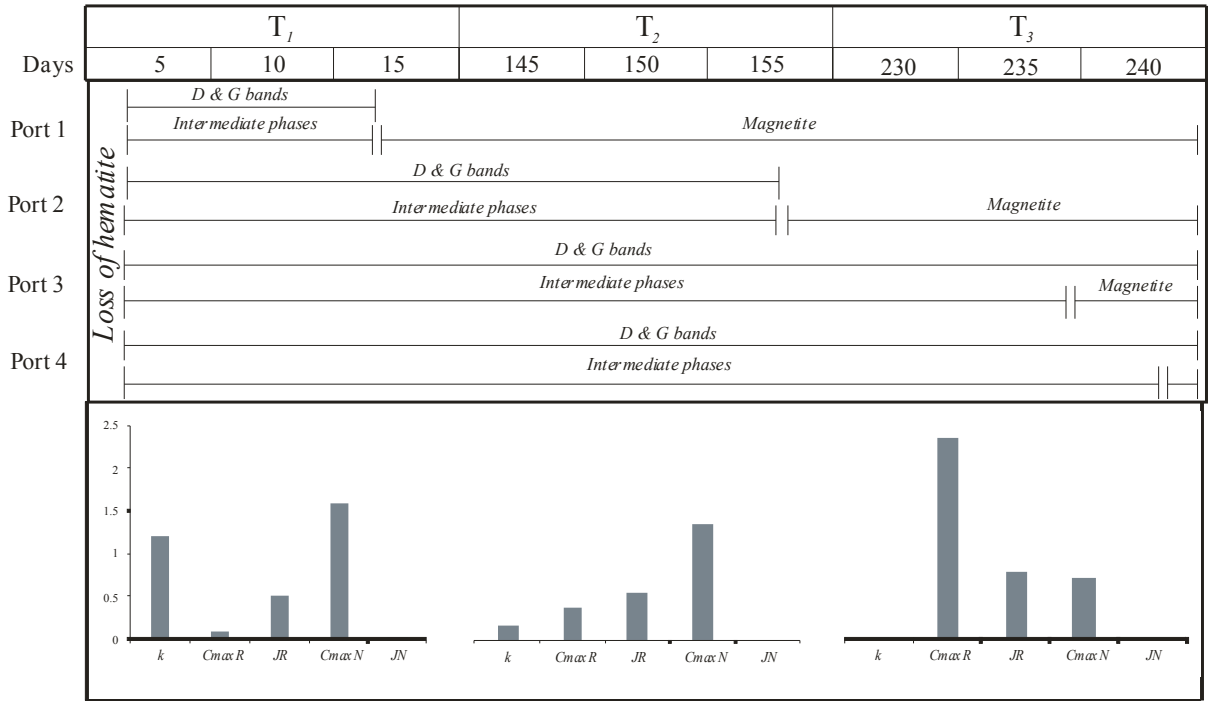

Figure 6.19: Image showing the movement of front through all 4 ports over time. Magnitude of sorption and kinetic parameters were also plotted against each time. (Note: Parameter J_R and J_N have been exaggerated 10x)

6.4.4. Reconciliation of Micro-Scale Observations and Macro-Scale Kinetics

The analysis of TCE reduction kinetics showed declines in both TCE non-reactive sorption and reactivity over time, with the more profound changes occurring at earlier times (Figure 6.19). This trend is consistent with previous findings (Devlin *et al.*, 1998). These changes coincided with the spectroscopy-based observations that near the inlet side of the column a near complete conversion of Fe^{3+} oxides (e.g., hematite) to mixed valent oxides (e.g., magnetite) occurred. This finding is also consistent with earlier work (Odziemkowski *et al.*, 1998). In addition, at the ports nearest the inlet, there was a complete loss of signal from sp^2 carbon from the grain surfaces. To our knowledge, this observation has not previously been reported. Near the outlet end of the column these same changes were underway, but had not progressed to the same degree by the end of the experiment (240 days).

In order to reconcile the above experimental results, it must first be recognized that while the spectroscopic data were very location specific, coinciding to changes on several grains at particular distances from the inlet, the kinetic data represent column averages. Together, these two views of the same column can provide a compelling picture of the column chemodynamics over time. For example, the fact that the mineral and carbon alterations did not progress at the same rates everywhere along the column simultaneously strongly suggests the existence of a reaction front that progressed along the column with time. Reaction fronts have been described for granular iron columns in the past, but these were primarily associated with carbonate precipitation (Jeen *et al.*, 2006; Zhang and Gillham, 2005). In this work, the 'front' can be defined as either 1) the disappearance of hematite, 2) the dominant emergence of magnetite, or 3) the disappearance of sp^2 carbon. However it is defined, the front represents a boundary between a more reactive zone in the column and a less reactive, or weathered zone. As the weathered zone increases in size, the column-averaged kinetics indicates ever declining reactivities.

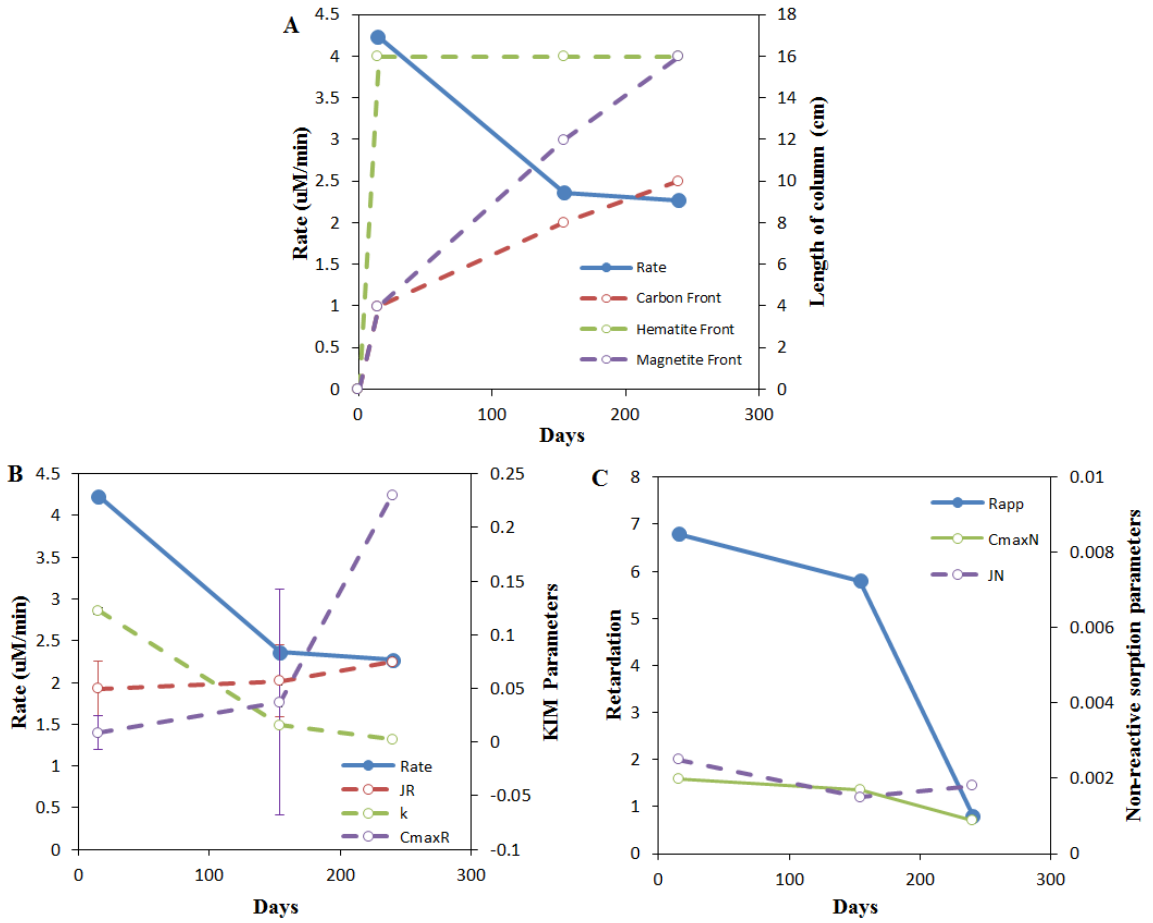

Figure 6.20: Graphical representations of A) Rate versus hematite, magnetite and carbon fronts B) comparison of rate with the KIM parameters and C) comparison of rate with non-reactive sorption parameters. Solid lines connect data points read from the left axes and broken lines connect data points read from the right axes.

To help determine which of the three 'fronts' is most relevant to the reactivity declines observed, correlations between reaction rates ($k_{app}C_o$) and both time and distance along the column were overlain on the approximate positions of the fronts, as indicated from the Raman analyses (Figure 6.20). Spectroscopic measurements collected through time indicate that the kinetics of hematite transformation and the appearance of magnetite was relatively fast (Figure 6.20A). In fact, hematite was removed from all ports within 2 days of contact with solution, suggesting a process more tied to a surface reaction involving water than with TCE. The

magnetite front appeared at 4cm from inlet within 15 days of experiment and moved through column in 240 days. Although the magnetite front moved slower than the hematite front, it did not exhibit the same declining rate of progression as the reactivity front did (Figure 6.20A). Of the three fronts (hematite, magnetite and carbon), the loss of sp^2 carbon front appears to show a behavior that is most consistent with the reactivity front behavior. While reactivity declined rapidly at first and then more slowly later in the experiment, the carbon front appeared to move rapidly into the column early in the experiment (up to day 150), and then slow in its progression later (days 150-240). Since at least one reported study demonstrated that carbon can serve as a reactive sorption site for aqueous organics (Oh *et al.*, 2002), the corresponding alteration of the surface carbon and decline in reactivity and k is evidence that the GI surface carbon serves as a reactive surface (Figure 6.20 B).

In addition to its importance to the reactivity front, changes to surface carbon also coincided well with the observed trends in retardation over time. Distinctly, with the weakening of Raman signals for surface carbon, the non-reactive sorption parameter, R_{app} was also determined to be decreasing in magnitude (Figure 6.20C). Therefore, carbon sites, known for their strong propensity to act as a sorbent of hydrophobic substances (Cornelissen *et al.*, 2005; Deng *et al.*, 1997) may represent the most important sites for TCE interactions with GI (Table 6.2).

If it can be concluded that surface carbon is an important location for TCE sorption and transformations, a closer examination of the nature of the surface carbon is merited. To begin this examination, it is noteworthy that the sorption affinity parameters, J_R and J_N, changed relatively little over the course of the experiment, suggesting that the dominant sorbing surface phase(s) remained so throughout the experiment. Since oxides can be virtually ruled out as

sorbing surfaces for hydrophobic organics (Smith, 1998; Klausen *et al.,* 1995), it follows that both J_R and J_N are most likely associated with surface carbon. However, the magnitude of J_R was estimated to be about an order of magnitude greater than that of J_N, suggesting the presence of at least two forms of carbon, with different sorption affinities for TCE.

To explore the possibility of two or more carbon types being present on the GI, the sp^2 carbon, as it presented on the two distinct sides of GI (shiny and red), was examined. On average, spectra collected from the red side was determined to indicate carbon that was more ordered or graphitic, on the basis of the relative intensities of the G bands, and low I_D/I_G ratios, compared to the carbon bands observed on the shiny side of the GI, and similar carbon bands recorded from electrolytic iron (appendix H). It is suggestive that two spectroscopically distinct carbon types, or end members of a continuum of carbon occurrences, were identifiable on the same samples that produced two distinct sorption affinities presumably related to carbon. The likelihood that these two observations are related is further supported by the studies of electrolytic iron (Chapter 5), which showed that the more micro-crystalline form of carbon exhibited very low sorption behavior. By process of elimination, the more ordered carbon form, dominating the red oxide layer, would be responsible for the higher sorption affinities, and is most closely associated with the reactive sites on the GI.

These finding suggests that surface carbon serves as a non-reactive sorption sites as well as a reactive one. The fact that none of the oxide phases is considered a good sorbing surface for aqueous hydrophobic organics, or that organic reduction reactions involving these phases without the presence of metallic iron proceed relatively slowly (Burris *et al.*, 1998; Smith, 2001) argues against the oxides dominating the reaction rates. Nonetheless, organic reduction reactions are well documented in association with iron oxide surfaces (Noubactep, 2008; Pecher *et al.*,

2002; Wilkin *et al.*, 2003), so there can little doubt that the oxides contribute something to the overall reaction rates.

6.5. Conclusions

Column experiment and spectroscopic investigations were conducted to document the surface changes on GI exposed to simulated contaminated groundwater, and to link those micro-scale changes to the macro-scale changes in the KIM parameters. It was observed that R_{app} for GI followed a non-linear trend over the range of input TCE concentrations and was greatest for $C_o <$ 100 μmol. Retardation factors were found to be higher in young columns than aged ones, with R_{app} dropping significantly during the periods 140 – 154 days, and 220 – 240 days. Trends in KIM parameters suggested systematic changes in kinetic and sorption parameters over time. In columns 0-15 days old, high TCE reduction rates were observed in conjunction with relatively large values of k and small values of C_{maxR}. These findings are consistent with those reported by Huang (2011) and suggest the kinetics were dominated by a small number of highly reactive sites. GI observed decline in affinity to reactive sites (J_R) from 0-15 days to 140-154 days but not noticeable difference was found between 140-154 to 220- 240 days. At later times (220-240 days), k tended to decline and C_{maxR} to increase, suggesting that the kinetics were becoming dominated by a larger number of less reactive sites with aging of the GI. Throughout these changes the sorption affinity changed relatively little, indicating a general consistency in the sorption behavior of the reactive sites, i.e., carbon dominated throughout the experiment.

Spectroscopic analysis of the surface phases on GI in space and time revealed 3 possible fronts that could be related to the reactivity decline in the GI over time. Once again, the data indicated the closest correspondence between reactivity and surface phase changes involved carbon.

Both the kinetic and spectroscopic work identifies variations in carbon, based on sorption behavior and degree of microcrystallinity, respectively. Connelly GI was characterized by a reactive, high affinity carbon type, and a non-reactive, low affinity type. The former was found to exhibit a relatively more ordered crystalline form compared to the latter, based on Raman analyses of the oxidized and shiny sides of the GI, and analogous tests on electrolytic iron that only display a shiny side. From these findings, it is concluded that the dominant, but not exclusive, reactive sites on Connelly GI are associated with carbon in the oxide layer. As the iron ages, the carbon is increasingly isolated from the solution by burial beneath an ever-increasing thickness of oxide layer. It is anticipated that over much greater time periods than were investigated here, the GI-TCE kinetics will become dominated by reductions on the oxides rather than the carbon, and the overall reactivity of the material will be correspondingly less than it was at early times.

References

Allin, K., 2000. Effect of water Geochemistry on the reactivity of granular iron., Earth Sciences. Waterloo, Ontario.

Bear, J., 1979. Hydraulics of Groundwater. McGraw- Hill International Book Co, New York.

Bi, E., Bowen, I.A.N., Devlin, J.F., 2009a. Effect of Mixed Anions (HCO_3^--SO_4^{2-}-ClO_4^-) on Granular Iron (Fe^0) Reactivity. Environmental Science and Technology, v. 43, no. 15, 7p.

Bi, E., Devlin, J.F., Huang, B., 2009b. Effects of Mixing Granular Iron with Sand on the Kinetics of Trichloroethylene Reduction. Ground Water Monitoring and Remediation, v. 29, no. 2, 56-62.

Bi, E., Devlin, J.F., Huang, B., Firdous, R., 2010. Transport and Kinetic Studies To Characterize Reactive and Nonreactive Sites on Granular Iron. Environmental Science and Technology, v. 44, no. 14, 5564-5569.

Blowes, D.W., Ptacek, C.J., Benner, S.G., McRae, C.W.T., Bennett, T.A., Puls, R.W., 2000. Treatment of inorganic contaminants using permeable reactive barriers. Journal of Contaminant Hydrology, v. 45, no. 1–2, 123-137.

Burris, D., Allen-King, R., Manoranjan, V., Campbell, T., Loraine, G., Deng, B., 1998. Chlorinated Ethene Reduction by Cast Iron: Sorption and Mass Transfer. Journal of Environmental Engineering, v. 124, no. 10, 1012-1019.

Burris, D.R., Wells, J.R., Campbell, T.J., Roberts, A.L., 1997. Trichloroethylene and tetrachloroethylene reduction in a metallic iron-water-vapor batch system. Environmental Toxicology and Chemistry, v. 16, no. 4, 0p.

Chawla, S.L., Gupta, R.K., 1993. Materials selection for Corrosion Control. ASM International, Materials Park, OH, 7 pp.

Cohen, M., 1978. The passivity and breakdown of passivity on iron. The Electrochemical Society, Pennington, NJ., 521-545 pp.

Cornelissen, G., Gustafsson, Ö., Bucheli, T.D., Jonker, M.T.O., Koelmans, A.A., van Noort, P.C.M., 2005. Extensive Sorption of Organic Compounds to Black Carbon, Coal, and Kerogen in Sediments and Soils: Mechanisms and Consequences for Distribution, Bioaccumulation, and Biodegradation. Environmental Science & Technology, v. 39, no. 18, 6881-6895.

de Faria, D.L.A., Venâncio Silva, S., de Oliveira, M.T., 1997. Raman microspectroscopy of some iron oxides and oxyhydroxides. Journal of Raman Spectroscopy, v. 28, no. 11, 873-878.

Deng, B., Campbell, T.J., Burris, D.R., 1997. Hydrocarbon Formation in Metallic Iron/Water Systems. Environmental Science & Technology, v. 31, no. 4, 1185-1190.

Devlin, J.F., 1994. A Simple and Powerful Method of Parameter Estimation Using Simplex Optimization. Ground Water, v. 32, no. 2, 323-327.

Devlin, J.F., 1996. A Method to Assess Analytical Uncertainties Over Large Concentration Ranges With Reference to Volatile Organics in Water. Ground Water Monitoring and Remediation, v. 16, no. 3, 179-185.

Devlin, J.F., 2009. Development and Assessment of a Rate Equation for Chemical Transformations in Reactive Porous Media. Environmental Science and Technology, v. 43, no. 11, 4113-4118.

Devlin, J.F., Allin, K.O., 2005. Major Anion Effects on the Kinetics and Reactivity of Granular Iron in Glass-Encased Magnet Batch Reactor Experiments. Environmental Science and Technology, v. 39, no. 6, 1868-1874.

Devlin, J.F., Klausen, J., Schwarzenbach, R.P., 1998. Kinetics of Nitroaromatic Reduction on Granular Iron in Recirculating Batch Experiments. Environmental Science and Technology, v. 32, no. 13, 1941-1947.
Dünnwald, J., Otto, A., 1989. An investigation of phase transitions in rust layers using raman spectroscopy. Corrosion Science, v. 29, no. 9, 1167-1176.
Farrell, J., Melitas, N., Kason, M., Li, T., 2000. Electrochemical and Column Investigation of Iron-Mediated Reductive Dechlorination of Trichloroethylene and Perchloroethylene. Environmental Science and Technology, v. 34, no. 12, 2549-2556.
Farrell, J., Wang, J., O'Day, P., Conklin, M., 2001. Electrochemical and spectroscopic study of arsenate removal from water using zero-valent iron media. Environ Sci Technol, v. 35, no. 10, 2026-2032.
Ferrari, A.C., Robertson, J., 2000. Interpretation of Raman spectra of disordered and amorphous carbon. Physical Review B, v. 61, no. 20, 14095-14107.
Furukawa, Y., Kim, J.-w., Watkins, J., Wilkin, R.T., 2002. Formation of Ferrihydrite and Associated Iron Corrosion Products in Permeable Reactive Barriers of Zero-Valent Iron. Environmental Science & Technology, v. 36, no. 24, 5469-5475.
Gillham, R.W., O'Hannesin, S.F., 1994. Enhanced Degradation of Halogenated Aliphatics by Zero-Valent Iron. Ground Water, v. 32, no. 6, 958-967.
Gillham, R.W., Vogan, J., Gui, L., Duchene, M., Son, J., 2010. Iron Barrier Walls for Chlorinated Solvent Remediation.In Situ Remediation of Chlorinated Solvent Plumes, In: Stroo, H.F., Ward, C.H. (Eds.). Springer New York, pp. 537-571.
Gotpagar, J., Grulke, E., Tsang, T., Bhattacharyya, D., 1997. Reductive dehalogenation of trichloroethylene using zero-valent iron. Environmental Progress, v. 16, no. 2, 137-143.
Gu, B., Watson, D.B., Wu, L., Phillips, D.H., White, D.C., Zhou, J., 2002. Microbiological characteristics in a zero-valent iron reactive barrier. Environ Monit Assess, v. 77, no. 3, 293-309.
Hanesch, M., 2009. Raman spectroscopy of iron oxides and (oxy)hydroxides at low laser power and possible applications in environmental magnetic studies. Geophysical Journal International, v. 177, no. 3, 8p.
Hansson, E.B., Odziemkowski, M.S., Gillham, R.W., 2006. Formation of poorly crystalline iron monosulfides: Surface redox reactions on high purity iron, spectroelectrochemical studies. Corrosion Science, v. 48, no. 11, 3767-3783.
Hansson, E.B., Odziemkowski, M.S., Gillham, R.W., 2008. Influence of Na2S on the degradation kinetics of CCl4 in the presence of very pure iron. Journal of Contaminant Hydrology, v. 98, no. 3-4, 128-134.
Hardy, L.I., Gillham, R.W., 1996. Formation of Hydrocarbons from the Reduction of Aqueous CO2 by Zero-Valent Iron. Environmental Science & Technology, v. 30, no. 1, 57-65.
Huang, B., 2011. Separating the Kinetic and Sorption Parameters of Mixed Chlorinated Solvents in Contact with Granular Iron, Geology. University of Kansas, Lawrence, p. 163.
Jeen, S.W., Gillham, R.W., Blowes, D.W., 2006. Effects of carbonate precipitates on long-term performance of granular iron for reductive dechlorination of TCE. Environ Sci Technol, v. 40, no. 20, 6432-6437.
Jeen, S.W., Mayer, K.U., Gillham, R.W., Blowes, D.W., 2007. Reactive transport modeling of trichloroethene treatment with declining reactivity of iron. Environmental Science and Technology, v. 41, no. 4, 1432-1438.
Knight, D.S., White, W.B., 1989. Characterization of diamond films by Raman spectroscopy. Journal of Materials Research, v. 4, no. 2, 385-393.

Landis, R.L., Gillham, R. W., Reardon, E. J., Fagan, R., Focht, R. M., Vogan, J.L., 2001. An examination of zero-valent iron sources used in permeable reactive barriers., 3rd International Containment Technology Conference. Florida State University, Tallahassee, Orlando, FL, p. 5.

Liang, L., Korte, N., Gu, B., Puls, R., Reeter, C., 2000. Geochemical and microbial reactions affecting the long-term performance of in situ 'iron barriers'. Advances in Environmental Research, v. 4, no. 4, 273-286.

Liang, L.Y., N. Korte, JD, Goodlaxson, J, Clausen al. , 1997. Byproduct formation during the reduction of TCE by zero-valence iron and palladized iron. Ground Water Monitoring and Remediation, v. 17, no. 1, 122-127.

Lo, I.M.-C., Surampalli, R.Y., Lai, K.C.K., Environmental and Water Resources Institute (U.S.). Hazardous Toxic and Radioactive Waste Management Committee., 2007. Zero-valent iron reactive materials for hazardous waste and inorganics removal. American Society of Civil Engineers, Reston, Va.

Mackenzie, P.D., Horney, D.P., Sivavec, T.M., 1999. Mineral precipitation and porosity losses in granular iron columns. Journal of Hazardous Materials, v. 68, no. 1–2, 1-17.

Marietta, M.L., Devlin, J.F., 2005. In Bringing Groundwater Quality Research to the Watershed Scale 4th International Groundwater Quality Conference. IAHS, Waterloo, Canada, pp. 376-382.

Marshall, C.P., Edwards, H.G., Jehlicka, J., 2010. Understanding the application of Raman spectroscopy to the detection of traces of life. Astrobiology, v. 10, no. 2, 229-243.

Marshall, A.O., Emry, J.R., Marshall, C.P., 2012. Multiple generations of carbon in the apex chert and implications for preservation of microfossils. Astrobiology, v. 12, no. 2, 160-166.

Marshall, C.P., Marshall, A.O., 2011. Hematite and carbonaceous materials in geological samples: A cautionary tale. Spectrochimica Acta Part A: Molecular and Biomolecular Spectroscopy, v. 80, no. 1, 133-137.

Min, J.E., Park, I.S., Ko, S., Shin, W.S., Park, J.W., 2009. Effect of phosphate and sediment bacteria on trichloroethylene dechlorination with zero valent iron. Journal of Environment Science and Health, Part A Environmental Science, v. 44, no. 4, 362-369.

Moore, A.M., De Leon, C.H., Young, T.M., 2003. Rate and Extent of Aqueous Perchlorate Removal by Iron Surfaces. Environmental Science and Technology, v. 37, no. 14, 3189-3198.

Neff, D., Reguer, S., Bellot-Gurlet, L., Dillmann, P., Bertholon, R., 2004. Structural characterization of corrosion products on archaeological iron: an integrated analytical approach to establish corrosion forms. Journal of Raman Spectroscopy, v. 35, no. 8-9, 739-745.

Noubactep, C., 2008. A critical review on the process of contaminant removal in Fe0-H2O systems. Environ Technol, v. 29, no. 8, 909-920.

Odziemkowski, M., Gillham, R., 1997. Surface redox reactions on commercial grade granular iron (steel) and their influence on the reductive dechlorination of solvent. Micro Raman Spectroscopic Studies, 213th ACS National Meeting, April, pp. 13-17.

Odziemkowski, M.S., Schuhmacher, T.T., Gillham, R.W., Reardon, E.J., 1998. Mechanism of oxide film formation on iron in simulating groundwater solutions: Raman spectroscopic studies. Corrosion Science, v. 40, no. 2–3, 371-389.

Oh, S.-Y., Cha, D.K., Chiu, P.C., 2002. Graphite-Mediated Reduction of 2,4-Dinitrotoluene with Elemental Iron. Environmental Science & Technology, v. 36, no. 10, 2178-2184.

Pecher, K., Haderlein, S.B., Schwarzenbach, R.P., 2002. Reduction of Polyhalogenated Methanes by Surface-Bound Fe(II) in Aqueous Suspensions of Iron Oxides. Environmental Science & Technology, v. 36, no. 8, 1734-1741.

Phillips, D.H., Gu, B., Watson, D.B., Roh, Y., 2003. Impact of sample preparation on mineralogical analysis of zero-valent iron reactive barrier materials. Journal of Environment Quality, v. 32, no. 4, 1299-1305.

Phillips, D.H., Gu, B., Watson, D.B., Roh, Y., Liang, L., Lee, S.Y., 2000. Performance Evaluation of a Zerovalent Iron Reactive Barrier: Mineralogical Characteristics. Environmental Science and Technology, v. 34, no. 19, 4169-4176.

Pimenta, M.A., Dresselhaus, G., Dresselhaus, M.S., Cancado, L.G., Jorio, A., Saito, R., 2007. Studying disorder in graphite-based systems by Raman spectroscopy. Physical Chemistry Chemical Physics, v. 9, no. 11, 1276-1290.

Ritter, K., Odziemkowski, M.S., Gillham, R.W., 2002. An in situ study of the role of surface films on granular iron in the permeable iron wall technology. Journal of Contaminant Hydrology, v. 55, no. 1-2, 87-111.

Ritter, K., Odziemkowski, M.S., Simpgraga, R., Gillham, R.W., Irish, D.E., 2003. An in situ study of the effect of nitrate on the reduction of trichloroethylene by granular iron. Journal of Contaminant Hydrology, v. 65, no. 1-2, 121-136.

Roh, Y., Lee, S.Y., Elless, M.P., 2000. Characterization of corrosion products in the permeable reactive barriers. Environmental Geology, v. 40, no. 1-2, 184-194.

Rouzaud, J.N., Oberlin, A., Beny-Bassez, C., 1983. Carbon films: Structure and microtexture (optical and electron microscopy, Raman spectroscopy). Thin Solid Films, v. 105, no. 1, 75-96.

Sasaki, K., Blowes, D.W., Ptacek, C.J., Gould, W.D., 2008. Immobilization of Se(VI) in mine drainage by permeable reactive barriers: column performance. Applied Geochemistry, v. 23, no. 5, 1012-1022.

Schultze, J., 1978. Electron transfer reactions on passive films. J. W. Schultze, Free Univ. of Berlin, W. Germany, Passivity of Metals, Frankenthal and Kruger(eds.), 82-101.

Sivavec, T.M., Horney, D.P., 1995. Reductive Dechlorination of Chlorinated Ethenes by Iron Metal. Abstracts of Papers of the American Chemical Society, v. 209, 128-ENVR.

Smith, M.P., 2001. Using 4-chloroaniline to Investigate the sorption characteristics of granular iron Earth Sciences. University of Waterloo, Waterloo, Ontario, Canada.

Su, C.M., Puls, R.W., 1999. Kinetics of trichloroethene reduction by zerovalent iron and tin: Pretreatment effect, apparent activation energy, and intermediate products. Environmental Science and Technology, v. 33, no. 1, 163-168.

Sumoondur, A., Shaw, S., Ahmed, I., Benning, L., 2008. Green rust as a precursor for magnetite: an in situ synchrotron based study. Mineralogical Magazine, v. 72, no. 1, 201-204.

Tamaura, Y., Ito, K., Katsura, T., 1983. Transformation of [gamma]-FeO(OH) to Fe3O4 by adsorption of iron(II) ion on [gamma]-FeO(OH). Journal of the Chemical Society, Dalton Transactions, v. 0, no. 2, 189-194.

Thibeau, R.J., Brown, C.W., Heidersbach, R.H., 1978. Raman Spectra of Possible Corrosion Products of Iron. Applied Spectroscopy, v. 32, no. 6, 532-535.

Tuinstra, F., Koenig, J.L., 1970. Raman Spectrum of Graphite. The Journal of Chemical Physics, v. 53, no. 3, 1126-1130.

Uhlig, H.H., 1956. Initial oxidation rate of metals and the logarithmic equation. Acta Metallurgica, v. 4, no. 5, 541-554.

Vikesland, P.J., Klausen, J., Zimmermann, H., Roberts, A.L., Ball, W.P., 2003. Longevity of granular iron in groundwater treatment processes: changes in solute transport properties over time. J Contam Hydrol, v. 64, no. 1-2, 3-33.

Wilkin, R.T., Acree, S.D., Ross, R.R., Beak, D.G., Lee, T.R., 2009. Performance of a zerovalent iron reactive barrier for the treatment of arsenic in groundwater: Part 1. Hydrogeochemical studies. Journal of Contaminant Hydrology, v. 106, no. 1–2, 1-14.

Wilkin, R.T., Puls, R.W., Sewell, G.W., 2003. Long-term performance of permeable reactive barriers using zero-valent iron: geochemical and microbiological effects. Ground Water, v. 41, no. 4, 493-503.

Zhang, Y., Gillham, R.W., 2005. Effects of gas generation and precipitates on performance of Fe0 PRBs. Ground Water, v. 43, no. 1, 113-121.

7. Conclusions and Recommendations.

Previous studies utilized the Kinetic Iron Model (KIM) (Devlin, 2009) to yield unique estimates of surface-reaction rate constant (k) and sorption parameters (C_{maxR}, J_R), and documented the contribution of the associated processes to reactivity as iron aged in contact with aqueous chlorinated solvents. In this work, the use of KIM was extended to establish cross-scale links between iron grain surface chemistry and the macroscopic kinetic measurements mentioned above. Image analysis techniques were used to explore factors that were important at pore scale. A novel column design was developed with which it was possible to obtain data sets from both the micro and macro scales. Spectroscopic and scanning electron microscope techniques were used to investigate micro-scale characteristics on the iron grains as a function of age.

With the KIM, unique estimates of reaction and sorption parameters were obtained and analyzed through original data processing software. Long-term column experiments revealed that young GI kinetics were dominated by a relatively small number of highly reactive sites (k). As iron aged in TCE solution and water, k declined, indicating that the iron surface lost these highly reactive sites, but C_{maxR} increased, suggesting that the kinetics were becoming dominated by a larger number of less reactive sites.

Pore scale investigations on GI diluted with sand supports an earlier hypothesis suggested by Bi *et al*. (2009) that observable reactivity was a function of GI surface area available to solution, which was in turn a function of the sand content. With the help of image analysis on the sectioned columns, it was found that the addition of sand to GI opened up pore spaces between iron grains, exposing more grain surface to solution. This was clearly reflected in a reported reactivity maximum associated with the addition of 15% sand by weight to GI (Bi *et al.*, 2009). Both the kinetic and visualization techniques support this finding. Barriers constructed without

sand will achieve grain packings that limit solution availability to the iron surface, particularly when the iron grains are platy in texture, as in case of Connelly Iron.

The (indirect) effect of grain shape on the reactivity of commercially available GI has received very little attention and was never experimentally established. This work, for the first time, addressed this issue and demonstrated that reactivity of GI varies in columns packed in varying styles. It was found that columns packed with grains oriented preferentially horizontally and those packed randomly led to quite similar GI reactivities. However, these grain orientations may not be very representative of packings in PRBs, which are expected to be effectively packed with grains oriented parallel to the flow direction, i.e., equivalently to a vertical direction in the column experiments conducted here. The laboratory tests of columns with vertically packed grains exhibited 2-4 times higher reaction rates than columns with the other packings, with important implications for the execution of benchtop treatability studies in columns. The differences in grain surface availability to solution due to packing variations were assessed by image analysis of sectioned columns. The sections showed significant differences in the spatial distribution of grains and pore network as a function of packing. However, it was found that pore scale differences were insufficient to explain the observed reactivity difference of 2-4 times between packings. It was suggested that micro-scale changes on grain surface account for the remaining reaction rates.

Separate column experiments together with spectroscopic investigations were conducted to document the changes to the GI surface that resulted from exposure to water, and TCE in solution. The data were also used to relate the observed micro-scale changes to the macro-scale changes in the KIM parameters. KIM parameters suggested systematic changes in kinetic and sorption parameters over time. The change in kinetic behavior of GI occurred simultaneously

with the progressive invasion of a reactivity front that moved through the column over time. The initial decline in reactivity (*dC/dt*) due to declining *k* was to some degree offset by the increase in C_{maxR} allowing the GI to maintain its reactivity for a longer period of time than might be expected. Similar to reactivity front, an absorption front, defined by a decline in TCE retardation over time (R_{app}) also moved through the iron media as it aged. It was observed that R_{app} for GI followed a non-linear trend as a function of input TCE concentrations and was greatest at low initial concentrations and decreased with increasing concentrations and age.

Based on macro and micro scale examinations it is concluded that the most profound changes to the TCE reduction and grain surfaces occurred within the first 150 days of experiment. As discussed previously, major changes in KIM parameters were accompanied by declines in *k* estimates and increases in C_{maxR}, whereas significant declines in retardation were associated with the loss of non-reactive sorption sites, reflected in the C_{maxN} parameter. Compared to these parameters, little change was observed in the sorption affinities for both reactive and non-reactive sites, J_R and J_N, indicating a general consistency in the sorption behavior, and the possibility that the sorbing surface was chemically similar throughout the experiments.

Spectroscopic analysis revealed 3 possible fronts that could be related to the reactivity decline in the GI. The spatial and temporal changes associated with carbon, as observed on Raman spectra, corresponded well in timing to the declining reactivity. Attributing the carbon front as the primary influence on reactivity front is a novel contribution of this work. Additionally, changes to surface carbon also coincided well with the observed trends in retardation over time, validating its importance to non-reactive sites as well.

Based on spectroscopic findings and sorption behavior, variations in carbonaceous material were examined. Connelly GI was found to contain a reactive, hydrophobic carbon type with a relatively high affinity for TCE, and a non-reactive, low-affinity type. The former was found to exhibit a relatively more ordered crystalline form compared to the latter, based on Raman analyses of two morphologically distinct sides on the Connelly iron grains: a oxidized side with a strong presence of red minerals (oxides) and a metallic side, similar in appearance to electrolytic iron. From these findings, and comparisons with the electrolytic iron (which has no highly oxidized surface area when new) it is concluded that the dominant reactive sites on Connelly GI are associated with carbon in the oxide layer. As the iron ages, these carbon sites become increasingly coated with oxides and become inaccessible to the solution. It is anticipated that for very long-term exposures to TCE (thousands of pore volumes) the GI/TCE reaction kinetics will become dominated by reductions on the oxides rather than the carbon, and the overall reactivity of the material will be correspondingly less than it was at early times.

7.1. Recommendations

Column experiments are required over much greater time periods than were investigated in this work to observe the carbon front move completely through the column and to document and compare the TCE reduction kinetics and changes to surface carbon at early times, middle, and much later times carbon is virtually inaccessible to the solution.

Improvements in the column design are necessary to better link the scale specific processes. This can be done by adding sampling ports along the length of column to collect effluents samples from locations other than the end of the column. This will help in delineating the exact position of reactivity front between sampling ports, although additional design changes may become necessary to ensure that TCE is present in all samples for some period of time in order

for the KIM analysis to be possible. This constraint was the reason sampling ports for solution were not included in the current design. Both iron grain and effluents samples collected from the same location could provide a more accurate correspondence between micro-scale and macro-scale changes along the reactivity front(s).

At present, the BEARKIMPE program is designed to process six experiments in a suite. An improvement in the code is required to handle a larger data set and to provide more options for the user to stop the code, refit curves or delete sheets, for convenience in data processing.

References

Bi, E., Devlin, J.F., Huang, B., 2009. Effects of Mixing Granular Iron with Sand on the Kinetics of Trichloroethylene Reduction. Ground Water Monitoring and Remediation, v. 29, no. 2, 56-62.

Devlin, J.F., 2009. Development and Assessment of a Rate Equation for Chemical Transformations in Reactive Porous Media. Environmental Science and Technology, v. 43, no. 11, 4113-4118.

APPENDICES

Appendix A. Statistical Assessment of KIM parameters

In order to assess the possibility that the addition of 15% by weight sand to a granular iron porous medium increases the sorption capacity of the metal for TCE, the KIM (eq A.1) was used to estimate the Langmuir parameters. The KIM was derived by Devlin (2009) and previously applied to the reduction of nitroaromatic compounds on granular iron.

$$\left(\frac{dC}{dt}\right)_o = \frac{kC_{max}\frac{Fe}{V}}{\frac{1}{J} + \frac{C_{max}\frac{Fe}{V}}{1+JC} + C_o} C_o \tag{A.1}$$

where k is the first order rate constant for reaction on the iron surface (min^{-1}), C_{max} represents maximum sorption capacity of the iron ($\mu mol\ g^{-1}$), J is sorption affinity to reactive sites on the iron (μM^{-1}) and Fe/V is the iron mass to water volume ratio ($g\ L^{-1}$). To estimate these parameters, series of column experiments were performed in which the magnitude of the influent concentration, C_o, was increased stepwise and the pumping continued to steady state at each step. The initial TCE reduction rate, $(dC/dt)_o$, was estimated by fitting the breakthrough curves

Table A. 1: Summary of column conditions and fitted KIM parameters. Parameter estimates given are means from the Monte Carlo analysis (see text).

Medium Description	Iron % by weight	Porosity	Fe/V_p (g/L)	k (min^{-1})	C_{max} ($\mu molg^{-1}$)	J (μM^{-1})
80 g iron	100%	0.55	4577	2.7E-02	3.0E-02	4.5E-02
68 g iron : 12 g sand	85%	0.46	4416	9.4E-03	1.0E-01	3.9E-02
60 g iron : 20 g sand	75%	0.49	3548	3.8E-02	5.1E-02	2.1E-03
40 g iron : 40 g sand	50%	0.47	2223	3.0E-02	2.1E-02	1.2E-02
Mean over all experiments				2.6E-02	5.1E-02	2.5E-02
StDev				1.2E-02	3.6E-02	2.1E-02
t-Inv	1.40003					
1-prob	0.744					

to a solution of the advection-dispersion equation with first order decay, and then multiplying the fitted rate constant, k_{app}, by C_o. These rates were then plotted against C_o and the resulting curve fitted with eq A.1 (see Figure 2.5B in Chapter 2) (Table A.1).

The fitting procedure was based on Gaussian nonlinear regression (Devlin, 2009), and made use of a Monte Carlo algorithm to obtain estimates of the parameter uncertainties. In general, the parameters exhibited near-normal distributions from which

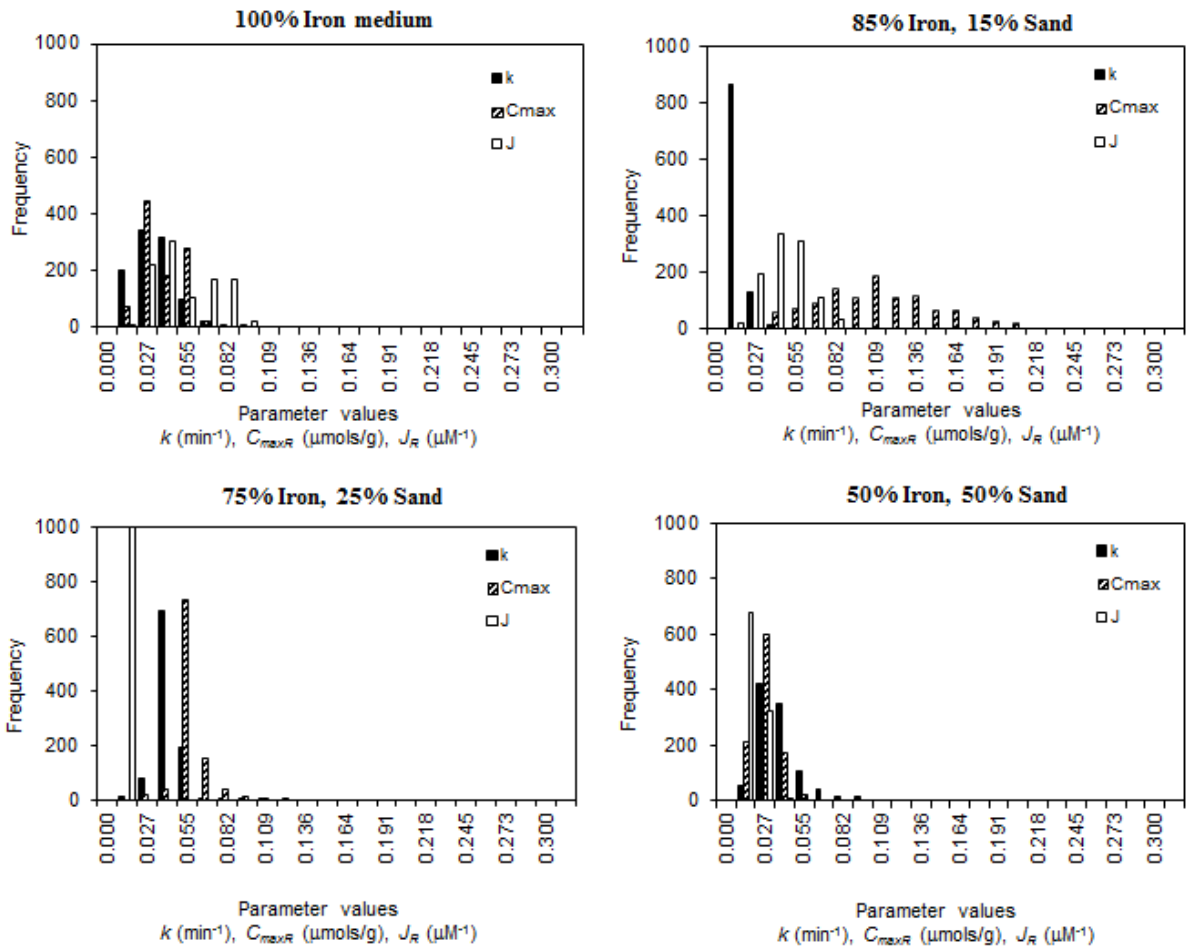

Figure A. 0.1: KIM parameter distributions from the Monte Carlo analysis performed during parameter identification.

means (Table A.1) and standard deviations (Table A.2) could be derived for each experiment.

In order to assess whether any experiment-specific mean (n = 1000) was significantly different from the overall mean values of all experiments (n = 4) (Table A.1), G-values were calculated (eq A.2, Table A. 2) and compared to the t-statistic for the 4 experiments (Table A.1).

$$G = \frac{|u_{experiment} - u_{overall}|}{\sigma_{experiment}} \tag{A.2}$$

where $u_{experiment}$ is the mean of a parameter for a particular experiment (i.e., involving a particular iron-sand mixture), $u_{overall}$ is the mean of the experiment specific means of a parameter (i.e., k, J, or C_{max}), and s is the parameter specific standard deviation for the experiment. A parameter was considered significantly different from the overall mean if the G-value exceeded the t-statistic for n = 4 (t = 1.400), which corresponds to a 75% confidence level.

Table A. 2: Summary of parameter standard deviations and G - values.

	Standard Deviations			**G - values**		
Iron %	k (min^{-1})	C_{max} (μmolg^{-1})	J (μM^{-1})	k (min^{-1})	C_{max} (μmolg^{-1})	J (μM^{-1})
100.00%	1.4E-02	1.4E-02	2.0E-02	0.047158	0.579996	0.98819
85.00%	4.7E-03	3.8E-02	1.4E-02	1.386497	1.401084	0.694348
75.00%	8.9E-03	1.0E-02	7.1E-04	0.968408	0.015764	1.092164
50.00%	1.4E-02	8.3E-03	4.3E-03	0.370931	0.836852	0.590373

Inspection of Table A.2 reveals that at 75% confidence only C_{max} from the 85% iron experiment exceeds the t-statistic, although the k value from the same experiment very nearly matches the level of significance. It is concluded that the addition of 15% sand to the iron medium resulted in significant differences in the kinetic behavior of the reactive medium compared to the other mixtures.

Appendix B: Breakthrough curves and model fits.

Breakthrough curves (Figures B.1 through B.5) were produce by increasing C_o in sequential tests, and were fitted to Advection dispersion equation equation 3.1 of chapter 3 to obtain estimates of R_{app}, α and k_{app} (Table B.1)(Bear, 1979). Sorption to the granular iron surface was assumed to be described by Langmuir isotherm.

Table B. 1: Comparison of the values of apparent first order rate constants (k_{app}) and retardation factors (R_{app}) using eq. 3.1 in chapter 3 for VP, HP and RP columns.

VP-1			HP-1			RP-1		
C_o (μM)	k_{app} (s^{-1})	R_{app}	C_o (μM)	k_{app} (s^{-1})	R_{app}	C_o (μM)	k_{app} (s^{-1})	R_{app}
27.19	1.16E-03	15.69	35.47	1.13E-03	8.677	24.9	8.68E-04	12.72
78.8	9.70E-04	12.32	47.92	4.78E-05	6.22	73.19	3.57E-04	17.7
107.4	3.56E-04	8.493	140.1	3.52E-04	5.12	145.4	3.55E-04	7.47
183.6	8.30E-04	9.2	282.5	1.72E-04	2.81	258.5	4.60E-04	5.18
355.4	5.74E-04	6.1	409.3	1.05E-04	1.9	386.4	1.24E-04	6.6
504	4.59E-04	4.568	480.5	8.89E-05	1.78	534.3	3.65E-04	3.6
VP-2			HP-2			RP-2 (Ref 2)		
C_o (μM)	k_{app} (s^{-1})	R_{app}	C_o (μM)	k_{app} (s^{-1})	R_{app}	C_o (μM)	k_{app} (s^{-1})	R_{app}
30.2	6.85E-04	16.53	31.98	7.61E-04	13.03	61.05	9.12E-04	9.4
44.05	1.98E-04	22.85	39.98	3.48E-04	6.604	64.70	4.01E-04	10.4
75.89	1.16E-04	3.57	112.4	3.65E-04	3.681	79.09	4.87E-04	3.1
189.38	5.53E-04	8.13	254.9	2.97E-04	5.174	114.7	5.86E-04	4.6
336.35	2.00E-04	7.08	321.0	1.15E-04	3.775	214.9	2.30E-04	2.6
496.95	1.55E-04	3.00	498.1	6.79E-05	2.984	383.7	9.69E-05	1.9

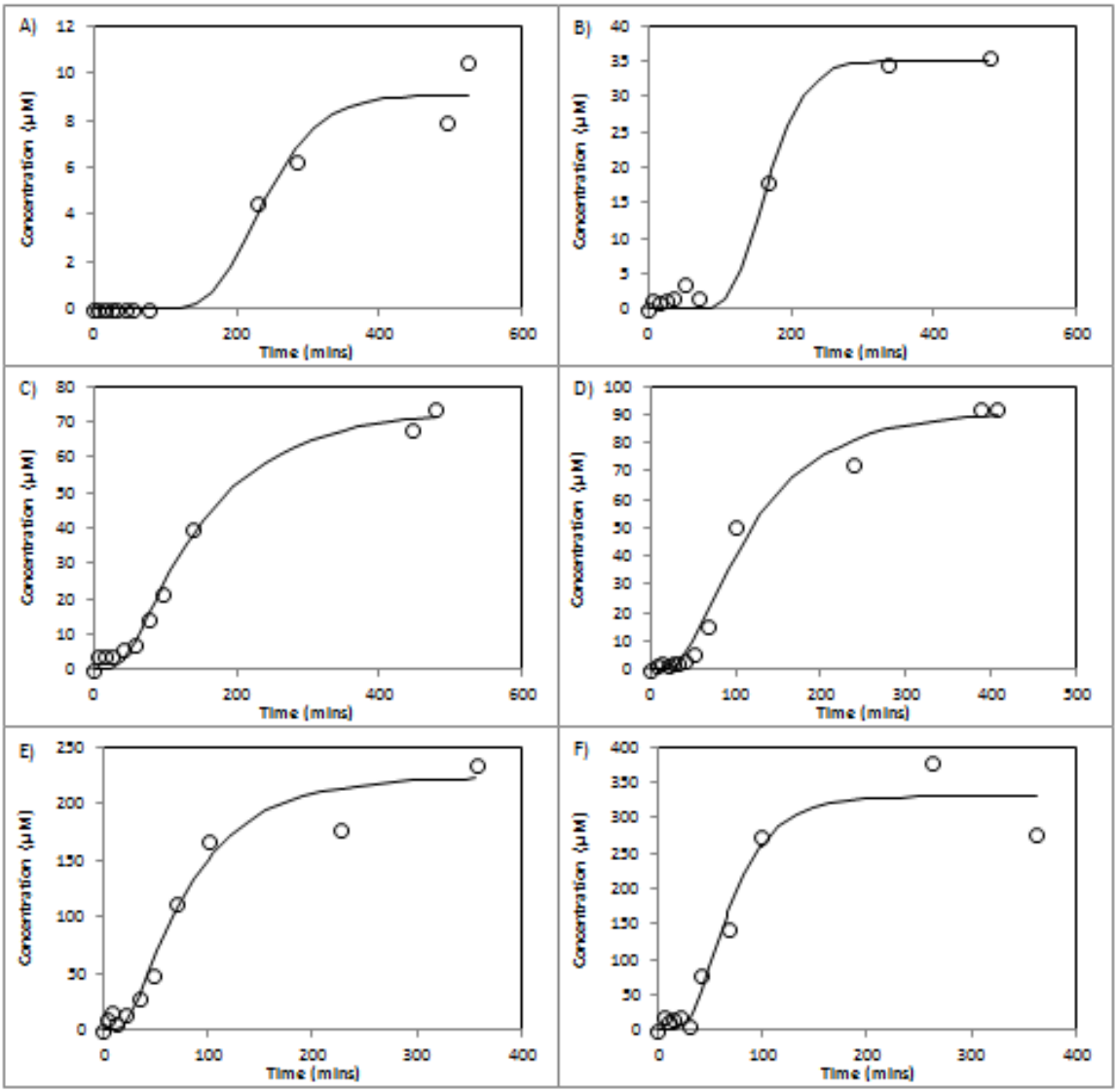

Figure B. 1: Breakthrough curves for VP1: A) C_O = 27.19 µM; B) *Co* = 78.8 µM; C) *Co* = 107.4 µM; D) *Co* = 183.6 µM; E) *Co* = 355.4; F) C_O = 515.0 µM. Symbols represent experimental data points and lines show the best fit using eq 3.1 of the chapter 3.

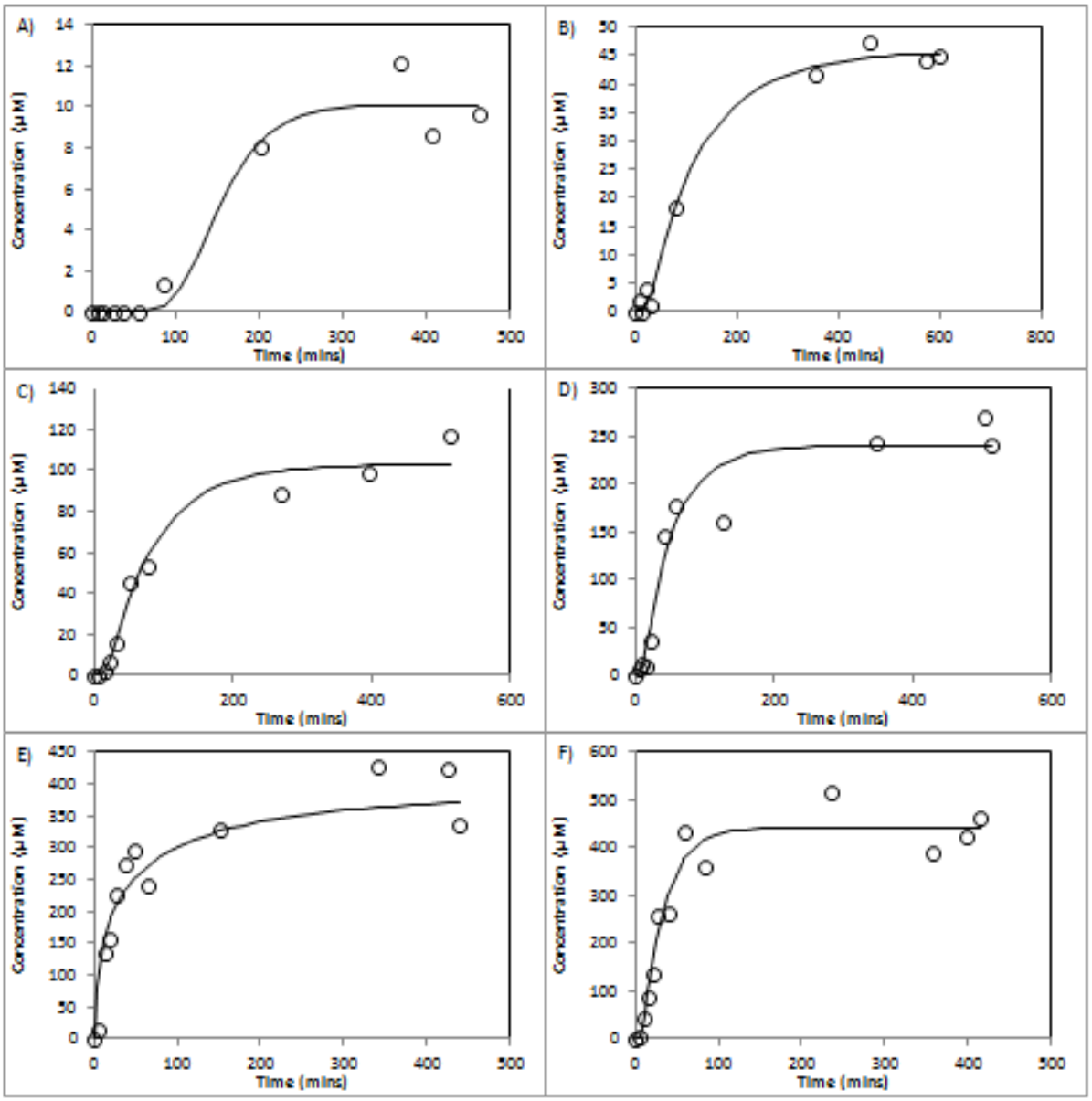

Figure B. 2: Breakthrough curves for HP1: A) C_O = 35.47 µM; B) C_o = 47.92 µM; C) C_o = 140.1 µM; D) C_o = 282.5 µM; E) C_o = 409.3; F) C_O = 480.5 µM. Symbols represent experimental data points and lines show the best fit using eq 3.1 of the chapter 3.

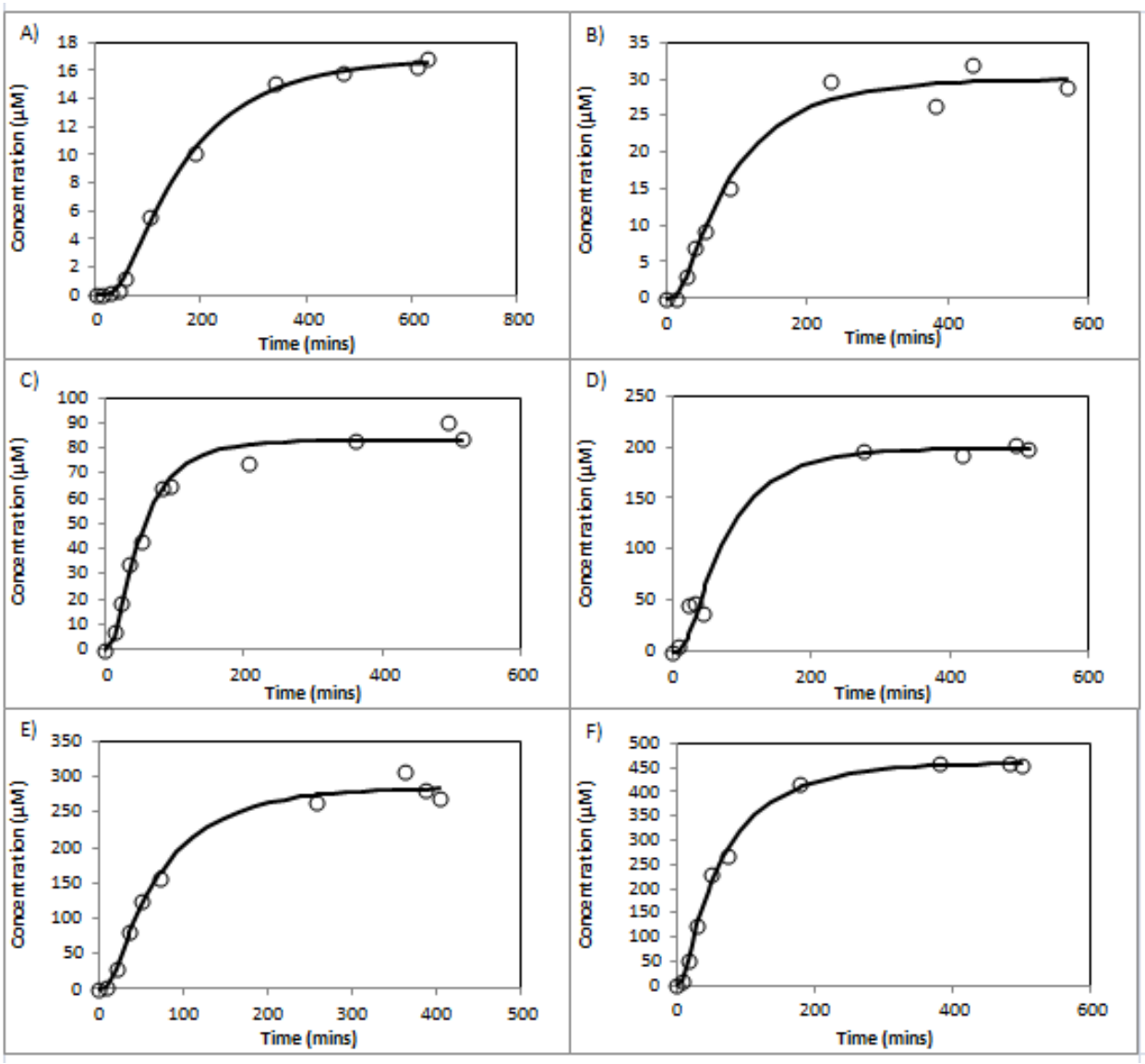

Figure B. 3: Breakthrough curves for RP1: A) C_O = 24.9 µM; B) C_o = 73.19 µM; C) C_o = 145.4 µM; D) C_o = 258.5 µM; E) C_o = 386.4; F) C_O = 534.3 µM. Symbols represent experimental data points and lines show the best fit using eq 3.1 of the chapter 3.

.

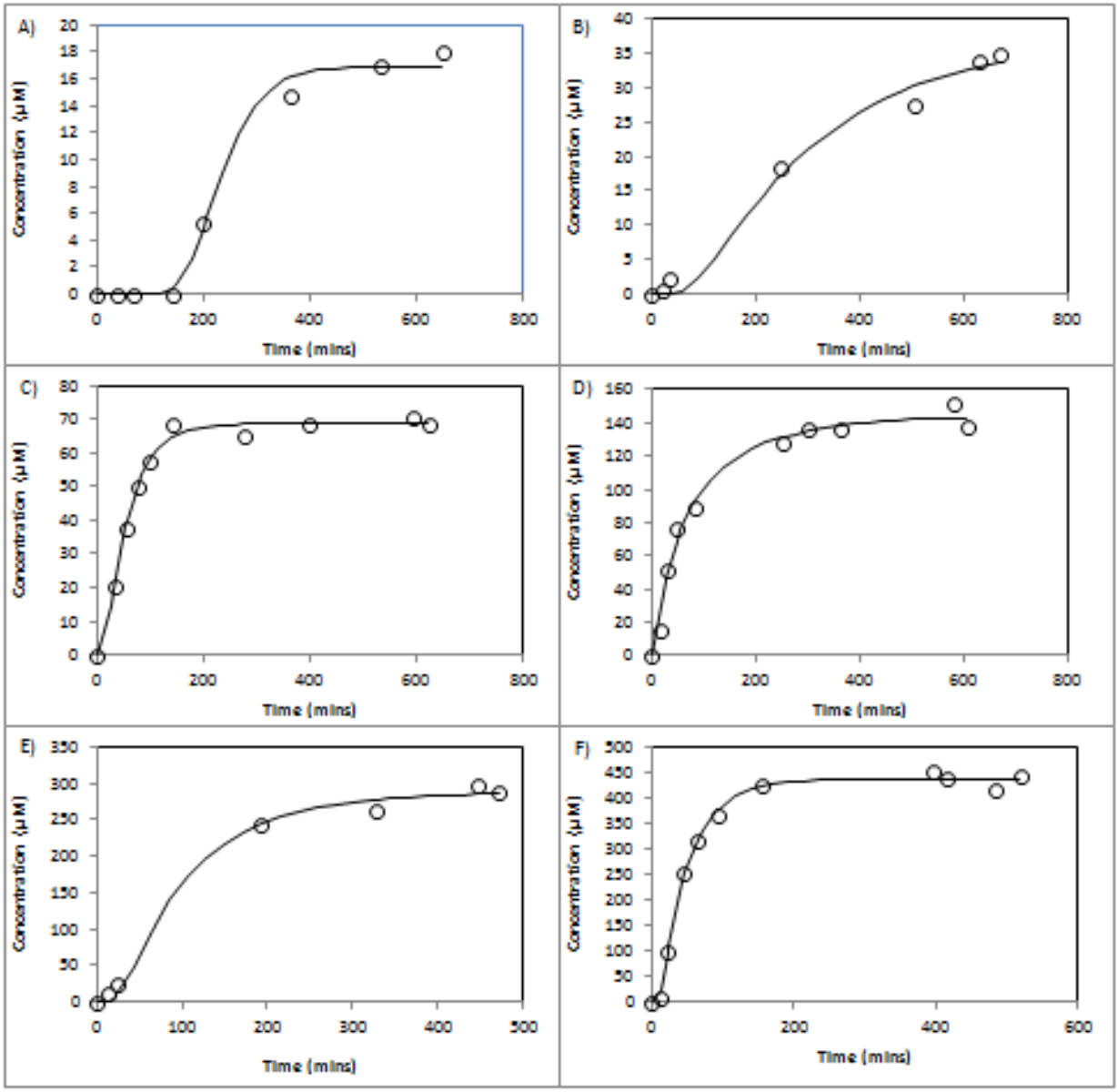

Figure B. 4: Breakthrough curves for VP2: A) C_O = 35.47 µM; B) C_O = 47.92 µM; C) C_O = 140.1 µM; D) C_O = 282.5 µM; E) C_O = 409.3; F) C_O = 480.5 µM. Symbols represent experimental data points and lines show the best fit using eq 3.1 of the chapter 3.

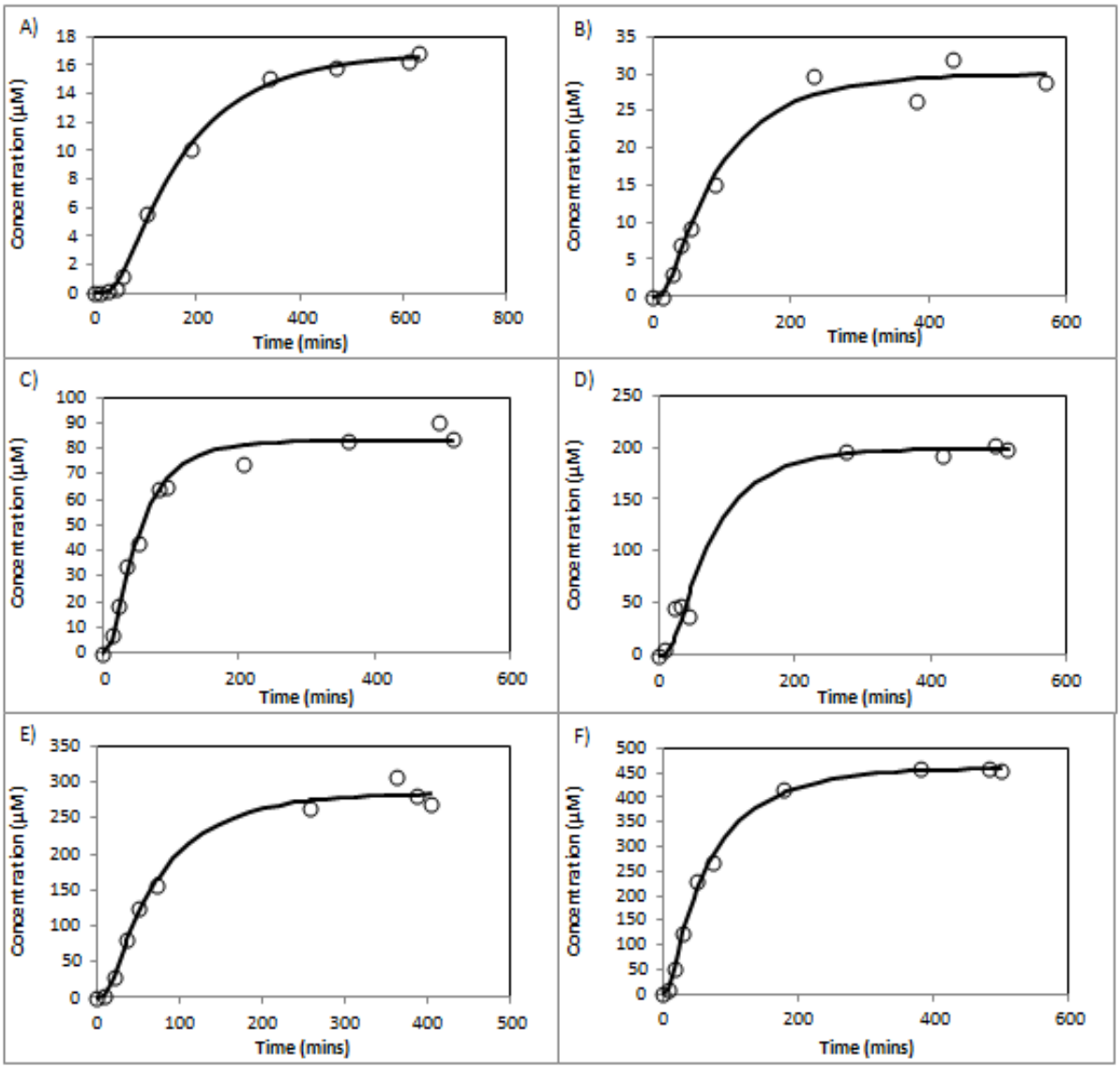

Figure B. 5: Breakthrough curves for HP2: A) C_O = 31.98 µM; B) C_o = 39.98 µM; C) C_O = 112.4 µM; D) C_O = 254.9 µM; E) C_O = 321.0; F) C_O = 498.1 µM. Symbols represent experimental data points and lines show the best fit using eq 3.1 of the chapter 3.

Appendix C: T-test of KIM parameters

A t-test was performed to compare the means of the estimated sorption and kinetic parameters between horizontal, random packing, and vertical packing (Table C.1).

Table C. 1: T-Test of the estimated KIM parameters from VP, HP and RP tests.

	Packing	C_{maxN} (uMg^{-1})	J_N (uM^{-1})	k (min^{-1})	C_{maxR}(uMg^{-1})	J_R(uM^{-1})
	VP-1	1.70	0.0026	0.0097	0.32	0.065
	VP-2	1.34	0.0034	0.01	0.11	0.099
Mean		1.52	0.003	0.00985	0.215	0.082
Stdev*		0.25	0.00056	0.00021	0.148	0.024
	HP-1	0.47	0.0044	0.01	0.06	0.07
	HP-2	0.54	0.0048	0.008	0.06	0.16
	RP-1	1.2	0.002	0.01	0.085	0.055
Mean		0.7366666	0.0037	0.010	0.068	0.095
Stdev*		0.4027819	0.0015	0.002	0.014	0.056
T-test		**9.74%**	**57.45%**	**92.64%**	**16.049%**	**78.78%**

* Standard deviation

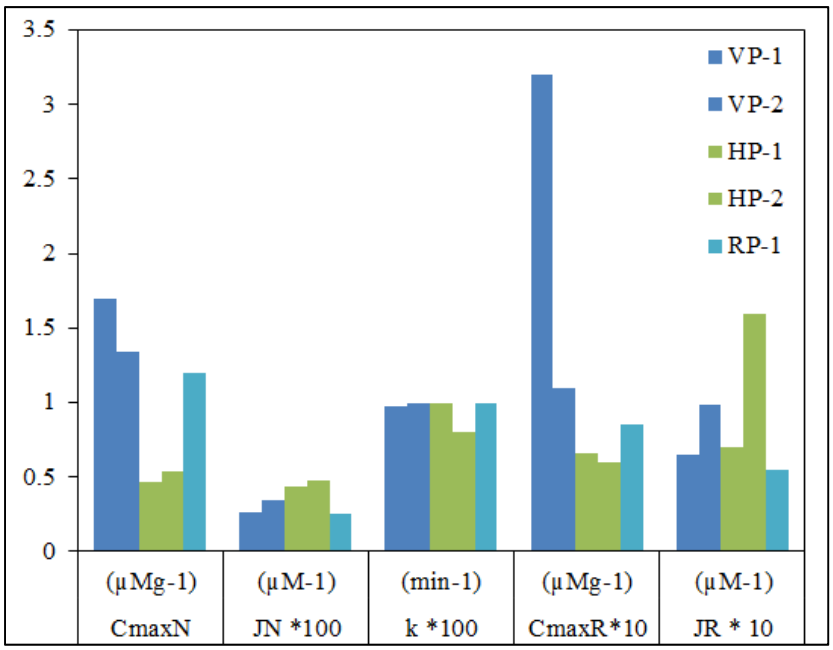

Figure C. 1: Comparison of KIM parameters between vertical packing, horizontal packing, and random packing.

Appendix D. Tracer test

A chloride tracer test was carried out on both VP and HP to assess the magnitude of physical non-equilibrium transport (PNE) on breakthrough curves (BTC). Flow conditions in HP would favor conditions for PNE, compare to VP columns. These conditions could be marked by enhanced tailing in the BTC for HP. However resulted BTC showed nearly identical degree of tailings (Figure C.1) and suggested minimal effect of diffusion on sorption (C_{max}) and rate constants (k).

Table D. 1: Data of tracer test for vertical and horizontal packings

Vertical Packing			Horizontal Packing		
Time (mins)	Drops	as Cl^-	Time (mins)	Drops	as Cl-
0	0	0	0	0	0
3	1	60	4	1	60
9	1	60	8	1	60
14	1	60	15	1	60
18	1	60	27	2	120
24	2	120	45	4	240
27	2	120	68	4	240
30	2	120	82	5	300
33	3	180	99	5	300
39	3	180	117	5	300
44	4	240	125	5	300
55	4	240	140	5	300
77	5	300			
95	5	300			
118	5	300			
140	5	300			
150	5	300			
155	5	300			
160	5	300			
170	5	300			
186	3	180	186	3	180
202	2	120	198	2	120
214	1	60	211	2	120
224	1	60	221	1	60
237	1	60	231	1	60

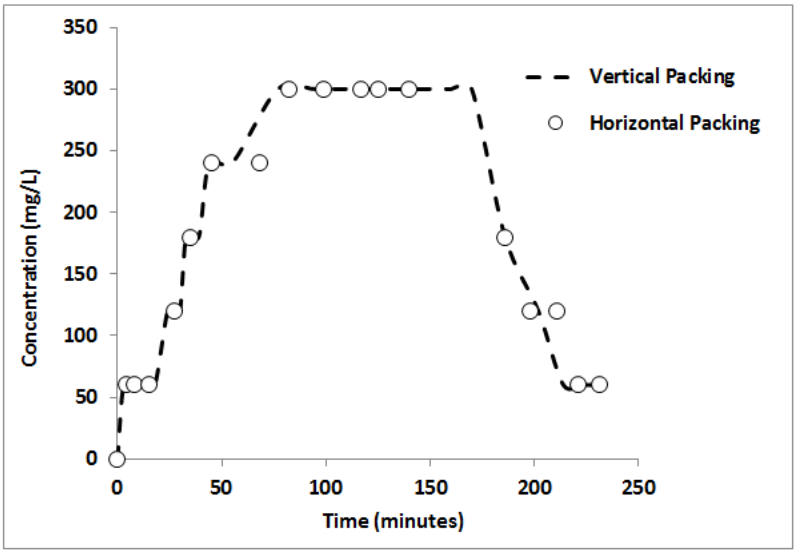

Figure D. 1: Breakthrough curves with tailings for (a) VP and (b) HP showing chloride concentration from 60 mg/l to 300 mg/l.

Appendix E: Morphological Analysis

Pore scale investigations were carried out by preparing the vertical and horizontal packings (in duplicates) in plastic vials of diameter 2.9 cm. Vials were flooded and subsequently cemented with epoxy (EPO-TEK 301). Vertical cross-sections of the cemented material were cut from the solid cylinders and mounted on slide. Sections were prepared by grinding the surface to 50 μm using Hillquist Thin Sectioner. 25 sections for each packing were prepared and subsequently photographed. Original images were cropped to extract a region of interest (ROI)

Table E. 1: Summary of the image characteristics of vertical and horizontal packing.

Packing type	Slice thickness (mm)	No. of slices	Original image size (pixel x pixel)	Image size for analysis (pixel x pixel)	Image size for analysis (mm x mm)
VP-1	0.05	25	615 x 382	410 x 308	21.87 x 16.43
HP-1	0.05	25	596 x 470	410 x 308	21.87 x 16.43
VP-2	0.05	25	439 x 390	400 x 175	27.20 x 11.90
HP-2	0.05	25	662 x 328	400 x 175	27.20 x 11.90

The range of pore sizes in the various packings investigated was examined in terms of pore volumes, grain perimeters, and areas can be found in Table E.2 while details of section wise grain perimeter and area estimated by Image J (Rasband, 2007) can be found in Table E.3. Both vertical packing showed higher estimated perimeters while areas remained higher for horizontal packings (Figure E.1, E.2). It is suggested that vertical packing supplemented better grain to solution contact which could foster more corrosion and resulted in enhanced reaction rates (factors of 2 to 4).

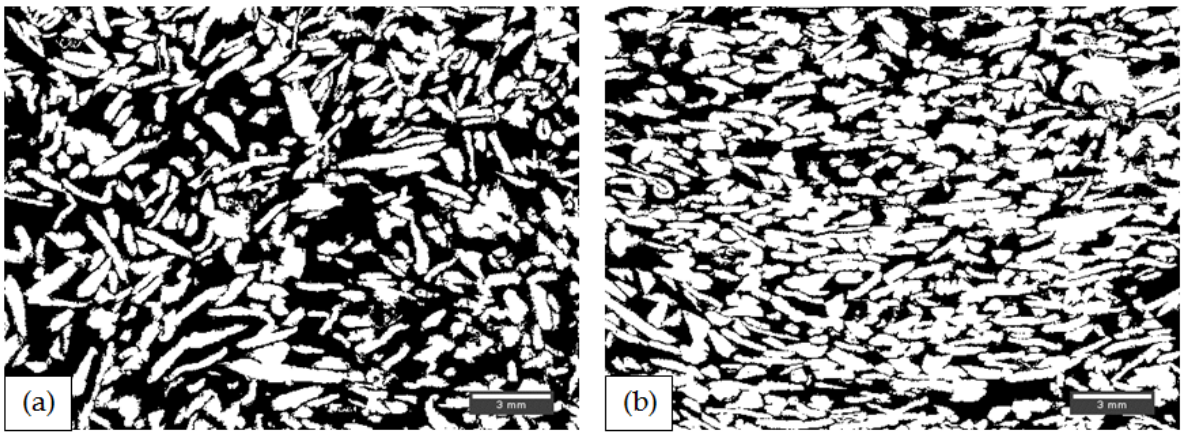

Figure E.1: Re-analysed sections at 600 dpi for (a)e vertical packing (VP) and (b) Horizontal packing.

Table E. 2: Summary of pore analysis for vertical and horizontal packings

Image type	Pore space Volume (mm^3)	Total Volume (mm^3)	Porosity %	Average grain perimeters (mm)	Average grain areas (mm^2)
VP-1	240.16	478.93	50.10	826.06	180.66
HP-1	195.09	478.93	40.70	631.10	213.27
VP-2	248.03	550.54	45.10	643.83	197.82
HP-2	238.74	550.01	43.40	602.18	208.51
VP-1*	-	-	54	1283.4	162.46
HP-1*	-	-	41	1160	210

***Reanalyzed data with higher resolution (600dpi) and based on single section study (Figure E 1).**

Table E. 3: Data output from grain analysis for both vertical and horizontal packings.

	Perimeter (mm)				Area (mm^2)			
	VP1	**HP1**	**VP2**	**HP2**	**VP1**	**HP1**	**VP2**	**HP2**
1	963.879	814.413	683.266	582.352	170.381	206.833	170.207	174.952
2	1006.128	625.609	656.545	646.789	164.013	208.601	177.112	179.816
3	893.504	733.454	579.702	735.95	171.326	214.079	180.146	179.633
4	863.386	714.456	448.078	589.72	173.266	215.011	177.244	187.042
5	865.169	559.749	558.624	545.235	170.92	221.023	179.609	188.678
6	845.764	640.126	619.445	496.534	179.423	216.076	180.639	184.642
7	781.59	607.93	619.54	530.27	186.292	217.516	180.353	186.142
8	673.176	616.999	583.092	591.457	184.846	217.078	180.168	187.35
9	808.222	682.275	539.104	502.818	184.282	211.03	180.357	189.612
10	808.003	520.634	624.506	487.846	186.671	216.486	178.313	190.006
11	784.973	464.541	560.596	510.929	187.988	215.812	182.93	193.768
12	801.738	612.262	560.982	382.934	189.408	213.255	179.511	192.917
13	778.924	633.098	570.678	540.756	190.926	211.217	181.608	191.857
14	636.345	678.778	549.952	448.958	193.044	213.549	184.327	193.121
15	738.319	597.148	534.894	557.962	185.106	212.433	179.948	191.138
16	888.017	628.029	457.345	525.092	181.134	211.973	181.24	188.613
17	888.544	718.214	455.589	683.825	180.519	213.888	183.396	187.698
18	832.914	622.601	523.009	580.407	179.316	208.124	175.94	187.956
19	762.903	556.927	622.399	599.51	180.134	213.386	174.703	186.101
20	798.728	548.124	602.457	566.753	179.235	215.144	178.78	185.762
21	847.142	621.323	622.38	429.698	182.492	208.28	175.93	189.33
22	756.69	591.672	586.244	400.242	183.557	210.459	175.824	194.567
23	756.257	657.245	577.19	569.207	181.795	211.91	172.743	184.451
24	931.565	662.902	639.682	552.17	171.872	207.872	170.544	184.194
25	900.933	639.73	696.674	683.825	170.454	210.89	165.374	187.698

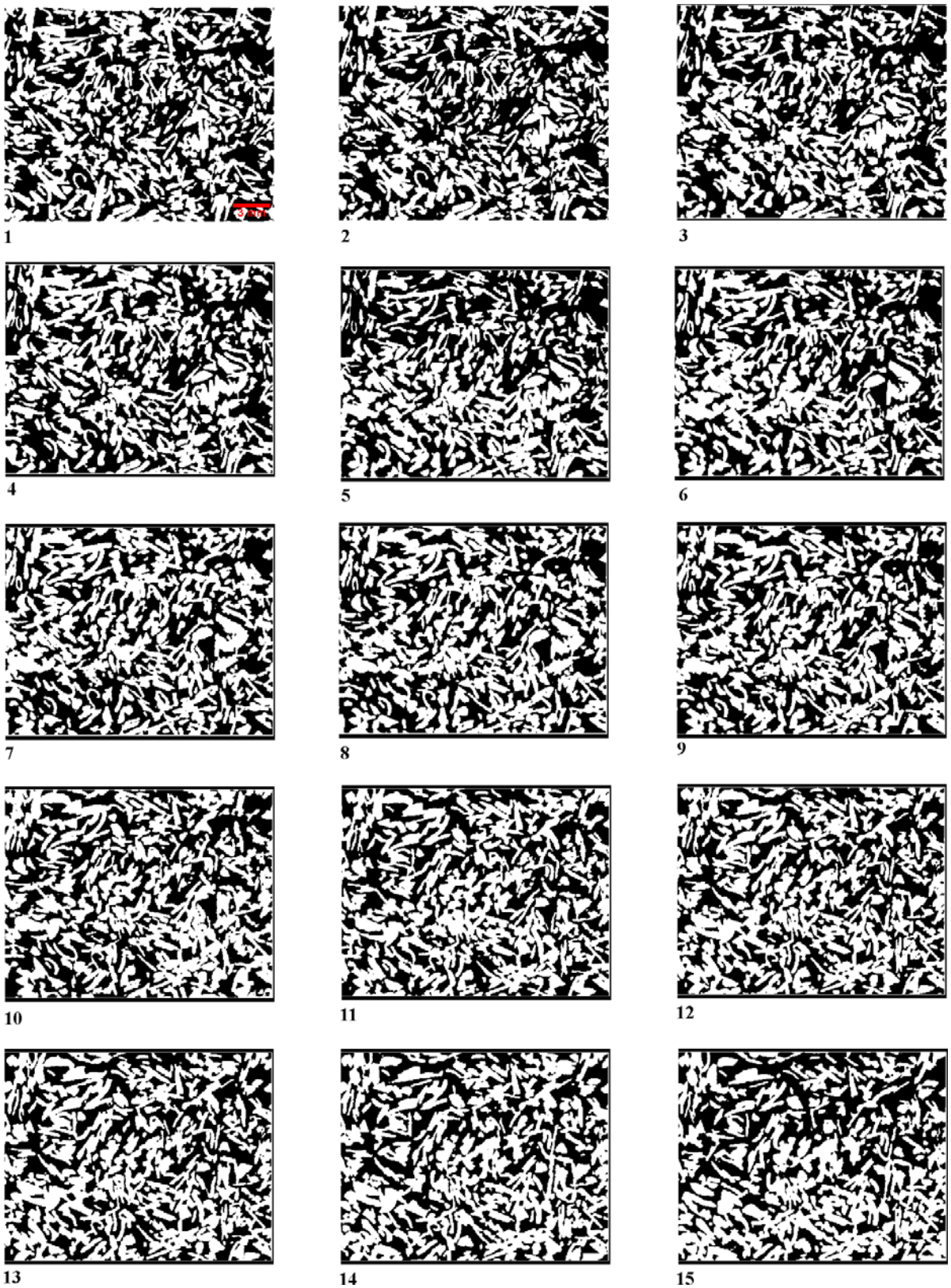

Figure E.2: 25 Serial Sections from the vertical packing (VP1).

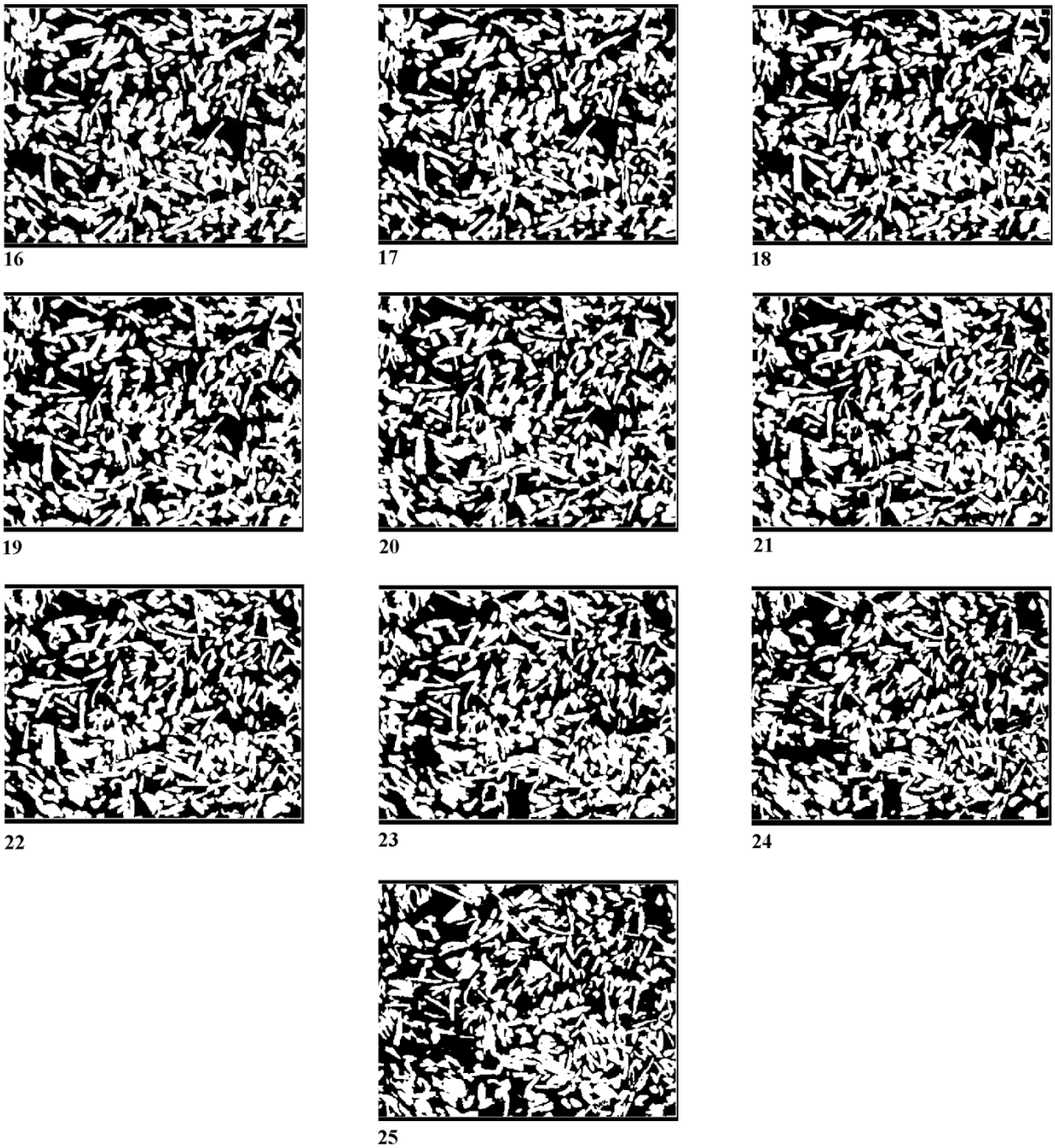

Figure E.2: 25 Serial Sections from the vertical packing (VP1) continued.

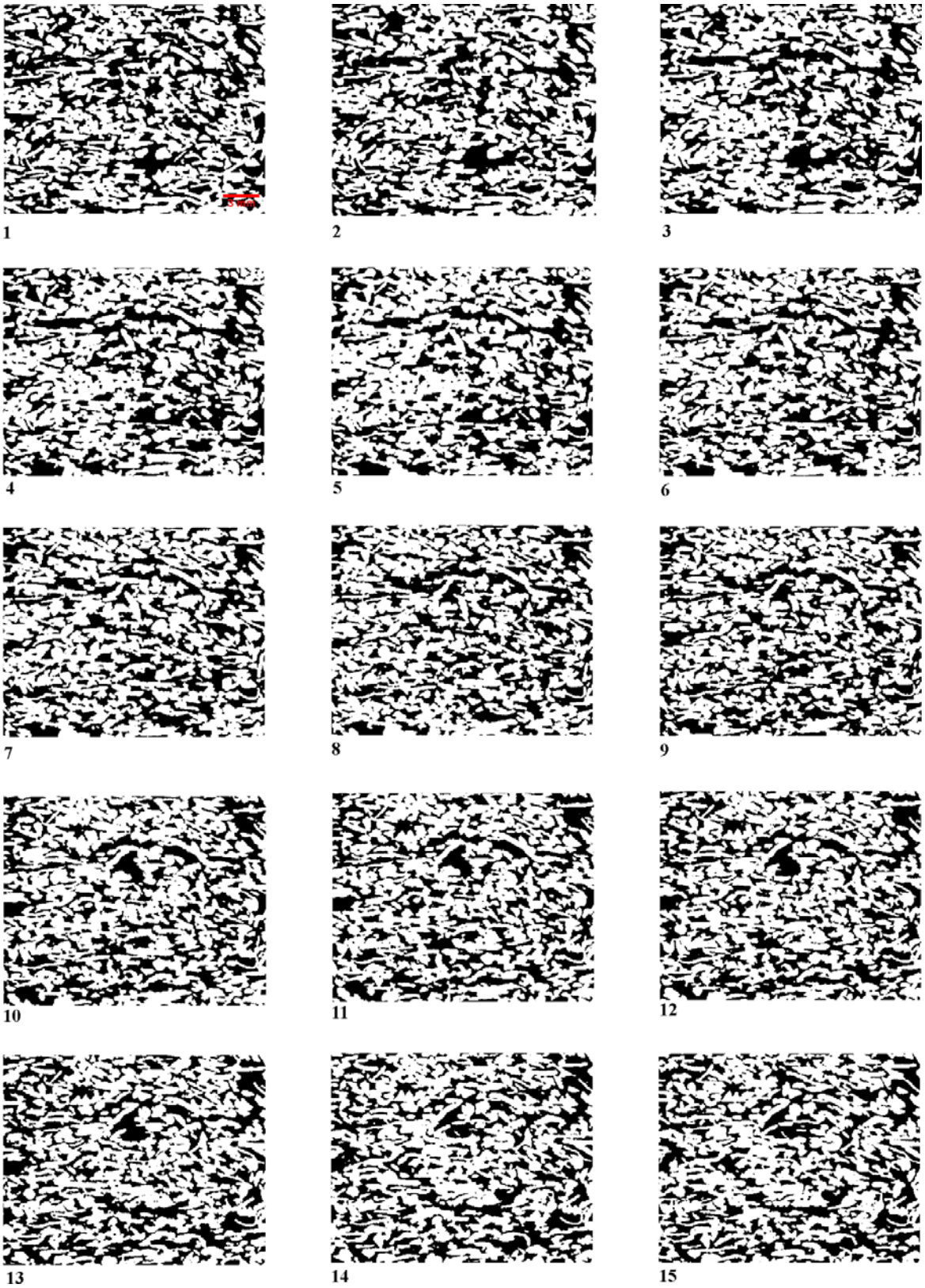

Figure E.3: 25 Serial Sections from the Horizontal packing (HP1).

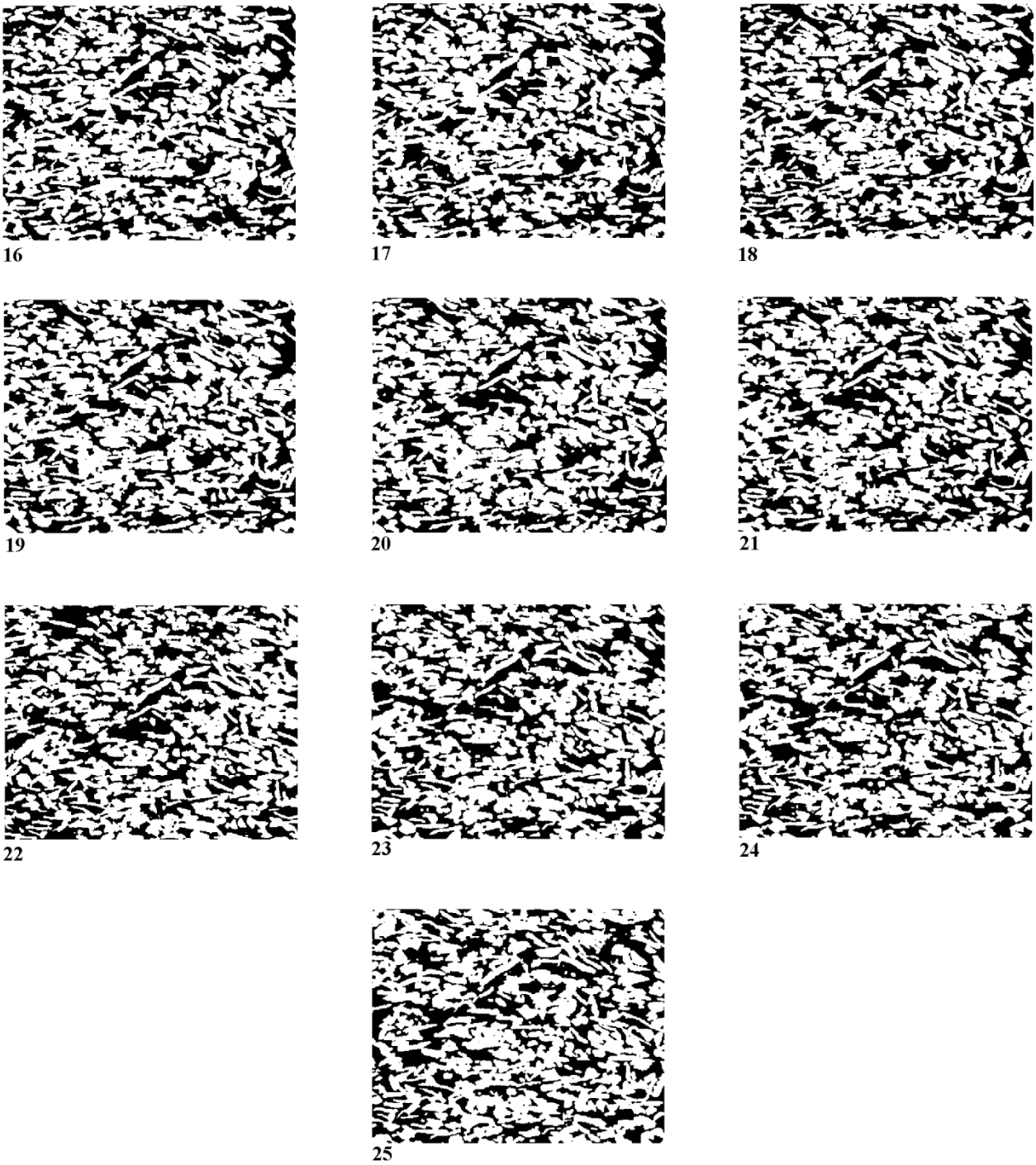

Figure E.3: 25 serial sections from horizontal packing (HP1) continued.

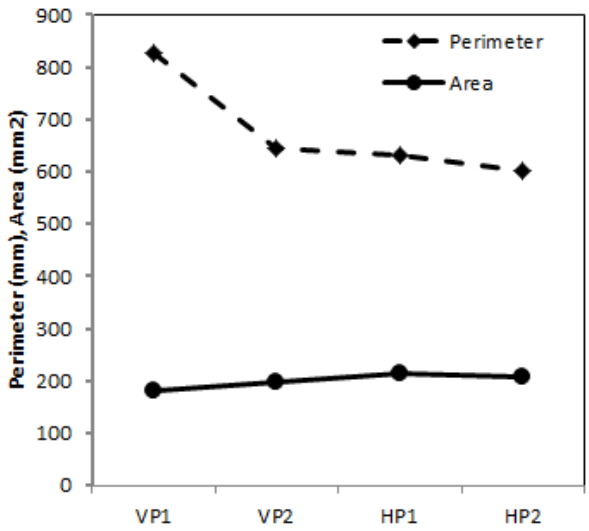

Figure E.4: Comparison of morphological parameters between vertical and horizontal packings.

Feret Angle

Feret angle (0-180 degrees) is the angle between the Feret's diameter and a line parallel to the x-axis of the image. Analyze particle algorithm was used to measure the orientation of grains in a section. For VP grains were aligned nearly at all angles whereas HP showed much narrow distribution of grains arrangement and mainly concentrated between 140º to 180º (Figure E.5).

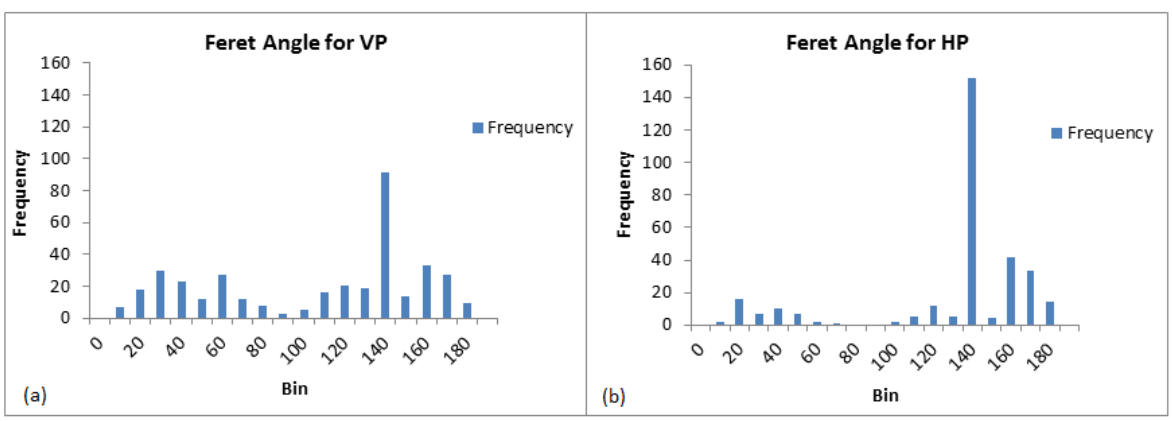

Figure E.5: Comparison of ferret angles between vertical and horizontal packing.

T-test of Pore Analysis parameters

A t-test was performed to compare the means of the estimated perimeters and areas between horizontal, and vertical packing (Table E.4).

Table E. 4: T-Test of the estimated pore analysis parameters from VP and HP.

Image type	Total area (mm^2)	Porosity %	Perimeter of grains (mm)	Area of Iron grains (mm^2)	Normalized perimeters (mm)	Normalized areas (mm^2)
VP 1	359.32	50.1	824.51	180.33	826.06	180.66
VP 2	323.68	45.1	578.88	177.87	643.83	197.82
Mean		47.6	701.69	179.1	734.94	189.24
Stdev*		3.53	173.68	1.739	128.85	12.133
Image type	**Total area (mm^2)**	**Porosity %**	**Perimeter of grains (mm)**	**Area of Iron grains (mm^2)**	**Normalized perimeters (mm)**	**Normalized areas (mm^2)**
HP 1	359.32	40.7	629.92	212.87	631.10	213.27
HP2	323.68	43.4	541.43	187.48	602.18	208.51
Mean		42.05	585.67	200.17	616.64	210.89
Stdev*		1.909	62.57	17.953	20.45	3.361
T-test		19.00%			32.83%	13.56%

* Standard deviation

Test for DPI versus Morphological parameters

Table E.5. Test for image dpi versus morphological parameters based on a single section.

dpi	%area	Perimeter
100	51.444	10.043
200	65.423	10.73
300	48.693	4.43
400	49.394	3.951
500	49.455	3.575
600	48.88	3.34

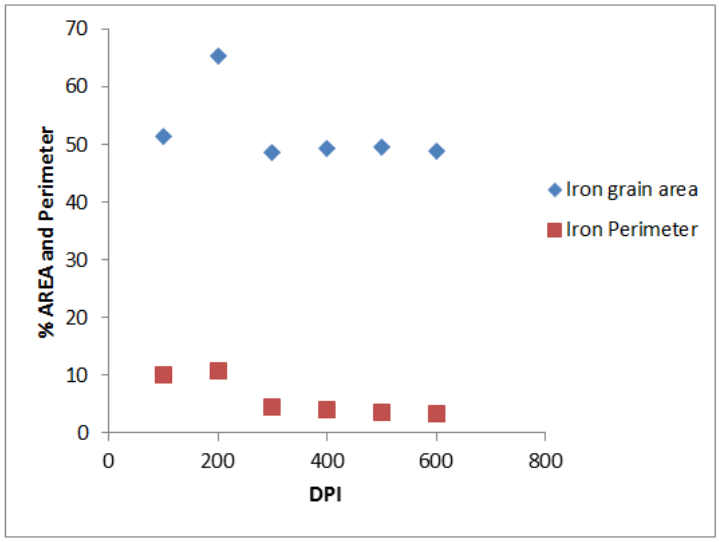

Figure E.6: Test result for dpi versus iron area% and average grain perimeter.

Appendix F: BEARKIMPE Code

UserForm 1 code

```
Private Sub CommandButton1_Click()

Dim FileToOpen
Dim FileName As String
Dim WkbkName As Object

10  FileToOpen = Application.GetOpenFilename("Text Files (*.xlsx), *.xlsx")
   FileName = ActiveWorkbook.Path + "\" + ActiveWorkbook.Name
   If FileToOpen = False Then Exit Sub
   If FileToOpen <> "" Then

      Msg = "Do you want to open " & FileToOpen & " ?"  ' Define message.
      Style = vbYesNo + vbDefaultButton1  ' Define buttons.
      Title = "Workbook to Open"  ' Define title.
      Response = MsgBox(Msg, Style, Title)

         If Response = vbYes Then    ' User chose Yes.
         Workbooks.Open (FileToOpen)    ' Perform some action.
         Else: GoTo 10   ' User chose No.
         End If

End If


Application.Run ("Lern")
UserForm1.Hide
UserForm2.Show



End Sub


Private Sub CommandButton2_Click()
   Unload Me
End Sub
```

Module 1 code

```
Sub Lern()
'Lern Macro
' Macro recorded 9/08/2010 by Rubina Firdous
'

'
   Application.ScreenUpdating = False
   Application.DisplayAlerts = False
    Range("A1:B1").Select
    Range("D1:E1").Select
    Range("G1:H1").Select
    Range("J1:K1").Select
    Range("M1:N1").Select
    Range("P1:Q1").Select
```

```
    Cells.Select
    Selection.Copy
    Windows("BEARKIMPE.xlsm").Activate
    ActiveWindow.WindowState = xlNormal
    ActiveWindow.WindowState = xlNormal
    Range("A1").Select
    ActiveSheet.Paste
    Range("A1").Select
    ActiveWindow.WindowState = xlNormal
    ActiveWindow.WindowState = xlNormal
    ActiveWindow.WindowState = xlNormal

For Each WkbkName In Application.Workbooks()
            If WkbkName.Name <> "BEARKIMPE.xlsm" Then WkbkName.Close (False)
        Next
End Sub
```

UserForm 2 code

```
Private Sub CommandButton1_Click()

 Dim TargetConcentration As Integer
 Dim i As Double
 Dim R, foundcell As Range
 Dim Graph As ChartObject
 Dim cw, rh As Long
 Dim Co(6) As Double
 'Dim Ctarget(6) As String - public variable
 Dim TextBox(6) As String
 Dim X As Double

'makes userform input for C Concentration into variable for code
Ctarget(1) = UserForm2.Co1
Ctarget(2) = UserForm2.Co2
Ctarget(3) = UserForm2.Co3
Ctarget(4) = UserForm2.Co4
Ctarget(5) = UserForm2.Co5
Ctarget(6) = UserForm2.Co6

'CTarget(1) = Str(25)
'CTarget(2) = Str(50)
'CTarget(3) = Str(100)
'CTarget(4) = Str(200)
'CTarget(5) = Str(300)
'CTarget(6) = Str(400)


Application.ScreenUpdating = False


 Sheets("Sheet1").Name = "BearPE2"
 Range("A1,D1,G1,J1,M1,P1").Value = "Time (min)"
Range("B1,E1,H1,K1,N1,Q1").Value = "Concentration (uM)"
```

```
'Loop calculates concentration and makes separate worksheets for 6 Cos


 Sheets("BearPE2").Activate
 ActiveSheet.Range("A1:B12").Select
 Range(Selection, Selection.End(xlDown)).Copy
 Worksheets.Add(After:=Worksheets(Worksheets.Count)).Name = Co1
 ActiveCell.Offset(0, 0).Select
 ActiveSheet.Paste

Sheets("BearPE2").Activate
 Range("D1:E15").Select
 Range(Selection, Selection.End(xlDown)).Copy
 Worksheets.Add(After:=Worksheets(Worksheets.Count)).Name = Co2
 ActiveCell.Offset(0, 0).Select
 ActiveSheet.Paste

 Sheets("BearPE2").Activate
 ActiveSheet.Range("G1:H15").Select
 Range(Selection, Selection.End(xlDown)).Copy
 Worksheets.Add(After:=Worksheets(Worksheets.Count)).Name = Co3
 ActiveCell.Offset(0, 0).Select
 ActiveSheet.Paste
 Sheets("BearPE2").Activate
 ActiveSheet.Range("J1:K15").Select
 Range(Selection, Selection.End(xlDown)).Copy
 Worksheets.Add(After:=Worksheets(Worksheets.Count)).Name = Co4
 ActiveCell.Offset(0, 0).Select
 ActiveSheet.Paste
 Sheets("BearPE2").Activate
 ActiveSheet.Range("M1:N15").Select
 Range(Selection, Selection.End(xlDown)).Copy
 Worksheets.Add(After:=Worksheets(Worksheets.Count)).Name = Co5
 ActiveCell.Offset(0, 0).Select
 ActiveSheet.Paste
 Sheets("BearPE2").Activate
 ActiveSheet.Range("P1:Q15").Select
 Range(Selection, Selection.End(xlDown)).Copy
 Worksheets.Add(After:=Worksheets(Worksheets.Count)).Name = Co6
 ActiveCell.Offset(0, 0).Select
 ActiveSheet.Paste
Sheets(Ctarget(1)).Activate

'Loop plots chart in all 6 spreedsheets
For i = 1 To 6
Next i


'graph is created for the observed data. statements identifies size and location, title, chart type, series selection, axes
formatting, plot area formatting, title formatting


   cw = Columns(1).Width
   rh = Rows(1).Height
   Set Graph = ActiveSheet.ChartObjects.Add(cw * 5, rh * 1, cw * 10, rh * 25)
```

```
    Graph.Name = " Breakthrough Curve"
    Graph.Chart.ChartType = xlXYScatter

Graph.Chart.SeriesCollection.NewSeries
 With Graph.Chart.SeriesCollection(1)
        .Values = ActiveSheet.Range("B2:B20")
        .XValues = ActiveSheet.Range("A2:A20")
        .Name = "Observed"
        .MarkerSize = 6
        .MarkerStyle = xlMarkerStyleCircle


End With

'    Graph.Chart.SeriesCollection.Add Source:=ActiveSheet.Range("B2:B" & LastRowNewSheet)

    With Graph.Chart.Axes(xlCategory)
        .HasTitle = True
        .AxisTitle.Caption = "Time (min)"
        .CategoryNames = Range("A2:A20" & LastRowNewSheet)
    End With

    With Graph.Chart.Axes(xlValue)
        .HasTitle = True
    With .AxisTitle
        .Caption = "Concentration (uM) "
    End With
    End With

    Graph.Chart.Axes(xlValue).HasMajorGridlines = False
    Graph.Chart.Axes(xlCategory).HasMajorGridlines = False
    Graph.Chart.ChartArea.Interior.Color = RGB(255, 255, 255)
    Graph.Chart.PlotArea.Interior.Color = RGB(255, 255, 255)
    Graph.RoundedCorners = True
    With Graph.Chart.ChartTitle
        .Caption = " Breakthrough Curve"
        .Font.Size = 14
        .Font.Bold = True
    End With

Sheets(Ctarget(2)).Activate
'graph is created for the observed data. statements identifies size and location, title, chart type, series selection, axes
formatting, plot area formatting, title formatting


    cw = Columns(1).Width
    rh = Rows(1).Height
    Set Graph = ActiveSheet.ChartObjects.Add(cw * 5, rh * 1, cw * 10, rh * 25)
    Graph.Name = " Breakthrough Curve"
    Graph.Chart.ChartType = xlXYScatter

Graph.Chart.SeriesCollection.NewSeries
 With Graph.Chart.SeriesCollection(1)
        .Values = ActiveSheet.Range("B2:B20")
        .XValues = ActiveSheet.Range("A2:A20")
        .Name = "Observed"
```

```
        .MarkerSize = 6
        .MarkerStyle = xlMarkerStyleCircle


End With

'    Graph.Chart.SeriesCollection.Add Source:=ActiveSheet.Range("B2:B" & LastRowNewSheet)

    With Graph.Chart.Axes(xlCategory)
        .HasTitle = True
        .AxisTitle.Caption = "Time (min)"
        .CategoryNames = Range("A2:A20" & LastRowNewSheet)
    End With

    With Graph.Chart.Axes(xlValue)
        .HasTitle = True
    With .AxisTitle
        .Caption = "Concentration (uM) "
    End With
    End With

    Graph.Chart.Axes(xlValue).HasMajorGridlines = False
    Graph.Chart.Axes(xlCategory).HasMajorGridlines = False
    Graph.Chart.ChartArea.Interior.Color = RGB(255, 255, 255)
    Graph.Chart.PlotArea.Interior.Color = RGB(255, 255, 255)
    Graph.RoundedCorners = True
    With Graph.Chart.ChartTitle
        .Caption = " Breakthrough Curve"
        .Font.Size = 14
        .Font.Bold = True
    End With

Sheets(Ctarget(3)).Activate
'graph is created for the observed data. statements identifies size and location, title, chart type, series selection, axes
formatting, plot area formatting, title formatting


    cw = Columns(1).Width
    rh = Rows(1).Height
    Set Graph = ActiveSheet.ChartObjects.Add(cw * 5, rh * 1, cw * 10, rh * 25)
    Graph.Name = " Breakthrough Curve"
    Graph.Chart.ChartType = xlXYScatter

Graph.Chart.SeriesCollection.NewSeries
 With Graph.Chart.SeriesCollection(1)
        .Values = ActiveSheet.Range("B2:B20")
        .XValues = ActiveSheet.Range("A2:A20")
        .Name = "Observed"
        .MarkerSize = 6
        .MarkerStyle = xlMarkerStyleCircle


End With

'    Graph.Chart.SeriesCollection.Add Source:=ActiveSheet.Range("B2:B" & LastRowNewSheet)
```

```
    With Graph.Chart.Axes(xlCategory)
        .HasTitle = True
        .AxisTitle.Caption = "Time (min)"
        .CategoryNames = Range("A2:A20" & LastRowNewSheet)
    End With

    With Graph.Chart.Axes(xlValue)
        .HasTitle = True
    With .AxisTitle
        .Caption = "Concentration (uM) "
    End With
    End With

    Graph.Chart.Axes(xlValue).HasMajorGridlines = False
    Graph.Chart.Axes(xlCategory).HasMajorGridlines = False
    Graph.Chart.ChartArea.Interior.Color = RGB(255, 255, 255)
    Graph.Chart.PlotArea.Interior.Color = RGB(255, 255, 255)
    Graph.RoundedCorners = True
    With Graph.Chart.ChartTitle
        .Caption = " Breakthrough Curve"
        .Font.Size = 14
        .Font.Bold = True
    End With

Sheets(Ctarget(4)).Activate
'graph is created for the observed data. statements identifies size and location, title, chart type, series selection, axes
formatting, plot area formatting, title formatting


    cw = Columns(1).Width
    rh = Rows(1).Height
    Set Graph = ActiveSheet.ChartObjects.Add(cw * 5, rh * 1, cw * 10, rh * 25)
    Graph.Name = " Breakthrough Curve"
    Graph.Chart.ChartType = xlXYScatter

Graph.Chart.SeriesCollection.NewSeries
 With Graph.Chart.SeriesCollection(1)
        .Values = ActiveSheet.Range("B2:B20")
        .XValues = ActiveSheet.Range("A2:A20")
        .Name = "Observed"
        .MarkerSize = 6
        .MarkerStyle = xlMarkerStyleCircle


End With

'    Graph.Chart.SeriesCollection.Add Source:=ActiveSheet.Range("B2:B" & LastRowNewSheet)

    With Graph.Chart.Axes(xlCategory)
        .HasTitle = True
        .AxisTitle.Caption = "Time (min)"
        .CategoryNames = Range("A2:A20" & LastRowNewSheet)
    End With

    With Graph.Chart.Axes(xlValue)
        .HasTitle = True
```

```
    With .AxisTitle
        .Caption = "Concentration (uM) "
    End With
    End With

    Graph.Chart.Axes(xlValue).HasMajorGridlines = False
    Graph.Chart.Axes(xlCategory).HasMajorGridlines = False
    Graph.Chart.ChartArea.Interior.Color = RGB(255, 255, 255)
    Graph.Chart.PlotArea.Interior.Color = RGB(255, 255, 255)
    Graph.RoundedCorners = True
    With Graph.Chart.ChartTitle
        .Caption = " Breakthrough Curve"
        .Font.Size = 14
        .Font.Bold = True
    End With

Sheets(Ctarget(5)).Activate
'graph is created for the observed data. statements identifies size and location, title, chart type, series selection, axes
formatting, plot area formatting, title formatting


    cw = Columns(1).Width
    rh = Rows(1).Height
    Set Graph = ActiveSheet.ChartObjects.Add(cw * 5, rh * 1, cw * 10, rh * 25)
    Graph.Name = " Breakthrough Curve"
    Graph.Chart.ChartType = xlXYScatter

Graph.Chart.SeriesCollection.NewSeries
 With Graph.Chart.SeriesCollection(1)
        .Values = ActiveSheet.Range("B2:B20")
        .XValues = ActiveSheet.Range("A2:A20")
        .Name = "Observed"
        .MarkerSize = 6
        .MarkerStyle = xlMarkerStyleCircle


End With

'    Graph.Chart.SeriesCollection.Add Source:=ActiveSheet.Range("B2:B" & LastRowNewSheet)

    With Graph.Chart.Axes(xlCategory)
        .HasTitle = True
        .AxisTitle.Caption = "Time (min)"
        .CategoryNames = Range("A2:A20" & LastRowNewSheet)
    End With

    With Graph.Chart.Axes(xlValue)
        .HasTitle = True
    With .AxisTitle
        .Caption = "Concentration (uM) "
    End With
    End With

    Graph.Chart.Axes(xlValue).HasMajorGridlines = False
    Graph.Chart.Axes(xlCategory).HasMajorGridlines = False
    Graph.Chart.ChartArea.Interior.Color = RGB(255, 255, 255)
```

```
    Graph.Chart.PlotArea.Interior.Color = RGB(255, 255, 255)
    Graph.RoundedCorners = True
    With Graph.Chart.ChartTitle
        .Caption = " Breakthrough Curve"
        .Font.Size = 14
        .Font.Bold = True
    End With

Sheets(Ctarget(6)).Activate
'graph is created for the observed data. statements identifies size and location, title, chart type, series selection, axes
formatting, plot area formatting, title formatting


    cw = Columns(1).Width
    rh = Rows(1).Height
    Set Graph = ActiveSheet.ChartObjects.Add(cw * 5, rh * 1, cw * 10, rh * 25)
    Graph.Name = " Breakthrough Curve"
    Graph.Chart.ChartType = xlXYScatter

Graph.Chart.SeriesCollection.NewSeries
 With Graph.Chart.SeriesCollection(1)
        .Values = ActiveSheet.Range("B2:B20")
        .XValues = ActiveSheet.Range("A2:A20")
        .Name = "Observed"
        .MarkerSize = 6
        .MarkerStyle = xlMarkerStyleCircle


End With

'    Graph.Chart.SeriesCollection.Add Source:=ActiveSheet.Range("B2:B" & LastRowNewSheet)

    With Graph.Chart.Axes(xlCategory)
        .HasTitle = True
        .AxisTitle.Caption = "Time (min)"
        .CategoryNames = Range("A2:A20" & LastRowNewSheet)
    End With

    With Graph.Chart.Axes(xlValue)
        .HasTitle = True
    With .AxisTitle
        .Caption = "Concentration (uM) "
    End With
    End With

    Graph.Chart.Axes(xlValue).HasMajorGridlines = False
    Graph.Chart.Axes(xlCategory).HasMajorGridlines = False
    Graph.Chart.ChartArea.Interior.Color = RGB(255, 255, 255)
    Graph.Chart.PlotArea.Interior.Color = RGB(255, 255, 255)
    Graph.RoundedCorners = True
    With Graph.Chart.ChartTitle
        .Caption = " Breakthrough Curve"
        .Font.Size = 14
        .Font.Bold = True
    End With
```

```
'Deleting Excess Worksheets and activating screen update
For Each Ws In ThisWorkbook.Worksheets
   If Application.WorksheetFunction.CountA(Ws.Cells) = 0 Then
   Application.DisplayAlerts = False
   Ws.Delete
   Application.DisplayAlerts = True
End If
Next

Application.ScreenUpdating = True

' maximize window, set active sheet to lowest Co, launch userform 3, and hide userform 2

ActiveWindow.WindowState = xlMaximized
Worksheets(1).Activate
UserForm2.Hide
UserForm3.Show

End Sub
```

UserForm 3 code

```
Private Sub Run_Click()

Dim NSIM As Integer
Dim NumSheets As Integer
Dim MaxCnt As Integer
Dim ILO As Integer
Dim IHI As Integer
Dim Scal As Double
Dim ERRMIN As Double
Dim ERPCNT As Double
Dim C(10) As Double
Dim E(10) As Double
Dim P(10, 10) As Double
Dim F(32, 10) As Double
Dim Co As Double
Dim Dstar As Double
Dim ColumnLength As Double
Dim RSS As Double
Dim OLDNOBS As Double
Dim X(10) As Double
Dim ChartObject As String
'Dim Phix(10) As Double
'Dim X(10) As Double
'Dim Data(2000, 10) As Double
'Dim Resi(2000) As Double
'Dim U(2000) As Double
'Dim W(2000) As Double
'Dim YCALC(2000) As Double
'Dim R(10) As Double
'Dim NP As Integer
'Dim NP1 As Integer
```

```
'Dim NOBS As Integer
'Dim bsw As Integer
'Dim Kount As Integer
'Dim Colength As Double
'dimensions that are commented out are available in the "Public_Variables" Module for use as an array transfer to a
public function
DiffusionCoeff = CDbl(DiffusionCoeff.Text)
Colength = CDbl(Colength.Text)
ApparentVel = CDbl(ApparentVel.Text)
Disper = CDbl(Disper.Text)
Retardation = CDbl(Retardation.Text)
FirstOrderDecay = CDbl(FirstOrderDecay.Text)

ActiveSheet.Range("V1") = "First guess of Parameters"
ActiveSheet.Range("v2") = "D* = "
ActiveSheet.Range("v3") = "Col L = "
ActiveSheet.Range("v4") = "vapp = "
ActiveSheet.Range("v5") = "D = "
ActiveSheet.Range("v6") = "R = "
ActiveSheet.Range("v7") = "k = "

ActiveSheet.Range("w2") = DiffusionCoeff
ActiveSheet.Range("w3") = Colength
ActiveSheet.Range("w4") = ApparentVel
ActiveSheet.Range("w5") = Disper
ActiveSheet.Range("w6") = Retardation
ActiveSheet.Range("w7") = FirstOrderDecay

Worksheets(2).Activate

NP = 4
NP1 = NP + 1
manip = "" 'manip is a debugging variable used to denote which manipulation is going on (reflection, expansion,
contraction)
NSIM = 1
MaxCnt = 500
ER = 1
ERRMIN = 0.0001
Dstar = DiffusionCoeff * 60
ColumnLength = Colength.Text
X(1) = ApparentVel * 60
X(2) = Disper
X(3) = Retardation
X(4) = FirstOrderDecay * 60

If X(4) > 0 Then X(4) = Log(X(4))


For i = 1 To 10
   Phix(i) = 0
Next

' fix input sets values negative to allow code to hold negative parameter constant
If GWV.Value = True Then Phix(1) = 1
If Dis.Value = True Then Phix(2) = 1
If RF.Value = True Then Phix(3) = 1
```

```
If FODC.Value = True Then Phix(4) = 1
If X(4) = 0 Then Phix(4) = 1 'if a zero is enetered for the first order decay constant, then it is automatically fixed

'count total sheets to process and set up loop to go through them all with BearPE code

NumSheets = Worksheets.Count
For q = 2 To NumSheets
   Worksheets(q).Activate

Co = CDbl(InputBox("Enter Initial Concentration (ug/l)", "Co Input Required"))

   NOBS = ActiveSheet.Range("A2").End(xlDown).Row - 1
   OLDNOBS = ActiveSheet.Range("E2").End(xlDown).Row
   'clearing data from Columns E&F from "undo" function in userform 3
   ActiveSheet.Range("E2:F" & OLDNOBS).Clear

   'clearing data array to remove previous data

   For i = 1 To 2000
      For J = 1 To NP1
         data(i, J) = 0#
      Next
   Next

   For i = 1 To NOBS
         data(i, 1) = ActiveSheet.Cells(i + 1, 1)
         data(i, 2) = ActiveSheet.Cells(i + 1, 2)
   Next

'starting error function value
 E(1) = ErrorFun(X, Dstar, data, NOBS, Kount, Resi, U, W, YCALC, Co, NP, BSW, manip)

   'INITIALIZE THE SIMPLEX
   Kount = 0

   For J = 1 To NP
      P(1, J) = X(J)
   Next

   For i = 2 To NP1

      For J = 1 To NP
         P(i, J) = X(J)
      Next

   P(i, i - 1) = 1.1 * X(i - 1)
      If (Phix(i - 1) = 1) Then P(i, i - 1) = X(i - 1)
      If (Abs(X(i - 1)) < 0.000000000001) Then P(i, i - 1) = 0.0001
      If (X(4) = 0#) Then P(5, 4) = 0#
      Next

'Find PLOW Ad PHIGH / BEST = PLOW / WORST = PHIGH
31   ILO = 1
     IHI = 1

      For i = 1 To NP1
```

```
        For J = 1 To NP
            X(J) = P(i, J)
        Next

       E(i) = ErrorFun(X, Dstar, data, NOBS, Kount, Resi, U, W, YCALC, Co, NP, BSW, manip)
       If (E(i) < E(ILO)) Then ILO = i
       If (E(i) > E(IHI)) Then IHI = i
     Next

'FIND PNHI THE NEXT HIGHEST NEXT=PNHI

41   NHI = ILO
     For i = 1 To NP1
         If (E(i) >= E(NHI) And i <> IHI) Then NHI = i
43   Next

'COMPUTE THE CENTROID
     For J = 1 To NP
         C(J) = -P(IHI, J)
         For i = 1 To NP1
             C(J) = C(J) + P(i, J)
44         Next
         C(J) = C(J) / NP
46   Next

i = 1

51 GoTo 52

52 'STOPPING CRITERION
     If (Kount > MaxCnt) Then
       UserForm3.Hide
       UserForm4.Show
         If MsgBox("EXECUTION TERMINATED; MAXCOUNT EXCEEDED. Please Enter Correct Distance
from Source and Retry Manually", vbCritical) = vbOK Then
             Exit Sub
     End If
     End If

ERPCNT = Abs(E(ILO) - E(IHI)) / E(ILO) * 100

If (Abs(E(ILO) - E(IHI)) / E(ILO) < ERRMIN) Then GoTo 200
If Kount = 0 Then GoTo 61
If (ER < 0.000001) Then GoTo 200

GoTo 61

'REFLECTION
61   For J = 1 To NP
         R(J) = 1.9985 * C(J) - 0.9985 * P(IHI, J)
62   Next
     manip = "REFLECT"
     ER = ErrorFun(R, Dstar, data, NOBS, Kount, Resi, U, W, YCALC, Co, NP, BSW, manip)

'REFLECTION AGAIN IF SUCCESSFUL
```

```
    If (ER < E(ILO)) Then GoTo 91
    If (ER >= E(IHI)) Then GoTo 122

'REPLACE WORST VERTEX WITH NEW ONE
79   For J = 1 To NP
        P(IHI, J) = R(J)
80   Next

    NSIM = NSIM + 1
    E(IHI) = ER
    If (ER > E(NHI)) Then GoTo 51
    IHI = NHI
    GoTo 41

'EXPAND THE SIMPLEX
91   ILO = IHI
    IHI = NHI
    For J = 1 To NP
        X(J) = 1.95 * R(J) - 0.95 * C(J)
93   Next
    manip = "EXPAND"
    EX = ErrorFun(X, Dstar, data, NOBS, Kount, Resi, U, W, YCALC, Co, NP, BSW, manip)
    If (EX < ER) Then GoTo 104

'R IS BETTER THAN X
    For J = 1 To NP
        P(ILO, J) = R(J)
99   Next

    NSIM = NSIM + 1
    E(ILO) = ER
    GoTo 110

'X IS BETTER THAN R
104  For J = 1 To NP
        P(ILO, J) = X(J)
105  Next

    'IF(IDB > 0) then EX,(X(j),j=1,NP)
    NSIM = NSIM + 1
    E(ILO) = EX
110  GoTo 41

i = 1

'CONTRACT THE SIMPLEX
122  For J = 1 To NP
        R(J) = 0.5015 * C(J) + 0.4985 * P(IHI, J)
123  Next
    manip = "CONTRACT"
    ER = ErrorFun(R, Dstar, data, NOBS, Kount, Resi, U, W, YCALC, Co, NP, BSW, manip)
    If (ER < E(ILO)) Then GoTo 91
    If (ER < E(IHI)) Then GoTo 79

'Scale
Scal = CDbl(InputBox("Enter Scale to Continue: <0 Expands, >0 Shrinks, =0 Stops", "Scale Factor Required"))
```

```
If (Scal = 0#) Then GoTo 200
137   For i = 1 To NP1
          For J = 1 To NP
              P(i, J) = P(i, J) + Scal * (P(ILO, J) - P(i, J))
138       Next
139   Next
      GoTo 31

'WRITING THE OUTPUT

200

ActiveSheet.Range("C1") = "Calculated Conc (ug/l)"
ActiveSheet.Range("D1") = "Residuals"

For i = 1 To NOBS
    ActiveSheet.Cells(i + 1, 3) = YCALC(i)
    ActiveSheet.Cells(i + 1, 4) = Resi(i)
Next

ActiveSheet.Range("A1:D" & NOBS + 1).Select 'Follwowing With statement formats A through D columns for
headers and data alignment
With Selection
    .ColumnWidth = 10
    .NumberFormat = "General"
    .HorizontalAlignment = xlCenter
    .VerticalAlignment = xlCenter
    .WrapText = True
End With



ActiveSheet.ChartObjects(" Breakthrough Curve").Activate
For Each Series In ActiveChart.SeriesCollection
        Series.Delete
        Next Series 'deletes all series to prevent more than two series from being added to the same chart
        ActiveChart.SeriesCollection.NewSeries
 With ActiveChart.SeriesCollection(1)
        .Values = ActiveSheet.Range("B2:B" & NOBS + 1)
        .XValues = ActiveSheet.Range("A2:A" & NOBS + 1)
        .Name = "Observed"
        .MarkerSize = 6
        .MarkerStyle = xlMarkerStyleCircle
    End With

ActiveChart.SeriesCollection.NewSeries 'plots calculated data
 With ActiveChart.SeriesCollection(2)
        .Values = ActiveSheet.Range("C2:C" & NOBS + 1)
        .XValues = ActiveSheet.Range("A2:A" & NOBS + 1)
        .Name = "Calculated"
        .MarkerSize = 6
        .ChartType = xlXYScatterSmoothNoMarkers
    End With
'places text in spreadsheet to identify output parameters
ActiveSheet.Range("G28") = "OPTIMIZED PARAMETER ESTIMATES"
ActiveSheet.Range("G30") = "VELOCITY(m/sec)"
```

```
ActiveSheet.Range("G31") = "DISPERSIVITY (m)"
ActiveSheet.Range("G32") = "RF"
ActiveSheet.Range("G33") = "FODC ( /sec)"
ActiveSheet.Range("G34") = "RESDIUAL SUM OF SQUARES ="
ActiveSheet.Range("G39") = "INITIAL GUESSES AND INPUT OF PARAMETERS"
ActiveSheet.Range("G41") = "VELOCITY(m/sec)"
ActiveSheet.Range("G42") = "DISPERSIVITY (m)"
ActiveSheet.Range("G43") = "RF"
ActiveSheet.Range("G44") = "FODC ( /sec)"
ActiveSheet.Range("G45") = "ColumnLength (m)"
ActiveSheet.Range("G46") = "DIFFUSION COEFF (m^2/sec)"
ActiveSheet.Range("G47") = "Co (ug/l)"
ActiveSheet.Range("M40") = "FIX"
ActiveSheet.Range("G1").ColumnWidth = 10 ' allows all text to be seen


'places values for optimized parameter estimates
ActiveSheet.Range("J30") = X(1) / 60
ActiveSheet.Range("J31") = X(2)
ActiveSheet.Range("J32") = X(3)
ActiveSheet.Range("J33") = Exp(X(4)) / 60
ActiveSheet.Range("K34") = E(ILO)

If (Co) = True Then
ActiveSheet.Range("J47") = CDbl(InitialConcentration.Text)
End If

' places values for initial guesses
ActiveSheet.Range("J41") = CDbl(ApparentVel.Text)
ActiveSheet.Range("J42") = CDbl(Disper.Text)
ActiveSheet.Range("J43") = CDbl(Retardation.Text)
ActiveSheet.Range("J44") = CDbl(FirstOrderDecay.Text)
ActiveSheet.Range("J45") = CDbl(Colength.Text)
ActiveSheet.Range("J46") = CDbl(DiffusionCoeff.Text)
ActiveSheet.Range("J47") = Co
'denoting parameters fixed at input
If GWV.Value = True Then ActiveSheet.Range("M41") = "Y"
If Dis.Value = True Then ActiveSheet.Range("M42") = "Y"
If RF.Value = True Then ActiveSheet.Range("M43") = "Y"
If FODC.Value = True Then ActiveSheet.Range("M44") = "Y"
If GWV.Value = False Then ActiveSheet.Range("M41") = " "
If Dis.Value = False Then ActiveSheet.Range("M42") = " "
If RF.Value = False Then ActiveSheet.Range("M43") = " "
If FODC.Value = False Then ActiveSheet.Range("M44") = " "
ActiveSheet.Range("M45:M46") = "Y" 'distance and diffusion coeff never varied

'code for confidence int
Confit = CONFINT(X, Dstar, data, NOBS, Kount, Resi, U, W, YCALC, Co, NP, BSW, Phix, R, C)

Next

UserForm3.Hide


SheetCounter = 1
Sheets(Ctarget(SheetCounter)).Activate
```

```
UserForm9.Show


End Sub

Public Function ErrorFun(X, Dstar As Double, data, NOBS As Integer, Kount As Integer, Resi, U, W, YCALC, Co
As Double, NP As Integer, BSW As Integer, manip As String) As Double

   'COMPUTES THE ERROR FUNCTION FOR THE DATA SET
    'SMALLER VALUE IS BETTER

Dim SMRESI As Double
Dim u1 As Double
Dim u2 As Double
Dim uA As Double
Dim uB As Double
      u1 = 0#
      u2 = 0#

      ErrorFun = 0#
      SMRESI = 0#

If Bisquare.Value = True Then BSW = 1
If Relative.Value = True Then BSW = 2
If None.Value = True Then BSW = 0

'Sometimes negative values are predicted by the optimizer that are not real and will cause VBA run time errors.
'The following function simply converts them to positive values prior to evaluating the error function
 For J = 1 To NP - 1
        If X(J) < 0 Then X(J) = -X(J)
 Next
If (X(4) <> 0#) Then X(4) = Exp(X(4))

For i = 1 To 2000
    Resi(i) = 0#
    U(i) = 0#
    W(i) = 0#
10 Next

For i = 1 To NOBS

'CHANGE THE NEXT STATEMENT TO CHANGE THE FUNCTION BEING FIT
      'SquareRoot = num ^ (1 / 2)
      DCOEF = Dstar + X(1) * X(2)
      ColumnLength = CDbl(Colength.Text)
      'If (Data(i, 1) <= 0#) Then
          'EXPU1 = 0#
          'GoTo 20
      'Else
          u1 = (X(1) * ColumnLength / (2 * DCOEF)) * (1 - (1 + (4 * X(4) * DCOEF) / X(1) ^ 2) ^ 0.5)
          EXPU1 = Exp(u1)
      'End If

20    'If (Data(i, 1) <= ColumnLength / X(1)) Then
          'ERFCU2 = 0#
```

```
        'GoTo 30
     'Else
        u2 = (X(3) * ColumnLength - X(1) * data(i, 1) * (1 + (4 * X(4) * DCOEF / X(1) ^ 2)) ^ 0.5) / (2 * (DCOEF *
X(3) * data(i, 1)) ^ 0.5)

        ERFCU2 = ERFC(u2)
        uA = uA
    'End If

30   GoTo 40

40   YCALC(i) = 0.5 * Co * (EXPU1 * ERFCU2)
    Resi(i) = data(i, 2) - YCALC(i)
    SMRESI = SMRESI + Abs(Resi(i))
60   Next

    If (BSW = 1) Then
        C = 4# * SMRESI / CDbl(NOBS)
        For i = 1 To NOBS
            U(i) = Resi(i) / C
            W(i) = (1 - U(i) * U(i)) ^ 2
            If (U(i) > 1#) Then W(i) = 0#
            ErrorFun = ErrorFun + W(i) * Resi(i) * Resi(i)
70        Next
    End If

    If (BSW = 2) Then
        For i = 1 To NOBS
            If (data(i, 2) = 0#) Then
                W(i) = 0#
            Else
                W(i) = 1# / (data(i, 2) ^ 2#)
            End If
            ErrorFun = ErrorFun + W(i) * Resi(i) * Resi(i)
75        Next
    End If

    If (BSW = 0) Then
      For i = 1 To NOBS
          ErrorFun = ErrorFun + Resi(i) * Resi(i)
80     Next

    End If

    Kount = Kount + 1

   If (X(4) > 0#) Then X(4) = Log(X(4))


'fills calculated data and residuals into spreasheet for debugging purposes. X(1) through X(4) units are converted to
those used in BEARPE for comparison

    'ActiveSheet.Cells(Kount, 17) = X(1)/60
    'ActiveSheet.Cells(Kount, 18) = X(2)
    'ActiveSheet.Cells(Kount, 19) = X(3)
    'ActiveSheet.Cells(Kount, 20) = X(4)/60
```

```
    'ActiveSheet.Cells(Kount, 23) = manip
    'ActiveSheet.Cells(Kount, 24) = ErrorFun



End Function


Public Function ERFC(arg As Double)


'COMPLIMENTARY ERROR FUNCTION SUBROUTINE REAL*8 FUNCTION ERFC(ARG)
'COMPUTES THE COMPLIMENTARY ERROR FUNCTIOn FOR AN ARGUMENT
'IMPLICIT REAL*8 (A-H,L,M,O-Z)
'PARAMETER (P=0.3275911, A1=0.254829592, A2=-0.284496736,
'   1          A3=1.421413741, A4=-1.453152027, A5=1.061405429)
'TU = 1 / (1 + p * Abs(ARG))

'    ERFC=(A1*TU+A2*TU**2+A3*TU**3+A4*TU**4+A5*TU**5)
'   1      *EXP(-(ARG**2))
'    IF(ARG .LT. 0) ERFC=2-ERFC

'    RETURN
'    END


Dim P As Double
Dim A1 As Double
Dim A2 As Double
Dim A3 As Double
Dim A4 As Double
Dim A5 As Double
Dim TU As Double

P = 0.3275911
A1 = 0.254829592
A2 = -0.284496736
A3 = 1.421413741
A4 = -1.453152027
A5 = 1.061405429


TU = 1 / (1 + P * Abs(arg))

    ERFC = (A1 * TU + A2 * TU ^ 2 + A3 * TU ^ 3 + A4 * TU ^ 4 + A5 * TU ^ 5) * Exp(-(arg ^ 2))

    If (arg < 0) Then ERFC = 2 - ERFC


'*********** FUNCTION DERFC(ARG)
'   ROUTINE FOR ERFC (ARG) BY SERIES EXPANSION
'   DOUBLE PRECISION VERSION


 '    Dim IL As Integer
 '    Dim LJL As Integer
```

```
'     Dim JLJ As Integer
'     Dim XOX As Double
'     Dim SUMXOX As Double
'     Dim Fact As Double
'     Dim UOX As Double
'     Dim US As Double
'     Dim ZOZ As Double
'     Dim TXOX As Double
'     Dim OLDFACT As Double


'     Pi = 3.14159265358
'     SUMXOX = 1#
'     XOX = Abs(arg)
'     If (XOX > 3.4) Then GoTo 5160

'  THIS SERIES EXPANSION IS FOR ARG <= 3.4

'     Fact = 1#
'     IL = 1
'     UOX = XOX * XOX
'     US = UOX
'5085  Fact = Fact * IL
'     ZOZ = -1#
'     If ((IL / 2) * 2 = IL) Then ZOZ = 1#
'     TXOX = UOX / ((2# * IL + 1#) * Fact)
'     SUMXOX = SUMXOX + ZOZ * TXOX
'     UOX = UOX * US
'     IL = IL + 1


'     STOP THIE SUMMATION WHEN THE CURRENT TERM
'     IS LESS THAN 1E-20


'     If (TXOX > 1E-20) Then GoTo 5085
'     ERFC = 1# - 2# * XOX / (Pi) ^ 0.5 * SUMXOX
'     If (arg < 0#) Then ERFC = 2# - ERFC
'     GoTo 5430
'5160  If (XOX > 14#) Then GoTo 5410

'   THIS SERIES EXPANSION IS FOR ARG>3.4

'     UOX = 2# * XOX * XOX
'     LJL = 1
'     JLJ = 1
'     Fact = 1#
'5300  OLDFAC = Fact
'     Fact = Fact / UOX * JLJ

'  STOP THE SUMMATION WHEN THE CURRENT TERM BECOMES LARGER THAN
'  THE PREVIOUS TERM

'     If (Fact > OLDFAC) Then GoTo 5333
'     ZOZ = -1#
'     If ((LJL / 2) * 2 = LJL) Then ZOZ = 1#
```

```
'     TXOX = ZOZ * Fact
'     SUMXOX = SUMXOX + TXOX
'     LJL = LJL + 1
'     JLJ = JLJ + 2
'5333  ERFC = Exp(-XOX * XOX) / (Pi) ^ 0.5 / XOX * SUMXOX
'     GoTo 5420
'5410  ERFC = 0#
'5420  If (arg < 0#) Then ERFC = 2# - ERFC
5430 End Function

Public Function CONFINT(X, Dstar As Double, data, NOBS As Integer, Kount As Integer, Resi, U, W, YCALC,
Co As Double, NP As Integer, BSW As Integer, Phix, R, C) As Double

Dim NME(4) As String

NME(1) = "VELOCITY(m/sec)"
NME(2) = "DISPERSIVITY(m)"
NME(3) = "RF"
NME(4) = "FODC(1/sec)"


ActiveSheet.Range("G50:K60").Clear

  'DEFINING NPP TO BE THE NUMBER OF PARAMETERS BEING FIT
     NPP = 0
     For i = 1 To NP
         If Phix(i) = 0 Then NPP = NPP + 1
10    Next
     If NPP = 0 Then GoTo 300

   'DETERMINING THE CRITICAL RESIDUAL SUM OF SQUARES
   'WHICH DEFINES THE UPPER AND LOWER CONFIDENCE INTERVAL

     ER = ErrorFun(X, Dstar, data, NOBS, Kount, Resi, U, W, YCALC, Co, NP, BSW, manip)
     'FESTI = FESTIM(NOBS, NPP, IDB) alternative below
     ActiveSheet.Range("G51") = NOBS 'allows NOBS to be used in Excel's FINV function
     ActiveSheet.Range("G50") = "=FInv(0.05, G51-4, 4)" '0.05 = 95% confidence interval, G51 = NOBS, 4 = NP,
degrees of freedom = NOBS-NP, NP
     FESTI = ActiveSheet.Range("G50").Value
     'Fnpp = float(NPP)
     'FNOBS = float(NOBS)
     'RSSCRIT = ER * (1 + Fnpp / (FNOBS - Fnpp) * FESTI)
      RSSCRIT = ER * (1 + NPP / (NOBS - NPP) * FESTI)

'    LOOPING THROUGH THE PARAMETERS TO DETERMINE CONFIDENCE INTERVALS

For i = 1 To NP
    For J = 1 To NP
      R(J) = X(J)
      C(J) = X(J)
90  Next

     If Phix(i) = 1 Then GoTo 199

'   LOOKING FOR THE UPPER LIMIT
         NCOUNT = 1
```

```
100

   'IF(FLOAT(I) .EQ. 4. .AND. X(I) .LT. 0.) THEN
    If i = 4 And X(i) < 0 Then
            R(i) = R(i) - 0.1 * X(i)
        Else
            R(i) = R(i) + 0.1 * X(i)
        End If
        ER = ErrorFun(R, Dstar, data, NOBS, Kount, Resi, U, W, YCALC, Co, NP, BSW, manip)
        If R(4) < -100 Or R(4) > 100 Then GoTo 120
        If NCOUNT > 1 Then
            If Abs((ERCHK - ER) / ER * 100) < 0.001 Then
                R(i) = -1#
                GoTo 120
            End If
        Else
            NCOUNT = 2
        End If
        ERCHK = ER
        If ER < RSSCRIT Then GoTo 100

110

      'IF(FLOAT(I) .EQ. 4. .AND. X(I) .LT. 0.) THEN
      If i = 4 And X(i) < 0 Then

         R(i) = R(i) + 0.01 * X(i)
         Else
         R(i) = R(i) - 0.01 * X(i)
      End If

   ER = ErrorFun(R, Dstar, data, NOBS, Kount, Resi, U, W, YCALC, Co, NP, BSW, manip)
      If ER > RSSCRIT Then GoTo 110

    'LOOKING FOR THE LOWER LIMIT
120
      'IF(FLOAT(I) .EQ. 4. .AND. X(I) .LT. 0.) THEN
       If i = 4 And X(i) < 0 Then
            C(i) = C(i) + 0.1 * X(i)
        Else
            C(i) = C(i) - 0.1 * X(i)
        End If
       'IF(C(I) .LT. 0. .AND. FLOAT(I) .NE. 4.) THEN
       If C(i) < 0 And i <> 4 Then
            C(i) = C(i) + 0.1 * X(i)
125           C(i) = C(i) - 0.01 * X(i)
            If C(i) < 0 Then
                C(i) = 0#
                GoTo 249
            End If
        End If

        ER = ErrorFun(C, Dstar, data, NOBS, Kount, Resi, U, W, YCALC, Co, NP, BSW, manip)
        If C(4) < -100 Or C(4) > 100 Then GoTo 249
        If ER < RSSCRIT Then GoTo 120
```

```
130
        'IF(FLOAT(I) .EQ. 4. .AND. X(I) .LT. 0.) THEN
        If i = 4 And X(i) < 0 Then
            C(i) = C(i) - 0.01 * X(i)
        Else
            C(i) = C(i) + 0.01 * X(i)
        End If

        ER = ErrorFun(C, Dstar, data, NOBS, Kount, Resi, U, W, YCALC, Co, NP, BSW, manip)
        If ER > RSSCRIT Then GoTo 130

249
        If i = 4 Then
            X(i) = Exp(X(i))
            If R(i) < -99 Then
                R(i) = 0#
            Else
                R(i) = Exp(R(i))
            End If
            C(i) = Exp(C(i))
        End If

259  'Writing to the output file

       ActiveSheet.Range("G50") = "95% CONFIDENCE INTERVALS FOR ESTIMATED PARAMETERS"
       ActiveSheet.Range("G51") = "Parameter"
       ActiveSheet.Range("I51") = "Low"
       ActiveSheet.Range("J51") = "Optimized"
       ActiveSheet.Range("K51") = "High"
       ActiveSheet.Range("G60") = "CRITICAL RSS VALUE ="
       ActiveSheet.Range("J60") = RSSCRIT

       If R(i) > 0 Then

          ActiveSheet.Cells(i + 52, 7) = NME(i)
          ActiveSheet.Cells(i + 52, 9) = C(i) 'lower limit
          ActiveSheet.Cells(i + 52, 10) = X(i) 'optimized
          ActiveSheet.Cells(i + 52, 11) = R(i) 'upper limit

            If i = 1 Then 'converts velocity to m/sec
                ActiveSheet.Cells(i + 52, 9) = C(i) / 60 'lower limit
                ActiveSheet.Cells(i + 52, 10) = X(i) / 60 'optimized
                ActiveSheet.Cells(i + 52, 11) = R(i) / 60 'upper limit
            End If

            If i = 4 Then ' converts FODC to /sec
                ActiveSheet.Cells(i + 52, 9) = C(i) / 60 'lower limit
                ActiveSheet.Cells(i + 52, 10) = X(i) / 60 'optimized
                ActiveSheet.Cells(i + 52, 11) = R(i) / 60 'upper limit
            End If

        Else
         ActiveSheet.Range("G52") = "No Convergence"
        End If
199
200   Next
```

```
        If R(i) = 0 Then

            ActiveSheet.Cells(i + 52, 7) = ""
            ActiveSheet.Cells(i + 52, 9) = ""
            ActiveSheet.Cells(i + 52, 10) = ""
            ActiveSheet.Cells(i + 52, 11) = ""
        End If

299
300
    If X(4) > 0 Then
        X(4) = Log(X(4))
    Else
        X(4) = 0#
    End If

End Function

UserForm 4 code
Private Sub EnterDefaults_Click()
Dim sh As String

sh = ActiveSheet.Name

Worksheets(1).Activate
DiffusionCoeff = ActiveSheet.Range("w2")
Colength = ActiveSheet.Range("w3")
ApparentVel = ActiveSheet.Range("w4")
Disper = ActiveSheet.Range("w5")
Retardation = ActiveSheet.Range("w6")
FirstOrderDecay = ActiveSheet.Range("w7")

Sheets(sh).Activate


End Sub

Private Sub EnableButton_Click()

Dim White As String
Dim Grey As String

White = "&H80000005"
Grey = "&H8000000B"

If UserForm4.EnableButton.Value = True Then
   InCo.BackColor = White
   InCo.Enabled = True
End If

End Sub

Private Sub DisableButton_Click()
```

```
Dim White As String
Dim Grey As String

White = "&H80000005"
Grey = "&H8000000B"

If UserForm4.DisableButton.Value = True Then
   InCo.BackColor = Grey
   InCo.Enabled = False
End If

End Sub


Private Sub Run_Click()

Dim NSIM As Integer
Dim NumSheets As Integer
Dim MaxCnt As Integer
Dim ILO As Integer
Dim IHI As Integer
Dim Scal As Double
Dim ERRMIN As Double
Dim ERPCNT As Double
Dim C(10) As Double
Dim E(10) As Double
Dim P(10, 10) As Double
Dim F(32, 10) As Double
Dim Co As Double
Dim Dstar As Double
Dim ColumnLength As Double
Dim RSS As Double
Dim OLDNOBS As Double
Dim X(10) As Double
Dim ChartObject As String
Dim InitialConcentration As Double
Dim Edit As Integer
'Dim Phix(10) As Double
'Dim X(10) As Double
'Dim Data(2000, 10) As Double
'Dim Resi(2000) As Double
'Dim U(2000) As Double
'Dim W(2000) As Double
'Dim YCALC(2000) As Double
'Dim R(10) As Double
'Dim NP As Integer
'Dim NP1 As Integer
'Dim NOBS As Integer
'Dim bsw As Integer
'Dim Kount As Integer
'Dim Colength As Double
'Dim Co As Double
'dimensions that are commented out are available in the "Public_Variables" Module for use as an array transfer to a
public function

NP = 4
```

```
NP1 = NP + 1
manip = "" 'manip is a debugging variable used to denote which manipulation is going on (reflection, expansion,
contraction)
NSIM = 1
MaxCnt = 500
ER = 1
ERRMIN = 0.0001
If EnableButton = True Then
   Co = CDbl(InCo.Text)
   Edit = 1
Else
   Co = ActiveSheet.Range("J47")
End If

Dstar = CDbl(DiffusionCoeff.Text) * 60
ColumnLength = CDbl(Colength.Text)
X(1) = CDbl(ApparentVel) * 60
X(2) = CDbl(Disper)
X(3) = CDbl(Retardation.Text)
X(4) = CDbl(FirstOrderDecay.Text) * 60

If X(4) > 0 Then X(4) = Log(X(4))


For i = 1 To 10
   Phix(i) = 0
Next

' fix input sets values negative to allow code to hold negative parameter constant
If GWV.Value = True Then Phix(1) = 1
If Dis.Value = True Then Phix(2) = 1
If RF.Value = True Then Phix(3) = 1
If FODC.Value = True Then Phix(4) = 1
If X(4) = 0 Then Phix(4) = 1 'if a zero is enetered for the first order decay constant, then it is automatically fixed

'count total sheets to process and set up loop to go through them all with BearPE code

NumSheets = Worksheets.Count
'For q = 2 To NumSheets
   'Worksheets(q).Activate



   NOBS = ActiveSheet.Range("A2").End(xlDown).Row - 1
   OLDNOBS = ActiveSheet.Range("E2").End(xlDown).Row
   'clearing data from Columns E&F from "undo" function in userform 3
   ActiveSheet.Range("E2:F" & OLDNOBS).Clear

   'clearing data array to remove previous data

   For i = 1 To 2000
      For J = 1 To NP1
         data(i, J) = 0#
      Next
   Next
```

```
   For i = 1 To NOBS
         data(i, 1) = ActiveSheet.Cells(i + 1, 1)
         data(i, 2) = ActiveSheet.Cells(i + 1, 2)
   Next

'starting error function value
 E(1) = ErrorFun(X, Dstar, data, NOBS, Kount, Resi, U, W, YCALC, Co, NP, BSW, manip)

   'INITIALIZE THE SIMPLEX
   Kount = 0

   For J = 1 To NP
      P(1, J) = X(J)
   Next

   For i = 2 To NP1

      For J = 1 To NP
         P(i, J) = X(J)
      Next

   P(i, i - 1) = 1.1 * X(i - 1)
      If (Phix(i - 1) = 1) Then P(i, i - 1) = X(i - 1)
      If (Abs(X(i - 1)) < 0.000000000001) Then P(i, i - 1) = 0.0001
      If (X(4) = 0#) Then P(5, 4) = 0#
      Next

'Find PLOW Ad PHIGH / BEST = PLOW / WORST = PHIGH
31   ILO = 1
     IHI = 1

      For i = 1 To NP1

         For J = 1 To NP
            X(J) = P(i, J)
         Next

        E(i) = ErrorFun(X, Dstar, data, NOBS, Kount, Resi, U, W, YCALC, Co, NP, BSW, manip)
        If (E(i) < E(ILO)) Then ILO = i
        If (E(i) > E(IHI)) Then IHI = i
      Next

'FIND PNHI THE NEXT HIGHEST NEXT=PNHI

41    NHI = ILO
     For i = 1 To NP1
         If (E(i) >= E(NHI) And i <> IHI) Then NHI = i
43    Next

'COMPUTE THE CENTROID
     For J = 1 To NP
        C(J) = -P(IHI, J)
        For i = 1 To NP1
            C(J) = C(J) + P(i, J)
44        Next
        C(J) = C(J) / NP
```

```
46    Next

i = 1

51 GoTo 52

52 'STOPPING CRITERION
     If (Kount > MaxCnt) Then
       UserForm3.Hide
       UserForm4.Show
          If MsgBox("EXECUTION TERMINATED; MAXCOUNT EXCEEDED. Please Enter Correct Distance
from Source and Retry Manually", vbCritical) = vbOK Then
             Exit Sub
     End If
     End If

ERPCNT = Abs(E(ILO) - E(IHI)) / E(ILO) * 100

If (Abs(E(ILO) - E(IHI)) / E(ILO) < ERRMIN) Then GoTo 200
If Kount = 0 Then GoTo 61
If (ER < 0.000001) Then GoTo 200

GoTo 61

'REFLECTION
61    For J = 1 To NP
         R(J) = 1.9985 * C(J) - 0.9985 * P(IHI, J)
62    Next
     manip = "REFLECT"
     ER = ErrorFun(R, Dstar, data, NOBS, Kount, Resi, U, W, YCALC, Co, NP, BSW, manip)

'REFLECTION AGAIN IF SUCCESSFUL
     If (ER < E(ILO)) Then GoTo 91
     If (ER >= E(IHI)) Then GoTo 122

'REPLACE WORST VERTEX WITH NEW ONE
79    For J = 1 To NP
         P(IHI, J) = R(J)
80    Next

     NSIM = NSIM + 1
     E(IHI) = ER
     If (ER > E(NHI)) Then GoTo 51
     IHI = NHI
     GoTo 41

'EXPAND THE SIMPLEX
91    ILO = IHI
     IHI = NHI
     For J = 1 To NP
         X(J) = 1.95 * R(J) - 0.95 * C(J)
93    Next
     manip = "EXPAND"
     EX = ErrorFun(X, Dstar, data, NOBS, Kount, Resi, U, W, YCALC, Co, NP, BSW, manip)
     If (EX < ER) Then GoTo 104
```

```
'R IS BETTER THAN X
    For J = 1 To NP
        P(ILO, J) = R(J)
99    Next

    NSIM = NSIM + 1
    E(ILO) = ER
    GoTo 110

'X IS BETTER THAN R
104   For J = 1 To NP
        P(ILO, J) = X(J)
105   Next

    'IF(IDB > 0) then EX,(X(j),j=1,NP)
    NSIM = NSIM + 1
    E(ILO) = EX
110   GoTo 41

i = 1

'CONTRACT THE SIMPLEX
122   For J = 1 To NP
        R(J) = 0.5015 * C(J) + 0.4985 * P(IHI, J)
123   Next
    manip = "CONTRACT"
    ER = ErrorFun(R, Dstar, data, NOBS, Kount, Resi, U, W, YCALC, Co, NP, BSW, manip)
    If (ER < E(ILO)) Then GoTo 91
    If (ER < E(IHI)) Then GoTo 79

'Scale
Scal = CDbl(InputBox("Enter Scale to Continue: <0 Expands, >0 Shrinks, =0 Stops", "Scale Factor Required"))
If (Scal = 0#) Then GoTo 200
137   For i = 1 To NP1
        For J = 1 To NP
            P(i, J) = P(i, J) + Scal * (P(ILO, J) - P(i, J))
138       Next
139   Next
    GoTo 31

'WRITING THE OUTPUT

200

ActiveSheet.Range("C1") = "Calculated Conc (ug/l)"
ActiveSheet.Range("D1") = "Residuals"

For i = 1 To NOBS
   ActiveSheet.Cells(i + 1, 3) = YCALC(i)
   ActiveSheet.Cells(i + 1, 4) = Resi(i)
Next

ActiveSheet.Range("A1:D" & NOBS + 1).Select 'Follwowing With statement formats A through D columns for
headers and data alignment
With Selection
   .ColumnWidth = 10
```

```
    .NumberFormat = "General"
    .HorizontalAlignment = xlCenter
    .VerticalAlignment = xlCenter
    .WrapText = True
End With



ActiveSheet.ChartObjects(" Breakthrough Curve").Activate
For Each Series In ActiveChart.SeriesCollection
        Series.Delete
        Next Series 'deletes all series to prevent more than two series from being added to the same chart
        ActiveChart.SeriesCollection.NewSeries
 With ActiveChart.SeriesCollection(1)
        .Values = ActiveSheet.Range("B2:B" & NOBS + 1)
        .XValues = ActiveSheet.Range("A2:A" & NOBS + 1)
        .Name = "Observed"
        .MarkerSize = 6
        .MarkerStyle = xlMarkerStyleCircle
    End With

ActiveChart.SeriesCollection.NewSeries 'plots calculated data
 With ActiveChart.SeriesCollection(2)
        .Values = ActiveSheet.Range("C2:C" & NOBS + 1)
        .XValues = ActiveSheet.Range("A2:A" & NOBS + 1)
        .Name = "Calculated"
        .MarkerSize = 6
        .ChartType = xlXYScatterSmoothNoMarkers
    End With
'places text in spreadsheet to identify output parameters
ActiveSheet.Range("G28") = "OPTIMIZED PARAMETER ESTIMATES"
ActiveSheet.Range("G30") = "VELOCITY(m/sec)"
ActiveSheet.Range("G31") = "DISPERSIVITY (m)"
ActiveSheet.Range("G32") = "RF"
ActiveSheet.Range("G33") = "FODC ( /sec)"
ActiveSheet.Range("G34") = "RESDIUAL SUM OF SQUARES ="
ActiveSheet.Range("G39") = "INITIAL GUESSES AND INPUT OF PARAMETERS"
ActiveSheet.Range("G41") = "VELOCITY(m/sec)"
ActiveSheet.Range("G42") = "DISPERSIVITY (m)"
ActiveSheet.Range("G43") = "RF"
ActiveSheet.Range("G44") = "FODC ( /sec)"
ActiveSheet.Range("G45") = "ColumnLength (m)"
ActiveSheet.Range("G46") = "DIFFUSION COEFF (m^2/sec)"
ActiveSheet.Range("G47") = "Co (ug/l)"
ActiveSheet.Range("M40") = "FIX"
ActiveSheet.Range("G1").ColumnWidth = 10 ' allows all text to be seen


'places values for optimized parameter estimates
ActiveSheet.Range("J30") = X(1) / 60
ActiveSheet.Range("J31") = X(2)
ActiveSheet.Range("J32") = X(3)
ActiveSheet.Range("J33") = Exp(X(4)) / 60
ActiveSheet.Range("K34") = E(ILO)
' places values for initial guesses
ActiveSheet.Range("J41") = CDbl(ApparentVel.Text)
```

```
ActiveSheet.Range("J42") = CDbl(Disper.Text)
ActiveSheet.Range("J43") = CDbl(Retardation.Text)
ActiveSheet.Range("J44") = CDbl(FirstOrderDecay.Text)
ActiveSheet.Range("J45") = CDbl(Colength.Text)
ActiveSheet.Range("J46") = CDbl(DiffusionCoeff.Text)
'ActiveSheet.Range("J47") = CDbl(InCo.Text)

If InCo.Enabled = True Then
ActiveSheet.Range("J47") = CDbl(InCo.Text)
End If
'denoting parameters fixed at input
If GWV.Value = True Then ActiveSheet.Range("M41") = "Y"
If Dis.Value = True Then ActiveSheet.Range("M42") = "Y"
If RF.Value = True Then ActiveSheet.Range("M43") = "Y"
If FODC.Value = True Then ActiveSheet.Range("M44") = "Y"
If GWV.Value = False Then ActiveSheet.Range("M41") = " "
If Dis.Value = False Then ActiveSheet.Range("M42") = " "
If RF.Value = False Then ActiveSheet.Range("M43") = " "
If FODC.Value = False Then ActiveSheet.Range("M44") = " "
ActiveSheet.Range("M45:M46") = "Y" 'distance and diffusion coeff never varied

'code for confidence int
Confit = CONFINT(X, Dstar, data, NOBS, Kount, Resi, U, W, YCALC, Co, NP, BSW, Phix, R, C)

'Next

UserForm4.Hide
UserForm9.Show

End Sub

Public Function ErrorFun(X, Dstar As Double, data, NOBS As Integer, Kount As Integer, Resi, U, W, YCALC, Co
As Double, NP As Integer, BSW As Integer, manip As String) As Double

  'COMPUTES THE ERROR FUNCTION FOR THE DATA SET
   'SMALLER VALUE IS BETTER

Dim SMRESI As Double
Dim u1 As Double
Dim u2 As Double
Dim uA As Double
Dim uB As Double
     u1 = 0#
     u2 = 0#

     ErrorFun = 0#
     SMRESI = 0#

If Bisquare.Value = True Then BSW = 1
If Relative.Value = True Then BSW = 2
If None.Value = True Then BSW = 0

'Sometimes negative values are predicted by the optimizer that are not real and will cause VBA run time errors.
'The following function simply converts them to positive values prior to evaluating the error function
 For J = 1 To NP - 1
       If X(J) < 0 Then X(J) = -X(J)
```

```
 Next
If (X(4) <> 0#) Then X(4) = Exp(X(4))

For i = 1 To 2000
   Resi(i) = 0#
   U(i) = 0#
   W(i) = 0#
10 Next

For i = 1 To NOBS

'CHANGE THE NEXT STATEMENT TO CHANGE THE FUNCTION BEING FIT
     'SquareRoot = num ^ (1 / 2)
     DCOEF = Dstar + X(1) * X(2)
     ColumnLength = CDbl(Colength.Text)
     'Co = CDbl(InCo.Text)
     'If (Data(i, 1) <= 0#) Then
         'EXPU1 = 0#
         'GoTo 20
     'Else
         u1 = (X(1) * ColumnLength / (2 * DCOEF)) * (1 - (1 + (4 * X(4) * DCOEF) / X(1) ^ 2) ^ 0.5)
         EXPU1 = Exp(u1)
     'End If

20   'If (Data(i, 1) <= ColumnLength / X(1)) Then
         'ERFCU2 = 0#
         'GoTo 30
      'Else
         u2 = (X(3) * ColumnLength - X(1) * data(i, 1) * (1 + (4 * X(4) * DCOEF / X(1) ^ 2)) ^ 0.5) / (2 * (DCOEF *
X(3) * data(i, 1)) ^ 0.5)

         ERFCU2 = ERFC(u2)
         uA = uA
     'End If

30   GoTo 40

40   YCALC(i) = 0.5 * Co * (EXPU1 * ERFCU2)
     Resi(i) = data(i, 2) - YCALC(i)
     SMRESI = SMRESI + Abs(Resi(i))
60   Next

     If (BSW = 1) Then
         C = 4# * SMRESI / CDbl(NOBS)
         For i = 1 To NOBS
             U(i) = Resi(i) / C
             W(i) = (1 - U(i) * U(i)) ^ 2
             If (U(i) > 1#) Then W(i) = 0#
             ErrorFun = ErrorFun + W(i) * Resi(i) * Resi(i)
70         Next
     End If

     If (BSW = 2) Then
         For i = 1 To NOBS
             If (data(i, 2) = 0#) Then
                 W(i) = 0#
```

```
            Else
                W(i) = 1# / (data(i, 2) ^ 2#)
            End If
            ErrorFun = ErrorFun + W(i) * Resi(i) * Resi(i)
        Next
    End If

    If (BSW = 0) Then
      For i = 1 To NOBS
          ErrorFun = ErrorFun + Resi(i) * Resi(i)
     Next

    End If

    Kount = Kount + 1

   If (X(4) > 0#) Then X(4) = Log(X(4))



End Function


Public Function ERFC(arg As Double)


'COMPLIMENTARY ERROR FUNCTION SUBROUTINE REAL*8 FUNCTION ERFC(ARG)
'COMPUTES THE COMPLIMENTARY ERROR FUNCTIOn FOR AN ARGUMENT
'IMPLICIT REAL*8 (A-H,L,M,O-Z)
'PARAMETER (P=0.3275911, A1=0.254829592, A2=-0.284496736,
'    1          A3=1.421413741, A4=-1.453152027, A5=1.061405429)
'TU = 1 / (1 + p * Abs(ARG))

'    ERFC=(A1*TU+A2*TU**2+A3*TU**3+A4*TU**4+A5*TU**5)
'    1      *EXP(-(ARG**2))
'    IF(ARG .LT. 0) ERFC=2-ERFC

'    RETURN
'    END


Dim P As Double
Dim A1 As Double
Dim A2 As Double
Dim A3 As Double
Dim A4 As Double
Dim A5 As Double
Dim TU As Double

P = 0.3275911
A1 = 0.254829592
A2 = -0.284496736
A3 = 1.421413741
A4 = -1.453152027
A5 = 1.061405429
```

```
TU = 1 / (1 + P * Abs(arg))

    ERFC = (A1 * TU + A2 * TU ^ 2 + A3 * TU ^ 3 + A4 * TU ^ 4 + A5 * TU ^ 5) * Exp(-(arg ^ 2))

    If (arg < 0) Then ERFC = 2 - ERFC


'*********** FUNCTION DERFC(ARG)
'   ROUTINE FOR ERFC (ARG) BY SERIES EXPANSION
'   DOUBLE PRECISION VERSION


 '    Dim IL As Integer
 '    Dim LJL As Integer
 '    Dim JLJ As Integer
 '    Dim XOX As Double
 '    Dim SUMXOX As Double
 '    Dim Fact As Double
 '    Dim UOX As Double
 '    Dim US As Double
 '    Dim ZOZ As Double
 '    Dim TXOX As Double
 '    Dim OLDFACT As Double


  '    Pi = 3.14159265358
  '    SUMXOX = 1#
  '    XOX = Abs(arg)
  '    If (XOX > 3.4) Then GoTo 5160

'  THIS SERIES EXPANSION IS FOR ARG <= 3.4

  '    Fact = 1#
   '   IL = 1
    '  UOX = XOX * XOX
    '  US = UOX
'5085  Fact = Fact * IL
'     ZOZ = -1#
'     If ((IL / 2) * 2 = IL) Then ZOZ = 1#
'     TXOX = UOX / ((2# * IL + 1#) * Fact)
'     SUMXOX = SUMXOX + ZOZ * TXOX
'     UOX = UOX * US
'     IL = IL + 1


'    STOP THIE SUMMATION WHEN THE CURRENT TERM
'    IS LESS THAN 1E-20


 '    If (TXOX > 1E-20) Then GoTo 5085
 '    ERFC = 1# - 2# * XOX / (Pi) ^ 0.5 * SUMXOX
 '    If (arg < 0#) Then ERFC = 2# - ERFC
 '    GoTo 5430
'5160  If (XOX > 14#) Then GoTo 5410
```

```
'   THIS SERIES EXPANSION IS FOR ARG>3.4

  '    UOX = 2# * XOX * XOX
  '    LJL = 1
  '    JLJ = 1
  '    Fact = 1#
'5300  OLDFAC = Fact
'      Fact = Fact / UOX * JLJ

'  STOP THE SUMMATION WHEN THE CURRENT TERM BECOMES LARGER THAN
'  THE PREVIOUS TERM

'      If (Fact > OLDFAC) Then GoTo 5333
'      ZOZ = -1#
'      If ((LJL / 2) * 2 = LJL) Then ZOZ = 1#
'      TXOX = ZOZ * Fact
'      SUMXOX = SUMXOX + TXOX
'      LJL = LJL + 1
'      JLJ = JLJ + 2
'5333  ERFC = Exp(-XOX * XOX) / (Pi) ^ 0.5 / XOX * SUMXOX
'      GoTo 5420
'5410  ERFC = 0#
'5420  If (arg < 0#) Then ERFC = 2# - ERFC
5430 End Function

Public Function CONFINT(X, Dstar As Double, data, NOBS As Integer, Kount As Integer, Resi, U, W, YCALC,
Co As Double, NP As Integer, BSW As Integer, Phix, R, C) As Double

Dim NME(4) As String

NME(1) = "VELOCITY(m/sec)"
NME(2) = "DISPERSIVITY(m)"
NME(3) = "RF"
NME(4) = "FODC(1/sec)"


ActiveSheet.Range("G50:K60").Clear

  'DEFINING NPP TO BE THE NUMBER OF PARAMETERS BEING FIT
      NPP = 0
      For i = 1 To NP
          If Phix(i) = 0 Then NPP = NPP + 1
10    Next
      If NPP = 0 Then GoTo 300

   'DETERMINING THE CRITICAL RESIDUAL SUM OF SQUARES
   'WHICH DEFINES THE UPPER AND LOWER CONFIDENCE INTERVAL

      ER = ErrorFun(X, Dstar, data, NOBS, Kount, Resi, U, W, YCALC, Co, NP, BSW, manip)
      'FESTI = FESTIM(NOBS, NPP, IDB) alternative below
      ActiveSheet.Range("G51") = NOBS 'allows NOBS to be used in Excel's FINV function
      ActiveSheet.Range("G50") = "=FInv(0.05, G51-4, 4)" '0.05 = 95% confidence interval, G51 = NOBS, 4 = NP,
degrees of freedom = NOBS-NP, NP
      FESTI = ActiveSheet.Range("G50").Value
      'Fnpp = float(NPP)
      'FNOBS = float(NOBS)
```

```
     'RSSCRIT = ER * (1 + Fnpp / (FNOBS - Fnpp) * FESTI)
      RSSCRIT = ER * (1 + NPP / (NOBS - NPP) * FESTI)

'    LOOPING THROUGH THE PARAMETERS TO DETERMINE CONFIDENCE INTERVALS

For i = 1 To NP
   For J = 1 To NP
      R(J) = X(J)
      C(J) = X(J)
90  Next

    If Phix(i) = 1 Then GoTo 199

'   LOOKING FOR THE UPPER LIMIT
         NCOUNT = 1
100

    'IF(FLOAT(I) .EQ. 4. .AND. X(I) .LT. 0.) THEN
     If i = 4 And X(i) < 0 Then
            R(i) = R(i) - 0.1 * X(i)
         Else
            R(i) = R(i) + 0.1 * X(i)
         End If
         ER = ErrorFun(R, Dstar, data, NOBS, Kount, Resi, U, W, YCALC, Co, NP, BSW, manip)
         If R(4) < -100 Or R(4) > 100 Then GoTo 120
         If NCOUNT > 1 Then
            If Abs((ERCHK - ER) / ER * 100) < 0.001 Then
               R(i) = -1#
               GoTo 120
            End If
         Else
            NCOUNT = 2
         End If
         ERCHK = ER
         If ER < RSSCRIT Then GoTo 100

110

       'IF(FLOAT(I) .EQ. 4. .AND. X(I) .LT. 0.) THEN
       If i = 4 And X(i) < 0 Then

          R(i) = R(i) + 0.01 * X(i)
          Else
          R(i) = R(i) - 0.01 * X(i)
       End If

   ER = ErrorFun(R, Dstar, data, NOBS, Kount, Resi, U, W, YCALC, Co, NP, BSW, manip)
       If ER > RSSCRIT Then GoTo 110

     'LOOKING FOR THE LOWER LIMIT
120
       'IF(FLOAT(I) .EQ. 4. .AND. X(I) .LT. 0.) THEN
        If i = 4 And X(i) < 0 Then
            C(i) = C(i) + 0.1 * X(i)
         Else
            C(i) = C(i) - 0.1 * X(i)
```

```
        End If
       'IF(C(I) .LT. 0. .AND. FLOAT(I) .NE. 4.) THEN
       If C(i) < 0 And i <> 4 Then
           C(i) = C(i) + 0.1 * X(i)
125          C(i) = C(i) - 0.01 * X(i)
           If C(i) < 0 Then
               C(i) = 0#
               GoTo 249
           End If
        End If

        ER = ErrorFun(C, Dstar, data, NOBS, Kount, Resi, U, W, YCALC, Co, NP, BSW, manip)
        If C(4) < -100 Or C(4) > 100 Then GoTo 249
        If ER < RSSCRIT Then GoTo 120

130
        'IF(FLOAT(I) .EQ. 4. .AND. X(I) .LT. 0.) THEN
        If i = 4 And X(i) < 0 Then
            C(i) = C(i) - 0.01 * X(i)
        Else
            C(i) = C(i) + 0.01 * X(i)
        End If

        ER = ErrorFun(C, Dstar, data, NOBS, Kount, Resi, U, W, YCALC, Co, NP, BSW, manip)
        If ER > RSSCRIT Then GoTo 130

249
        If i = 4 Then
            X(i) = Exp(X(i))
            If R(i) < -99 Then
                R(i) = 0#
            Else
                R(i) = Exp(R(i))
            End If
            C(i) = Exp(C(i))
        End If

259  'Writing to the output file

       ActiveSheet.Range("G50") = "95% CONFIDENCE INTERVALS FOR ESTIMATED PARAMETERS"
       ActiveSheet.Range("G51") = "Parameter"
       ActiveSheet.Range("I51") = "Low"
       ActiveSheet.Range("J51") = "Optimized"
       ActiveSheet.Range("K51") = "High"
       ActiveSheet.Range("G60") = "CRITICAL RSS VALUE ="
       ActiveSheet.Range("J60") = RSSCRIT

       If R(i) > 0 Then

          ActiveSheet.Cells(i + 52, 7) = NME(i)
          ActiveSheet.Cells(i + 52, 9) = C(i) 'lower limit
          ActiveSheet.Cells(i + 52, 10) = X(i) 'optimized
          ActiveSheet.Cells(i + 52, 11) = R(i) 'upper limit

             If i = 1 Then 'converts velocity to m/sec
                ActiveSheet.Cells(i + 52, 9) = C(i) / 60 'lower limit
```

```
            ActiveSheet.Cells(i + 52, 10) = X(i) / 60 'optimized
            ActiveSheet.Cells(i + 52, 11) = R(i) / 60 'upper limit
        End If

        If i = 4 Then ' converts FODC to /sec
            ActiveSheet.Cells(i + 52, 9) = C(i) / 60 'lower limit
            ActiveSheet.Cells(i + 52, 10) = X(i) / 60 'optimized
            ActiveSheet.Cells(i + 52, 11) = R(i) / 60 'upper limit
        End If

      Else
       ActiveSheet.Range("G52") = "No Convergence"
      End If
199
200   Next

     If R(i) = 0 Then

        ActiveSheet.Cells(i + 52, 7) = ""
        ActiveSheet.Cells(i + 52, 9) = ""
        ActiveSheet.Cells(i + 52, 10) = ""
        ActiveSheet.Cells(i + 52, 11) = ""
     End If

299
300
    If X(4) > 0 Then
        X(4) = Log(X(4))
    Else
        X(4) = 0#
    End If

End Function



Private Sub Finished_Click()
UserForm5.Show
UserForm4.Hide
End Sub

UserForm 5 code

Private Sub CollectData_Click()

Dim pm As Double
Dim NSIM As Integer
Dim NumSheets As Integer
Dim wks As Double
Dim MaxCnt As Integer
Dim ILO As Integer
Dim IHI As Integer
Dim Scal As Double
Dim ERRMIN As Double
Dim ERPCNT As Double
Dim C(10) As Double
```

```
Dim E(10) As Double
Dim P(10, 10) As Double
Dim F(32, 10) As Double
Dim Co As Double
Dim Dstar As Double
Dim ColumnLength As Double
Dim RSS As Double
Dim OLDNOBS As Double
Dim X(10) As Double
Dim ChartObject As String



'create results worksheet
Worksheets.Add(After:=Worksheets(Worksheets.Count)).Name = "RF"

pm = CDbl(FeV.Text)
pm = ActiveSheet.Range("A1")

'Selecting the optimized data from all worksheets and placing it in RF WKS
'loop to copy the opimized FODC, Co, R and report the findings in the RF
For i = 2 To 6

Worksheets(2).Activate
 ActiveSheet.Range("J47,J54,J55,J56").Select
 Selection.Copy
 Worksheets("RF").Select
 Range("A30").Select
 ActiveSheet.Paste

 Next
Worksheets(3).Activate
 ActiveSheet.Range("J47,J54,J55,J56").Select
 Selection.Copy
 Worksheets("RF").Select
 Range("B30").Select
 ActiveSheet.Paste

Worksheets(4).Activate
 ActiveSheet.Range("J47,J54,J55,J56").Select
 Selection.Copy
 Worksheets("RF").Select
 Range("C30").Select
 ActiveSheet.Paste

 Worksheets(5).Activate
 ActiveSheet.Range("J47,J54,J55,J56").Select
 Selection.Copy
 Worksheets("RF").Select
 Range("D30").Select
 ActiveSheet.Paste

 Worksheets(6).Activate
 ActiveSheet.Range("J47,J54,J55,J56").Select
 Selection.Copy
```

```
 Worksheets("RF").Select
 Range("E30").Select
 ActiveSheet.Paste

 Worksheets(7).Activate
 ActiveSheet.Range("J47,J54,J55,J56").Select
 Selection.Copy
 Worksheets("RF").Select
 Range("F30").Select
 ActiveSheet.Paste
'places text in spreadsheet to identify output parameters
ActiveSheet.Range("A8") = "Co (ug/l)"
ActiveSheet.Range("B8") = "R"
ActiveSheet.Range("C8") = "k (1/sec)"
ActiveSheet.Range("D8") = "Dispersivity"
ActiveSheet.Range("E8") = "k (1/Min)"
ActiveSheet.Range("A1") = "FeV"
ActiveSheet.Range("B1") = CDbl(FeV.Text)
ActiveSheet.Range("A2") = "Cmax"
ActiveSheet.Range("A3") = "J"
ActiveSheet.Range("A4") = "RSS"
ActiveSheet.Range("F8") = "Calc R"
ActiveSheet.Range("G8") = "Res Sq"

Range("A30").Select
   Selection.Cut Destination:=Range("A9")
   Range("B30").Select
   Selection.Cut Destination:=Range("A10")
   Range("C30").Select
   Selection.Cut Destination:=Range("A11")
   Range("D30").Select
   Selection.Cut Destination:=Range("A12")
   Range("E30").Select
   Selection.Cut Destination:=Range("A13")
   Range("F30").Select
   Selection.Cut Destination:=Range("A14")
   Range("A32").Select
   Selection.Cut Destination:=Range("B9")
   Range("B32").Select
   Selection.Cut Destination:=Range("B10")
   Range("C32").Select
   Selection.Cut Destination:=Range("B11")
   Range("D32").Select
   Selection.Cut Destination:=Range("B12")
   Range("E32").Select
   Selection.Cut Destination:=Range("B13")
   Range("F32").Select
   Selection.Cut Destination:=Range("B14")
   Range("A33").Select
   Selection.Cut Destination:=Range("C9")
   Range("B33").Select
   Selection.Cut Destination:=Range("C10")
   Range("C33").Select
   Selection.Cut Destination:=Range("C11")
   Range("D33").Select
   Selection.Cut Destination:=Range("C12")
```

```
    Range("E33").Select
    Selection.Cut Destination:=Range("C13")
    Range("F33").Select
    Selection.Cut Destination:=Range("C14")
    Range("A31").Select
    Selection.Cut Destination:=Range("D9")
    Range("B31").Select
    Selection.Cut Destination:=Range("D10")
    Range("C31").Select
    Selection.Cut Destination:=Range("D11")
    Range("D31").Select
    Selection.Cut Destination:=Range("D12")
    Range("E31").Select
    Selection.Cut Destination:=Range("D13")
    Range("F31").Select
    Selection.Cut Destination:=Range("D14")
    Range("D7").Select
    Range("A30:F33").Clear


'Converting k (1/sec) to k (1/min)

    ActiveSheet.Range("E9").Select
    Application.CutCopyMode = False
    ActiveCell.FormulaR1C1 = "=60*RC[-2]"
    Range("E9").Select
    Selection.AutoFill Destination:=Range("E9:E14"), Type:=xlFillDefault
    Range("E9:E14").Select


   'graph is created for the observed data. statements identifies size and location, title, chart type, series selection,
axes formatting, plot area formatting, title formatting

    cw = Columns(1).Width
    rh = Rows(1).Height
    Set Graph = ActiveSheet.ChartObjects.Add(cw * 7, rh * 1, cw * 8, rh * 20)
    Graph.Name = " Retardation Curve"
    Graph.Chart.ChartType = xlXYScatter
    Graph.Chart.SeriesCollection.NewSeries

 With Graph.Chart.SeriesCollection(1)
        .Values = ActiveSheet.Range("B9:B14")
        .XValues = ActiveSheet.Range("A9:A14")
        .Name = "Retardation"
        .MarkerSize = 8
        .MarkerStyle = xlMarkerStyleCircle
    End With
    With Graph.Chart.Axes(xlCategory)
        .HasTitle = True
        .AxisTitle.Caption = "Co (uM)"
    With Graph.Chart.Axes(xlValue)
        .HasTitle = True
        .AxisTitle.Caption = "RETARDATION"
    End With
    End With
```

```
    ActiveSheet.Buttons.Add(144.6, 45, 78.6, 29.4).Select
    Selection.OnAction = "SolverMacro1"
    ActiveSheet.Shapes("Button 1").Select
    Selection.Characters.Text = "Non-Reactive Sorption"
    With Selection.Characters(Start:=1, Length:=21).Font
        .Name = "Calibri"
        .FontStyle = "Regular"
        .Size = 11
        .Strikethrough = False
        .Superscript = False
        .Subscript = False
        .OutlineFont = False
        .Shadow = False
        .Underline = xlUnderlineStyleNone

    End With
    UserForm5.Hide

    End Sub
   Sub SolverMacro1()
'
' SolverMacro1 Macro
'

'
    Range("F9").Select
    ActiveCell.FormulaR1C1 = _
        "=1+R[-8]C[-4]*((R[-6]C[-4]*R[-7]C[-4])/(1+R[-6]C[-4]*RC[-5])^2)"
    Range("F9").Select
    ActiveCell.FormulaR1C1 = "=1+R1C2*((R3C2*R2C2)/(1+R3C2*RC[-5])^2)"
    Range("F9").Select
    Selection.AutoFill Destination:=Range("F9:F14")
    Range("F9:F14").Select
    Range("G9").Select
    ActiveCell.FormulaR1C1 = "=(RC[-1]-RC[-5])^2"
    Range("G9").Select
    ActiveSheet.ChartObjects(" Retardation Curve").Activate
    ActiveSheet.ChartObjects(" Retardation Curve").Activate
    Range("G9").Select
    Selection.AutoFill Destination:=Range("G9:G14")
    Range("G9:G14").Select
    Range("B4").Select
    ActiveCell.FormulaR1C1 = "=SUM(R[5]C[5]:R[10]C[5])"
    Range("B2").Select
    ActiveCell.FormulaR1C1 = "0.5"
    Range("B3").Select
    ActiveCell.FormulaR1C1 = "0.001"
    Range("B4").Select
    SolverOk SetCell:="$B$4", MaxMinVal:=2, ValueOf:="0", ByChange:="$B$2:$B$3"
    SolverSolve

    ActiveSheet.ChartObjects(" Retardation Curve").Activate
    ActiveChart.SeriesCollection.NewSeries
    ActiveChart.SeriesCollection(2).Name = "=""Calc R"""
    ActiveChart.SeriesCollection(2).XValues = "='RF'!$A$9:$A$14"
    ActiveChart.SeriesCollection(2).Values = "='RF'!$F$9:$F$14"
```

```
    ActiveSheet.ChartObjects(" Retardation Curve").Activate
    ActiveChart.SeriesCollection(2).Select
    Selection.ChartType = xlXYScatterSmoothNoMarkers
   ActiveSheet.ChartObjects(" Retardation Curve").Activate
    ActiveChart.SeriesCollection(2).Select
    With Selection.Format.Line
        .Visible = msoTrue
        .ForeColor.ObjectThemeColor = msoThemeColorAccent1
        .ForeColor.TintAndShade = 0
        .ForeColor.Brightness = 0
    End With
    With Selection.Format.Line
        .Visible = msoTrue
        .ForeColor.ObjectThemeColor = msoThemeColorText1
        .ForeColor.TintAndShade = 0
        .ForeColor.Brightness = 0
        .Transparency = 0
    End With
    ActiveChart.SeriesCollection(2).Smooth = True

End Sub

Module 2
Sub SolverMacro1()
'
' SolverMacro1 Macro
'

'
    Range("F9").Select
    ActiveCell.FormulaR1C1 = _
        "=1+R[-8]C[-4]*((R[-6]C[-4]*R[-7]C[-4])/(1+R[-6]C[-4]*RC[-5])^2)"
    Range("F9").Select
    ActiveCell.FormulaR1C1 = "=1+R1C2*((R3C2*R2C2)/(1+R3C2*RC[-5])^2)"
    Range("F9").Select
    Selection.AutoFill Destination:=Range("F9:F14")
    Range("F9:F14").Select
    Range("G9").Select
    ActiveCell.FormulaR1C1 = "=(RC[-1]-RC[-5])^2"
    Range("G9").Select
    ActiveSheet.ChartObjects(" Retardation Curve").Activate
    ActiveSheet.ChartObjects(" Retardation Curve").Activate
    Range("G9").Select
    Selection.AutoFill Destination:=Range("G9:G14")
    Range("G9:G14").Select
    Range("B4").Select
    ActiveCell.FormulaR1C1 = "=SUM(R[5]C[5]:R[10]C[5])"
    Range("B2").Select
    ActiveCell.FormulaR1C1 = "0.5"
    Range("B3").Select
    ActiveCell.FormulaR1C1 = "0.001"
    Range("B4").Select
    SolverOk SetCell:="$B$4", MaxMinVal:=2, ValueOf:="0", ByChange:="$B$2:$B$3"
    SolverSolve Userfinish:=True

    ActiveSheet.ChartObjects(" Retardation Curve").Activate
```

```
    ActiveChart.SeriesCollection.NewSeries
With ActiveChart.SeriesCollection(1)
    .Name = "=""Obs R"""
    .Values = ActiveSheet.Range("$b$9:$b$14")
    .XValues = ActiveSheet.Range("$a$9:$a$14")
    .MarkerSize = 6
    .MarkerStyle = xlMarkerStyleCircle
End With

ActiveChart.SeriesCollection.NewSeries 'plots calculated data
With ActiveChart.SeriesCollection(2)
    .Name = "=""Calc R"""
    .Values = ActiveSheet.Range("$f$9:$f$14")
    .XValues = ActiveSheet.Range("$a$9:$a$14")
    .ChartType = xlXYScatterSmoothNoMarkers
End With

UserForm6.Show
End Sub
```

UserForm 6 code

```
Private Sub KIM2PE_Click()


Dim NumSheets As Integer
Dim wks As Double
Dim FeV As Double
Dim KIM2PE As Action




'create results worksheet
Worksheets.Add(After:=Worksheets(Worksheets.Count)).Name = "KIM2PE"


    Sheets("RF").Select
    ActiveSheet.Range("A8:A14,E8:E14").Copy
    Sheets("KIM2PE").Select
    ActiveCell.Offset(0, 0).Select
    ActiveSheet.Paste
    ActiveSheet.Range("C1") = "Fe/V"

    Sheets("RF").Select
    ActiveSheet.Range("B1").Copy
    Sheets("KIM2PE").Select
    ActiveSheet.Range("C2").Select
    ActiveSheet.Paste
    Selection.AutoFill Destination:=Range("C2:C7")


    'Run Matrix for L-H Model for J and kCmax
    Range("C9").Select
    ActiveCell.Value = "-1"
    Selection.AutoFill Destination:=Range("C9:C14")
```

```
    Range("D9").Select
    ActiveCell.FormulaR1C1 = "=R[-7]C[-1]/R[-7]C[-2]"

    Selection.AutoFill Destination:=Range("D9:D14")
    Range("D9:D14").Select
    ActiveWindow.SmallScroll Down:=3
    Range("C16:H17").Select
    Selection.FormulaArray = "=TRANSPOSE(R[-7]C:R[-2]C[1])"
    ActiveWindow.SmallScroll Down:=3
    Range("C19:D20").Select
    Selection.FormulaArray = "=MMULT(R[-3]C:R[-2]C[5],R[-10]C:R[-5]C[1])"
    Range("C22:D23").Select
    Selection.FormulaArray = "=MINVERSE(R[-3]C:R[-2]C[1])"
    Range("C25:H26").Select
    Selection.FormulaArray = "=MMULT(R[-6]C:R[-5]C[1],R[-16]C:R[-11]C[1])"
    Selection.ClearContents
    Selection.FormulaR1C1 = "=MMULT(R[-3]C:R[-2]C[1],R[-9]C:R[-8]C[5])"
    Selection.ClearContents
    Selection.FormulaArray = "=MMULT(R[-3]C:R[-2]C[1],R[-9]C:R[-8]C[5])"
    ActiveWindow.SmallScroll Down:=-3
    Range("C28:C29").Select
    Selection.FormulaArray = "=MMULT(R[-3]C:R[-2]C[5],R[-26]C[-2]:R[-21]C[-2])"


    'WRITING THE OUTPUT


ActiveSheet.Range("D1") = "Obs Rate (uM/Min)"
ActiveSheet.Range("E1") = "Calc Rate (uM/min)"
ActiveSheet.Range("F1") = "Residuals"
ActiveSheet.Range("A9") = "J"
ActiveSheet.Range("A10") = "k*Cmax"

'Gathering the values of J and kCmax and converting 1/J to J
With Range("B9").Select
    ActiveCell.FormulaR1C1 = "=1/R[19]C[1]"
    Range("B10").Select
    ActiveCell.FormulaR1C1 = "=R[19]C[1]"
Range("D2").Select
    ActiveCell.FormulaR1C1 = "=RC[-3]*RC[-2]"
    Range("D2").Select
    Selection.AutoFill Destination:=Range("D2:D7")
    Range("D2:D7").Select
    Range("E2").Select
    ActiveCell.FormulaR1C1 = "=(R10C2*RC[-2]*RC[-4])/(1/R9C2+RC[-4])"
    Selection.AutoFill Destination:=Range("E2:E7")
    Range("F2").Select
    ActiveCell.FormulaR1C1 = "=RC[-1]-RC[-2]"
    Range("F2").Select
    Selection.AutoFill Destination:=Range("F2:F7")
    Range("F2:F7").Select


End With

'Matrix for linearized equation for KIM for the estimation of k, Cmax, J for simplex optimizer
```

```
 ActiveCell.Offset(29, -4).Range("A1").Select
   ActiveCell.FormulaR1C1 = "STEP 2"
   ActiveCell.Offset(0, 1).Range("A1").Select
   ActiveCell.FormulaR1C1 = "=(R[-29]C[-2]+R9C2)/R[-29]C"
   ActiveCell.Offset(1, 0).Range("A1").Select
   ActiveWindow.SmallScroll Down:=6
   ActiveCell.Offset(-1, 0).Range("A1").Select
   Selection.AutoFill Destination:=ActiveCell.Range("A1:A6"), Type:= _
      xlFillDefault
   ActiveCell.Range("A1:A6").Select
   ActiveCell.Offset(0, 1).Range("A1").Select
   ActiveWindow.SmallScroll Down:=-18
   ActiveCell.FormulaR1C1 = "=1/R[-29]C[-2]"
   ActiveCell.Offset(1, 0).Range("A1").Select
   ActiveWindow.SmallScroll Down:=9
   ActiveCell.Offset(-1, 0).Range("A1").Select
   Selection.AutoFill Destination:=ActiveCell.Range("A1:A6")
   ActiveCell.Range("A1:A6").Select
   ActiveWindow.SmallScroll Down:=0
   ActiveCell.Offset(7, -1).Range("A1:F2").Select
   Selection.FormulaArray = "=TRANSPOSE(R[-7]C:R[-2]C[1])"
   ActiveCell.Offset(3, 0).Range("A1:B2").Select
   Selection.FormulaArray = "=MMULT(R[-3]C:R[-2]C[5],R[-10]C:R[-5]C[1])"
   ActiveWindow.SmallScroll Down:=9
   ActiveCell.Offset(3, 0).Range("A1:B2").Select
   Selection.FormulaArray = "=MINVERSE(R[-3]C:R[-2]C[1])"
   ActiveCell.Offset(3, 0).Range("A1:F2").Select
   Selection.FormulaArray = "=MMULT(R[-3]C:R[-2]C[1],R[-9]C:R[-8]C[5])"
   ActiveCell.Offset(3, 0).Range("A1:A2").Select
   Selection.FormulaArray = "=MMULT(R[-3]C:R[-2]C[5],R[-19]C[2]:R[-14]C[2])"
   ActiveCell.Offset(-19, 2).Range("A1").Select
   ActiveCell.FormulaR1C1 = "=(1/1+R9C2*R[-29]C[-4])"
   ActiveCell.Offset(1, 0).Range("A1").Select

   ActiveWindow.SmallScroll Down:=18
   ActiveCell.Offset(-1, 0).Range("A1").Select
   Selection.AutoFill Destination:=ActiveCell.Range("A1:A6")
   ActiveCell.Range("A1:A6").Select
   ActiveWindow.SmallScroll Down:=-24
   ActiveCell.Offset(-20, -4).Range("A1").Select
   ActiveCell.FormulaR1C1 = "k"
   ActiveCell.Offset(1, 0).Range("A1").Select
   ActiveCell.FormulaR1C1 = "Cmax"
   ActiveCell.Offset(-1, 1).Range("A1").Select
   ActiveCell.FormulaR1C1 = "=R[40]C[1]"
   ActiveCell.Offset(1, 0).Range("A1").Select
   ActiveCell.FormulaR1C1 = "=1/R[38]C[1]"
   ActiveCell.Offset(1, 0).Range("A1").Select
   ActiveWindow.SmallScroll Down:=-15



UserForm6.Hide
UserForm7.Show

End Sub
```

UserForm 7 code

```
Private Sub Run_Click()
'Adding worksheet after KIM2PE for KIMPE optimizer

Dim pm As Double
Dim NSIM As Integer
Dim NumSheets As Integer
Dim MaxCnt As Integer
Dim ILO As Integer
Dim IHI As Integer
Dim Scal As Double
Dim ERRMIN As Double
Dim ERPCNT As Double
Dim C(10) As Double
Dim E(10) As Double
Dim P(10, 10) As Double
Dim F(32, 10) As Double
Dim Co As Double
Dim Dstar As Double
Dim ColumnLength As Double
Dim RSS As Double
Dim OLDNOBS As Double
Dim X(10) As Double
Dim ChartObject As String
Dim Kount As Integer
Dim Phix(10) As Double
'Dim X(10) As Double
'Dim Data(2000, 10) As Double
'Dim Resi(2000) As Double
'Dim U(2000) As Double
'Dim W(2000) As Double
'Dim YCALC(2000) As Double
'Dim R(10) As Double
'Dim NP As Integer
'Dim NP1 As Integer
'Dim NOBS As Integer
'Dim bsw As Integer
'Dim Kount As Long
'Dim Colength As Double
'dimensions that are commented out are available in the "Public_Variables" Module for use as an array transfer to a
public function

Sheets("KIM2PE").Activate
pm = ActiveSheet.Range("c2")

Worksheets.Add(After:=Worksheets(Worksheets.Count)).Name = "KIMPE"
ActiveSheet.Range("A12") = "J (um/l)"
ActiveSheet.Range("A13") = "k (1/min)"
ActiveSheet.Range("A14") = "Cmax (um/g)"

'Writing output of Matrix
Sheets("KIM2PE").Select
ActiveSheet.Range("A1:C7").Copy
Sheets("KIMPE").Select
```

```
ActiveSheet.Range("A1:C7").Select
ActiveSheet.Paste
Sheets("KIM2PE").Select
ActiveSheet.Range("B12,B9,B11").Copy
Sheets("KIMPE").Select
ActiveSheet.Range("B12:B14").Select
ActiveSheet.Paste

'Following With statement formats A through B columns for headers and data alignment
 ActiveSheet.Range("A1").Select

With Selection
   .ColumnWidth = 12
   .NumberFormat = "General"
   .HorizontalAlignment = xlCenter
   .VerticalAlignment = xlCenter
   .WrapText = True
End With
'Starting optimizer


NP = 3
NP1 = NP + 1
manip = "" 'manip is a debugging variable used to denote which manipulation is going on (reflection, expansion,
contraction)
NSIM = 1
MaxCnt = 500
ER = 1
ERRMIN = 0.0001

X(1) = CDbl(Cmax.Text)
X(2) = CDbl(affn.Text)
X(3) = CDbl(k.Text)
If X(3) > 0 Then X(3) = Log(X(3))

For i = 1 To 10
   Phix(i) = 0
Next

' fix input sets values negative to allow code to hold negative parameter constant
 'If k.Value = True Then Phix(1) = 1
'If Cmax.Value = True Then Phix(2) = 1
'If affn.Value = True Then Phix(3) = 1

 'if a zero is enetered for the first order decay constant, then it is automatically fixed

   ActiveSheet.Range("C2").Select
   ActiveCell.FormulaR1C1 = "=RC[-1]*RC[-2]"
   Range("C2").Select
   Selection.AutoFill Destination:=Range("C2:C7")




   NOBS = ActiveSheet.Range("A2").End(xlDown).Row - 1
```

```
    OLDNOBS = ActiveSheet.Range("E2").End(xlDown).Row
    'clearing data from Columns E&F from "undo" function in userform 3
    ActiveSheet.Range("E2:F" & OLDNOBS).Clear

    'clearing data array to remove previous data

    For i = 1 To 2000
       For J = 1 To NP1
          data(i, J) = 0#
       Next
    Next

    For i = 1 To NOBS
          data(i, 1) = ActiveSheet.Cells(i + 1, 1)
          data(i, 2) = ActiveSheet.Cells(i + 1, 2)
    Next

'starting error function value
 E(1) = ErrorFun(X, Dstar, data, NOBS, Kount, Resi, U, W, YCALC, Co, NP, BSW, manip, pm)

    'INITIALIZE THE SIMPLEX
    Kount = 0

    For J = 1 To NP
       P(1, J) = X(J)
    Next

    For i = 2 To NP1

       For J = 1 To NP
          P(i, J) = X(J)
       Next

    P(i, i - 1) = 1.1 * X(i - 1)
       If (Phix(i - 1) = 1) Then P(i, i - 1) = X(i - 1)
       If (Abs(X(i - 1)) < 0.000000000001) Then P(i, i - 1) = 0.0001
       If (X(1) = 0#) Then P(2, 1) = 0#
       Next

'Find PLOW Ad PHIGH / BEST = PLOW / WORST = PHIGH
31   ILO = 1
     IHI = 1

      For i = 1 To NP1

          For J = 1 To NP
             X(J) = P(i, J)
          Next

         E(i) = ErrorFun(X, Dstar, data, NOBS, Kount, Resi, U, W, YCALC, Co, NP, BSW, manip, pm)
         If (E(i) < E(ILO)) Then ILO = i
         If (E(i) > E(IHI)) Then IHI = i
      Next

'FIND PNHI THE NEXT HIGHEST NEXT=PNHI
```

```
41    NHI = ILO
      For i = 1 To NP1
          If (E(i) >= E(NHI) And i <> IHI) Then NHI = i
43    Next

'COMPUTE THE CENTROID
      For J = 1 To NP
          C(J) = -P(IHI, J)
          For i = 1 To NP1
              C(J) = C(J) + P(i, J)
44          Next
          C(J) = C(J) / NP
46    Next

i = 1

51 GoTo 52

52 'STOPPING CRITERION
      If (Kount > MaxCnt) Then
        UserForm1.Hide
        UserForm2.Show
          If MsgBox("EXECUTION TERMINATED; MAXCOUNT EXCEEDED. Please Enter Correct Distance
from Source and Retry Manually", vbCritical) = vbOK Then
              Exit Sub
      End If
      End If

ERPCNT = Abs(E(ILO) - E(IHI)) / E(ILO) * 100

If (Abs(E(ILO) - E(IHI)) / E(ILO) < ERRMIN) Then GoTo 200
If Kount = 0 Then GoTo 61
If (ER < 0.000001) Then GoTo 200

GoTo 61

'REFLECTION
61    For J = 1 To NP
          R(J) = 1.9985 * C(J) - 0.9985 * P(IHI, J)
62    Next
      manip = "REFLECT"
      ER = ErrorFun(R, Dstar, data, NOBS, Kount, Resi, U, W, YCALC, Co, NP, BSW, manip, pm)

'REFLECTION AGAIN IF SUCCESSFUL
      If (ER < E(ILO)) Then GoTo 91
      If (ER >= E(IHI)) Then GoTo 122

'REPLACE WORST VERTEX WITH NEW ONE
79    For J = 1 To NP
          P(IHI, J) = R(J)
80    Next

      NSIM = NSIM + 1
      E(IHI) = ER
      If (ER > E(NHI)) Then GoTo 51
      IHI = NHI
```

```
    GoTo 41

'EXPAND THE SIMPLEX
91    ILO = IHI
    IHI = NHI
    For J = 1 To NP
        X(J) = 1.95 * R(J) - 0.95 * C(J)
93    Next
    manip = "EXPAND"
    EX = ErrorFun(X, Dstar, data, NOBS, Kount, Resi, U, W, YCALC, Co, NP, BSW, manip, pm)
    If (EX < ER) Then GoTo 104

'R IS BETTER THAN X
    For J = 1 To NP
        P(ILO, J) = R(J)
99    Next

    NSIM = NSIM + 1
    E(ILO) = ER
    GoTo 110

'X IS BETTER THAN R
104   For J = 1 To NP
        P(ILO, J) = X(J)
105   Next

    'IF(IDB > 0) then EX,(X(j),j=1,NP)
    NSIM = NSIM + 1
    E(ILO) = EX
110   GoTo 41

i = 1

'CONTRACT THE SIMPLEX
122   For J = 1 To NP
        R(J) = 0.5015 * C(J) + 0.4985 * P(IHI, J)
123   Next
    manip = "CONTRACT"
    ER = ErrorFun(R, Dstar, data, NOBS, Kount, Resi, U, W, YCALC, Co, NP, BSW, manip, pm)
    If (ER < E(ILO)) Then GoTo 91
    If (ER < E(IHI)) Then GoTo 79

'Scale
Scal = CDbl(InputBox("Enter Scale to Continue: <0 Expands, >0 Shrinks, =0 Stops", "Scale Factor Required"))
If (Scal = 0#) Then GoTo 200
137   For i = 1 To NP1
        For J = 1 To NP
            P(i, J) = P(i, J) + Scal * (P(ILO, J) - P(i, J))
138       Next
139   Next
    GoTo 31

'WRITING THE OUTPUT

200
ActiveSheet.Range("C1") = "Obs Rate (uM/Min)"
```

```
ActiveSheet.Range("D1") = "Calc Rate (uM/min)"
ActiveSheet.Range("E1") = "Residuals"

For i = 1 To NOBS
   ActiveSheet.Cells(i + 1, 4) = YCALC(i)
   ActiveSheet.Cells(i + 1, 5) = Resi(i)
Next

ActiveSheet.Range("A1:D" & NOBS + 1).Select 'Follwowing With statement formats A through D columns for
headers and data alignment
With Selection
   .ColumnWidth = 10
   .NumberFormat = "General"
   .HorizontalAlignment = xlCenter
   .VerticalAlignment = xlCenter
   .WrapText = True
End With



   'graph is created for the observed data. statements identifies size and location, title, chart type, series selection,
axes formatting, plot area formatting, title formatting


   cw = Columns(1).Width
   rh = Rows(1).Height
   Set Graph = ActiveSheet.ChartObjects.Add(cw * 6, rh * 1, cw * 8, rh * 10)
   'Graph.Name = " Rate Curve"
   Graph.Chart.ChartType = xlXYScatter
   Graph.Activate

   With ActiveChart.SeriesCollection.NewSeries
      .XValues = ActiveSheet.Range("A2:A" & NOBS + 1)
      .Values = ActiveSheet.Range("C2:C" & NOBS + 1)
      .Name = "Obs Rate"
      .MarkerSize = 6
      .MarkerStyle = xlMarkerStyleCircle
   End With

ActiveChart.SeriesCollection.NewSeries 'plots calculated data
 With ActiveChart.SeriesCollection(2)
      .Values = ActiveSheet.Range("D2:D" & NOBS + 1)
      .XValues = ActiveSheet.Range("A2:A" & NOBS + 1)
      .Name = "Calculated"
      .MarkerSize = 6
      .ChartType = xlXYScatterSmoothNoMarkers
   End With



'    Graph.Chart.SeriesCollection.Add Source:=ActiveSheet.Range("B2:B" & LastRowNewSheet)

   With Graph.Chart.Axes(xlCategory)
      .HasTitle = True
      .AxisTitle.Caption = "Co (min)"
```

```
        .CategoryNames = Range("A2:A7" & LastRowNewSheet)
    End With

    With Graph.Chart.Axes(xlValue)
        .HasTitle = True
    With .AxisTitle
        .Caption = "Rate (uM/l/min) "
    End With
    End With

    Graph.Chart.Axes(xlValue).HasMajorGridlines = False
    Graph.Chart.Axes(xlCategory).HasMajorGridlines = False
    Graph.Chart.ChartArea.Interior.Color = RGB(255, 255, 255)
    Graph.Chart.PlotArea.Interior.Color = RGB(255, 255, 255)
    Graph.RoundedCorners = True
    'With Graph.Chart.ChartCaption = "Rate Curve"
        '.Font.Size = 14
        '.Font.Bold = True
   ' End With



'places text in spreadsheet to identify output parameters
ActiveSheet.Range("G28") = "OPTIMIZED PARAMETER ESTIMATES"
ActiveSheet.Range("G30") = "Cmax"
ActiveSheet.Range("G31") = "Affn"
ActiveSheet.Range("G32") = "k"

ActiveSheet.Range("G34") = "RESDIUAL SUM OF SQUARES ="
ActiveSheet.Range("G39") = "INITIAL GUESSES AND INPUT OF PARAMETERS"
ActiveSheet.Range("G41") = "Cmax"
ActiveSheet.Range("G42") = "Affn"
ActiveSheet.Range("G43") = "k"

ActiveSheet.Range("G1").ColumnWidth = 10 ' allows all text to be seen


'places values for optimized parameter estimates
ActiveSheet.Range("J30") = X(1)
ActiveSheet.Range("J31") = X(2)
ActiveSheet.Range("J32") = Exp(X(3))

ActiveSheet.Range("K34") = E(ILO)



' places values for initial guesses
ActiveSheet.Range("J41") = CDbl(Cmax.Text)
ActiveSheet.Range("J42") = CDbl(affn.Text)
ActiveSheet.Range("J43") = CDbl(k.Text)



'code for confidence int
Confit = CONFINT(X, Dstar, data, NOBS, Kount, Resi, U, W, YCALC, Co, NP, BSW, Phix, R, C, pm)
```

```
UserForm7.Hide
UserForm8.Show
UserForm8.Hide
End Sub

Public Function ErrorFun(X, Dstar, data, NOBS, Kount, Resi, U, W, YCALC, Co, NP, BSW, manip, pm)
'Public Function ErrorFun(X, Dstar As Double, data, NOBS As Integer, Kount As Integer, Resi, U, W, YCALC, Co
As Double, NP As Integer, BSW As Integer, manip As String, pm As Double)

  'COMPUTES THE ERROR FUNCTION FOR THE DATA SET
   'SMALLER VALUE IS BETTER

Dim SMRESI As Double
Dim u1 As Double
Dim u2 As Double
     u1 = 0#
     u2 = 0#

     ErrorFun = 0#
     SMRESI = 0#

If Bisquare.Value = True Then BSW = 1
If Relative.Value = True Then BSW = 2
If None.Value = True Then BSW = 0

'Sometimes negative values are predicted by the optimizer that are not real and will cause VBA run time errors.
'The following function simply converts them to positive values prior to evaluating the error function
 For J = 1 To NP - 1
       If X(J) < 0 Then X(J) = -X(J)
 Next
If (X(3) <> 0#) Then X(3) = Exp(X(3))

For i = 1 To 2000
   Resi(i) = 0#
   U(i) = 0#
   W(i) = 0#
10 Next

For i = 1 To NOBS
          data(i, 1) = ActiveSheet.Cells(i + 1, 1)
          data(i, 2) = ActiveSheet.Cells(i + 1, 2)
          data(i, 3) = ActiveSheet.Cells(i + 1, 3)

  pm = 4444


u1 = X(3) * X(1) * pm * data(i, 1)

     'End If

20   'If (Data(i, 1) <= ColumnLength / X(1)) Then
         'ERFCU2 = 0#
         'GoTo 30
```

```
 'Else
    u2 = ((1 / X(2)) + ((X(1) * pm) / (1 + X(2) * data(i, 1))) + data(i, 1))


40   YCALC(i) = (u1 / u2)
    Resi(i) = data(i, 3) - YCALC(i)
    SMRESI = SMRESI + Abs(Resi(i))
60   Next

    If (BSW = 1) Then
        C = 1# * SMRESI / CDbl(NOBS)
        For i = 1 To NOBS
            U(i) = Resi(i) / C
            W(i) = (1 - U(i) * U(i)) ^ 2
            If (U(i) > 1#) Then W(i) = 0#
            ErrorFun = ErrorFun + W(i) * Resi(i) * Resi(i)
70        Next
    End If

    If (BSW = 2) Then
        For i = 1 To NOBS
            If (data(i, 2) = 0#) Then
                W(i) = 0#
            Else
                W(i) = 1# / (data(i, 2) ^ 2#)
            End If
            ErrorFun = ErrorFun + W(i) * Resi(i) * Resi(i)
75        Next
    End If

    If (BSW = 0) Then
      For i = 1 To NOBS
          ErrorFun = ErrorFun + Resi(i) * Resi(i)
80      Next

    End If

   Kount = Kount + 1


  If (X(3) > 0#) Then X(3) = Log(X(3))

'fills calculated data and residuals into spreasheet for debugging purposes. X(1) through X(4) units are converted to
those used in BEARPE for comparison

    'ActiveSheet.Cells(Kount, 17) = X(1)
    'ActiveSheet.Cells(Kount, 18) = X(2)
    'ActiveSheet.Cells(Kount, 19) = X(3)
    'ActiveSheet.Cells(Kount, 23) = manip
    'ActiveSheet.Cells(Kount, 24) = ErrorFun



End Function
```

```
Public Function ERFC(arg As Double)


'COMPLIMENTARY ERROR FUNCTION SUBROUTINE REAL*8 FUNCTION ERFC(ARG)
'COMPUTES THE COMPLIMENTARY ERROR FUNCTIOn FOR AN ARGUMENT
'IMPLICIT REAL*8 (A-H,L,M,O-Z)
'PARAMETER (P=0.3275911, A1=0.254829592, A2=-0.284496736,
'   1          A3=1.421413741, A4=-1.453152027, A5=1.061405429)
'TU = 1 / (1 + p * Abs(ARG))

'    ERFC=(A1*TU+A2*TU**2+A3*TU**3+A4*TU**4+A5*TU**5)
'   1      *EXP(-(ARG**2))
'    IF(ARG .LT. 0) ERFC=2-ERFC

'    RETURN
'    END


Dim P As Double
Dim A1 As Double
Dim A2 As Double
Dim A3 As Double
Dim A4 As Double
Dim A5 As Double
Dim TU As Double

P = 0.3275911
A1 = 0.254829592
A2 = -0.284496736
A3 = 1.421413741
A4 = -1.453152027
A5 = 1.061405429


TU = 1 / (1 + P * Abs(arg))

    ERFC = (A1 * TU + A2 * TU ^ 2 + A3 * TU ^ 3 + A4 * TU ^ 4 + A5 * TU ^ 5) * Exp(-(arg ^ 2))

    If (arg < 0) Then ERFC = 2 - ERFC


'*********** FUNCTION DERFC(ARG)
'   ROUTINE FOR ERFC (ARG) BY SERIES EXPANSION
'   DOUBLE PRECISION VERSION


'    Dim IL As Integer
'    Dim LJL As Integer
'    Dim JLJ As Integer
'    Dim XOX As Double
'    Dim SUMXOX As Double
'    Dim Fact As Double
'    Dim UOX As Double
'    Dim US As Double
'    Dim ZOZ As Double
'    Dim TXOX As Double
```

```
'     Dim OLDFACT As Double


'     Pi = 3.14159265358
'     SUMXOX = 1#
'     XOX = Abs(arg)
'     If (XOX > 3.4) Then GoTo 5160

'  THIS SERIES EXPANSION IS FOR ARG <= 3.4

'     Fact = 1#
'     IL = 1
'     UOX = XOX * XOX
'     US = UOX
'5085  Fact = Fact * IL
'     ZOZ = -1#
'     If ((IL / 2) * 2 = IL) Then ZOZ = 1#
'     TXOX = UOX / ((2# * IL + 1#) * Fact)
'     SUMXOX = SUMXOX + ZOZ * TXOX
'     UOX = UOX * US
'     IL = IL + 1


'    STOP THIE SUMMATION WHEN THE CURRENT TERM
'    IS LESS THAN 1E-20


'     If (TXOX > 1E-20) Then GoTo 5085
'     ERFC = 1# - 2# * XOX / (Pi) ^ 0.5 * SUMXOX
'     If (arg < 0#) Then ERFC = 2# - ERFC
'     GoTo 5430
'5160  If (XOX > 14#) Then GoTo 5410

'   THIS SERIES EXPANSION IS FOR ARG>3.4

'     UOX = 2# * XOX * XOX
'     LJL = 1
'     JLJ = 1
'     Fact = 1#
'5300  OLDFAC = Fact
'     Fact = Fact / UOX * JLJ

'  STOP THE SUMMATION WHEN THE CURRENT TERM BECOMES LARGER THAN
'  THE PREVIOUS TERM

'     If (Fact > OLDFAC) Then GoTo 5333
'     ZOZ = -1#
'     If ((LJL / 2) * 2 = LJL) Then ZOZ = 1#
'     TXOX = ZOZ * Fact
'     SUMXOX = SUMXOX + TXOX
'     LJL = LJL + 1
'     JLJ = JLJ + 2
'5333  ERFC = Exp(-XOX * XOX) / (Pi) ^ 0.5 / XOX * SUMXOX
'     GoTo 5420
'5410  ERFC = 0#
'5420  If (arg < 0#) Then ERFC = 2# - ERFC
```

```
5430 End Function

Public Function CONFINT(X, Dstar, data, NOBS, Kount, Resi, U, W, YCALC, Co, NP, BSW, Phix, R, C, pm)

Dim NME(3) As String


NME(1) = "Cmax"
NME(2) = "affn"
NME(3) = "k"


ActiveSheet.Range("G50:K60").Clear

  'DEFINING NPP TO BE THE NUMBER OF PARAMETERS BEING FIT
     NPP = 0
     For i = 1 To NP
         If Phix(i) = 0 Then NPP = NPP + 1
10    Next
     If NPP = 0 Then GoTo 300

   'DETERMINING THE CRITICAL RESIDUAL SUM OF SQUARES
   'WHICH DEFINES THE UPPER AND LOWER CONFIDENCE INTERVAL

     ER = ErrorFun(X, Dstar, data, NOBS, Kount, Resi, U, W, YCALC, Co, NP, BSW, manip, pm)
     'FESTI = FESTIM(NOBS, NPP, IDB) alternative below
     ActiveSheet.Range("G51") = NOBS 'allows NOBS to be used in Excel's FINV function
     ActiveSheet.Range("G50") = "=FInv(0.05, G51-4, 4)" '0.05 = 95% confidence interval, G51 = NOBS, 4 = NP,
degrees of freedom = NOBS-NP, NP
     FESTI = ActiveSheet.Range("G50").Value
     'Fnpp = float(NPP)
     'FNOBS = float(NOBS)
     'RSSCRIT = ER * (1 + Fnpp / (FNOBS - Fnpp) * FESTI)
      RSSCRIT = ER * (1 + NPP / (NOBS - NPP) * FESTI)

'    LOOPING THROUGH THE PARAMETERS TO DETERMINE CONFIDENCE INTERVALS

For i = 1 To NP
    For J = 1 To NP
      R(J) = X(J)
      C(J) = X(J)
90  Next

    If Phix(i) = 1 Then GoTo 199

'   LOOKING FOR THE UPPER LIMIT
         NCOUNT = 1
100

    'IF(FLOAT(I) .EQ. 3. .AND. X(3) .LT. 0.) THEN
     If i = 3 And X(i) < 0 Then
            R(i) = R(i) - 0.1 * X(i)
         Else
            R(i) = R(i) + 0.1 * X(i)
         End If
         ER = ErrorFun(R, Dstar, data, NOBS, Kount, Resi, U, W, YCALC, Co, NP, BSW, manip, pm)
```

```
        If Kount > 10000 Then
          ActiveSheet.Range("G49") = "CONFIDENCE INTERVALS DID NOT CONVERGE"
          GoTo 400
        End If
        If R(3) < -100 Or R(3) > 100 Then GoTo 120
        If NCOUNT > 1 Then
            If Abs((ERCHK - ER) / ER * 100) < 0.001 Then
                R(i) = -1#
                GoTo 120
            End If
        Else
            NCOUNT = 2
        End If
        ERCHK = ER
        If ER < RSSCRIT Then GoTo 100

110

      'IF(FLOAT(I) .EQ. 3. .AND. X(I) .LT. 0.) THEN
      If i = 3 And X(i) < 0 Then

         R(i) = R(i) + 0.01 * X(i)
         Else
         R(i) = R(i) - 0.01 * X(i)
      End If

   ER = ErrorFun(R, Dstar, data, NOBS, Kount, Resi, U, W, YCALC, Co, NP, BSW, manip, pm)
   If Kount > 10000 Then
          ActiveSheet.Range("G49") = "CONFIDENCE INTERVALS DID NOT CONVERGE"
          GoTo 400
   End If
      If ER > RSSCRIT Then GoTo 110

     'LOOKING FOR THE LOWER LIMIT
120
      'IF(FLOAT(I) .EQ. 3. .AND. X(I) .LT. 0.) THEN
       If i = 3 And X(i) < 0 Then
            C(i) = C(i) + 0.1 * X(i)
        Else
            C(i) = C(i) - 0.1 * X(i)
        End If
       'IF(C(I) .LT. 0. .AND. FLOAT(I) .NE. 3.) THEN
       If C(i) < 0 And i <> 1 Then
            C(i) = C(i) + 0.1 * X(i)
125           C(i) = C(i) - 0.01 * X(i)
            If C(i) < 0 Then
                C(i) = 0#
                GoTo 249
            End If
        End If

        ER = ErrorFun(C, Dstar, data, NOBS, Kount, Resi, U, W, YCALC, Co, NP, BSW, manip, pm)
        If Kount > 10000 Then
          ActiveSheet.Range("G49") = "CONFIDENCE INTERVALS DID NOT CONVERGE"
          GoTo 400
        End If
```

```
    If C(3) < -100 Or C(3) > 100 Then GoTo 249
    If ER < RSSCRIT Then GoTo 120

130
    'IF(FLOAT(I) .EQ. 3. .AND. X(I) .LT. 0.) THEN
    If i = 3 And X(i) < 0 Then
        C(i) = C(i) - 0.01 * X(i)
    Else
        C(i) = C(i) + 0.01 * X(i)
    End If

    ER = ErrorFun(C, Dstar, data, NOBS, Kount, Resi, U, W, YCALC, Co, NP, BSW, manip, pm)
    If Kount > 10000 Then
      ActiveSheet.Range("G49") = "CONFIDENCE INTERVALS DID NOT CONVERGE"
      GoTo 400
    End If
    If ER > RSSCRIT Then GoTo 130

249
    If i = 3 Then
        X(i) = Exp(X(i))
        If R(i) < -99 Then
            R(i) = 0#
        Else
            R(i) = Exp(R(i))
        End If
        C(i) = Exp(C(i))
    End If

259 'Writing to the output file

    ActiveSheet.Range("G50") = "95% CONFIDENCE INTERVALS FOR ESTIMATED PARAMETERS"
    ActiveSheet.Range("G51") = "Parameter"
    ActiveSheet.Range("I51") = "Low"
    ActiveSheet.Range("J51") = "Optimized"
    ActiveSheet.Range("K51") = "High"
    ActiveSheet.Range("G60") = "CRITICAL RSS VALUE ="
    ActiveSheet.Range("J60") = RSSCRIT

    If R(i) > 0 Then

       ActiveSheet.Cells(i + 52, 7) = NME(i)
       ActiveSheet.Cells(i + 52, 9) = C(i) 'lower limit
       ActiveSheet.Cells(i + 52, 10) = X(i) 'optimized
       ActiveSheet.Cells(i + 52, 11) = R(i) 'upper limit

        If i = 1 Then 'converts velocity to m/sec
            ActiveSheet.Cells(i + 52, 9) = C(i)  'lower limit
            ActiveSheet.Cells(i + 52, 10) = X(i) 'optimized
            ActiveSheet.Cells(i + 52, 11) = R(i)  'upper limit
        End If
        If i = 2 Then 'converts velocity to m/sec
            ActiveSheet.Cells(i + 52, 9) = C(i)  'lower limit
            ActiveSheet.Cells(i + 52, 10) = X(i) 'optimized
            ActiveSheet.Cells(i + 52, 11) = R(i)  'upper limit
        End If
```

```
            If i = 3 Then ' converts FODC to /sec
                ActiveSheet.Cells(i + 52, 9) = C(i)  'lower limit
                ActiveSheet.Cells(i + 52, 10) = X(i)  'optimized
                ActiveSheet.Cells(i + 52, 11) = R(i) 'upper limit
            End If

        Else
         ActiveSheet.Range("G52") = "No Convergence"
        End If
199
200   Next

      If R(i) = 0 Then

         ActiveSheet.Cells(i + 52, 7) = ""
         ActiveSheet.Cells(i + 52, 9) = ""
         ActiveSheet.Cells(i + 52, 10) = ""
         ActiveSheet.Cells(i + 52, 11) = ""
      End If

299
300
 If X(3) > 0 Then
        X(3) = Log(X(3))
    Else
        X(3) = 0#
    End If
400
 i = i
End Function

UserForm 8 code

Private Sub CommandButton1_Click()

'create results worksheet
Worksheets.Add(After:=Worksheets(Worksheets.Count)).Name = "MonteCarlo"

Sheets("KIMPE").Select
   ActiveSheet.Range("A1:A7,C1:C7").Copy
   Sheets("MonteCarlo").Select
   ActiveCell.Offset(0, 0).Select
   ActiveSheet.Paste
Sheets("KIMPE").Select
   ActiveSheet.Range("g30:g32,j30:j32").Copy
   Sheets("MonteCarlo").Select
   ActiveCell.Range("A12:B14").Select
   ActiveSheet.Paste

'reorder parameters to match Monte Carlo order
   ActiveSheet.Range("a14:b14").Cut
   ActiveSheet.Range("a11:b11").Select
   ActiveSheet.Paste
```

```
   Response = MsgBox("Analysis Complete. Do you wish to save your project with a unique name?", vbYesNo)

If Response = vbYes Then    ' User chose Yes.
        NewName = InputBox("Enter New File Name", "Save As")
        ActiveWorkbook.SaveAs FileName:=ThisWorkbook.Path & NewName, FileFormat:=xlNormal,
Password:="", WriteResPassword:="", ReadOnlyRecommended:=False, CreateBackup:=False
        Else: GoTo 10    ' User chose No.
End If

   UserForm8.Hide

10 End Sub

UserForm 9 code
Private Sub AcceptCurve_Click()

a = DiffusionCoeff
If SheetCounter = 6 Then
   UserForm9.Hide
   UserForm4.Show
   GoTo 10
End If
SheetCounter = SheetCounter + 1
Sheets(Ctarget(SheetCounter)).Activate

10  SheetCounter = SheetCounter
End Sub

Private Sub RefitCurve_Click()

UserForm9.Hide
UserForm4.Show

End Sub
```

Appendix G: Connelly Iron Specifications

CONNELLY – GPM, INC.

ESTABLISHED 1875
3154 SOUTH CALIFORNIA AVENUE CHICAGO, ILLINOIS 60608-5176
PHONE: (773) 247-7231 • www.ConnellyGPM.com • FAX: (773) 247-7239

April 7, 2011

SCREEN SPECIFICATION
ETI CC-1004

U.S. SCREEN NUMBER	(Opening Size)	
4	(4.75 mm)	100% PASSING
8	(2.36 mm)	95 - 100% PASSING
16	(1.18 mm)	75 - 90
30	(0.600 mm)	25 - 45
50	(0.300 mm)	0 - 10
100	(0.150 mm)	0 - 5

MATERIAL WEIGHS APPROXIMATELY 140 - 160 POUNDS PER CUBIC FOOT

TYPICAL ANALYSIS OF IRON AGGREGATE

Metallic Iron	87-93%
Total Carbon	2.85-3.23
Manganese	0.14-0.60
Sulphur	0.067-0.107
Phosphorous	0.000-0.132
Silicon	1.0-1.85
Nickel	0.05-0.21
Chromium	0.03-0.23
Vanadium	ND
Molybdenum	0.08-0.15
Titanium	0.004-0.1
Copper	0.11-0.20
Aluminum	0-0.005
Cobalt	ND
Magnesium	0.01
Boron	0.01
Zinc	0.01
Zirconium	0.01

GALEN B. DIXON
Technical Director

D:\WORD\WT\MscMemLST\SPECS&FORMS\1004SPECE-ml.DOC

Material Safety Data Sheet
May be used to comply with
OSHA's Hazard Communication Standard,
29 CFR 1910.1200. Standard must be
consulted for specific requirements.

U.S. Department of Labor
Occupational Safety and Health Administration
(Non-Mandatory From)
Form Approved
OMB No. 1218-0072

IDENTITY (As Used on Label and List)
IRON AGGREGATE

NOTE: Blank spaces are not permitted. If an item is not applicable or information unavailable, the space must be so marked.

Section I

Manufacturer's Name CONNELLY-GPM, INC.	Emergency Telephone Number (773) 247-7231
Address (Number, Street, City, State, and ZIP Code) 3154 South California Avenue	Telephone Number for Information (773) 247-7231
Chicago, IL 60608-5176	Date Revised 3/18/2008 Date Printed 4/7/2011
	Signature of Preparer (optional)

Section II - Hazardous Ingredients/Identity Information

Hazardous Components (Specific Chemical Identity; Common Name)			(as fume) OSHA PEL*	ACGIH TLV*	Other Limits Recommended	% (optional)
IRON	CAS #7439-89-6	+85%	10 mg/m³	5 mg/m³	10 mg/m³	+85%
CARBON (carbon black)	CAS #1333-86-4	<3.5%	3.5 mg/m³	3.5 mg/m³	7 mg/m³	<3.5%
SILICON	CAS #7440-21-3	<2%	(1)	(2)	20 mg/m³	<2%
CHROMIUM	CAS #7440-47-3	<.25%	1.0 mg/m³	0.5 mg/m³		<.25%
COPPER	CAS #7440-50-8	<.25%	1.0 mg/m³	1.0 mg/m³		<.25%
MANGANESE	CAS #7439-96-5	<.75%	5 mg/m³	5 mg/m³		<.75%
NICKEL	CAS #7440-02-2	<.25%	1.0 mg/m³	1.0 mg/m³		<.25%

All other constituents below 0.2%

*8 hour time weighted average

1) <1% Quartz 15 mg/m³ of total dust, or 5 mg/m³ respirable dust
2) >1% Quartz 10 mg/m³ of total dust, or 5 mg/m³ respirable dust

Section III - Physical/Chemical Characteristics

Boiling Point Iron Dust	3000 °C	Specific Gravity (H_2O = 1) Approximate @ 60°F	7.8
Vapor Pressure (mm Hg) @ 1787°C	1	Melting Point	1371-1480°F
Vapor Density (AIR = 1)	N/A	Evaporation Rate (Butyl Acetate = 1)	N/A

Solubility in Water
INSOLUBLE

Apearance and Odor
Odorless Gray/Black Powder

Section IV - Fire and Explosion Hazard Data

Flash Point (Method Used) Not Available	Flammable Limits	LEL	UEL

Extinguishing Media
Dry chemicals or sand or universal type foam

Special Fire Fighting Procedures
Firefighters should wear self-contained breathing apparatus and protective clothing.

Unusual Fire and Explosion Hazards
Dust can present fire and explosion hazards when exposed to fire, chemical reaction, or contact with powerful oxidizers.

(Reproduce locally)

OSHA 174 Sept 1985

Section V - Reactivity Data

Stability	Unstable:		Contitions to Avoid:
	Stable:	x	Contact with powerful oxidizers such as strong acids.

Incompatibility (Materials to Avoid)

Powerful oxidizers such as strong acids.

Hazardous Decomposition or Byproducts

Hydrogen, Carbon-Monoxide, Carbon Dioxide

Hazardous	May Occur		Contitions to Avoid:
Polymerization	Will Not Occur	x	

Section VI - Health Hazard Data

Route(s) of Entry	Inhalation?	Skin?	Ingestion?
	yes	no	yes (not likely)

Health Hazards (Acute and Chronic)

Chronic overexposure to iron oxide fume may cause apparently benign pneumoconiosis.
Acute overexposure may cause eye, nose, mouth, and skin irritation.

Carcinogenicity:	NTP?	IARC Monographs?	OSHA Regulated
	NO INFORMATION AVAILABLE		

Signs and Symptoms of Exposure

NO INFORMATION AVAILABLE

Medical Conditions Generally Aggravated by Exposure

NO INFORMATION AVAILABLE

Emergency First Aid Procedures

INHALATION: Remove to fresh air. Seek medical attention.
INGESTION: Seek medical attention.
SKIN CONTACT: Brush off excess. Wash with soap and water.
EYE CONTACT: Flush with running water. Seek medical attention.

Section VII - Precautions for Safe Handling

Steps to Be Taken in Case Material is Released or Spilled

If large quantities of dust are spilled, remove by vacuuming or wet sweeping. To prevent inhalation of large quantities of airborne dust, clean up personnel should wear respirators and protective clothing.

Waste Disposal Method

Sanitary landfill
Follow Federal, State, and Local Guidelines.

Precautions to Be Taken In Handling and Storing

Do not store near powerful oxidizers such as strong acids. Keep material in a cool dry location.

Other Precautions

Section VIII - Control Measures

Respiratory Protection (Specify Type)

NIOSH approved respirator for dusts and fumes.

Ventilation	Local Exhaust	Special
	YES	
	Mechanical (General)	Other

Protective Gloves	Eye Protection
Cloth	NIOSH approved safety glasses/goggles

Other Protective Clothing or Equipment

Skull cap, hard hat to keep dust out of hair.

Work/Hygenic Practices

Use good housekeeping practices to keep dust to a minimum.

Appendix H: Raman Spectra Collected on Shinny Side of Connelly Iron and Electrolytic Iron.

Sampling Port 1: Shinny

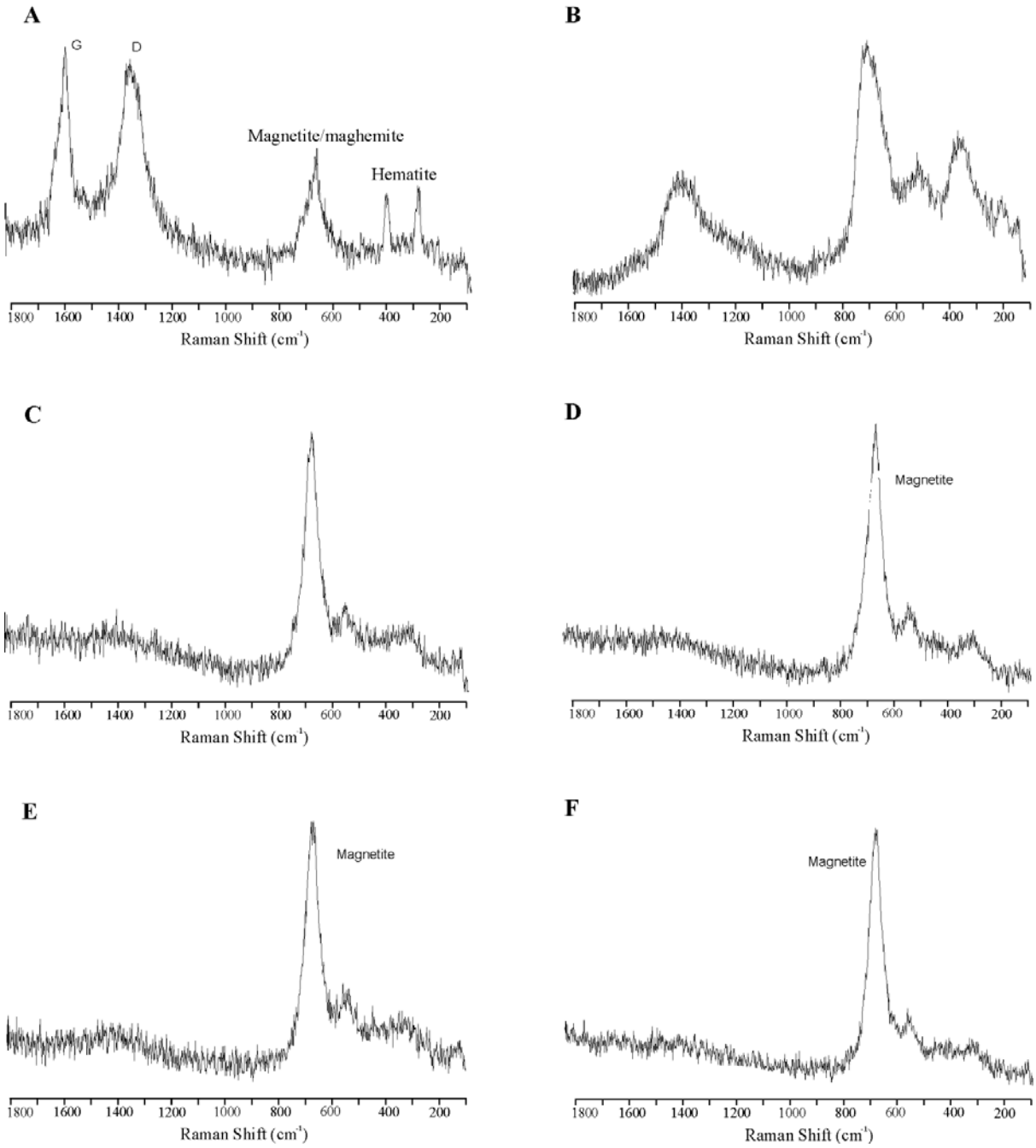

Figure H. 1: Raman spectra collected on the shinny side of grain at port 1 for A) 2 days B) 12 days C)15 days D) 152 days E) 154 days and F) 240 days of column aging.

Sampling Port 2: Shinny

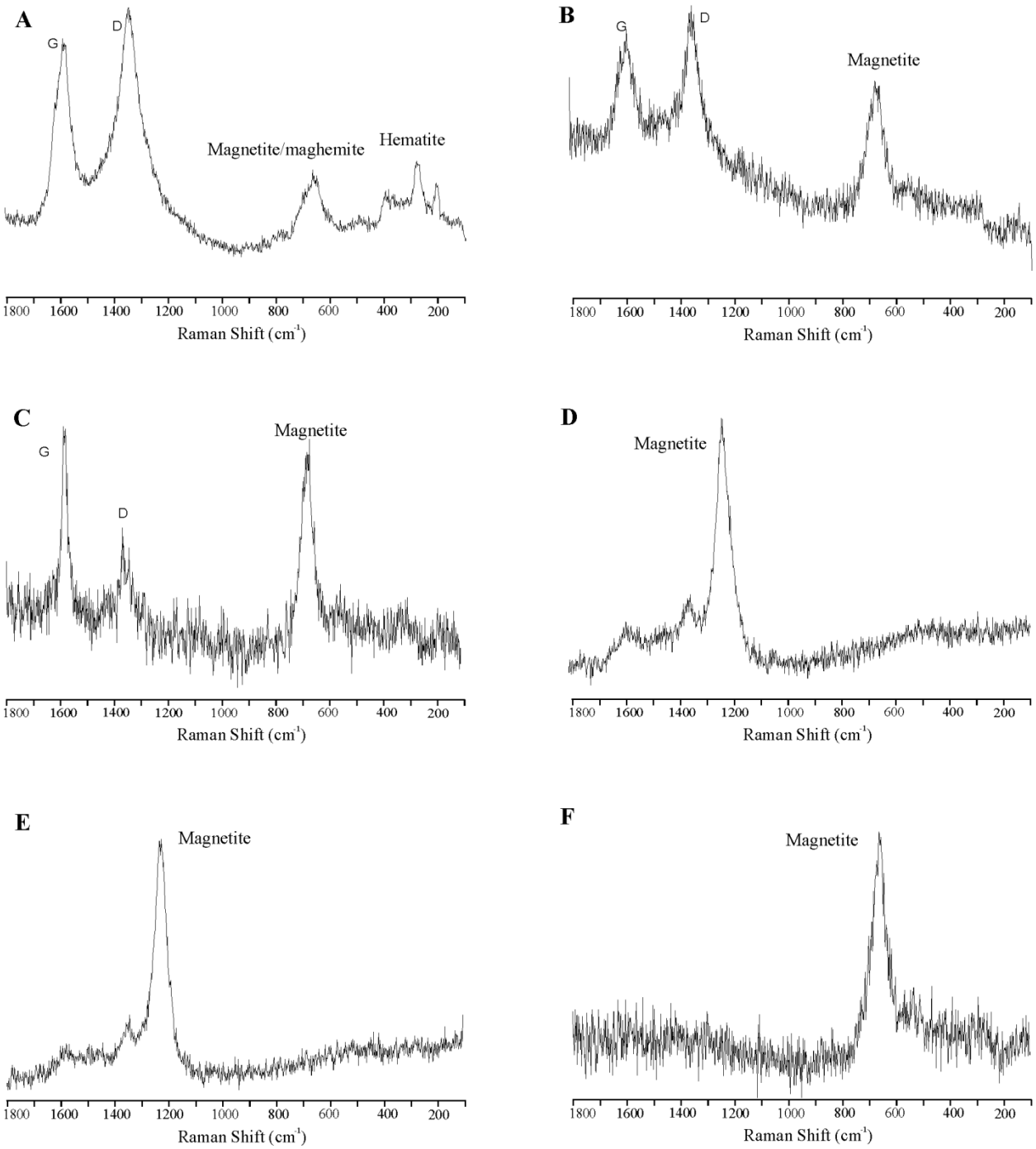

Figure H. 2: Raman spectra collected on the shinny side of grain at port 2 for A) 2 days B) 12 days C)15 days D) 152 days E) 154 days and F) 240 days of column aging.

Sampling Port 3: Shinny

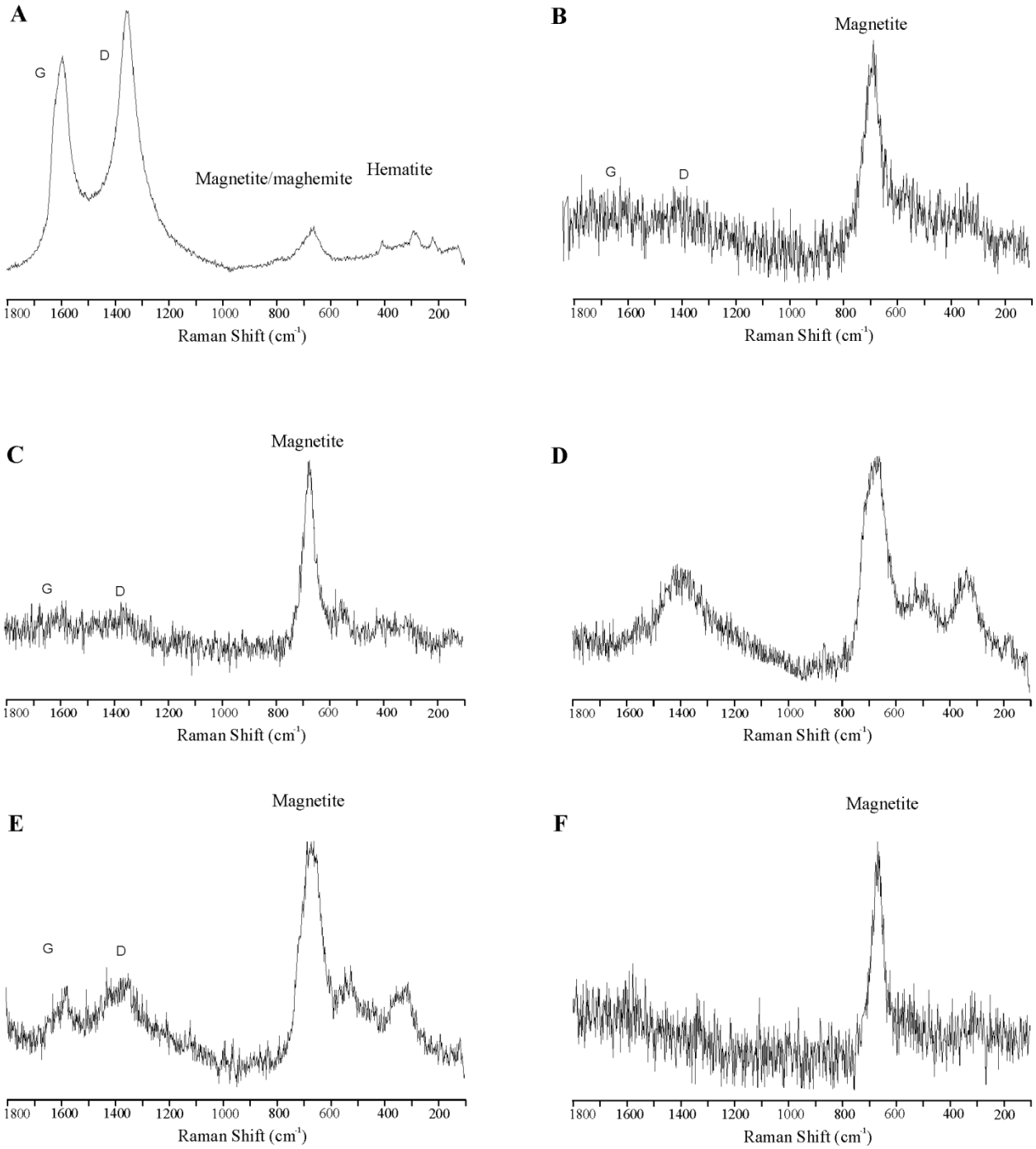

Figure H. 3: Raman spectra collected on the shinny side of grain at port 3 for A) 2 days B) 12 days C)15 days D) 152 days E) 154 days and F) 240 days of column aging.

Sampling Port 4: Shinny

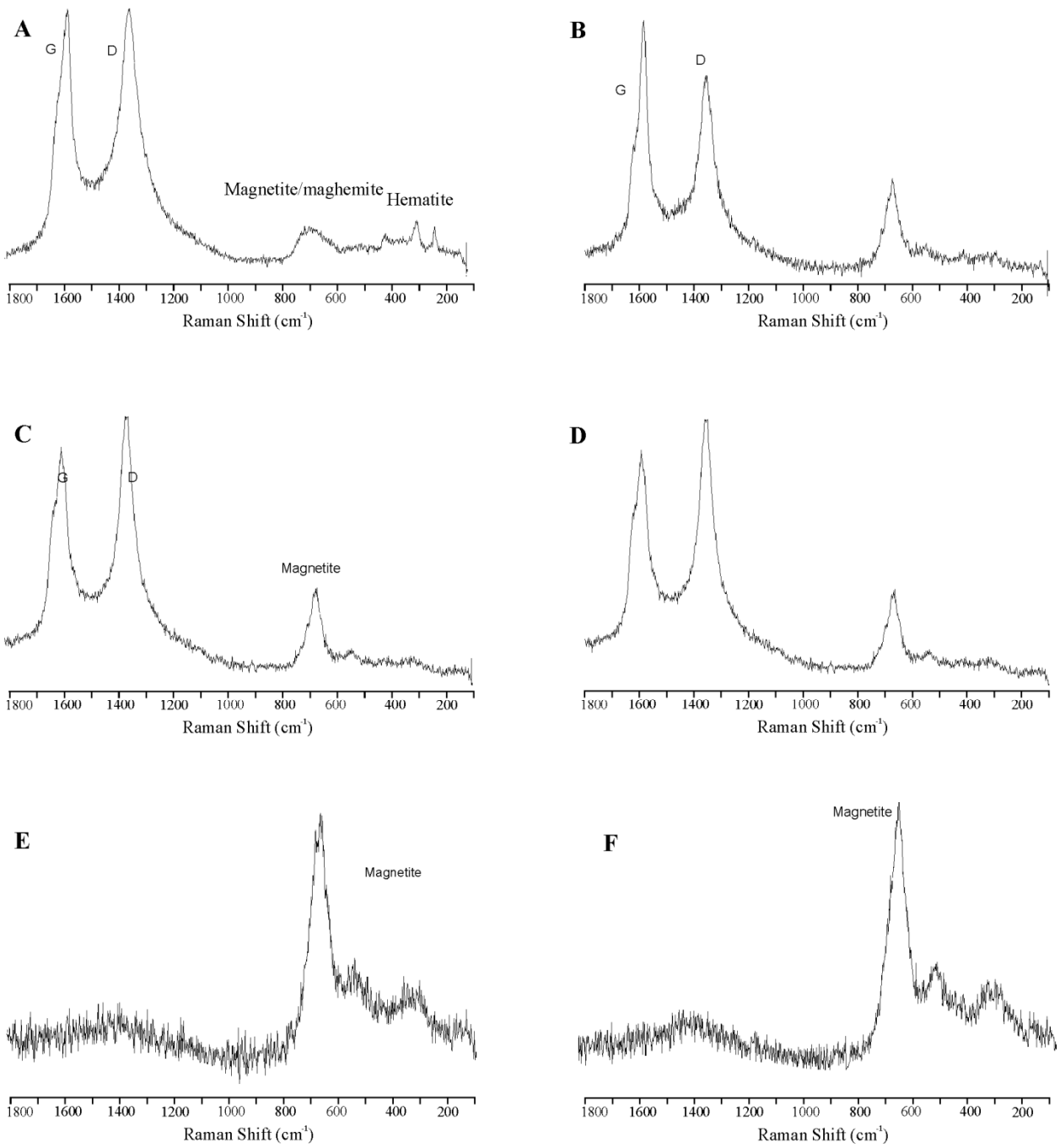

Figure H. 4: Raman spectra collected on the shinny side of grain at port 4 for A) 2 days B) 12 days C)15 days D) 152 days E) 154 days and F) 240 days of column aging.

Table H.1: Raman shifts, intensities (ID and IG), and Full width half maximum (FWHM) of Carbon D and G bands.

Co (uM)	IMAGE #	D band	ID	G band	IG	ID/IG	$FWHM_{ID}$	$FWHM_{IG}$
	1	1353	1381	1584	1397	0.988547		
0	CI1	1346	5907	1575	6663	0.886538	98.66	31.9
0	CI2	1346	13488	1571	42826	0.314949	49.165	30.25
0	CI3	1340	5681	1580	4181	1.358766		
0	CI4	1346	6609	1578	6628	0.997133	96.37	41.57
0	CI5	1344	6609		6637	0.995781		
	SYSTAMATIC ANLYSIS SET 1							
	redraw1	1348	3655	1575	4711.9	0.775696	56.64	62.35
	redraw4	1350	8216	1577	9245.9	0.88861	60.44	47.27
	redraw5	1348	7260	1571	8880	0.817568	54.74	51.07
	shinyraw2	1352	7979	1584	8661	0.921256	69.94	62.35
	shinyraw6	1321	3250	1586	3231	1.005881	107.73	71.58
	VIAL 1							
	50µM							
50	RC	1351	1137	1580	1179	0.964377	77.55	33.96
50	RD	1346	3507	1575	4971	0.705492	52.97	32.065
50	RL	1342	1517	1588	1502	1.009987	81.35	83.13
50	RM	1351	3401	1588	3283	1.035943	105.82	68.04
50	SE	1346	1506	1582	1561	0.964766	81.3	37.76
50	SG	1353	1428	1580	1916	0.745303	68.05	28.38
50	SH	1346	1397	1586	1411	0.990078	104.04	71.82
	VIAL2							
50	50µM							
50	RA	1350	5542	1588	5407	1.024968	109.74	68.05
50	RC	1343	994	1588	1018	0.976424		
50	SC	1348	2558	1575	2754	0.928831	62.47	45.36
50	SE	1344	3847	1582	3520	1.092898	69.95	54.86
	100µM							
100	SB	1365	2527	1582	2496	1.01242		
100	SC	1355	2110	1580	2112	0.999053	54.86	47.26
100	SD	1353	1127	1584	1146	0.983421	139.85	33.96
100	SE	1351	1269	1580	1419	0.894292	56.65	28.26
	200µM							

200	RA	1342	2827	1588	2959	0.95539	64.25	-56.77
200	RB	1350	2582	1588	2666	0.968492	81.13	66.15
200	RC	1355	2497	1588	2576	0.969332		
200	RD	1348	972	1584	967	1.005171		
200	SA	1348	1240	1580	1260	0.984127	62.35	41.57
200	SB	1350	4919	1584	5435	0.90506	47.27	37.77
200	SC	1351	6671	1584	6438	1.036191	58.55	56.65
200	SD	1351	8650	1586	7996	1.081791	54.75	60.45
200	SE	1353	2623	1588	2466	1.063666	50.95	56.65
200	SF	1351	3017	1584	2920	1.033219	54.75	58.55
	300µM						100.23	54.94
300	RE	1350	3232	1590	3164	1.021492	49.15	68.12
300	SB	1350	2907	1594	2788	1.042683		
300	SC	1346	2309	1584	2335	0.988865		
	400µM							
400	SA		4609	1584	5105	0.90284	47.26	20.9
	VIAL3							
	50µM							
50	RA	1348	1408	1576	2144	0.656716	47.38	22.68
50	RB	1346	3700	1575	4002	0.924538	117.27	24.58
50	SB	1353	1639	1582	2738	0.598612	49.16	28.26
50	SE	1346	3347	1576	3376	0.99141	117.22	49.25
	100µM							
100	RB	1348	979	1576	943	1.038176		
100	RC	1351	3496	1578	3209	1.089436		
100	RE	1348	1048	1573	1225	0.85551	128.62	24.58
100	RF	1346	2991	1588	2930	1.020819		
100	SA	1357	1051	1582	1170	0.898291	52.76	34.08
100	SB	1353	6339	1576	6457	0.981725	52.96	35.85
100	SC	1348	1560	1575	2273	0.686318	60.45	26.48
	200µM							
200	RA	1363	2393	1590	2406	0.994597		
		1350	3018	1590	2796	1.079399		
	400µM							

400	SB	1352	1573	1579	1599	0.98374		
400	SC	1352	1511	1579	1567	0.964263		
400		1350	4593	1586	4708	0.975573		
400		1342	4519	1584	4652	0.97141		
	VIAL4							
	50µM							
50	RB	1359	1259	1576	1723	0.730702	77.55	26.48
50	SA	1353	1376	1578	2247	0.612372	47.26	20.9
50	SB	1350	1712	1580	2562	0.668228	51.06	30.16
50	SC	1348	1789	1578	2358	0.758694	51.06	33.95
	100µM							
100	RA	1355	1084	1575	1098	0.98725		
100	RC	1353	3404	1576	3630	0.937741	56.65	37.75
100	SA	1346	4657	1573	4650	1.001505	62.35	52.92
100	SC	1353	1544	1580	1519	1.016458	68.05	35.85
100	SD	1353	2036	1573	3289	0.619033	81.23	22.67
	200µM							
200	SA	1350	3563	1584	3926	0.907539	79.45	30.17
200	SC	1350	1404	1586	1279	1.097733		
200	RB	1342	2675	1584	2662	1.004884		
		1348	2592	1599	2570	1.00856		
	300µM							
300	RA	1350	1146	1588	1110	1.032432	113.42	66.14
300	RB	1353	3284	1584	3168	1.036616	98.33	53
300	RC	1333	1137	1575	1190	0.955462		
300	SA	1352	2943	1586	2985	0.98593	54.74	45.48
300	SC	1352	2373	1582	2804	0.846291	47.27	33.96
300	SD	1352	2264	1575	3365	0.672808	46.57	30.28
300	SE	1353	2049	1580	3271	0.626414	50.96	24.58
400	RB	1335	1788	1588	1855	0.963881		
400	RC	1346	5239	1592	5270	0.994118		
400	SB	1352	5775	1582	5981	0.965558		

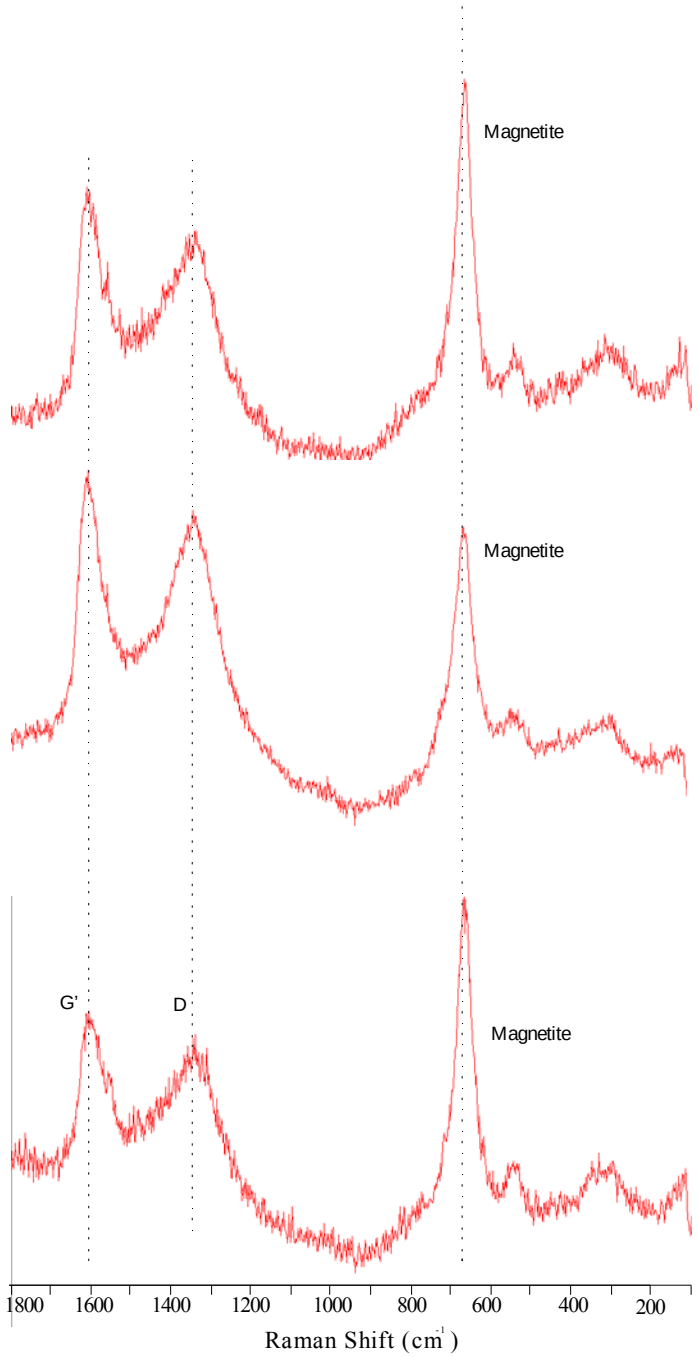

Figure H. 5: Raman spectras collected on the Electrolytic Iron showing magnetite band at 670cm^{-1} and two carbonaceous material bands at 1606 cm^{-1} is G' and at 1336 cm^{-1} is D band.

References

Bear, J., 1979. Hydraulics of Groundwater. McGraw- Hill International Book Co, New York.

Devlin, J.F., 2009. Development and Assessment of a Rate Equation for Chemical Transformations in Reactive Porous Media. Environmental Science and Technology, v. 43, no. 11, 4113-4118.

Rasband, W., 2007. ImageJ: National Institute of Health, 1.46b ed, Bethesda, MD, USA, p. http://rsb.info.nih.gov/ij/index.html.